N°d'ordre NNT :2023ISAL0020

THESE de DOCTORAT DE L'INSA LYON,
Membre de l'Université de Lyon

Ecole Doctorale N° 34
Ecole doctorale Matériaux de Lyon

Spécialité/ discipline de doctorat : **Matériaux**

Soutenue publiquement le 23/03/2023, par :
Aslihan SAYILAN

Tribological Behaviour of Ti-Based Thin Films: A Small Scale *In Situ* Investigation

Devant le jury composé de :

LANGLADE, Cécile	Professeure, UTBM	Rapporteuse
MARTIN, Nicolas	Professeur, FEMTO-ST	Rapporteur
PICHON, Luc	Professeur, Université de Poitiers	Examinateur
VAZ, Jose Filipe	Maître de Conférences Universidade do Minho	Examinateur
SANCHEZ LOPEZ, Juan Carlos	HDR-Chercheur scientifique, CSIC	Examinateur
STEYER, Philippe	Professeur, INSA de Lyon	Directeur de thèse
DESCARTES, Sylvie	HDR-Ingénieur de Recherche, INSA de Lyon	Co-directrice
MARY, Nicolas	Maître de Conférences, INSA de Lyon	Encadrant

ANALYSIS SUMMARY
magister

INSA INSTITUT NATIONAL DES SCIENCES APPLIQUÉES LYON

TH0954_Aslihan SAYILAN_Manuscrit

8% Similarities

< 1% Text between quotes
0% similarities between quotation marks
< 1% Language not recognised

Document name: TH0954_Aslihan SAYILAN_Manuscrit.pdf
Document ID: efde4a87acbc7835db35c4bef34eb148572c2ffb
Original document size: 12.96 Mo

Submitter: Mickael Lallart
Submission date: 1/20/2023
Upload type: interface
analysis end date: 1/20/2023

Number of words: 59,971
Number of characters: 414,263

Location of similarities in the document:

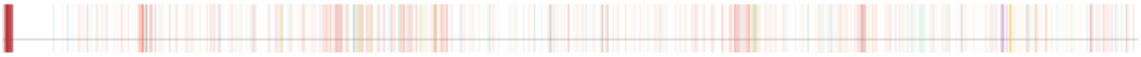

Main sources detected

No.	Description	Similarities	Locations	Additional information
1	**Document from another user** #8DF3c0 The document is from another group 16 similar sources	< 1%		identical words : < 1% (281 words)
2	**1_thesis_dabankah_Thesis_Dabankah.pdf** #17e527 The document is from my group 21 similar sources	< 1%		identical words : < 1% (286 words)
3	**manuscrit_thèse_PilarSango.pdf** #5b5449 The document is from my group 8 similar sources	< 1%		identical words : < 1% (266 words)
4	**www.wtc-2022.org** https://www.wtc-2022.org/abstract/export/abstract-A102102AS.pdf 15 similar sources	< 1%		identical words : < 1% (237 words)
5	**hdl.handle.net** | Proceedings of the VIII Iberian Conference on Tribology : Conferenc... http://hdl.handle.net/10317/4812 109 similar sources	< 1%		identical words : < 1% (231 words)

Sources with incidental similarities

No.	Description	Similarities	Locations	Additional information
1	**hal.umontpellier.fr** | Atomic layer deposition for biosensing applications https://hal.umontpellier.fr/hal-01919095/file/Biosensors and Bioelectronics, 2018, 122, 147-159.pdf	< 1%		identical words : < 1% (40 words)
2	**www.sciencedirect.com** | Dry cutting performance of partially filtered arc deposited ... https://www.sciencedirect.com/science/article/pii/S0257897201014219	< 1%		identical words : < 1% (22 words)
3	**www.sciencedirect.com** | Identification of critical load for scratch adhesion strength-- https://www.sciencedirect.com/science/article/pii/S0257897215301705	< 1%		identical words : < 1% (22 words)
4	**www.sciencedirect.com** | Electrospun fibro-porous polyurethane coatings for impla... https://www.sciencedirect.com/science/article/abs/pii/S0142961212012008	< 1%		identical words : < 1% (17 words)
5	**doi.org** | Die pCO2-/pO2-Optode: Eine neue p CO2- bzw. pO2-Meßsonde zur Messun-- https://doi.org/10.1515/znc-1975-7-819	< 1%		identical words : < 1% (18 words)

Ignored source

These sources have been excluded by the document owner from the calculation of the similarity percentage.

No.	Description	Similarities	Locations	Additional information
1	**www.sciencedirect.com** | Tribological analysis of TiN film during run-in period: An i... https://www.sciencedirect.com/science/article/pii/S0257897223000038	4%		identical words : 4% (2,430 words)

Referenced sources (without similarities detected)

These sources were cited in the paper without finding any similarities.

1 https://doi.org/10.1016/j.surfcoat.2014.11.020
2 https://doi.org/10.2319/0003-3219(2009)
3 https://doi.org/10.1186/1475-925x-5-22
4 https://doi.org/10.1016/j.msec.2016.01.029
5 https://doi.org/10.1016/j.apsusc.2019.144617

Département FEDORA – INSA Lyon - Ecoles Doctorales

SIGLE	ECOLE DOCTORALE	NOM ET COORDONNEES DU RESPONSABLE
CHIMIE	**CHIMIE DE LYON** **https://www.edchimie-lyon.fr** Sec. : Renée EL MELHEM Bât. Blaise PASCAL, 3e étage secretariat@edchimie-lyon.fr	**M. Stéphane DANIELE** C2P2-CPE LYON-UMR 5265 Bâtiment F308, BP 2077 43 Boulevard du 11 novembre 1918 69616 Villeurbanne **directeur@edchimie-lyon.fr**
E.E.A.	**ÉLECTRONIQUE, ÉLECTROTECHNIQUE, AUTOMATIQUE** **https://edeea.universite-lyon.fr** Sec. : Stéphanie CAUVIN Bâtiment Direction INSA Lyon Tél : 04.72.43.71.70 secretariat.edeea@insa-lyon.fr	**M. Philippe DELACHARTRE** INSA LYON Laboratoire CREATIS Bâtiment Blaise Pascal, 7 avenue Jean Capelle 69621 Villeurbanne CEDEX Tél : 04.72.43.88.63 **philippe.delachartre@insa-lyon.fr**
E2M2	**ÉVOLUTION, ÉCOSYSTÈME, MICROBIOLOGIE, MODÉLISATION** **http://e2m2.universite-lyon.fr** Sec. : Bénédicte LANZA Bât. Atrium, UCB Lyon 1 Tél : 04.72.44.83.62 secretariat.e2m2@univ-lyon1.fr	**Mme Sandrine CHARLES** Université Claude Bernard Lyon 1 UFR Biosciences Bâtiment Mendel 43, boulevard du 11 Novembre 1918 69622 Villeurbanne CEDEX **sandrine.charles@univ-lyon1.fr**
EDISS	**INTERDISCIPLINAIRE SCIENCES-SANTÉ** **http://ediss.universite-lyon.fr** Sec. : Bénédicte LANZA Bât. Atrium, UCB Lyon 1 Tél : 04.72.44.83.62 secretariat.ediss@univ-lyon1.fr	**Mme Sylvie RICARD-BLUM** Institut de Chimie et Biochimie Moléculaires et Supramoléculaires (ICBMS) - UMR 5246 CNRS - Université Lyon 1 Bâtiment Raulin - 2ème étage Nord 43 Boulevard du 11 novembre 1918 69622 Villeurbanne Cedex Tél : +33(0)4 72 44 82 32 **sylvie.ricard-blum@univ-lyon1.fr**
INFOMATHS	**INFORMATIQUE ET MATHÉMATIQUES** **http://edinfomaths.universite-lyon.fr** Sec. : Renée EL MELHEM Bât. Blaise PASCAL, 3e étage Tél : 04.72.43.80.46 infomaths@univ-lyon1.fr	**M. Hamamache KHEDDOUCI** Université Claude Bernard Lyon 1 Bât. Nautibus 43, Boulevard du 11 novembre 1918 69 622 Villeurbanne Cedex France Tél : 04.72.44.83.69 **hamamache.kheddouci@univ-lyon1.fr**
Matériaux	**MATÉRIAUX DE LYON** **http://ed34.universite-lyon.fr** Sec. : Yann DE ORDENANA Tél : 04.72.18.62.44 yann.de-ordenana@ec-lyon.fr	**M. Stéphane BENAYOUN** Ecole Centrale de Lyon Laboratoire LTDS 36 avenue Guy de Collongue 69134 Ecully CEDEX Tél : 04.72.18.64.37 **stephane.benayoun@ec-lyon.fr**
MEGA	**MÉCANIQUE, ÉNERGÉTIQUE, GÉNIE CIVIL, ACOUSTIQUE** **http://edmega.universite-lyon.fr** Sec. : Stéphanie CAUVIN Tél : 04.72.43.71.70 Bâtiment Direction INSA Lyon mega@insa-lyon.fr	**M. Jocelyn BONJOUR** INSA Lyon Laboratoire CETHIL Bâtiment Sadi-Carnot 9, rue de la Physique 69621 Villeurbanne CEDEX **jocelyn.bonjour@insa-lyon.fr**
ScSo	**ScSo*** **https://edsciencessociales.universite-lyon.fr** Sec. : Mélina FAVETON INSA : J.Y. TOUSSAINT Tél : 04.78.69.77.79 melina.faveton@univ-lyon2.fr	**M. Bruno MILLY** Université Lumière Lyon 2 86 Rue Pasteur 69365 Lyon CEDEX 07 **bruno.milly@univ-lyon2.fr**

*ScSo : Histoire, Géographie, Aménagement, Urbanisme, Archéologie, Science politique, Sociologie, Anthropologie

Table of Content

List of Figures

List of Tables

ABSTRACT

The nature of interface in contact with skin, clothes or joints is one of the prime interests in the field of metallic biosensors. This interface can be enhanced through PVD processes in terms of chemistry and microstructure. Furthermore, dynamic evaluation of the contact interface at the early stage is essential to better understand the wear mechanism and to anticipate the efficient service life of the corresponding bio-device. Therefore, within this thesis, a laboratory-made micro-tribometer was developed and presented. This particular reciprocating ball-on-disk stage is coupled with an environmental SEM (eSEM) to characterise, at small scale, the tribological behaviour of the system under realistic *in situ* conditions.

To express the proof of concept, a preliminary analysis was performed with a conventional TiN PVD hard coatings, used as a model surface. The testing procedure for the dynamic approach during the run-in period throughout 100 cycles was defined in the controlled atmosphere in eSEM chamber (both in high vacuum and 50% relative humidity (RH)). When the tribological tests were performed, the wear track of the films was examined *in situ* after every 10 cycles, while the ball track was analysed in *post mortem* mode. Once validated, the mini-tribometer stage was applied for a more realistic metal used in biosensor systems: titanium. Indeed, this metal presents a high biocompatible character, coupled with interesting mechanical properties. The wear character of pure Ti film is still an issue, due to its columnar microstructure, which can be modified with an addition of proper alloying elements. In this sense, silver is an outstanding material to be alloyed with titanium for bio-sensor applications regarding its anti-bacterial character and ductile nature, as well its remarkable sliding behaviour in nanoparticle form. Within this thesis, Ti-Ag films were deposited with magnetron sputtering PVD process with several Ag contents. Various types of multiscale characterization (microstructural, chemical, electrical, mechanical) were performed to analyse the effect of Ag in the film composition. It was shown that increasing Ag content led to a denser microstructure with Ag-based nano-/micro-meter sized clusters distributed into the film matrix. Moreover, from a functional point of view, it also provided a slight improvement on hardness, Young's modulus and electrical conductivity of the films. During the *in situ* tribological analysis, the small-scale strategy of characterization that was specifically developed in this PhD, has highlighted a strong influence of the contact environment on its tribological behaviour. In particular, the effect of the humidity rate of the contact region on the tribological behaviour was deeply investigated, and the effect of Ag content on tribological behaviour of Ti-Ag films was studied. It was seen that temperature change to modify the humidity affects the tribological behaviour of polymer counter-face and Ag.

RESUME

La nature de l'interface en contact avec la peau, les vêtements ou les articulations est d'un intérêt primordial dans le domaine des biocapteurs métalliques. Cette interface peut être améliorée par des procédés PVD en termes de chimie et de microstructure. De plus, l'évaluation dynamique de l'interface de contact à un stade précoce est essentielle pour mieux comprendre le mécanisme d'usure et pour anticiper la durée de vie efficace du bio-dispositif correspondant. Par conséquent, dans le cadre de cette thèse, un micro-tribomètre fabriqué en laboratoire a été développé et présenté. Cette platine à billes sur disque est couplée à un MEB environnemental (eSEM) pour caractériser, à petite échelle, le comportement tribologique du système dans des conditions *in situ* réalistes.

Pour exprimer la preuve de concept, une analyse préliminaire a été réalisée avec un revêtement dur PVD TiN conventionnel, utilisé comme surface modèle. La procédure d'essai pour l'approche dynamique pendant la période de rodage tout au long de 100 cycles a été définie dans l'atmosphère contrôlée de la chambre eSEM (à la fois sous vide poussé et à 50% d'humidité relative (RH)). Lors des essais tribologiques, la trace d'usure des films a été examinée *in situ* tous les 10 cycles, tandis que la trace de la bille a été analysée en mode post mortem. Une fois validée, la platine du mini-tribomètre a été appliquée à un métal plus réaliste utilisé dans les systèmes de biocapteurs : le titane. En effet, ce métal présente un caractère biocompatible élevé, couplé à des propriétés mécaniques intéressantes. L'usure du film de titane pur reste un problème, en raison de sa microstructure colonnaire, qui peut être modifiée par l'ajout d'éléments d'alliage appropriés. Dans ce sens, l'argent est un matériau exceptionnel à allier au titane pour les applications de biocapteurs, en raison de son caractère antibactérien et de sa nature ductile, ainsi que de son remarquable comportement de glissement sous forme de nanoparticules. Dans le cadre de cette thèse, des films Ti-Ag ont été déposés par un procédé PVD de pulvérisation magnétron avec plusieurs teneurs en Ag. Différents types de caractérisation multi-échelle (microstructurelle, chimique, électrique, mécanique) ont été réalisés pour analyser l'effet de l'Ag dans la composition du film. Il a été démontré que l'augmentation de la teneur en Ag conduit à une microstructure plus dense avec des clusters de taille nano-/micro-métrique à base d'Ag distribués dans la matrice du film. De plus, d'un point de vue fonctionnel, cela a également permis une légère amélioration de la dureté, du module d'Young et de la conductivité électrique des films. Au cours de l'analyse tribologique *in situ*, la stratégie de caractérisation à petite échelle qui a été spécifiquement développée dans cette thèse, a mis en évidence une forte influence de l'environnement de contact sur son comportement tribologique. En particulier, l'effet du taux d'humidité de la région de contact sur le comportement tribologique a été étudié en profondeur, et l'effet de la teneur en Ag sur le comportement tribologique des films Ti-Ag a été étudié. Il a été constaté que le changement de température pour modifier l'humidité affecte le comportement tribologique de la contre-face en polymère et de l'Ag.

1. INTRODUCTION

The background was introduced and the problematics of this study was discussed.
Then the objective and the outline of this PhD was defined in the introduction chapter.

1. INTRODUCTION

1.1. Background and Context

Thin films are having a significant place in various fields of applications as transportation industry, medicine, energy etc. In a general viewpoint, Physical Vapour Deposition (PVD) is a reasonably favourable technique to prepare these films thanks to its efficiency and environmental-friendly character. With the technological developments on biosensors, thin films deposited with PVD technique is increasingly preferable.

The development of biosensors could be identified in three generations until reaching the use of thin films for this specific application. The first generation is defined as mediator-less amperometric biosensors. After that, second generation biosensors had a separated component (e.g. a co-reactor or auxiliary enzyme) which was fixed to the sensor itself to provide higher efficiency. Finally, for the third-generation sensors, bio-receptor is the integral part of main sensing element. The enzymes and mediator are placed on the same electrodes which provides higher feasibility in addition to the lower cost [1]. In Table 1.1, the chronological development of biosensors is explained.

Table 1.1: Chronological development of bio-sensors

	1st generation	
1962	Clark et al.	Enzyme electrode for oxygen detection [3]
1967	Clark	Enzyme electrode with glucose oxidase immobilisation [4]
1969	Guilbaut & Montalvo	First potentiometric enzyme electrode (to detect urea) [5]
1973	Guilbaut &Lubrano	Lactate enzyme sensor with Pt electrode for H_2O_2 detection [6]
1974	Mosbach et al.	First thermistor [2]
1975	Lubbers & Opitz	Optical biosensor (to detect alcohol) [2]
	2nd generation	
1976	Clemens et al.	Electrochemical biosensor (to detect glucose in artificial pancreas) [7]

1976	La Roche	Lactate analyser [8]
	3rd generation	
1980	Peterson	Fiber optic pH sensor (to detect blood gases in vivo) [9]
1982	Schultz	Fiber optic biosensors (to detect glucose) [10]
1983	Liedberg	First surface plasmon resonance biosensor (immune-sensor) [11]
1999	Poncharal et al.	First nano-sized bio-sensor [12]
2018	Girbi et al.	Nerve on chip biosensor (to detect nerve impulse) [13]

Previously wet-contact Ag/AgCl based electrodes were used for bio-sensing applications (Figure 2.3) [14]. However, for new generation biosensors, polymers are highly demanded materials based on their low cost and good biocompatibility. Nevertheless, for reliable signal acquisition, high electrical conductivity is required and thin films over polymeric substrates could be used to enhance this characteristic in addition to bio-functionalization of electrode [15]. Also, the optical [16] or mechanical properties of biosensors could be modified for thin films [17]. The conductive polymers could be also used instead of thin films but since the thin films provide the reproducibility in long term and reduce the instability for detection, they are a significant alternative substance to be used in biosensor design [18]. Another requirement of thin films for biosensor applications is the miniaturisation of the sensing devices. With the latest technological enhancements, it is targeted to develop biosensors as micro- and nano-sized. Thereby, thin coatings could provide the expected feasibility and efficiency for these small size devices [19].

Since thin films can provide to achieve small scale devices [20] in addition to the advantage of the PVD technique to modify the film behaviour, various types of coating can be obtained [21]. Thereby, longer signal acquisition and more reliable measurements can be performed in addition to their low cost with these thin film-based biosensors without any requirement of skin preparation [22] in contrary to wet electrodes. Today, thin films are being used for various bio-potential electrodes such as electrocardiography, electromyography and electroencephalography [23]. Here, it is also important to consider the bio-adaptability, electrical conductivity and mechanical durability of these thin films regarding the final bio-applications.

When focusing in biological field, Titanium is a common material used for bio-applications since it is highly bio-compatible, whereas silver is a well-known anti-bacterial material. By combining their special properties, Ti-Ag PVD film were developed in a first aim to be used for bio-sensor applications. Regarding this aspect, their electrical and mechanical properties were studied and it was seen that increasing Ag content in the Ti-film provides enhanced fracture resistance thanks to the ductile character of the silver. Therefore, a longer and continuous signal acquisition can be provided for a sensor [24]. However, by considering the friction of a sensor against human body (joints and skin) or clothes, the wear behaviour of them is also quite significant to estimate their durability and service life. Even though pure titanium does not have high wear resistance, silver in nanoparticle form is known with its enhanced sliding behaviour [25] in addition to its anti-bacterial behaviour [23]. Therefore, it is expected that changing Ag content will provide a crucial effect on the tribological response of these films. However, previously the wear behaviour of these films was not investigated.

On the other hand, both Ti and Ag have a strong tendency to oxidisation. Thus, while investigating the friction and wear character of Ti-Ag films, it is necessary to consider the effect of contact environment.

It is known that during the early stages of the contact, the friction behaviour could be different than the steady state. Also, based on the effect of environment (e. g. humidity) the modifications on the tribological behaviour of these films can be investigated detailly in this stage. To examine the progress on the wear behaviour of Ti-based films at the early stage (run-in period) of the contact, *in situ* characterization is needed. Moreover, small scale investigation provides to deeply and comprehensively study the tribological responses of these films.

1.2. Objective

In this study, it is aimed to better understand the tribological behaviours of Ti-based thin films with the role of environment in small scale approach *in situ* conditions. Therefore, it was aimed to perform the tribological-tests with a novel approach in controlled environment. Firstly, it was needed to be assured that the designed concept for this specific purpose is qualified. The tests were performed with a laboratory made ball-on-disk micro-tribometer which is implementable into scanning electron microscope (SEM) chamber. First tests were performed with TiN hard coatings which were deposited with cathodic arc evaporation. After, it was aimed to investigate the functional properties of Ti-Ag films and the effect of Ag content on the film characteristics

for bio-sensor applications. Therefore, Ti-Ag films were deposited with magnetron sputtered PVD technique with varying Ag content. Finally, as another crucial purpose, the tribological behaviours of Ti-Ag films were targeted to examine. The effect on Ag content and the role of humidity were aimed to investigate *in situ* conditions in controlled environment. Hereby, the verified coupling of laboratory-made mini-tribometer with eSEM chamber was used to perform the tribo-tests on these films.

1.3 Outline

In this manuscript, the small scale tribological behaviour of Ti-based thin films were discussed with a small scale approach *in situ* conditions with the effect of the environment.

The first chapter as the *Introduction* expresses the background and the context of this research work. After that, it states all the objectives within the framework of this Ph.D. in addition to indicated its outline.

In the second chapter, the *State of the Art* is indicated. This chapter expresses the bio-sensors, details Ti-based PVD thin films and their properties in the literature in terms of their adhesion character, mechanical and electrical behaviours. Then, since this work is focused on friction and contact behaviour of Ti-based films, their tribological behaviour are discussed. Lastly a part dedicated to the role of environment on tribological behaviour of these films is taken a place in this chapter.

The third chapter was focused on *Materials and Methods*. In addition to the preparation of substrates and deposition process of the films, the used counter-faces (polymeric and steel balls) were explained. Furthermore, all the characterization techniques which were used for analysing microstructural, chemical, mechanical and electrical behaviours of TiN and Ti-Ag films were stated. Moreover, the laboratory-made micro-tribometer, the microscopes (SEM, TEM, optical microscope) were introduced. The special SEM which is operable in environmental mode as the tribometer implemented inside its chamber expressed detailly with its detectors. Then the complementary characterization methods were mentioned.

The main target of the fourth chapter is to introduce the *proof of the concept of the in situ small scale tribological study during run-in period in eSEM by using TiN films as the reference coatings.* Thus, in this chapter, the system to perform the tribological tests was validated. The procedure and the requirement of testing both *in situ* and *post mortem* conditions were explained

in addition to the confirmation of the fact that the developed tribo-microscope system allows to perform the tribological tests in different environments.

In fifth chapter, *Functional Characterization of Ti-Ag Magnetron Sputtered PVD films with the Preliminary Tribological Tests*. Their microstructure, morphology, density, chemical composition, mechanical and electrical properties were explained. Then the first tribological tests performed with the steel ball in high vacuum with the *post mortem* conditions were stated and the challenges based on the contact environment and film adhesion were detected. By considering the difficulties of the tribological analysis of these films, their adhesion performance was aimed to be enhanced and new series of films were deposited with and interlayer and statically analysed to be able to continue the *in situ* tribological tests.

The sixth chapter is dedicated to *Dynamic Tribological Analysis of Ti-Ag films in Small Scale*. In this part, it is firstly started with analysis of the microstructural, mechanical and electrical behaviours of these second set of Ti-Ag film series with interlayer. Then, *in situ* tribological tests were performed to examine firstly the effect of environment. Here, the tests were performed in various humidity levels in addition to the ambient air conditions. Finally, the effect of Ag content on the friction and wear character of these films against polymeric counter-part was examined and indicated detailly. Three different films with increasing Ag content were tested and their friction maps, wear behaviours, and mean coefficient of frictions were discussed.

Lastly, seventh chapter was taken a place as the *Conclusion* and chapter eight was dedicated to following *Perspectives* regarding this PhD.

References (Chapter 1)

[1] Jones, J. G., & Zhou, D. M. (1994). A first look at Biosensors. *Biotechnology Advances*, *12*(4), 693–701. https://doi.org/10.1016/0734-9750(94)90011-6

[2] Naresh, V., & Lee, N. (2021). A review on biosensors and recent development of nanostructured materials-enabled biosensors. *Sensors*, *21*(4), 1109. https://doi.org/10.3390/s21041109

[3] Heineman, W. R., & Jensen, W. B. (2006). Leland C. Clark Jr. (1918–2005). *Biosensors and Bioelectronics*, *21*(8), 1403–1404. https://doi.org/10.1016/j.bios.2005.12.005

[4] Updike, S. J., & Hicks, G. P. (1967). The enzyme electrode. *Nature*, *214*(5092), 986–988. https://doi.org/10.1038/214986a0

[5] Guilbault, G. G., & Tarp, M. (1974). A specific enzyme electrode for urea. *Analytica Chimica Acta*, *73*(2), 355–365. https://doi.org/10.1016/s0003-2670(01)85472-6

[6] Guilbault, G. G., & Lubrano, G. J. (1973). An enzyme electrode for the amperometric determination of glucose. *Analytica Chimica Acta*, *64*(3), 439–455. https://doi.org/10.1016/s0003-2670(01)82476-4

[7] Lübbers, D. W., & Opitz, N. (1975). A new probe for measurement of PCO2 or po2 in fluids and gases. *Zeitschrift Für Naturforschung C*, *30*(7-8), 532–533. https://doi.org/10.1515/znc-1975-7-819

[8] Clemens, A. H., Hough, D. L., & D'Orazio, P. A. (1982). Development of the biostator glucose clamping algorithm. *Clinical Chemistry*, *28*(9), 1899–1904. https://doi.org/10.1093/clinchem/28.9.1899

[9] Yoo, E.-H., & Lee, S.-Y. (2010). Glucose Biosensors: An overview of use in clinical practice. *Sensors*, *10*(5), 4558–4576. https://doi.org/10.3390/s100504558

[10] Schultz, J. S. (1982, August 17). Oxygen Sensor of Plasma Constituents.

[11] Liedberg, B., & Johansen, K. (1983). Affinity biosensing based on surface plasmon resonance detection. *Affinity Biosensors*, 31–54. https://doi.org/10.1385/0-89603-539-5:31

[12] Poncharal, P., Wang, Z. L., Ugarte, D., & de Heer, W. A. (1999). Electrostatic deflections and electromechanical resonances of carbon nanotubes. *Science*, *283*(5407), 1513–1516. https://doi.org/10.1126/science.283.5407.1513

[13] Gribi, S., du Bois de Dunilac, S., Ghezzi, D., & Lacour, S. P. (2018). A microfabricated nerve-on-a-chip platform for rapid assessment of neural conduction in explanted peripheral nerve fibers. *Nature Communications*, *9*(1). https://doi.org/10.1038/s41467-018-06895-7

[14] Lopes, C. J. R. (2018). *Development of Ti-based intermetallic thin films for enhanced biomedical sensing performance* (thesis).

[15] Tvarozek, V., Hianik, T., Novotny, I., Rehacek, V., Ziegler, W., Ivanic, R., & Andel, M. (1998). Thin films in biosensors. *Vacuum*, *50*(3-4), 251–262. https://doi.org/10.1016/s0042-207x(98)00050-5

[16] Qiu, G., Ng, S. P., & Wu, C.-M. L. (2018). Label-free surface plasmon resonance biosensing with titanium nitride thin film. *Biosensors and Bioelectronics*, *106*, 129–135. https://doi.org/10.1016/j.bios.2018.02.006

[17] Narayan, R. J. (2005). Nanostructured diamondlike carbon thin films for medical applications. *Materials Science and Engineering: C*, *25*(3), 405–416. https://doi.org/10.1016/j.msec.2005.01.026

[18] Dominik, M., Leśniewski, A., Janczuk, M., Niedziółka-Jönsson, J., Hołdyński, M., Wachnicki, Ł., Godlewski, M., Bock, W. J., & Śmietana, M. (2017). Titanium oxide thin films obtained with physical and chemical vapour deposition methods for optical biosensing purposes. *Biosensors and Bioelectronics*, *93*, 102–109. https://doi.org/10.1016/j.bios.2016.09.079

[19] Shul'ga, A. A., Strikha, V. I., Patskovsky, S. V., Dzydevich, S. V., El'skaya, A. V., Soldatkin, A. P., & Bubryak, O. A. (1992). Thin-film conductometric biosensors for glucose and urea determination. *Biosensors '92 Proceedings*, 81–88. https://doi.org/10.1016/b978-1-85617-161-8.50016-1

[20] Davis, F., & Higson, S. P. J. (2005). Structured thin films as functional components within biosensors. *Biosensors and Bioelectronics*, *21*(1), 1–20. https://doi.org/10.1016/j.bios.2004.10.001

[21] Baptista, A., Silva, F. J. G., Porteiro, J., Míguez, J. L., Pinto, G., & Fernandes, L. (2018). On the physical vapour deposition (PVD): Evolution of magnetron sputtering processes for industrial applications. *Procedia Manufacturing*, *17*, 746–757. https://doi.org/10.1016/j.promfg.2018.10.125

[22] Tvarozek, V., Hianik, T., Novotny, I., Rehacek, V., Ziegler, W., Ivanic, R., & Andel, M. (1998). Thin films in biosensors. *Vacuum*, *50*(3-4), 251–262. https://doi.org/10.1016/s0042-207x(98)00050-5

[23] Lopes, C. J. R. (2018). *Development of Ti-based intermetallic thin films for enhanced biomedical sensing performance* (thesis).

[24] Etiemble, A., Lopes, C., Nkou Bouala, G. I., Borges, J., Malchère, A., Langlois, C., Vaz, F., & Steyer, P. (2019). Fracture resistance of ti-ag thin films deposited on polymeric substrates for biosignal acquisition applications. *Surface and Coatings Technology*, *358*, 646–653. https://doi.org/10.1016/j.surfcoat.2018.11.078

[25] Wang, Q., Tu, J., Zhang, S., Lai, D., Peng, S., & Gu, B. (2006). Effect of AG content on microstructure and tribological performance of WS2–Ag Composite Films. *Surface and Coatings Technology*, *201*(3-4), 1666–1670. https://doi.org/10.1016/j.surfcoat.2006.02.039

2. STATE OF ART

The previous studies were reviwed about the preference of thin films for biosensors. The importance of Ti-based thin films was emphasized for these applications and the properties of Ti-based PVD films were indicated.

Scientific background was explained for tribological analysis in addition to the significance of the *in situ* small scale investigations. Finally, the role of environment on tribological behaviour of these films were asserted in the state of the art chapter.

2. STATE OF ART

Objective of the PhD is to contribute to a better understanding of the tribological behaviour of thin Ti-based films, adopting a small-scale *in situ* approach. A special emphasis will be put on the early stages of degradation on the one hand, on the effect of the atmosphere of the contact on the other hand. Therefore, this part devoted to the state of the art is structured into three parts concerning, as illustrated in Figure 2.1:

- 1: the thin film,
- 2: the tribological analysis of the surface,
- 3: the influence of the environment.

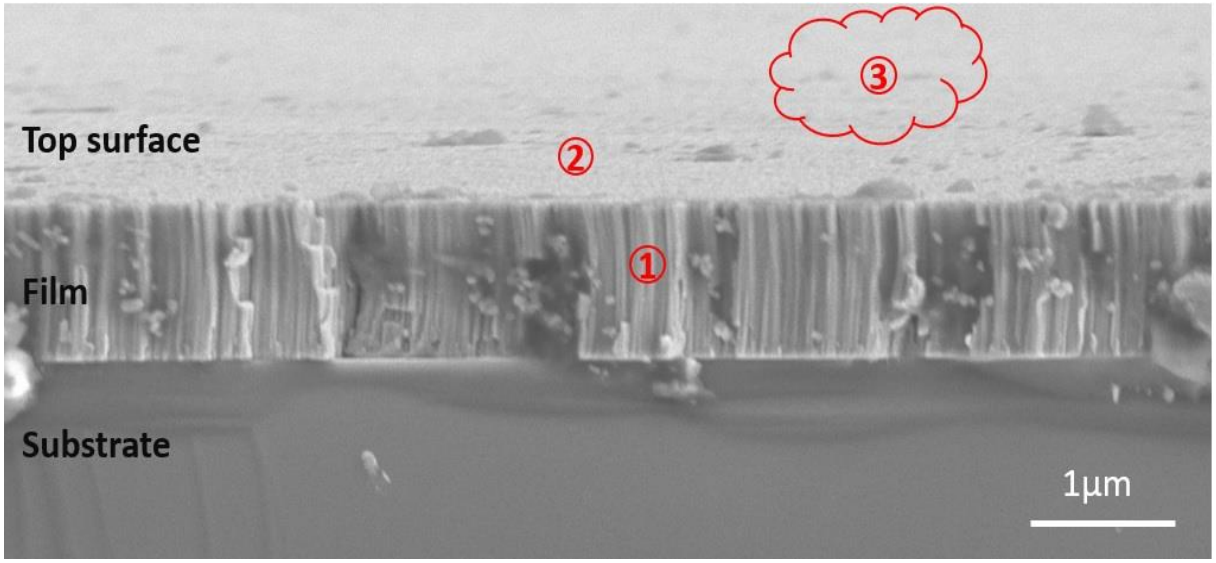

Figure 2.1: Schema of the film-substrate system pointing out 1) the film-substrate interface, 2) the film itself, and 3) the film-environment interface

2.1. Thin films

2.1.1. Towards vacuum-deposited films

For a long time, surface modification has been an efficient strategy to improve characteristics of the functional parts. Painting, plating, electrochemical (electroless or electro-deposition) were conventional processes leading to coated surfaces [1-3]. A new generation of coatings was proposed in the 80's with the development of physical vapor deposition techniques, which

drastically opened new perspectives. Besides, a key-advantage was the control of the deposition atmosphere (reactive or not), together with its environmental-friendly character [4].

The first emblematic film produced by such out-of-equilibrium processes was TiN, extensively studied for its outstanding tribological properties [5-8]. Since then, thin films (TFs) are covering various kinds of materials in the industry. Because of their specific thermal, mechanical, chemical and physical properties, they guaranty and extend the service life of materials while adding functional properties. In bio-environments, a controlled electrical conductivity allows TFs to be used as the part of biosensors [9,10]. For prosthesis, they improve fatigue life and wear resistance [11,12]. TFs are also used to cover machining parts, bearings, cutting tools [11]. Because of their low thickness, they are also suitable in small scale engineering applications such as MEMs and NEMs. They are also found in optical applications like OLEDs [10,12,13,14,15] or decorative purposes [20]. TF deposition methods are multiple; however, two techniques stand out: the physical vapour deposition (PVD) and the chemical vapour deposition (CVD) [16]. For both processes, the specific film properties are designed by the deposition parameters. As an example, Table 2.1 gives a non-exhaustive overview of the functionalities which can be changed through a modification of the surface.

Table 2.1: Relation between the thin film properties and the elaboration parameters

Property	**Parameter to modify the property**
Adhesion	Deposition current and voltage [17], deposition time [18], alloying elements [19,20], heat treatment [21], multilayer deposition [18,22,23,24]
Interfacial stress	Deposition current, voltage and pressure [35], alloying elements, film thickness, thermal expansion coefficient [25,26], multilayer deposition [26]
Fracture fatigue behaviour	Film thickness [27], film morphology and defects [28], alloying elements [11,12,13,17]
Hardness Young's modulus	Deposition voltage [30], alloying elements [31], film morphology [32,33], multi-layer deposition [34]

Electrical optical properties	Deposition voltage, current and pressure [35,36], deposition time [35], alloying elements [10,12], heat treatment [12,37], film morphology [35]
Wettability	Glancing angle deposition [38,39], alloying elements [40], surface treatment [38,41,42], heat treatment [42]
Roughness	Deposition voltage [43], glancing angle deposition [44], film thickness [43], alloying elements [45], surface treatments [43, 46, 47, 48]
Oxidation corrosion behaviour	Alloying elements [49,50], heat treatment, testing environment [51]
Wear behaviour	Film thickness [52,53], alloying elements [54-59], surface treatments [57], heat treatment [60], testing environment [27]

A modified surface constitutes in fact a system, where three critical regions can be distinguished:

(1) The film-substrate interface (internal surface): At this point, the adhesion properties and the interfacial stresses [18,22,23,61,62] are considered since they are at the origin of delamination, bending or crack initiation of film in service [63].

(2) Film itself: The film bulk properties are driving the fatigue and fracture behaviours, hardness, Young's modulus, electrical and optical properties [10,12, 13, 14, 15, 44, 64, 65]

(3) The film-environment interface (external surface): Controls the wettability [40], roughness [66], oxidation, corrosion [65,66] and wear behaviour in addition to the biocompatibility [68,69].

2.1.2. Ti-based films for Biosensors

In this project, it was focused on titanium and Ti-based films. The main reason was the fact that titanium and its alloys are well known materials to fulfil many specific requirements regarding

their physical mechanical and chemical properties. The bio-adaptable nature of titanium [33] in addition to its superior mechanical [31,64], and electrical properties put it forward rather than many other materials [13] in biomedical applications [12] in addition to their use in many other fields such as aerospace applications [68], bearings [11] and also the small scale engineering devices [12].

Bio-medical field (biosensors and bio-prosthesis) is one of the most important application of Ti-based TFs. Recently, Ti-based films found new perspectives in the field of biosensors. Sensors could be defined as a module or a device which provides detection of physical quantities by converting them into signal to monitor and analyse. Biosensors converts specifically the biological response to electrical signals with an integrated receptor-transducer system [70]. A transducer converts the energy from one to another form while the receptor gathers the data [71]. They can be classified according to their transducer types (electrochemical, optical, thermal, piezoelectric…) or to their bio-recognition types as enzymatic, anti-body, nucleic acid and whole-cell based sensors [72]. An optimal biosensor should provide reliability, repeatability, sensitivity, selectivity, linearity and rapid response [70]. Using thin films in biosensor applications (Figure 2.2) actually provides to avoid from skin preparation as the main difference than the wet electrodes in addition to the high reliability of the measurements [73].

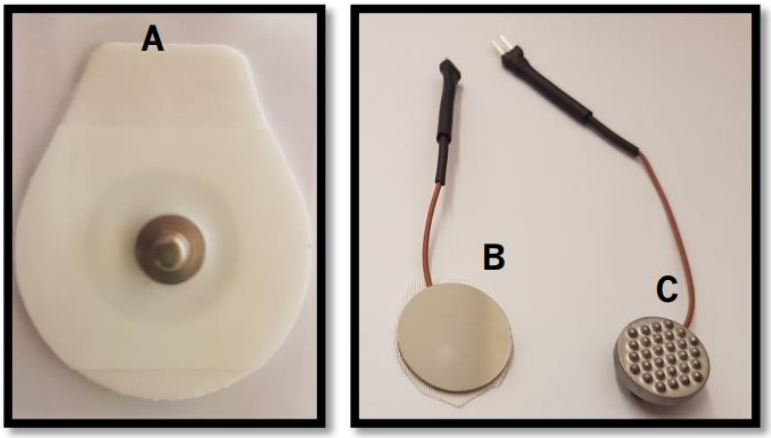

Figure 2.2: Electrodes as Ag/AgCl a) wet-based, and dry Ti-based metallic film deposited on b) steel and c) polyurethane substrates [73]

The first known use of thin film for biosensors was in 1989 by Koudelka et *al.* [74] under *in vivo* conditions on a silicon substrate, yet the sensing tools are ion-sensitive, instability

problems occurred. Since then, there have been many developments and in the previous studies, various types of thin films have been used to enhance the performances of biosensors. For example, Pu et *al.* [75] used graphene for this purpose, since it is the most well-known solid lubricant which provides a low friction and wear rate in addition to its superior mechanical and electrical character. Similarly, Narayan [76] studied on the use of diamond-like-carbon (DLC) film for the biosensors applications to optimise the fatigue, corrosion, and wear behaviour of these devices. Also, polymer thin films by embedding metallic nano-particles were developed for this purpose [77]. However, the use of metallic films is also very common for biosensors. For instance, Jonsson et *al*. [70] used gold for a surface plasmon resonance biosensor and it was examined that the thickness of the gold layer has an effect on the signals obtained. Furthermore, Shul'ga et *al.* [78] used gold, chromium, copper and nickel thin films on conductometric transducers of biosensor to detect glucose and urea.

First use of titanium as thin film for biosensor applications was performed by Urban et *al*. in 1990. Here, the Ti-film (50 nm) was preferred to use as the adhesion layer below platinum film (60 nm) for the electrode of the sensor to detect glucose and they obtained high reproducibility and stability [74]. Also, Qui et *al.* [79] deposited TiN film with 29.8 nm thickness to functionalise the sensor efficiently against biotin. TiN is a fantastic alternative material to the fold-based surface plasmon resonance (SPR) bio-sensors and its optical properties could be modified by changing deposition conditions and sizes of microstructure. In another study, Dominik et *al.* [80] worked on titanium oxide films for optical biosensing purposes and it was seen that any change on the TiO_x character affects the biofunctionalization and if it is going to be used as an optical based sensor, film composition modifies the refractive index and so the detection performance of the sensor. As another example, Gordin et *al.* [81] preferred to use commercially pure titanium and Ti-6Al-4V alloy with nitrogen addition to investigate their mechanical properties and biocompatibility. In this study, it was stated that, titanium has high strength, good corrosion resistance and biocompatibility; however, its friction and wear resistance is not sufficient, so the nitrogen addition was performed during the film deposition process. Also, Lopes [73] deposited Ti-based films in four different alloy form (Ti-Ag, Ti-Au, Ti-Cu and Ti-Al) to be used for biosensor applications and examined their electrical and mechanical properties. For that purpose, ductile metals were selected to provide the bio-potential character in addition to the choice of polymeric substrate to provide flexibility (Figure 2.3). It was seen that these Ti-based dry electrodes can provide more reliability and avoiding

from any allergic skin reactions by comparison to the conventional Ag/AgCl wet electrodes. Starting from pure Ti, effect of increasing alloying element content in the composition were also tested. Especially, Ti-Au and Ti-Cu films were exhibited outstanding signal acquisition for in vivo bio-sensing tests.

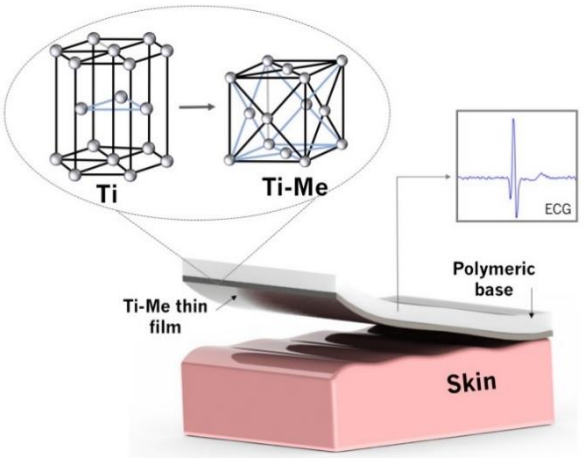

Figure 2.3: Ti-based bio-sensors with polymeric substrate on skin contact [73]

However, friction is a significant parameter for durability and efficiency of thin films [82]. Any surface may face up with tribological issues and tribology has a crucial role for the biological fields. Many body parts are exposing to a relative cyclic motion such as, blinking the eye-lids or a foetus moving in mothers' uterus. Another most well-known body parts which exposes to cyclic motion are joints. Regarding to this, in 2018, Etiemble et *al.* [83] deposited Ti-Ag films for biosensor applications to be used for hip joints and investigated their fracture resistance and electrical properties. It was seen that increasing Ag content in the film composition provided higher durability with longer signal acquisition (Figure 2.4). However, their friction and wear behaviour were not investigated in their study. Therefore, in this study it was aimed to characterize the tribological behaviour of Ti-based thin films in small scale *in situ* conditions.

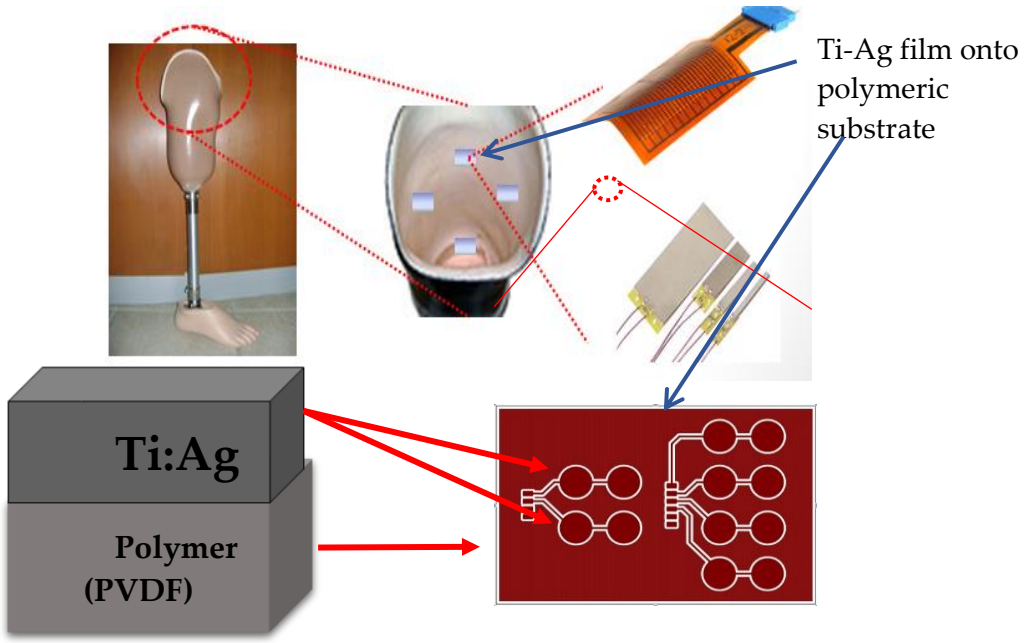

Figure 2.4: Ti-Ag films on polymeric substrate of a bio-sensor for hip-joint-prosthesis

Regarding this aspect, by considering the structure mentioned above, corresponding film properties and their modifications for Ti-based films were discussed in this chapter. During this research, the adhesion properties of the films were needed to be enhanced as one of the aspects which is a required characteristic to be considered for the film-substrate interface. Therefore, a detailed background research about the adhesion character of Ti-based films were expressed. Furthermore, the mechanical and electrical properties of film-itself were needed to be investigated for bio-material applications since the electrical signal acquisition is the key parameter for bio-sensors and mechanical properties are significant for joint-prosthesis. Finally, for the film-environment interface, the tribological behaviour of Ti-based PVD coatings were reviewed from previous works and explained detailly since the tribological analysis of Ti-based films is the main objective of this project. Even though there are several researches for the tribological behaviour of TiN films in various conditions, there is not much study about Ti-Ag films. Yet, several researches indicated below about the wear behaviour of Ti-based PVD films used to be enlightened for the current project.

2.1.2.1. Adhesion Behavior

A strong film adhesion for titanium and titanium-based coatings is critical for the service life of the final product. In previous studies it has been seen that deposition parameters [17], film thickness [18], surface treatments [84, 85], alloying elements addition [23] and multi-layer deposition of the films are the common techniques to enhance the adhesion [86]. Additionally, various sputtering techniques such as radio frequency or direct current physical vapour deposition may provide different adhesion character [22]. For example, Kondo et *al.* [85] investigated the effect of surface pre-treatments for DC magnetron sputtered titanium coatings and tested their adhesion performances with pull-out method to estimate the peeling susceptibility. To analyse the effect of surface pre-treatment, Ar ion bombardment and chemical etching with buffered HF were applied. It has been observed that chemical treatment is more efficient than Ar bombardment to enhance adhesion with respect to the interface evaluations after pulling-out with the epoxy. The main cause of decrease in adhesion of films for Ar bombarded samples has been based on the high concentration of Ar at the interface between Si substrate and the titanium film. Additionally, Lugscheider et *al.* [87] have done another research to investigate the effect of deposition method on adhesion for TiN films. The coatings have been deposited both with magnetron sputtered and cathodic arc PVD methods. Tape has been placed onto the samples and then pulled out to analyse the delamination and spalling of the deposits and better adhesion performance has been observed for the magnetron sputtering films than cathodic arc plated ones. Moreover, the adhesion performances of RF magnetron sputtered Ti, TiN and Au films, were considered by Kim et *al.* [22]. The scotch has been applied onto surfaces and then pulled with an accelerating force. No delamination for Ti-based coatings was obtained whereas the Au films were completely removed.

Additionally, the effect of deposition parameters, single- and double-layer film structures and film composition on adhesion behaviours of the films have been investigated in previous studies. For instance, TiAlN PVD films could be used in aggressive machining parts such as cutting tools; therefore, their tool life is quite important. Better adhesion properties enhance the tool life of these films. For example, Harris et *al.* [24] deposited TiN/TiAlN duplex coatings in order to compare their performances with TiAlN single layer ones. After the Daimler-Benz test, it has been proved that TiN/TiAlN double layer film performs better adhesion character and thereby, the tool life for this type of films is 20% longer than the single layer TiAlN coatings.

2.1.2.2. Mechanical Properties

Hardness and Young's modulus (H and E respectively) parameters have critical importance regarding TF applications such as dental implants, body prosthesis [32], tribune engines [34], microelectronic devices [88] or antimicrobial applications [89]. The microstructure, composition [33], and homogeneity of the film are the significant parameters to modify the hardness and Young's modulus values of materials [32]. To analyse the hardness and elastic modulus of TFs, mostly the values were drawn from the bulk materials; however, it is possible to deposit the films in plenty of composition which does not exist in bulk form via physical vapor deposition. Thus, it is not possible to assume the same values for bulk materials and their films in alloy form [90]. On the other hand, there is a strong influence of the substrate on the hardness and elastic modulus response of coatings because the films are mostly not enough thick to control the contact response [91]. The system response is similar to the contact modulus: for higher indentation loads the substrate response is more effective; while for lower applied loads, the coating response comes forward. Thus, small-scale indentation (nano-indentation) with a Berkovich indenter is the recommended method to estimate the hardness and contact modulus of thin films [92]. Vickers hardness test could also be applied for hardness measurements yet, the indentation depth has to be $1/10^{th}$ of the coating thickness [93].

It is known that the toughness and the wear behaviour of thin films could be correlated with their mechanical properties. Film toughness could be estimated with the H/E* ratio where E* is the reduced modulus [94] ($E^*=E/(1-\upsilon)$, while υ being the Poisson's ratio [95]). Also, resilience helps to estimate the friction resistance of a film. It can be described as the resistance against the plastic deformation and it is correlated with H^3/E^{*2} [94].

Mechanical properties of TFs could be investigated and enhanced through several methods. One of the main factors for this purpose is modification on the grain size of coatings. To provide the grain size refinement, diverse alloying elements could be incorporated into film during deposition such as carbon [88], silicon [30], silver [89], copper to increase the hardness [96]. Moreover, adding alloying elements provides the solid solution hardening and causes an energy barrier to block the dislocation movements out of the distorted lattice to enhance the mechanical properties [30]. By changing the concentration of incorporated elements in the film, the hardness and modulus could be increased with nanocomposite formation up to a critical enrichment [97]. In another study Etiemble et *al.* [11] investigated the effect of Ag content into

the Ti-film on fracture resistance of the film. It was seen that the crack propagation develops in a different way with increasing stain rate for Ti-rich (Ag/Ti=0.08) and Ag rich (Ag/Ti=2.14) films (Figure 2.5). Increasing Ag content in the Ti-Ag film provided to reduce the crack density and formation of the continuous cracks on the polymeric substrate. Therefore, it could be stated that proper alloying element may enhance the mechanical properties of Ti-based films. Depositing the coatings in multilayer form and changing the film thickness also aid to achieve the expected film hardness and elastic modulus values [33,34,97].

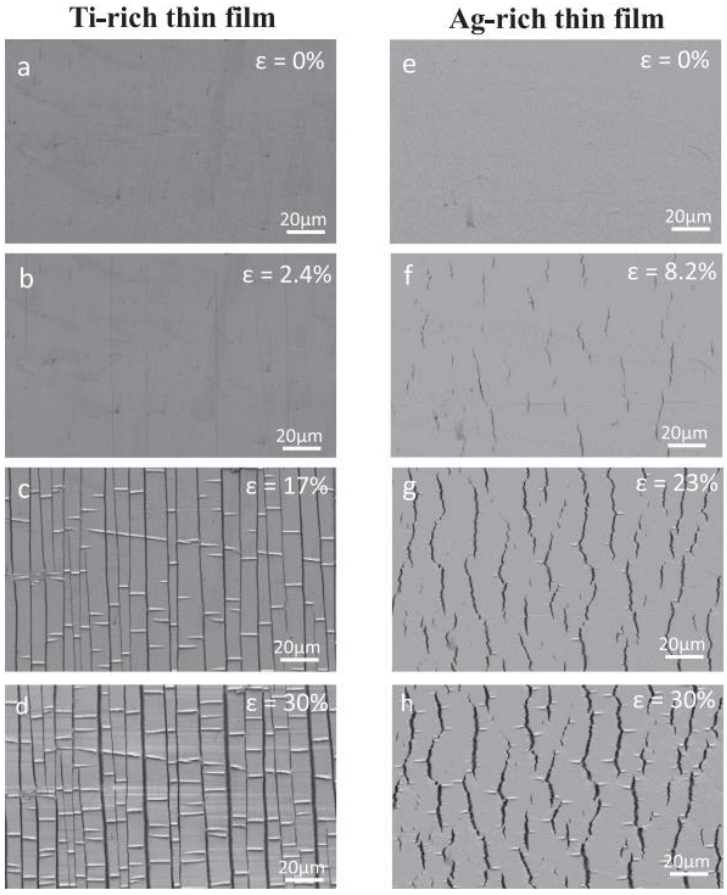

Figure 2.5: *In situ* tensile test of Ti rich ang Ag rich Ti-Ag films with different stain rates [11]

Titanium-based films are commonly used for various applications where high hardness and elastic modulus are required. For example, Zhou et *al.* [34] preferred to use Ti/TiN multilayer coating for the compressor blades of the engines for gas tribunes thanks to its high hardness. Also, Andrade et *al.* [98] have reported that with copper addition, the mechanical properties of titanium coatings could be enhanced. In another study, Wojcienszak et *al.* [32] suggested to use Ti-Cu coating which has higher hardness than pure titanium, thus it provides greater grindability

for dental implants. As an example of another Ti-based metallic films, Ewald et *al.* [45] analysed Ti-Ag films in terms of their mechanical behaviours; however, it was expressed that increasing silver content may not really enhanced the mechanical properties of these films and they are still comparable with pure titanium film. Additionally, Lopes [73] investigated the role of increasing alloying element on the mechanical properties of Ti-based metallic films. It was first seen that there is a Ti-based solid solution forms, then, with the increase of alloying elements intermetallic compounds were formed. Further increase on alloying elements caused the formation of the solid solution with corresponding alloying element matrix. These changes caused the modifications on the mechanical properties of the films. It was seen that with increasing Al and Ag content, the mechanical properties were enhanced in the intermetallic zone however with further increase of these elements in the film, hardness and Young's modulus were decreased (Figure 2.6). On the other hand, for Au and Cu, the films behaved a different character in terms of their mechanical susceptibility. On the contrary of Ti-Ag and Ti-Al films, firstly hardness and Young's modulus decreased with increasing Au and Cu content in the intermetallic zone and then either stabilised or increased with further increase of these alloying elements (Figure 2.7). Here, it can be noted that the type and the content of the alloying elements in the final composition of Ti-based film can vary the hardness and Young's modulus. The variations on the mechanical properties of the films were associated the modification on film microstructure. Here, with increasing alloying element content, the reduction on the grain size played a role on the modification of the hardness and elastic modulus values as well as the ductility of the four different alloying metals.

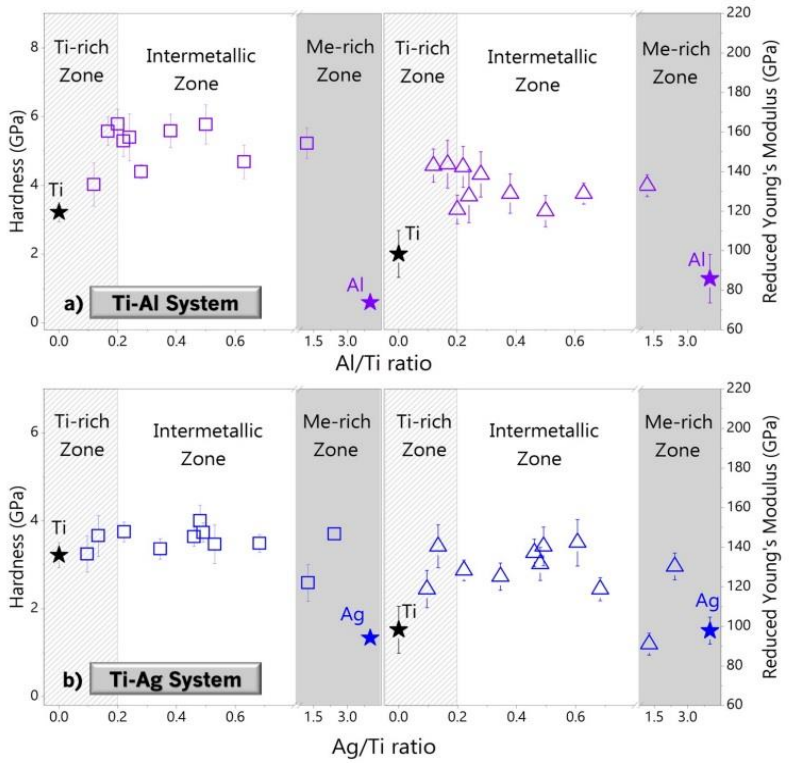

Figure 2.6: Mechanical properties of a) Ti-Al and b) Ti-Ag films with increasing alloying element content [73]

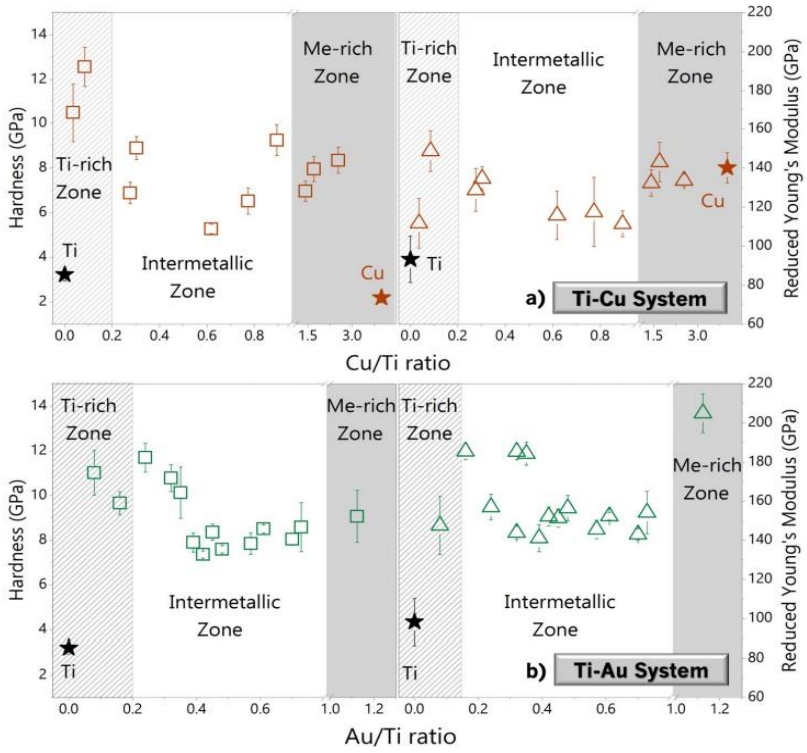

Figure 2.7: Mechanical properties of a) Ti-Cu and b) Ti-Au films with increasing alloying element content [73]

Conventionally, a way opened by PVD processes to harden surfaces relies on their ability to change a metal into a ceramic. In that area, transition metal nitrides, and specially titanium nitride, are one of the most important system. Incorporating the film with different elements may cause nanocomposite formation with improved mechanical properties [31]. Saladukhin et *al.* [30] stated that for transition metal nitride coatings, ternary films have mostly higher hardness than their parent binary systems. For example, (TiAl)N coatings are still harder than TiN films which were deposited in same conditions [99]. Similarly, (Ti,Zr)N film provides energy barrier against the dislocation movements in lattice regarding the solid solution strengthening and so it has higher hardness than TiN films. In another research, Chang et *al.* [97] investigated the effect of Al concentration on mechanical properties of magnetron sputtered $Ti_{1-x}Al_xN$ PVD film. It has been observed that the highest hardness and elastic modulus values were obtained for Al/(Al+Ti) =0.19 but when this ratio was reached 0.57, the decrease of hardness was seen due to the loss of the cubic structure.

To conclude, mechanical properties of titanium-based films could be controlled by several strategies. Grain refinement and solid solution strengthening are two of the major mechanisms to increase the hardness and elastic modulus which could be provided by incorporating various additive elements (N, Si, C, Zr, Al, Ag, Cu) into titanium films. Additionally, changing the coating's architecture at a nanometer scale (multi-layered design or nanocomposite structure) is also an alternative to reach high level mechanical values.

2.1.2.3 Electrical Properties

Electrical responses of thin films also have a great importance by considering their applications. Especially for future biosensor applications, TFs were aimed to be used for biosensor applications but also, they could be used in flexible electronic circuits [100], electro-physiological monitoring [13], heat mirrors [14], semiconductor industry [15], interconnects and electrode materials [10]. Thus, to tailor the electrical properties of these films, it is necessary to consider different factors such as their chemical composition, microstructure [35], film thickness [15], impurities [36], and the deposition parameters of these thin coatings [101].

Firstly, low resistivity is essential for electrodes and interconnects, and this could be achieved by adding different alloying elements during deposition. For example, silver is the metal which has the lowest resistivity. Thus, by incorporating the film with silver and changing the silver content into the film, it is possible to enhance the electrical response [10]. Also, microstructure

has a critical role on electrical character of the coating. Regarding the electron scattering at grain boundaries, lattice defects [101], film architecture [35] and impurities, the resistivity of the film could be differed [36]. Increasing film thickness may also cause film densification and the film may achieve the resistivity values almost as much as the bulk material of the same composition [15]. Additionally, the concentration of carriers and film conductivity increases with thickness for the metallic films [37]. Moreover, in terms of deposition parameters; bias voltage, Argon flow rate and partial pressures of deposition gases [36] are effective on the final electrical response of the film. Another important concern for the resistivity is the annealing process after deposition, which may enhance the electrical behaviour by modifying the film crystallinity [10,37]. Resistivity measurements are mostly done by four-point-probe technique (Figure 2.8) and when considering the resistivity value, it is necessary to be taken into account all the influential parameters (Matthiessen's rule) (Eq. 1).

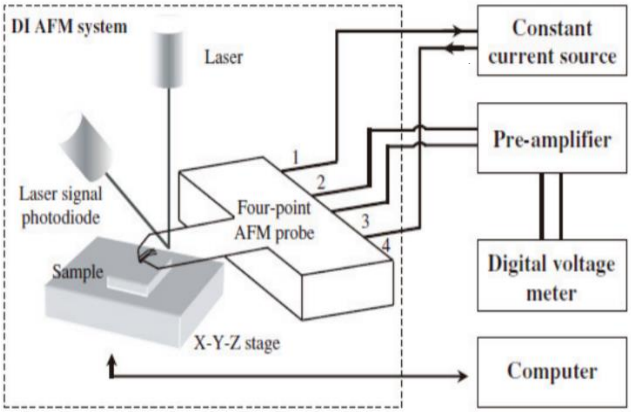

Figure 2.8: Schema of four-point atomic force microscope probe [102]

$$\rho = \rho_a + \rho_i + \rho_g + \rho_s \text{ (Eq. 1)}$$

Where, ρ_a is the bulk resistivity, ρ_i, ρ_g, ρ_s are resistivities from impurities, grain boundaries and roughness respectively [103].

Titanium-based TFs are quite appropriate materials for electrical applications such as flexible electronic circuits, bio-sensors [9] and health monitoring electrodes (e.g. electrocardiogram (ECG), electromyography (EMG) and electroencephalogram (EEG) (Figure 2.9)) regarding their high conductivity [13].

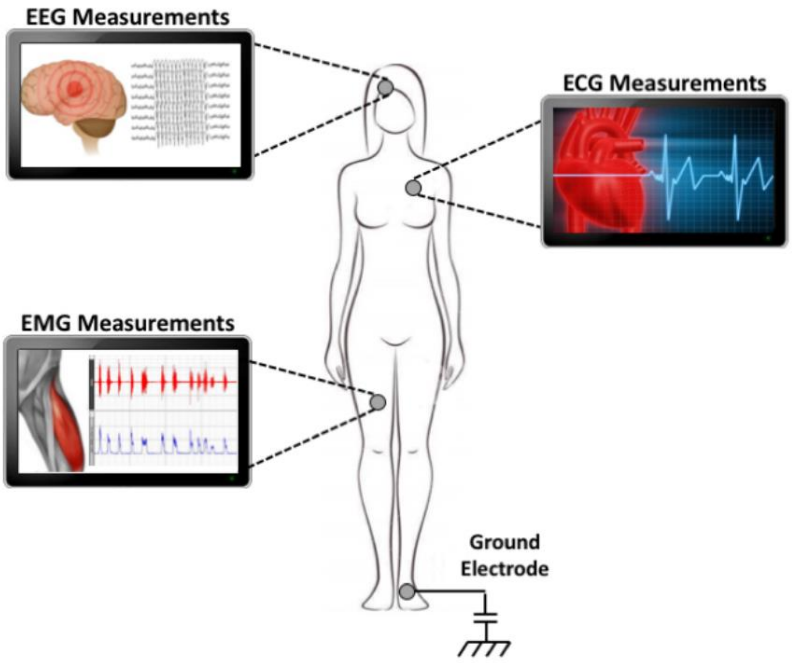

Figure 2.9: Bio-potential sensors placed on human body [73]

To study the effect of thickness on the resistivity of Ti-based TFs, Savaloni et *al.* [37] deposited TiO_2 films via PVD and with varying thicknesses. It has been examined that, carrier concentration and the film conductivity has been improved and the resistivity has been decreased for increasing thicknesses regarding the densification of the film microstructure and decrease of voids and valleys as it was seen by AFM investigations.

Additionally, Etiemble et *al.* [11] stated that electrically conductive materials (e.g. Ag, Au, Cu) are efficient for the films to be used for flexible electronic circuits; however, they have adhesion problem and high ductility. Thus, depositing these metals with titanium in an alloy form enhances the adhesion behaviour and the brittle character of the films. It has been observed that, with increasing silver content into titanium film, firstly the resistivity increased due to the formation of intermetallic phases (TiAg and Ti_2Ag) but then with the further increase of Ag, the electrical response has been increased due to low resistivity of silver for the Ag-richer zones. Another reason for the improvement of the electrical response is the enhanced fracture character due to the increasing film ductility with increasing Ag content which was examined by *in situ* tensile test. Regarding the high Ag content, the generated cracks have been short and discontinuous as it was shown in Figure 2.6; thereby, the electrical pathway was preserved and the signal acquisition was not interrupted all along the film.

In order to investigate the effect of the microstructural architecture of the films, Lopes et *al.* [35] have deposited Ti-Ag films via glancing angle physical vapour deposition technique in oblique, helical and zig-zag patterned microstructures (Figure 2.10). It was seen that, increasing the incident angle of deposition causes an increase in the obliqueness of the deposited columns. Thus, a more porous film micro-structure is obtained and it was concluded with higher resistivity for the films deposited in oblique form. However, helical-tailored Ti-Ag TFs have a more compact character than oblique and zig-zag micro-structured films and they have lower resistivity. Nevertheless, the highest conductivity has been exhibited for the films deposited with zero incident angle owing to quite densified microstructure and higher concentration of charge carriers. Thus, it could be stated that microstructural architecture of the films has a critical role on film resistivity.

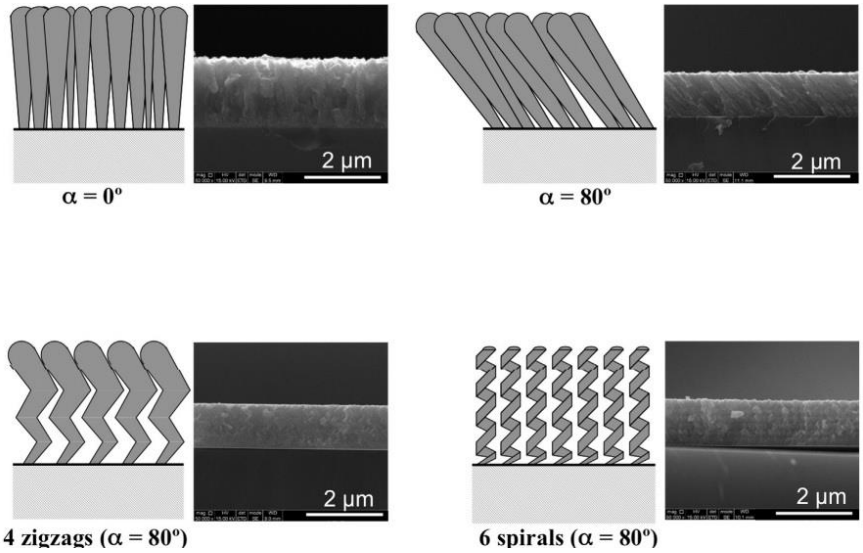

Figure 2.10: Examples of microstructure geometries of thin films deposited with glancing angle deposition [35]

The influence of deposition parameters such as flow rates of deposition gases, bias voltage, and substrate temperature has to be considered on electrical response of PVD Ti-based thin films. Arshi et *al.* [101] investigated the influence of Ar flow rate on the resistivity of TiN films. With increasing Ar flow from 5 sccm (standard cubic centimetre per minute) to 10-15 sccm the crystal structure of the film modified to a mixed-orientation {(1 1 1)-(2 0 0)} but with the further increase, a preferred orientation (1 1 1) has been obtained which causes higher resistivity because of the scattering of conduction electrons in vacancies of TiN film. In another research, Arshi et *al.* [36] also analysed the effect of nitrogen flow rate for TiN PVD films. It has been determined that from 0 to 3 sccm (standard cubic centimetres per minute) of nitrogen flow rate,

the resistivity varies with the phase transformation; however, for further increase up to 9 sccm, the resistivity of the film changes again because of the scattering of conduction electrons at grain boundaries. To examine the effect of bias voltage, Xi et *al.* [104] deposited TiN films with different bias from 0 to -150 V in their research. It has been asserted that for the films deposited with bias between 0 and -30V, the surface was smoother but when it changed to -60V, the film roughness and resistivity increased. However, for the films deposited with -150V bias, the resistivity decreased with decreasing roughness. So, it could be stated that with increasing bias voltage the roughness of the film differs which causes a change in the electrical performance of the film. Another critical point for the electrical response of Ti-based TFs is the substrate temperature. Savaloni et *al.* [31] expressed that resistivity of the TiO_2 film decreases with increasing temperature of substrate during deposition owing to the rise of diffusion of TiO_2 particles on the surface of the substrate with higher mobility.

Annealing as post treatment process after film deposition could also vary the electrical response of Ti-based films. For example, Kawamura et *al.* [10] stated that for Ti-Ag single layer, and also Ti/Ag and Ti/Ag/Ti multilayer films, the resistivity has been decreased with annealing (at 500°C) compared to as-deposited samples. The film crystallinity has been increased, the roughness of the film has been reduced and Ag grain size has been enlarged with heat treatment; therefore, the electrical response of the film has been improved.

To sum up, Ti-based PVD thin films are the efficient materials to be used in bio-medical applications regarding their electrical and mechanical properties in addition to ability to change film nature by tuning the deposition parameters, adding alloying elements or applying various post-treatments. In this Ph.D., the characteristics of film-substrate system were reviewed in terms of the properties of film-itself, their tribological behaviours and the tuning of their tribological susceptibility by changing environmental conditions. However, their mechanical, electrical and microstructural features in addition to their adhesion character can be enhanced with several processes such as alloying element addition, multi-layer deposition, surface treatments or modification on the deposition parameters.

2.2 Tribological Behavior

In most of the industrial fields such as bio-medicine, nuclear power, aerospace, railways and the machining tools, bearings, or in systems expose to sliding motion, the wear resistance has a great importance since the surfaces of these materials have to be subjected to friction [68, 69].

Similarly, for bio-prosthesis and bio-sensors, the wear resistance has a great importance for their service life [105, 106].

2.2.1 Tribometry systems and quantitative analysis

The friction and wear behaviours of materials can be estimated by tribometers. Tribometers can be classified in two main groups regarding the motion of their tip-heads which are rotational and reciprocating tribometers (Figure 2.11) [107, 108]. It has to be noted that, there are many parameters of tribometry system which have an important role to determine the wear resistance of TFs such as type of the contact, contact geometry, load, sliding speed, stress, surface conditions and testing environment [51]. Moreover, the wear performance of the TFs can be modified as the other film parameters by changing the film thickness [52, 53], adding alloying elements [54-59] into the film, and applying heat treatment [58, 60, 109]. These processes could provide solid lubrication [110], enhanced adhesion, changes on the crystal structure of the films and so the wear behaviour could be tailored [57].

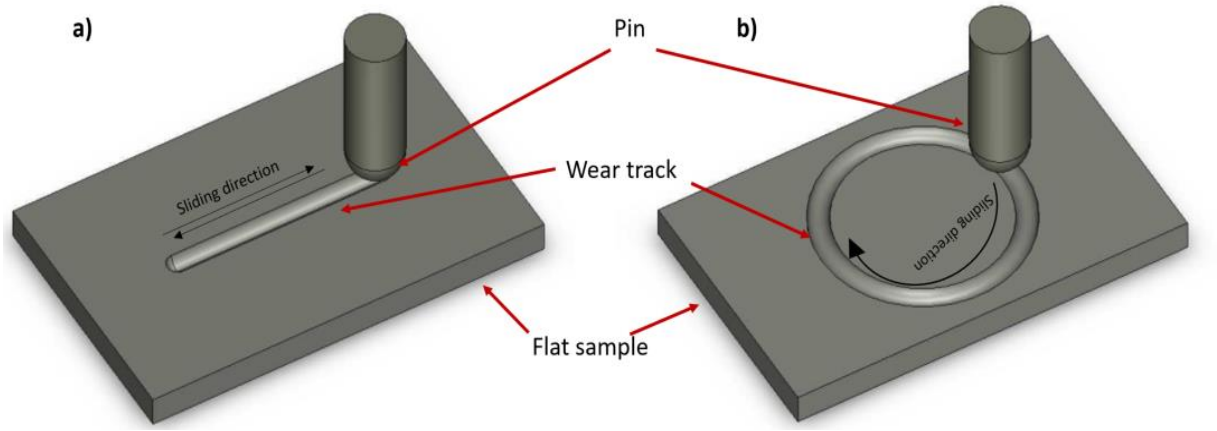

Figure 2.11: Tribometers due to sliding mechanisms as a) reciprocating, b) rotating [108]

To analyse the wear behaviour of thin films, tribometers or scratch testing systems could be used. The tribometer system could be provide ball on disk or pin on disk contact with an applied normal load, so the Hertzian contact pressure is obtained (Figure 2.12).

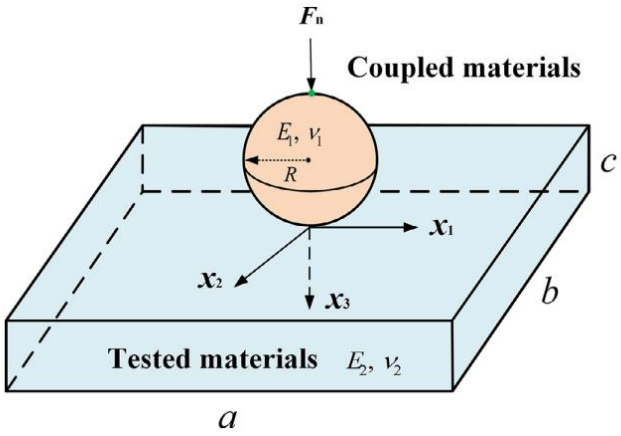

Figure 2.12: Hertzian contact of a ball-on-disk system [111]

Hertzian law is based on calculating the maximum and minimum of the contact pressure based of material properties in contact as well as the applied normal load. In this case it is necessary to calculate the contact radius (Eq. 2) Here a is the contact radius where F_N is the normal load, R is the radius of ball in contact, and E_r is the reduced Young's modulus.

$$a = \left(\frac{3F_N R}{4E_r}\right)^{1/3} \text{ (Eq. 2)}$$

Here the reduced Young's modulus can be defined as a parameter which is related with the Young's' modulus of two materials in contact (E_1 and E_2) and their Poisson's ratios (υ_1 and υ_2) (Eq. 3).

$$E_r = \left(\frac{1-\upsilon_1^2}{E_1} + \frac{1-\upsilon_2^2}{E_2}\right)^{-1} \text{ (Eq. 3)}$$

Here the contact area can be defined as:

$$A = \pi a^2 = \pi\left(\frac{3F_n R}{4E_r}\right)^{2/3} \text{ (Eq. 4)}$$

Therefore, finally the maximum (P_{max}) and the mean (P_{mean}) Hertzian contact pressures were calculated as it was shown in Eq. 5 and Eq. 6

$$P_{max} = \frac{3F_N}{2\pi a^2} \text{ (Eq. 5)}$$

$$P_{mean} = \frac{2}{3} P_{max} \text{ (Eq. 6) [123]}$$

Friction force (F_f) could be defined with Coulomb's law in dry friction conditions which is proportional with the normal load (F_N) and the friction coefficient (f) (Eq. 7).

$F_f = fF_N$ (Eq. 7) [112]

Wear volume could be calculated after a 3D interferometer analysis of the wear track. For the flat surfaces tested with reciprocating tribometer the wear volume could be expressed as below. (Eq. 8) The possible shape and 3D profile of the wear track is indicated in Figure 2.13.

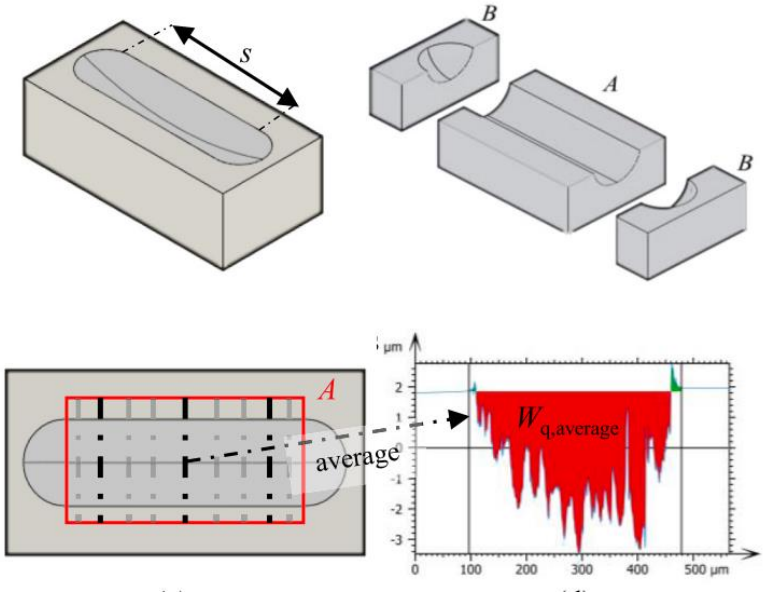

Figure 2.13: Shape and the profile of the wear track on a flat surface formed by reciprocating tribometer [113]

$$V_w = \underbrace{\frac{\pi . l^2 (d-s)^2}{64} . \frac{1}{R}}_{2B} + \underbrace{sW_{q,average}}_{A} \text{ (Eq. 8)}$$

Here, V_w is the total wear volume, l is the width of the wear track, d is the total length of the track and R is the radius of cross section of the wear track [113]. The wear rate (W_s) could be expressed as the ratio between the wear volume to applied normal load (F_N) along the sliding distance (L) (Eq. 9) [109].

$$W_s = \frac{V_w}{F_N x L} \text{ (Eq. 9) [76]}$$

Wear behaviour has a significant role for the final application of coatings. To examine the wear susceptibility of TFs, selected tribometer applies a certain normal load with a sliding motion to

form a wear track. The normal-load range and the nature of the contact could be varied depending on the materials in contact.

2.2.2. Tribology in Metal-Polymer Contact for Bio-Materials

Tribological phenomena appears in many body parts of living species. Especially for human beings, it can be considered for joints, skin, eyes, teeth and heat valves [114].

In several studies, titanium was used as commercially pure (cp)-Ti film [106] or in hard coating form as TiN [115, 116], or in several alloy forms such as TiAl, Ti6Al4V [117] or TiAg films [11]. Moreover, numerous polymeric materials were preferred as the counter-part to be coupled with Ti-based films. Even though, conventionally ultra-high molecular weight polyethylene is used, also PEEK, epoxy resin, hydrogels [114] and polyurethane have been selected as the polymeric counter-pars for body prosthesis [118]. Regarding the appropriate moduli, low weight, cost efficiency and easy preparation of polymers, they are good candidates to be coupled with metallic surfaces in relative motion for bio-materials. In the given particular examples below, polymers were used as articulating component and metal-based surfaces were used as femoral or tibial component for hip and knee joints to enhance the durability of the implants [119]. Additionally, in the case of the contact at joints, proper lubrication conditions should be also considered. For this purpose, the designed prosthesis was tested previously with water, bovine solution, saline solution [118] and simulated body fluid [115].

Regarding all aspects mentioned above, Wang et *al.* [119] examined the tribological behaviour of TiN coating on steel substrate against high density poly ethylene (HDPE). It was seen that both in water and simulated body fluid, the wear track has the similar behaviour with a friction coefficient ~0.1. However, the wear debris of poly-ethylene can cause a chronical inflammation around the soft tissue of the prosthesis (Figure 2.14).

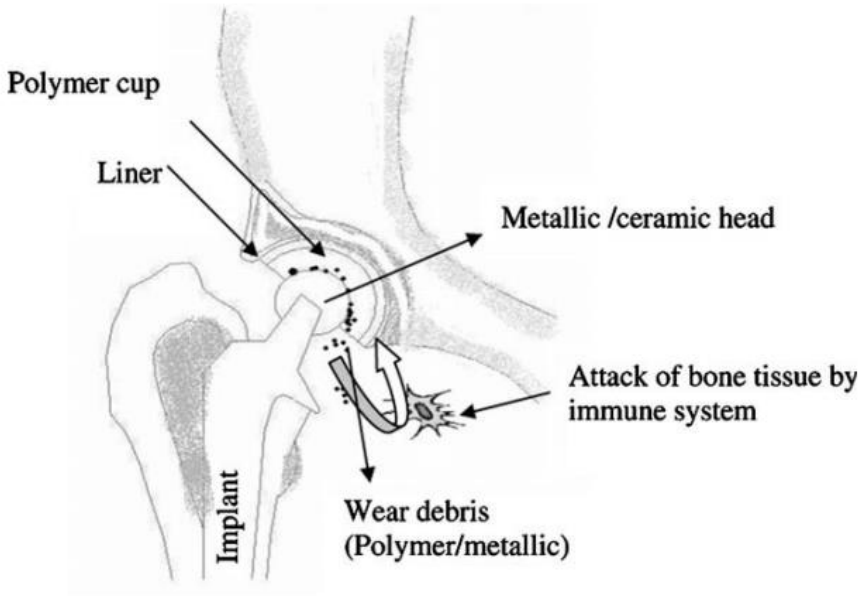

Figure 2.14: Forming of wear debris in a prosthesis based on friction [120]

On the other hand, polymeric counter-part has an efficient role on bio-material applications. Polyurethane (PU) is one of the significant materials to be used for this purpose. For example, Auger et *al*. replaced the UHMWPE cups with PU to be used for hip joint prosthesis. PU is elasto-hydrodynamically equivalent material for UHMWPE in addition to its low friction character. Also, Unsworth et al. correlated mechanical properties of PU with its friction character and indicated that it is a suitable material to be used for hip joints as a soft layer [118].

In this PhD, for the targeted bio-sensor application, wear involves an open contact. Therefore, interior inflammation in human body based on wear debris was not a main concern. However, for the reliable measurements with continuous signal acquisition, good wear resistance and low friction coefficient is still needed. Therefore, proper material choice is the critical point.

2.2.3. Tribology for Ti-based films

Titanium and some of its alloys have high hardness and chemical stability as it was mentioned before; however, they do not have enhanced wear resistance with their high friction coefficients regarding their highly columnar microstructure [5]. Therefore, several modifications on deposition process, film composition or crystal structure is needed. To investigate the tribological behaviour of Ti-based thin films, the counter face is often selected as a hard material

by considering the industrial applications; however, for the bio-sensor applications, it is significant to consider the skin contact and to select the counter-face material accordingly. In this point, a polymeric contact could be effective. Below, first the variations on the tribological behaviours of Ti-films against a hard counter-face were reviewed in terms of several aspects such as alloying element addition, changes on deposition parameters, multi-layer deposition. Secondly, tribological behaviours of Ti-based films against polymeric contact were discussed.

In previous studies, to investigate the tribological behaviour of Ti-based thin films against various counter-face materials, steel [52], alumina, SiN [121], or ruby [56] balls were used. Also, it was aimed to improve the tribological character of these films in several different methods. To enhance the wear behaviour of Ti-based coatings, Nolan et *al.* [56] used plasma nitriding technique during PVD film deposition of TiN and Ti_2N coatings. It was seen that plasma nitriding forms a strengthened nitrogen diffusion layer below the coating which enhances the wear character of the film against a ruby ball. Additionally, Kaneta et *al.* [52], studied the effect of film thickness on the wear character of Ti and TiN coatings on their tribological response against steel ball. It was examined that increasing thickness provides lower wear rate for pure Ti film whereas the wear rate is quite stable with the changes on the thickness of TiN film.

Alloying elements could also modify the wear and friction character of Ti-based coatings. Previously liquid lubrication was used to control the friction for these coatings; however, several elements such as noble metals could provide solid lubrication to improve the wear resistance of Ti-based TFs [58]. Regarding this aspect, Du et *al.* investigated the effect of Ag addition into TiN matrix and it was seen that 60% and 80% (at.) Ag addition provides higher wear resistance by comparison to pure TiN film [68]. Similarly, Zhou et *al*. [122] focused on appearance of wear track with silver addition for TiCN-Ag film. It was observed that adding a soft material such as Ag provides the formation of fcc-Ag phase which enhances the lubrication performance, and therefore the wear track has a smoother appearance with increasing Ag content even though there is an increment on applied normal load. It was explained that with increasing Ag content the microstructure of the film was changed from densely-packed crystals to spherical small grains, which were randomly placed in amorphous matrix. Such modified microstructure helped to increase the wear resistance. As another solid lubrication method, carbon addition could be considered. For example, Nolan et *al.* [56] analysed the effect of C content on wear character of titanium carbide- amorphous nanocomposite films (TiC-a:C). It

was seen that for the amorphous carbon content above 60-65%, the solid lubrication occurs and the tribological behaviour of the film is controlled by the presence of sp^2 bonds while the TiC nanocrystals regulate the carbon matrix and improve the wear resistance. The wear and friction characters of various Ti-based films with various other alloying elements were also compared in previous studies. Hsieh et *al.* [55] compared the friction coefficients and wear rates of TiN, TiSiN, TiCNO, TiAlN and AlTiN films against alumina ball. It was seen that TiCNO film has the lowest friction coefficient with the smallest wear rate, whereas Al containing films has the highest friction coefficient and the highest wear rate (Table 2.2). In another study, Aihua et *al.* [59] explained that the higher friction coefficient and wear rate of AlTiN film is dependent on the brittleness of the aluminium oxide which increases the chemical reactivity and causes aroused severe abrasive wear.

Table 2.2: Comparison of friction coefficients and wear rates of different Ti-based films [55]

	TiN	TiSiN	TiCNO	TiAlN	AlTiN	TiCN (C rich)	TiCN (N rich)
Friction coefficient	0.65	0.99	0.19	0.94	0.87	0.20	0.21
Wear rate (mm^3/m)x10^{-6}	4.34	8.01	1.12	19.70	46.62	1.93	2.58

Heat treatment also plays an important role on the wear behaviour of Ti-based coatings. Adochite et *al.* [60] stated that at room temperature the friction behaviour of Ag:TiO_2 film is based on film structure; however, the film starts to crystallize after 300°C and with further increase in temperature Ag starts to segregate through the surface which provides a reduction on friction coefficient and improves the wear behaviour of the film.

It also has to be noted that, as well as the modification on the Ti-based films, changes on the testing environment [123], testing parameters (load, speed) [124] and the material of the counter-face has a crucial role on the contact behaviour [123, 124].

The applied normal load and the sliding speed of the counter face could also modify the friction behaviour and the wear scar. Kateria et *al.* [124] studied the effect of sliding speed and the normal load on the friction coefficient of pure titanium coating. It was seen that friction coefficient decreases with increasing sliding speed, yet while the normal load increases the coefficient of friction also increases with larger deformation on the pure Ti TF. Additionally,

when Nolan et *al.* [56] examined the role of the normal load which was applied as 10 N, 20 N and 40N on TiN film, it was observed that there is relatively lower wear rate for the tests performed with 10 N and 20 N but, the highest wear rate was obtained with 40 N of normal load application.

Regarding the targeted final application of the titanium-based TFs, the choice of the counter-face material is also significant because the coefficient of friction and the wear behaviour of the coating differs against selected counter-face materials since the contact pressure is dependent on the mechanical properties of both of materials in the contact. In order to examine this issue, Kateria et *al.* [124] performed tests with steel, SiN and Al_2O_3 balls on pure Ti film, and it was seen that while the lowest wear rate has been obtained against SiN ball, the highest material loss was occurred for the test against Al_2O_3 ball.

The bio-compatibility and wear resistance of "Ti-based TF in polymeric contact" make them a suitable system for bio-sensors. Therefore, Ti-based TF to be used for bio-sensor applications which could be possibly exposed a relative motion has to be considered with the proper counter-part [125-127]. As it was explained, for most of the bio-sensors, polymers are preferred regarding their flexibility and durability [105]. Also, conductive polymers are developed for a reliable signal acquisition [125,127,128]. Normally, the relative motion like on pulse or cardiograph measurements [129], or movements on joint prosthesis of knees or hips, are endlessly repeating during the lifetime [130, 131]. To investigate the pulse rate or the deformation on joints, bio-sensors can take place. For this purpose, polyurethane is an efficient material to be used in bio-sensor applications in addition to its use for body-prosthesis [132]. It can provide bio-compatibility and reduce the bacterial adhesion. Marois et *al.* [133] stated that, regarding the in vivo and in vitro tests performed with PU, this material can be used in cardiovascular system, middle ear, for eyes, and endoprosthesis. Here, it was either used as a substrate with a coating of a metallic film [80] or as a functionalised layer for corresponding bio-sensing purpose [134, 135]. In the previous studies PU has been used for various sensing purposes as the component of many different bio-sensor mechanisms (Table 2.3) [136].

Table 2.3: PU use in different biosensor applications [136]

PU kind	Biosensor kind	Application
Aliphatic acrylated urethane diacrylate membrane	Ion-sensitive field effect transistor	Urea biosensor
Aliphatic acrylated urethane diacrylate membrane	Amperometric	Glucose determination
Asymmetric PU/hydrophilic PU membrane	Potentiometric	Enzymes bio-selective sensors
Photocurable oligomer of urethane and Bisphenol A (epoxy) diacrylate based membrane	Ion-sensitive field effect transistor	K^+ sensitive ion sensor
Tecoflex (SG-80A) based membrane	Potentiometric	NH_4^+, K^+ ion-selective sensor
Aromatic diisocyanate and poly(tetramethylene ether glycol) based PU membrane	Potentiometric	Ion selective sensor
PU/poly(vinyl alcohol) based membrane	Potentiometric	NH_4^+ and proton selective electrode
Tecoflex PU	Electrochemical	Ion selective sensor
Photocurable urethane-acrylate membrane from urethane diacrylate oligomer	Potentiometric	pH sensor
Tecoflex PU	Potentiometric	pH sensor for biomedical application
Hydrophilic PU based membrane	Electrochemical	Blood gas determination
Teflon and Tecoflex (SG-85 A) PU films	Amperometric	Glucose sensor
Tecoflex (SG-80A) PU based membrane	Amperometric	Formaldehyde monitoring
Tecoflex (EG 80A) PU based membrane	Electrochemical transducer	Lactate and glucose biosensors

In this PhD, polyurethane was selected as the counter-part material for Ti-Ag PVD films regarding its efficient role both for bio-prosthesis and bio-sensors. It was aimed to achieve soft contact with a reduced friction coefficient to provide more realistic contact conditions for the bio-sensor applications. Even though, in the previous studies, the durability of bio-sensors against relative motion was not investigated, polyurethane is a good candidate to be used as the counter part for examining the tribological behaviours of the Ti-based films to be used for biosensors.

To conclude, the tribological behaviours of Ti-based thin films were investigated and several techniques to improve their friction and wear characters were discussed. The alloying elements, their concentration in the film, change on bias voltage, current or temperature during deposition, and modification on surface roughness are possible processes to enhance the wear resistance of Ti-based PVD thin films. For the bio-sensor applications, it is necessary to provide continuous electrical signal acquisition to achieve the reliability of the measurements. Therefore, to deeply investigate the tribological behaviour of Ti-based TFs and to be assured for the continuous

electrical conductivity from the beginning of the contact, it is firstly focused on the early stage of the contact (run-in period) and the wear mechanism based on friction. Here, Ti-based films against polymeric contact were analysed. As the polymeric counter-face, poly-urethane (PU) was investigated regarding it bio-compatibility and flexibility.

2.2.4. *In situ* Small Scale Analysis at Early Stage of Contact

Regarding the developments on small scale engineering devices such as MEMS, NEMS, biosensors; the size of the contact [137] and the applied force to estimate the friction behaviour of surfaces have a great importance [138]. The real contact area between two surfaces is in microscopic or nanoscopic range and so it is not possible to characterise the tribological behaviour of these surfaces in larger scale [137]. As another reason to perform small scale tribological characterization is to increase the resolution and to be able to better understand the sliding contact conditions [139]. Since the scale has a significant role on tribological phenomena various microscopy and spectroscopy techniques have been used [140]. To examine the sliding contact in a better way is not easy since the interface is buried [139]. Nano-indenters couples with AFM is a well-known technique for small scale tribological analysis [151, 52]. Other microscopy techniques to perform micro or sub-micro scale investigations are also have a significant role on tribological investigation in small scale. For example, Achanta et *al.* [153] performed microscale investigation with lateral force microscopy to evaluate the very sensitive surface interactions with ultra-low force and in small length scale. Heinrichs et *al.* [154] used SEM, TEM, EDS and EEES (electron energy loss spectroscopy) for the *post mortem* analysis of the wear tracks after the tests performed on TiO_2 films against a polytetrafluoroethylene (PTFE) ball.

Additionally, tribologists willed to investigate the contact interface during sliding to understand the wear mechanism, formation of third bodies, material transfer and evolution of the microstructures. Thus, *in situ* characterization is needed. In the previous studies, *in situ* characterization to examine the material flow was performed in various scales [155-158]. There are several set-ups designed to perform the tribological tests especially in SEM. In SEM chamber, it is possible to achieve sub-micrometric investigations with high resolution in real time [155]. Michler et *al.* [155], Heinrichs et *al.* [156] and Gee et *al.* [158] designed various micro-scratchers with a pin sliding tip to perform *in situ* analysis in SEM.

Another significant point for the tribological analysis is examining the material behaviour against sliding during running-in period. Even though the tribological behaviour of materials was well-documented in the previous studies [159-162] crucial changes on surface roughness, grain size or the texture of the surface can be formed during running-in state [163, 164]. This stage takes place at the early times of the contact and the testing conditions during the running in period can affect the steady state times of sliding because during the running-in state large amount of plastic deformation can occur with the high wear rate [165]

By performing *in situ* tribological tests, mixing of the materials, chemical changes and role of the surrounding environment could be identified progressively. Thereby, the wear mechanism can be modelled and so the service life of the final products could be predicted for the corresponding applications [141]. Additionally, even though there are some studies to explain the damaging mechanism during running in period, usually [142], it is not considered. However, it could be efficiently investigated with *in situ* analysis for the early stages of the contact. In the future, *in situ* characterisation for tribology could even provide to perform simulations in atomic scale [139].

2.3. Effect of Environment in Tribology

It is known that many factors can modify the wear and friction behaviour of thin films significantly, such as roughness [41], crystal orientation, chemical composition and mechanical properties. However, as well as the properties of film itself, the operating environment also has a crucial role on the tribological response of thin films [42]. Also, it has to be noted that the operating conditions can control the friction and wear mechanisms [143]. Therefore, the effect of environment has to be considered while investigating their tribological behaviour because tribo-chemical reactions may occur at the interface between the surface and the sliding counter-face [41]. Also, physisorption of the environmental species could have a role on the modification of the friction and wear character of the TFs [42].

Previously, the effect of environment has been investigating for several types of thin films [41,42]. Depending on the materials in contact, the role of environment takes place on tribological behaviour of surfaces. For example, solid film lubricants are usually used to reduce the friction coefficient at contact. While the tribological behaviours of graphene and graphite films enhance with increasing humidity, the situation is contrary for diamond like carbon (DLC) films [144]. DLC films are the most well-known films which has tuning character on its

tribological response with changing environmental conditions based on the fact that carbon has many stable forms due to its ability to hybridise in various states regarding the various humidity levels [42]. DLC films have a self-lubrication character in dry air atmosphere against friction; however, with a slight increase in humidity the friction coefficient increases. Previously Gilmore et *al.* [145] studied the effect of Ti doping in DLC film on its tribological behaviour under as 5%, 65% and 85% relative humidity. It was seen that titanium tends to reduce the friction coefficient for all the relative humidity; nevertheless, the effect of titanium is quite the same even though the humidity increases. Another example for the films which have tuning on their tribological character based on the environmental conditions is MoS_2 which has a similar behaviour as DLC films. While it is self-lubricating in high vacuum, the friction coefficient increases with the existence of humidity in the atmosphere [144].

Tribological susceptibility of titanium based films is also sensitive to the environmental conditions [43-50]. It could be stated that, today one of the greatest challenges for the wear performance of Ti- based coatings is working environment [58]. Since titanium is quite tend to oxidise, a passive oxide layer forms on the surface of the film in humid environments which could also provide a solid lubrication and reduce the friction.

In this point, Manu et *al.* [144] investigated the tribological behaviour of commercially pure Ti with increasing humidity. It was seen that from 0 to 10% relative humidity the friction coefficient was slightly decreased. This characteristic was explained as the effect of dehumidification. The surface energy of the titanium surface was decreased regarding the small amount of adsorption of water molecules which helped to reduce the friction. However, with the further increase on humidity (up to 55%) the friction coefficient started to increase. This behaviour was correlated with the increasing thickness of the water adsorption layer which caused an increase in shear stress and stick-slip motion. Also, the surface energy was increased based on the formation of hydrogen bonds between OH and H molecules. However, surprisingly the friction coefficient decreased for the very higher relative humidity than 55%. This issue was based on the confinement of the excessive water molecules at the contact interface which restrict the interaction between two surfaces in contact (Figure 2.15).

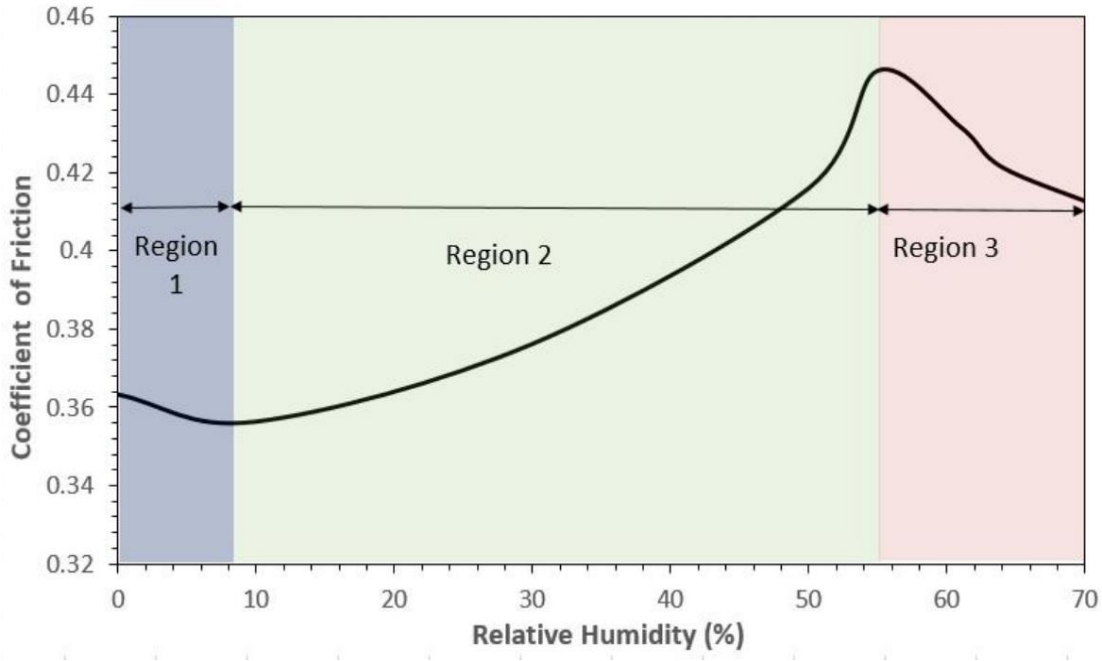

Figure 2.15: Tribological behaviour of cp-Ti with increasing relative humidity [144]

Additionally, the tribological behaviour of TiN films can be tuned with the changes on relative humidity. For example, in the study performed by Yoon et *al*. it was seen that the friction coefficient of TiN film was decreased with increasing relative humidity from 2% to 25% [146]. Also, Barril et *al.* [110] compared the wear rate of TiN film in aqueous solution and under dry contact in atmospheric conditions and it was seen that, passive oxide film forms on the surface of the coating (Eq. 10). Additionally, in aqueous solution, the wear behaviour of the Ti-based TF is also dependent on the aggressiveness of the liquid which makes necessary to consider the corrosion behaviour of the coating. On the other side, under dry contact, the tribological response of the film is controlled by the level of the relative humidity of the testing environment. Therefore, it was indicated that the frictional properties are dependent on the hydration of oxide layer which was formed on the film surface. In another study, Zhang et *al.* [123] observed that while the wear behaviour of Ti-based films tested in nitrogen environment, existence of N_2 in the testing environment, inhibits the formation of the oxide layer. Additionally, when the friction behaviour of titanium-zirconium-molybdenum coating was examined in salted and distilled water, it was seen that the coefficients of friction in both environmental conditions were low in the beginning. However, it started to increase gradually for the salty water environment regarding the aggressiveness of liquid which causes corrosion.

$$-TiN + 2H_2O \rightarrow TiO_2 + \frac{1}{2}N_2 + 4H^+ + 4e^-$$ (Eq. 10) [110]

Also, Whang et *al.* [147] investigated the effect of silver on tribological behaviour of WS_2 films with increasing humidity. Here, Ag is selected because it provides lower shear stress as a soft ductile material. It was aimed to improve the wear character of the films and it was seen that Ag addition help to reduce the friction coefficient under vacuum conditions. However, in humid conditions, the effect of Ag was negative on tribological behaviour of the films (Figure 2.16). It was seen that Ag has a sensitivity to environment in terms of its tribological behaviour. Therefore, in this PhD it was aimed to analyse the role of Ag on tribological behaviour of Ti-Ag films in various humidity levels to deeply understand its sensitivity.

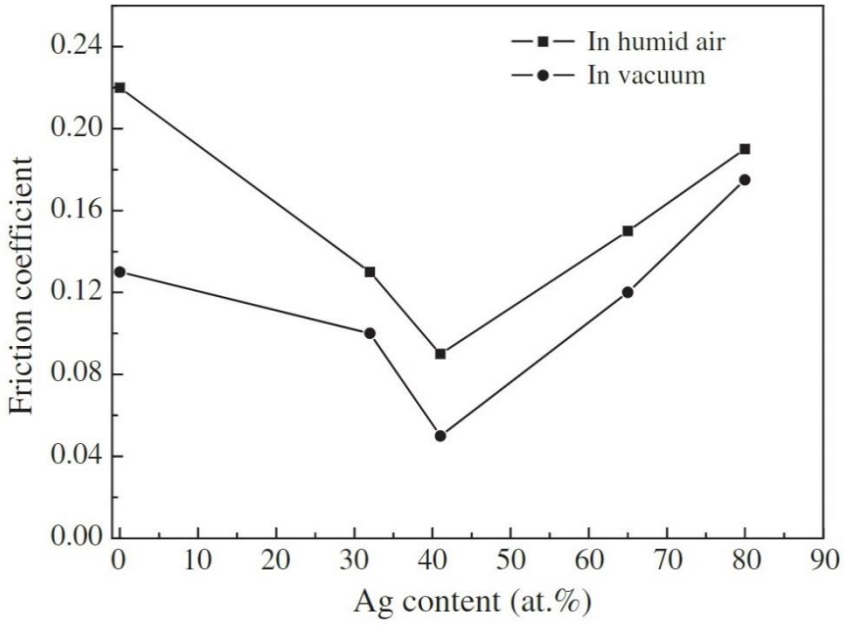

Figure 2.16: Effect of Ag in vacuum and humid environment on friction coefficient [147]

As well as the metallic film, the counter-part should also be considered. Therefore, the changes of the tribological behaviour also for the polymers based on the environmental conditions has to be considered. Because, environment (e.g. humidity) has a strong role on the modification of fretting life for most of the polymers. It is also important to consider that, the polymers to be used in bio-applications are subjected to humidity and natural lubricants such as synovial fluid at joints. Previously, Briscoe et *al.* [148] examined the friction behaviour of HDPE, PEEK and PA in different humidity levels. It was seen that for all these three types of polymers, the water adsorption is limited with their amorphous regions. However, when they adsorb water, their mechanical properties decrease and slight surface plasticization occur which helps to reduce the shear stress as well as the friction coefficient. This phenomenon is named as Rubenstein effect.

However, with the further increase of the adsorbed water molecules, based on softening of the polymer surface, both the contact area and the friction coefficient increase [149]. Even though there are some studies about the effect of humidity on the friction behaviour of several polymers, PU was not deeply examined. Only Khun et *al.* [150] stated that hydrogen bonding in PU regarding the adsorption of water molecules significantly modifies the morphology and physical properties of the material. However, in their study, the role of acidity and immersion time of PU into acid were investigated in terms of tribological aspect. Thereby, it is crucial to consider that changing relative humidity could also modify the friction and wear behaviour of PU counter-part.

To sum up, the tribological behaviour of the materials can be affected by the testing environment. Here; humidity, temperature, aggressivity of the environment could take place to modify the tribological behaviour of surfaces. In this chapter it was aimed to review the role of humidity on the Ti-based thin films' wear and friction characters. It was seen from the previous studies, titanium tends to oxide and form an oxide layer on the surface of the film. Depending on the level of humidity, the absorbed water molecules and formation of oxide layer can cause the tuning of the tribological character of the film. Moreover, for TiN film, this oxide layer helped to reduce the friction coefficient by behaving as solid lubricant. Even though there are some studies focused on the role of environment on tribological behaviour of pure Ti [144], some Ti-alloys [143] and even hard Ti based films (e.g. TiN) [146], there is no research was done about Ti-Ag films behaviour about this issue. Therefore, in this study, the role of environment based on the relative humidity level was examined on friction and wear behaviour specifically for Ti-Ag films. Since in the literature, it was indicated that, while Ag provides enhanced sliding behaviour in vacuum conditions, it causes a reduction on wear resistance of the films in humid environment. Therefore, in this manuscript, it was aimed to examine the modifications of tribological behaviour of Ti-Ag films detailly regarding the changing Ag content and increasing humidity.

References (Chapter 2)

[1] Chouirfa, H., Bouloussa, H., Migonney, V., & Falentin-Daudré, C. (2019). Review of titanium surface modification techniques and coatings for antibacterial applications. *Acta Biomaterialia*, *83*, 37–54. https://doi.org/10.1016/j.actbio.2018.10.036

[2] Wen, C. (2015). *Surface coating and modification of metallic biomaterials*. Woodhead Publishing.

[3] Elsner, C. I., Cavalcanti, E., Ferraz, O., & Di Sarli, A. R. (2003). Evaluation of the surface treatment effect on the anticorrosive performance of paint systems on Steel. *Progress in Organic Coatings*, *48*(1), 50–62. https://doi.org/10.1016/s0300-9440(03)00112-7

[4] Navinšek, B., Panjan, P., & Milošev, I. (1999). PVD coatings as an environmentally clean alternative to electroplating and electroless processes. *Surface and Coatings Technology*, *116-119*, 476–487. https://doi.org/10.1016/s0257-8972(99)00145-0

[5] Manory, R. R., Mollica, S., Ward, L., Purushotham, K. P., Evans, P., Noorman, J., & Perry, A. J. (2002). The effects of MEVVA ion implantation on the tribological properties of PVD-tin films deposited on steel substrates. *Surface and Coatings Technology*, *155*(2-3), 136–140. https://doi.org/10.1016/s0257-8972(02)00131-7

[6] Chen, Q., Li, A., Wu, G., Lu, Z., Zhang, G., & Tian, G. (2020). Structure vs chemistry: Tribological behavior of tin films in the nitrogen atmosphere. *Ceramics International*, *46*(18), 28053–28063. https://doi.org/10.1016/j.ceramint.2020.07.300

[7] Chen, Q., Wu, G., Li, D., Li, A., Shang, L., Lu, Z., Zhang, G., Wu, Z., & Tian, G. (2019). Understanding the unusual friction behavior of tin films in vacuum. *Tribology International*, *137*, 379–386. https://doi.org/10.1016/j.triboint.2019.05.024

[8] Yan, Z., Jiang, D., Gao, X., Hu, M., Wang, D., Fu, Y., Sun, J., Feng, D., & Weng, L. (2018). Friction and wear behavior of tin films against Ceramic and Steel Balls. *Tribology International*, *124*, 61–69. https://doi.org/10.1016/j.triboint.2018.03.031

[9] Cordill, M., Marx, V., & Kirchlechner, C. (2014). Ductile film delamination from compliant substrates using hard overlayers. *Thin Solid Films, 571*, 302-307. doi:10.1016/j.tsf.2014.02.093.

[10] Kawamura, M., Zhang, Z., Kiyono, R., & Abe, Y. (2013). Thermal stability and electrical properties of Ag–Ti films and Ti/Ag/Ti films prepared by sputtering. *Vacuum, 87*, 222-226. doi:10.1016/j.vacuum.2012.02.021

[11] Etiemble, A., Lopes, C., Bouala, G. I., Borges, J., Malchère, A., Langlois, C, Vaz, F., & Steyer, P. (2019). Fracture resistance of Ti-Ag thin films deposited on polymeric substrates for biosignal acquisition applications. *Surface and Coatings Technology, 358,* 646-653. doi:10.1016/j.surfcoat.2018.11.078.

[12] Manninen, N. K., Galindo, R. E., Benito, N., Figueiredo, N. M., Cavaleiro, A., Palacio, C., & Carvalho, S. (2011). Ag–Ti(C, N)-based coatings for biomedical applications: Influence of silver content on the structural properties. *Journal of Physics D: Applied Physics*, *44*(37), 375501. doi:10.1088/0022-3727/44/37/375501.

[13] Lopes, C., Gabor, C., Cristea, D., Costa, R., Domingues, R., Rodrigues, M., Borges, J., Alves, E., Barradas, N.P., Munteanu, D., Vaz, F. (2020). Evolution of the mechanical properties of Ti-based intermetallic thin films doped with different metals to be used as biomedical devices. *Applied Surface Science, 505*, 144617. doi:10.1016/j.apsusc.2019.144617

[14] Braic, V., Braic, M., Pavelescu, G., Melinte, D., & Necsoiu, D. (1995). Influence of deposition parameters on optical properties of titanium nitride thin films. *ROMOPTO 94: Fourth Conference in Optics*. doi:10.1117/12.203490

[15] Ding, G., Clavero, C., Schweigert, D., & Le, M. (2015). Thickness and microstructure effects in the optical and electrical properties of silver thin films. *AIP Advances, 5*(11), 117234. doi:10.1063/1.4936637

[16] Oluwatosin Abegunde, O., Titilayo Akinlabi, E., Philip Oladijo, O., Akinlabi, S., & Uchenna Ude, A. (2019). Overview of thin film deposition techniques. *AIMS Materials Science*, *6*(2), 174–199. https://doi.org/10.3934/matersci.2019.2.174

[17] Vlasveld, A., Harris, S., Doyle, E., Lewis, D., & Munz, W. (2002). Characterisation and performance of partially filtered arc TiAlN coatings. *Surface and Coatings Technology, 149*(2-3), 217–223. doi: 10.1016/s0257-8972(01)01448-7

[18] Heinke, W., Leyland, A., Matthews, A., Berg, G., Friedrich, C., & Broszeit, E. (1995). Evaluation of PVD nitride coatings, using impact, scratch and Rockwell-C adhesion tests. *Thin Solid Films, 270*(1-2), 431–438. doi: 10.1016/0040-6090(95)06934-8

[19] Kottfer, D., Ferdinandy, M., Kaczmarek, L., Maňková, I., & Beňo, J. (2013). Investigation of Ti and Cr based PVD coatings deposited onto HSS Co 5 twist drills. *Applied Surface Science*, *282*, 770–776. doi: 10.1016/j.apsusc.2013.06.051

[20] Reali, L. F., Lin, J., Wei, R., Torres, R., Laurindo, C. A. H., Soares, P., & Hatem, A. L. A. (2017). Adhesion evaluation of nanostructured coatings on titanium alloy for biomedical applications. *Procceedings of the 24th ABCM International Congress of Mechanical Engineering*. doi: 10.26678/abcm.cobem2017.cob17-2383

[21] Stan, G., Morosanu, C., Marcov, D., Pasuk, I., Miculescu, F., & Reumont, G. (2009). Effect of annealing upon the structure and adhesion properties of sputtered bio-glass/titanium coatings. *Applied Surface Science, 255*(22), 9132–9138. doi: 10.1016/j.apsusc.2009.06.117

[22] Kim, W., Kim, S., Lee, K.-S., Lee, T., & Kim, I. (2012). Titanium nitride thin film as an adhesion layer for surface plasmon resonance sensor chips. *Applied Surface Science, 261*, 749–752. doi: 10.1016/j.apsusc.2012.08.093

[23] Liang, T., Liu, Y., Fu, Z., Luo, T., & Zhang, K. (2005). Diffusion and adhesion properties of Cu films on polyimide substrates. *Thin Solid Films, 473*(2), 247–251. doi: 10.1016/j.tsf.2004.07.073

[24] Harris, S., Doyle, E., Vlasveld, A., & Dolder, P. (2001). Dry cutting performance of partially filtered arc deposited titanium aluminium nitride coatings with various metal nitride base coatings. *Surface and Coatings Technology, 146-147*, 305–311. doi: 10.1016/s0257-8972(01)01421-9

[25] Abadias, G., & Guerin, P. (2008). *In situ* stress evolution during magnetron sputtering of transition metal nitride thin films. *Applied Physics Letters, 93*(11), 111908. doi:10.1063/1.2985814

[26] Kitamura, T., Hirakata, H., & Itsuji, T. (2003). Effect of residual stress on delamination from interface edge between nano-films. *Engineering Fracture Mechanics, 70*(15), 2089-2101. doi:10.1016/s0013-7944(02)00254-0

[27] Cordill, M., & Taylor, A. (2015). Thickness effect on the fracture and delamination of titanium films. *Thin Solid Films, 589*, 209-214. doi:10.1016/j.tsf.2015.05.021.

[28] Massl, S., Thomma, W., Keckes, J., & Pippan, R. (2009). Investigation of fracture properties of magnetron-sputtered TiN films by means of a FIB-based cantilever bending technique. *Acta Materialia, 57*(6), 1768-1776. doi:10.1016/j.actamat.2008.12.018

[29] Bouzakis, K., Skordaris, G., Gerardis, S., Katirtzoglou, G., Makrimallakis, S., Pappa, M., Lill, E., & Msaoubi, R. (2009). Ambient and elevated temperature properties of TiN, TiAlN and TiSiN PVD films and their impact on the cutting performance of coated carbide tools. *Surface and Coatings Technology, 204*(6-7), 1061-1065. doi:10.1016/j.surfcoat.2009.07.001.

[30] Saladukhin, I., Abadias, G., Michel, A., Uglov, V., Zlotski, S., Dub, S., & Tolmachova, G. (2015). Structure and hardness of quaternary TiZrSiN thin films deposited by reactive magnetron co-sputtering. *Thin Solid Films, 581*, 25-31. doi:10.1016/j.tsf.2014.11.020

[31] Ivanov, Y., Koval, N., Krysina, O., Baumbach, T., Doyle, S., Slobodsky, T., Timchenko, A, Galimov, R. M., & Shmakov, A. (2012). Superhard nanocrystalline Ti–Cu–N coatings deposited by vacuum arc evaporation of a sintered cathode. *Surface and Coatings Technology, 207*, 430-434. doi:10.1016/j.surfcoat.2012.07.037

[32] Wojcieszak, D., Kaczmarek, D., Antosiak, A., Mazur, M., Rybak, Z., Rusak, A., Osekowska, M., Poniedzialek, A, Gamain, A, & Szponar, B. (2015). Influence of Cu–Ti

thin film surface properties on antimicrobial activity and viability of living cells. *Materials Science and Engineering: C, 56*, 48-56. doi:10.1016/j.msec.2015.06.013

[33] Wojcieszak, D., Mazur, M., Kalisz, M., & Grobelny, M. (2017). Influence of Cu, Au and Ag on structural and surface properties of bioactive coatings based on titanium. *Materials Science and Engineering: C, 71*, 1115-1121. doi:10.1016/j.msec.2016.11.091

[34] Zhou, D., Peng, H., Zhu, L., Guo, H., & Gong, S. (2014). Microstructure, hardness and corrosion behaviour of Ti/TiN multilayer coatings produced by plasma activated EB-PVD. *Surface and Coatings Technology, 258*, 102-107. doi:10.1016/j.surfcoat.2014.09.058

[35] Lopes, C., Pedrosa, P., Martin, N., Barradas, N. P., Alves, E., & Vaz, F. (2015). Study of the electrical behaviour of nanostructured Ti-Ag thin films, prepared by Glancing Angle Deposition, *Materials Letters*, 157, 188-192, doi: 10.1016/j.matlet.2015.05.0

[36] Arshi, N., Lu, J., Joo, Y. K., Lee, C. G., Yoon, J. H., & Ahmed, F. (2012). Influence of nitrogen gas flow rate on the structural, morphological and electrical properties of sputtered TiN films. *Journal of Materials Science: Materials in Electronics, 24*(4), 1194-1202. doi:10.1007/s10854-012-0905-4

[37] Savaloni, H., Khojier, K., & Alaee, M. S. (2007). Characteristics of nanostructure and electrical properties of Ti thin films as a function of substrate temperature and film thickness. *Journal of Materials Science, 42*(8), 2603-2611. doi:10.1007/s10853-006-1340-9.

[38] Melentiev, R., Fang, F., & Narala, S. K. (2020). Influence of different pretreatments on Ti-6Al-4V surface integrity and scratch-resistance of epoxy coating: Analysis of topography, microstructure, chemistry and wettability. *Surface and Coatings Technology, 404*, 126436. doi:10.1016/j.surfcoat.2020.126436

[39] Plirdpring, T., Samransuksamer, B., Horprathum, M., Lertvanithpol, T., Pattantsetakul, V., Limwichean, S. & Eiamchai, P. (2017). Preparation and surface wettability of nanostructure TiO 2 films. *Materials Today: Proceedings, 4*(5), 6331-6335. doi:10.1016/j.matpr.2017.06.135

[40] Maciejewski, M., Wojcieszak, D., Mazur, M., Zielinski, M., Kaczmarek, D., Domaradzki, J., & Prociow, E. (2010). Influence of droplet size and surface preparation of TiO. *2010 International Students and Young Scientists Workshop "Photonics and Microsystems"*. doi:10.1109/stysw.2010.5714179

[41] Kaur, M., & Singh, K. (2019). Review on titanium and titanium based alloys as biomaterials for orthopaedic applications. *Materials Science and Engineering: C, 102*, 844-862. doi:10.1016/j.msec.2019.04.064

[42] Wenzel, R. N. (1936). Resistance Of Solid Surfaces To Wetting By Water. *Industrial & Engineering Chemistry, 28*(8), 988-994. doi:10.1021/ie50320a024

[43] Ali, M., Hamzah, E., Qazi, I. A., & Toff, M. R. M. (2010). Effect of cathodic arc PVD parameters on roughness of tin coating on steel substrate. *Current Applied Physics, 10*(2), 471–474. https://doi.org/10.1016/j.cap.2009.07.007

[44] Jaiswal, J., Singh;Ramesh Chandra, M., Sanger, A., Kumar, A., Mourya, S., Chauhan, S., & Daipuriya, R. (2016). Enhanced optical absorbance of hydrophobic TI thin film: Role of Surface Roughness. *Advanced Materials Letters*, *7*(6), 485–490. https://doi.org/10.5185/amlett.2016.6056

[45] Ewald, A., Glückermann, S. K., Thull, R., & Gbureck, U. (2006). Antimicrobial titanium/silver PVD coatings on Titanium. *BioMedical Engineering OnLine*, *5*(1). https://doi.org/10.1186/1475-925x-5-22.

[46] Almaguer-Flores, A., XimÃ©nez-Fyvie, L. A., & Rodil, S. E. (2010). Oral bacterial adhesion on amorphous carbon and titanium films: Effect of surface roughness and culture media. *Journal of Biomedical Materials Research Part B: Applied Biomaterials*, *92B*(1), 196–204. https://doi.org/10.1002/jbm.b.31506.

[47] Lopes, H. P., Elias, C. N., Vieira, M. V. B., Vieira, V. T. L., de Souza, L. C., & dos Santos, A. L. (2016). Influence of surface roughness on the fatigue life of nickel-titanium rotary endodontic instruments. *Journal of Endodontics*, *42*(6), 965–968. https://doi.org/10.1016/j.joen.2016.03.001

[48] Bearinger, J. P., Orme, C. A., & Gilbert, J. L. (2003). *In situ* imaging and impedance measurements of titanium surfaces using AFM and SPIS. *Biomaterials*, *24*(11), 1837–1852. https://doi.org/10.1016/s0142-9612(02)00547-1

[49] Zhang, B. B., Wang, B. L., Li, L., & Zheng, Y. F. (2011). Corrosion behavior of ti–5ag alloy with and without thermal oxidation in artificial saliva solution. *Dental Materials*, *27*(3), 214–220. https://doi.org/10.1016/j.dental.2010.10.005

[50] Aziz-Kerrzo, M., Conroy, K. G., Fenelon, A. M., Farrell, S. T., & Breslin, C. B. (2001). Electrochemical studies on the stability and corrosion resistance of titanium-based implant materials. *Biomaterials*, *22*(12), 1531–1539. https://doi.org/10.1016/s0142-9612(00)00309-4

[51] Sawyer, W. G., & Wahl, K. J. (2008). Accessing Inaccessible Interfaces: *In Situ* Approaches to Materials Tribology. *MRS Bulletin*, *33*(12), 1145-1150. doi:10.1557/mrs2008.244

[52] Kaneta, M., Matsuda, K., Matsuda, J., & Utsumi, A. (1992). Friction and wear properties of titanium films formed on aluminium by laser thermal spraying. *Wear*, *156*(1), 161–173. https://doi.org/10.1016/0043-1648(92)90151-w

[53] Ravindran, K. A., Ramasamy, P., & Laddha, G. S. (1980). Frictional behaviour of thin films of Soft Metals. *Thin Solid Films*, *66*(2), 249–254. https://doi.org/10.1016/0040-6090(80)90227-8

[54] Zhou, R., Ju, H., Liu, S., Zhao, Z. T., Xu, J., Yu, L., Qian, H., Jia, S., Song, R., & Shen, J. (2022). The influences of ag content on the friction and wear properties of TiCN–Ag Films. *Vacuum*, *196*, 110719. https://doi.org/10.1016/j.vacuum.2021.110719

[55] Hsieh, J. H., Tan, A. L. K., & Zeng, X. T. (2006). Oxidation and wear behaviors of TI-based thin films. *Surface and Coatings Technology*, *201*(7), 4094–4098. https://doi.org/10.1016/j.surfcoat.2006.08.026

[56] Nolan, D., Huang, S. W., Leskovsek, V., & Braun, S. (2006). Sliding wear of titanium nitride thin films deposited on ti–6al–4v alloy by PVD and plasma nitriding processes. *Surface and Coatings Technology*, *200*(20-21), 5698–5705. https://doi.org/10.1016/j.surfcoat.2005.08.110

[57] Yerokhin, A. L., Nie, X., Leyland, A., & Matthews, A. (2000). Characterisation of oxide films produced by plasma electrolytic oxidation of a ti–6al–4v alloy. *Surface and Coatings Technology*, *130*(2-3), 195–206. https://doi.org/10.1016/s0257-8972(00)00719-2

[58] Cavaleiro, D., Veeregowda, D., Cavaleiro, A., Carvalho, S., & Fernandes, F. (2020). High temperature tribological behaviour of tisin(ag) films deposited by HIPIMS in doms mode. *Surface and Coatings Technology*, *399*, 126176. https://doi.org/10.1016/j.surfcoat.2020.126176

[59] Aihua, L., Jianxin, D., Haibing, C., Yangyang, C., & Jun, Z. (2012). Friction and wear properties of tin, TiAlN, Altin and craln PVD nitride coatings. *International Journal of Refractory Metals and Hard Materials*, *31*, 82–88. https://doi.org/10.1016/j.ijrmhm.2011.09.010

[60] Adochite, R. C., Munteanu, D., Torrell, M., Cunha, L., Alves, E., Barradas, N. P., Cavaleiro, A., Riviere, J. P., Le Bourhis, E., Eyidi, D., & Vaz, F. (2012). The influence of annealing treatments on the properties of AG:tio2 nanocomposite films prepared by magnetron sputtering. *Applied Surface Science*, *258*(8), 4028–4034. https://doi.org/10.1016/j.apsusc.2011.12.095

[61] Sarioglu, C., Demirler, U., Kazmanli, M. K., & Urgen, M. (2005). Measurement of residual stresses by X-ray diffraction techniques in MoN and Mo2N coatings deposited by arc PVD on high-speed steel substrate. *Surface and Coatings Technology*, *190*(2-3), 238-243. doi:10.1016/j.surfcoat.2004.08.184

[62] Abadias, G., Koutsokeras, L., Siozios, A., & Patsalas, P. (2013). Stress, phase stability and oxidation resistance of ternary Ti–Me–N (Me=Zr, Ta) hard coatings. *Thin Solid Films*, *538*, 56-70. doi:10.1016/j.tsf.2012.10.119

[63] Marshall, D. B., & Evans, A. G. (1984). Measurement of adherence of residually stressed thin films by indentation. I. Mechanics of interface delamination. *Journal of Applied Physics*, *56*(10), 2632-2638. doi:10.1063/1.333794

[64] Puchi-Cabrera, E., Berríos, J., & Teer, D. (2002). On the computation of the absolute hardness of thin solid films. *Surface and Coatings Technology*, *157*(2-3), 185-196. doi:10.1016/s0257-8972(02)00153-6

[65] Kuphasuk, C., Oshida, Y., Andres, C. J., Hovijitra, S. T., Barco, M.T., & Brown, D.T. (2001). Electrochemical corrosion of titanium and titanium-based alloys, *The Journal of Prosthetic Dentistry*, 85(2), 195-202, doi:10.1067/mpr.2001.113029

[66] Stępień, K. (2015). Testing the accuracy of surface roughness measurements carried out with a portable profilometer. *Key Engineering Materials*, *637*, 69–73. https://doi.org/10.4028/www.scientific.net/kem.637.69

[67] Fazel, M., Salimijazi, H. R., Golozar, M. A., & Garsivaz jazi, M. R. (2015). A comparison of corrosion, tribocorrosion and electrochemical impedance properties of pure TI and ti6al4v alloy treated by micro-arc oxidation process. *Applied Surface Science*, *324*, 751–756. https://doi.org/10.1016/j.apsusc.2014.11.030

[68] Du, D., Liu, D., Zhang, X., & Tang, J. (2019). Fretting fatigue behaviors and surface integrity of ag-tin soft solid lubricating films on titanium alloy. *Applied Surface Science*, *488*, 269–276. https://doi.org/10.1016/j.apsusc.2019.05.269

[69] Sousa, V. F. C., Silva, F. J. G., Alexandre, R., Fecheira, J. S., & Silva, F. P. N. (2021). Study of the wear behaviour of Tialsin and TiAlN PVD coated tools on milling operations of pre-hardened Tool Steel. *Wear*, *476*, 203695. https://doi.org/10.1016/j.wear.2021.203695

[70] Jones, J. G., & Zhou, D. M. (1994). A first look at Biosensors. *Biotechnology Advances*, *12*(4), 693–701. https://doi.org/10.1016/0734-9750(94)90011-6

[71] Naresh, V., & Lee, N. (2021). A review on biosensors and recent development of nanostructured materials-enabled biosensors. *Sensors*, *21*(4), 1109. https://doi.org/10.3390/s21041109

[72] Kawamura, A., Miyata, T. Biosensors. (2016). *Biomaterials nanoarchitectonics (Ed)*. Elsevier Science.

[73] Lopes, C. J. R. (2018). *Development of Ti-based intermetallic thin films for enhanced biomedical sensing performance* (thesis).

[74] Urban, G., Jobst, G., Kohl, F., Jachimowicz, A., Olcaytug, F., Tilado, O., Goiser, P., Nauer, G., Pittner, F., Schalkhammer, T., & Mann-Buxbaum, E. (1991). Miniaturized thin-film biosensors using covalently immobilized glucose oxidase. *Biosensors and Bioelectronics*, *6*(7), 555–562. https://doi.org/10.1016/0956-5663(91)80019-t

[75] Tvarozek, V., Hianik, T., Novotny, I., Rehacek, V., Ziegler, W., Ivanic, R., & Andel, M. (1998). Thin films in biosensors. *Vacuum*, *50*(3-4), 251–262. https://doi.org/10.1016/s0042-207x(98)00050-5

[76] Narayan, R. J. (2005). Nanostructured diamondlike carbon thin films for medical applications. *Materials Science and Engineering: C*, *25*(3), 405–416. https://doi.org/10.1016/j.msec.2005.01.026

[77] Prakash, S., Chakrabarty, T., Singh, A. K., & Shahi, V. K. (2013). Polymer thin films embedded with metal nanoparticles for electrochemical biosensors applications. *Biosensors and Bioelectronics*, *41*, 43–53. https://doi.org/10.1016/j.bios.2012.09.031

[78] Shul'ga, A. A., Strikha, V. I., Patskovsky, S. V., Dzydevich, S. V., El'skaya, A. V., Soldatkin, A. P., & Bubryak, O. A. (1992). Thin-film conductometric biosensors for glucose and urea determination. *Biosensors '92 Proceedings*, 81–88. https://doi.org/10.1016/b978-1-85617-161-8.50016-1

[79] Qiu, G., Ng, S. P., & Wu, C.-M. L. (2018). Label-free surface plasmon resonance biosensing with titanium nitride thin film. *Biosensors and Bioelectronics*, *106*, 129–135. https://doi.org/10.1016/j.bios.2018.02.006

[80] Dominik, M., Leśniewski, A., Janczuk, M., Niedziółka-Jönsson, J., Hołdyński, M., Wachnicki, Ł., Godlewski, M., Bock, W. J., & Śmietana, M. (2017). Titanium oxide thin films obtained with physical and chemical vapour deposition methods for optical biosensing purposes. *Biosensors and Bioelectronics*, *93*, 102–109. https://doi.org/10.1016/j.bios.2016.09.079

[81] Gordin, D. M., Gloriant, T., Chane-Pane, V., Busardo, D., Mitran, V., Höche, D., Vasilescu, C., Drob, S. I., & Cimpean, A. (2012). Surface characterization and biocompatibility of titanium alloys implanted with nitrogen by Hardion+ Technology. *Journal of Materials Science: Materials in Medicine*. https://doi.org/10.1007/s10856-012-4750-z

[82] Caballero, D., Pla-Roca, M., Bessueille, F., Mills, C. A., Samitier, J., & Errachid, A. (2006). Atomic Force Microscopy Characterization of a microcontact printed, self-assembled thiol monolayer for use in biosensors. *Analytical Letters*, *39*(8), 1721–1734. https://doi.org/10.1080/00032710600714014

[83] Etiemble, A., Lopes, C., Nkou Bouala, G. I., Borges, J., Malchère, A., Langlois, C., Vaz, F., & Steyer, P. (2019). Fracture resistance of ti-ag thin films deposited on polymeric substrates for biosignal acquisition applications. *Surface and Coatings Technology*, *358*, 646–653. https://doi.org/10.1016/j.surfcoat.2018.11.078

[84] Bouzakis, K.-D., Asimakopoulos, A., Skordaris, G., Pavlidou, E., & Erkens, G. (2007). The inclined impact test: A novel method for the quantification of the adhesion properties of PVD films. *Wear*, *262*(11-12), 1471–1478. doi: 10.1016/j.wear.2007.01.027

[85] Kondo, I., Yoneyama, T., Kondo, K., Takenaka, O., & Kinbara, A. (1992). Effects of different pretreatments on the surface structure of silicon and the adhesion of metal films. *Journal of Vacuum Science & Technology A: Vacuum, Surfaces, and Films*, *10*(5), 3166–3170. doi: 10.1116/1.577837

[86] Bouzakis, K.-D., Anastopoulos, J., Asimakopoulos, A., Michailidis, N., & Erkens, G. (2006). Wear development of cemented carbide inserts coated with mono and multilayer PVD films, considering their strength properties, adhesion and the cutting loads. *Surface and Coatings Technology*, *201*(7), 4395–4400. doi: 10.1016/j.surfcoat.2006.08.052

[87] Lugscheider, E., Bärwulf, S., Riester, M., & Hilgers, H. (1999). Magnetron sputtered titanium nitride thin films on thermoplastic polymers. *Surface and Coatings Technology, 116-119*, 1172–1178. doi: 10.1016/s0257-8972(99)00157-7

[88] Raman, K., Kiran, M., Ramamurty, U., & Rao, G. M. (2012). Structure and mechanical properties of TiC films deposited using combination of pulsed DC and normal DC magnetron co-sputtering. *Applied Surface Science, 258*(22), 8629-8635. doi:10.1016/j.apsusc.2012.05.064

[89] Ewald, A., Glückermann, S. K., Thull, R., & Gbureck, U. (2006). Antimicrobial titanium/silver PVD coatings on titanium. *BioMedical Engineering OnLine, 5*(1). doi:10.1186/1475-925x-5-22

[90] Rebholz, C., Leyland, A., Matthews, A., Charitidis, C., Logothetidis, S., & Schneider, D. (2006). Correlation of elastic modulus, hardness and density for sputtered TiAlBN thin films. *Thin Solid Films, 514*(1-2), 81-86. doi:10.1016/j.tsf.2006.02.038

[91] Bemporad, E., Pecchio, C., Rossi, S. D., & Carassiti, F. (2001). Characterization and hardness modelling of alternate TIN/TICN multilayer cathodic arc PVD coating on tool steel. *Surface and Coatings Technology, 146-147*, 363-370. doi:10.1016/s0257-8972(01)01416-5

[92] Korsunsky, A. M., & Constantinescu, A. (2006). Work of indentation approach to the analysis of hardness and modulus of thin coatings. *Materials Science and Engineering: A, 423*(1-2), 28-35. doi:10.1016/j.msea.2005.09.126

[93] Buckle, H. (1971). *The science of Hardness Testing and its Research Applications* (J. Westbrook & H. Conrad, Eds.). Erscheinungsort nicht ermittelbar: American Society for Metals. 453

[94] Martínez-Martínez, D., López-Cartes, C., Fernández, A., & Sánchez-López, J. C. (2009). Influence of the microstructure on the mechanical and tribological behavior of TIC/A-C

nanocomposite coatings. *Thin Solid Films*, *517*(5), 1662–1671. https://doi.org/10.1016/j.tsf.2008.09.091

[95] Kontomaris, S. V., Stylianou, A., Malamou, A., & Nikita, K. S. (2018). An alternative approach for the young's modulus determination of biological samples regarding AFM indentation experiments. *Materials Research Express*, *6*(2), 025407. https://doi.org/10.1088/2053-1591/aaef10

[96] El-Sherbiny, M., & Salem, F. (1986). Tribological Properties of PVD Silver Films. *A S L E Transactions*, *29*(2), 223–228. doi: 10.1080/05698198608981681

[97] Chang, C., & Yang, F. (2018). Effect of target composition on the microstructural, mechanical, and corrosion properties of TiAlN thin films deposited by high-power impulse magnetron sputtering. *Surface and Coatings Technology*, *352*, 330-337. doi:10.1016/j.surfcoat.2018.08.023

[98] Andrade, P., Coelho, A., Afonso, C., Contieri, R., Robert, M. H., & Caram, R. (2010). Effects of Composition on Solidification Microstructure of Cast Titanium Alloys. *Materials Science Forum*, *649*, 183-188. doi:10.4028/www.scientific.net/msf.649.183 Sawyer, W. G., & Wahl, K. J. (2008). Accessing Inaccessible Interfaces: In Situ Approaches to Materials Tribology. *MRS Bulletin*, *33*(12), 1145-1150. doi:10.1557/mrs2008.244

[99] Nose, M., Deguchi, Y., Mae, T., Honbo, E., Nagae, T., & Nogi, K. (2003). Influence of sputtering conditions on the structure and properties of Ti–Si–N thin films prepared by r.f.-reactive sputtering. *Surface and Coatings Technology*, *174-175*, 261-265. doi:10.1016/s0257-8972(03)00710-2

[100] Vijgen, R., & Dautzenberg, J. (1995). Mechanical measurement of the residual stress in thin PVD films. *Thin Solid Films*, *270*(1-2), 264-269. doi:10.1016/0040-6090(95)06984-4

[101] Arshi, N., Lu, J., Joo, Y. K., Lee, C. G., Yoon, J. H., & Ahmed, F. (2012). Study on structural, morphological and electrical properties of sputtered titanium nitride films under different argon gas flow. *Materials Chemistry and Physics*, *134*(2-3), 839-844. doi:10.1016/j.matchemphys.2012.03.078

[102] Poncharal, P., Wang, Z. L., Ugarte, D., & de Heer, W. A. (1999). Electrostatic deflections and electromechanical resonances of carbon nanotubes. *Science*, *283*(5407), 1513–1516. https://doi.org/10.1126/science.283.5407.1513

[103] Li, J., Wang, Y., & Ba, D. (2012). Characterization of Semiconductor Surface Conductivity by Using Microscopic Four-Point Probe Technique. *Physics Procedia, 32*, 347-355. doi:10.1016/j.phpro.2012.03.568

[104] Xi, Y., Bai, Y., Gao, K., Pang, X., Yang, H., Yan, L., & Volinsky, A. A. (2018). Residual stress and microstructure effects on mechanical, tribological and electrical properties of TiN coatings on 304 stainless steel. *Ceramics International, 44*(13), 15851-15858. doi:10.1016/j.ceramint.2018.05.266

[105] Myshkin, N., & Kovalev, A. (2018). Adhesion and surface forces in polymer tribology—a review. *Friction*, *6*(2), 143–155. https://doi.org/10.1007/s40544-018-0203-0

[106] Long, M., & Rack, H. J. (1998). Titanium alloys in total joint replacement—A Materials Science Perspective. *Biomaterials*, *19*(18), 1621–1639. https://doi.org/10.1016/s0142-9612(97)00146-4

[107] Kosinskiy, M., Ahmed, S. I., Liu, Y., & Schaefer, J. A. (2012). A compact reciprocating vacuum microtribometer. *Tribology International, 56*, 81-88. doi:10.1016/j.triboint.2012.06.019

[108] Perez Delgado, Y., Bonny, K., De Baets, P., Neis, P. D., Rodriguez Fereira, V., Malek, O., Vleugels, J., & Lauwers, B. (2011). Dry sliding friction and wear response of WC-co hardmetal pairs in linearly reciprocating and rotating contact. *International Journal Sustainable Construction & Design*, *2*(1), 12–18. https://doi.org/10.21825/scad.v2i1.20430

[109] Yang, K., Shi, X., Zhai, W., & Mahmoud Ibrahim, A. M. (2015). Wear rate of a tial matrix composite containing 10 wt% AG predicted using the Newton interpolation method. *RSC Advances*, *5*(82), 67102–67114. https://doi.org/10.1039/c5ra11086f

[110] Barril, S., Mischler, S., & Landolt, D. (2001). Triboelectrochemical investigation of the friction and wear behaviour of tin coatings in a neutral solution. *Tribology International*, *34*(9), 599–608. https://doi.org/10.1016/s0301-679x(01)00052-4

[111] Hua, N., Zhang, X., Liao, Z., Hong, X., Guo, Q., Huang, Y., Ye, X., Chen, W., Zhang, T., Jin, X., Wang, Q., & Liaw, P. K. (2020). Dry wear behavior and mechanism of a Fe-based bulk metallic glass: Description by Hertzian contact calculation and finite-element method simulation. *Journal of Non-Crystalline Solids*, *543*, 120065. https://doi.org/10.1016/j.jnoncrysol.2020.120065

[112] Huang, P., & Yang, Q. (2014). Theory and contents of Frictional Mechanics. *Friction*, *2*(1), 27–39. https://doi.org/10.1007/s40544-013-0034-y

[113] Ayerdi, J. J., Aginagalde, A., Llavori, I., Bonse, J., Spaltmann, D., & Zabala, A. (2021). Ball-on-flat linear reciprocating tests: Critical assessment of wear volume determination methods and suggested improvements for ASTM D7755 standard. *Wear*, *470-471*, 203620. https://doi.org/10.1016/j.wear.2021.203620

[114] E, S. F., Shi, L., Guo, Z. G., & Liu, W. M. (2015). The recent progress of tribological biomaterials. *Biosurface and Biotribology*, *1*(2), 81–97. https://doi.org/10.1016/j.bsbt.2015.06.002

[115] Wang, L., Su, J. F., & Nie, X. (2010). Corrosion and tribological properties and impact fatigue behaviors of tin- and DLC-coated stainless steels in a simulated body fluid environment. *Surface and Coatings Technology*, *205*(5), 1599–1605. https://doi.org/10.1016/j.surfcoat.2010.07.111

[116] Wang, S., Liao, Z., Liu, Y., & Liu, W. (2015). The tribological behaviors of three films coated on biomedical titanium alloy by chemical vapor deposition. *Journal of Materials Engineering and Performance*, *24*(11), 4462–4474. https://doi.org/10.1007/s11665-015-1732-6

[117] Ramos-Saenz, C. R., Sundaram, P. A., & Diffoot-Carlo, N. (2010). Tribological properties of TI-based alloys in a simulated bone–implant interface with Ringer's solution at fretting contacts. *Journal of the Mechanical Behavior of Biomedical Materials*, *3*(8), 549–558. https://doi.org/10.1016/j.jmbbm.2010.06.006

[118] Hall, R. (1997). Friction in hip prostheses. *Biomaterials*, *18*(15), 1017–1026. https://doi.org/10.1016/s0142-9612(97)00034-3

[119] Uwais, Z. A., Hussein, M. A., Samad, M. A., & Al-Aqeeli, N. (2017). Surface modification of metallic biomaterials for better tribological properties: A Review. *Arabian Journal for Science and Engineering*, *42*(11), 4493–4512. https://doi.org/10.1007/s13369-017-2624-x

[120] Geetha, M., Singh, A. K., Asokamani, R., & Gogia, A. K. (2009). TI based biomaterials, the ultimate choice for orthopaedic implants – A Review. *Progress in Materials Science*, *54*(3), 397–425. https://doi.org/10.1016/j.pmatsci.2008.06.004

[121] Kataria, S., Kumar, N., Dash, S., & Tyagi, A. K. (2010). Tribological and deformation behaviour of titanium coating under different sliding contact

[122] Zhou, Y., Li, L., Shao, W., Chen, Z., Wang, S., Xing, X., & Yang, Q. (2020). Mechanical and tribological behaviors of Ti-DLC films deposited on 304 Stainless Steel: Exploration with TI doping from micro to Macro. *Diamond and Related Materials*, *107*, 107870. https://doi.org/10.1016/j.diamond.2020.107870

[123] Zhang, Z., Li, X., Almandoz, E., Fuentes, G. G., & Dong, H. (2017). Sliding friction and wear behaviour of titanium-zirconium-molybdenum (TZM) alloy against al2o3 and SI3N4 balls under several environments and temperatures. *Tribology International*, *110*, 348–357. https://doi.org/10.1016/j.triboint.2016.10.049

[124] Kataria, S., Kumar, N., Dash, S., & Tyagi, A. K. (2010). Tribological and deformation behaviour of titanium coating under different sliding contact

[125] Arya, S. K., Saha, S., Ramirez-Vick, J. E., Gupta, V., Bhansali, S., & Singh, S. P. (2012). Recent advances in zno nanostructures and thin films for biosensor applications: Review. *Analytica Chimica Acta*, *737*, 1–21. https://doi.org/10.1016/j.aca.2012.05.048

[126] Friedrich, K. (2018). Polymer composites for Tribological Applications. *Advanced Industrial and Engineering Polymer Research*, *1*(1), 3–39. https://doi.org/10.1016/j.aiepr.2018.05.001

[127] Teles, F. R. R., & Fonseca, L. P. (2008). Applications of polymers for biomolecule immobilization in electrochemical biosensors. *Materials Science and Engineering: C*, *28*(8), 1530–1543. https://doi.org/10.1016/j.msec.2008.04.010

[128] Hesketh, P. J., Zivanovic, S., Pak, S., Ilic, B., & Clair, L. S. T. et al. (1998). Biosensors and Microfluidic Systems. In B. Bhushan (Ed.), *Tribology Issues and Opportunities In Mems* (Pp. 85–94). Essay, Kluwer Academic Publishers.

[129] Updike, S. J., & Hicks, G. P. (1967). The enzyme electrode. *Nature*, *214*(5092), 986–988. https://doi.org/10.1038/214986a0

[130] Guilbault, G. G., & Tarp, M. (1974). A specific enzyme electrode for urea. *Analytica Chimica Acta*, *73*(2), 355–365. https://doi.org/10.1016/s0003-2670(01)85472-6

[131] Guilbault, G. G., & Lubrano, G. J. (1973). An enzyme electrode for the amperometric determination of glucose. *Analytica Chimica Acta*, *64*(3), 439–455. https://doi.org/10.1016/s0003-2670(01)82476-4

[132] Soto, R. J., Schofield, J. B., Walter, S. E., Malone-Povolny, M. J., & Schoenfisch, M. H. (2016). Design considerations for silica-particle-doped nitric-oxide-releasing polyurethane glucose biosensor membranes. *ACS Sensors*, *2*(1), 140–150. https://doi.org/10.1021/acssensors.6b00623

[133] Marois , Y., & Guidoin, R. (n.d.). Biocompatibility of Polyurethanes. Texas. Retrieved 2013, from https://www.ncbi.nlm.nih.gov/books/NBK6422/.

[134] Ahmadi, Y., & Kim, K.-H. (2020). Functionalization and customization of Polyurethanes for Biosensing Applications: A state-of-the-art review. *TrAC Trends in Analytical Chemistry*, *126*, 115881. https://doi.org/10.1016/j.trac.2020.115881

[135] Wang, N., Burugapalli, K., Song, W., Halls, J., Moussy, F., Ray, A., & Zheng, Y. (2013). Electrospun fibro-porous polyurethane coatings for implantable glucose biosensors. *Biomaterials*, *34*(4), 888–901. https://doi.org/10.1016/j.biomaterials.2012.10.049

[136] Romaskevic, T., Budriene, S., Pielichowski, K., Pielichowski, K. (2006) Application of polyurethane-based materials for immobilization of enzymes and cells: a review, *Chemijia, 17*(4), 74-89.

[137] Stoyanov, P., & Chromik, R. (2017). Scaling effects on materials tribology: From Macro to Micro Scale. *Materials*, *10*(5), 550. https://doi.org/10.3390/ma10050550

[138] Singh, R. A., Pham, D.-C., Kim, J., Yang, S., & Yoon, E.-S. (2009). Bio-inspired dual surface modification to improve tribological properties at small-scale. *Applied Surface Science*, *255*(9), 4821–4828. https://doi.org/10.1016/j.apsusc.2008.12.004

[139] Jacobs, T. D. B., Greiner, C., Wahl, K. J., & Carpick, R. W. (2019). Insights into tribology from in situ nanoscale experiments. *MRS Bulletin*, *44*(06), 478–486. https://doi.org/10.1557/mrs.2019.122

[140] Sawyer, W. G., & Wahl, K. J. (2008). Accessing inaccessible interfaces: *in situ* approaches to materials tribology. *MRS Bulletin*, *33*(12), 1145–1150. https://doi.org/10.1557/mrs2008.244

[141] Gee, M., Kamps, T., Woolliams, P., Nunn, J., & Mingard, K. (2022). In situ real time observation of tribological behaviour of coatings. *Surface and Coatings Technology*, *442*, 128233. https://doi.org/10.1016/j.surfcoat.2022.128233

[142] Heinrichs, J., Olsson, M., & Jacobson, S. (2013). Influence of tool steel microstructure on initial material transfer in metal forming—In situ studies in the SEM. *Wear*, *302*(1-2), 1249-1256. doi:10.1016/j.wear.2013.01.114

[143] Rahaman, M. L., Zhang, L. C., & Ruan, H. H. (2014). Effects of environmental temperature and sliding speed on the tribological behaviour of a ti-based metallic glass. *Intermetallics*, *52*, 36–48. https://doi.org/10.1016/j.intermet.2014.03.011

[144] Manu, B. R., Schroeder, A. M., & Jayatissa, A. H. (2020). Characterization of the effect of moisture on tribology of titanium rubbed against different pin materials. *Chemical Science International Journal*, 1–10. https://doi.org/10.9734/csji/2020/v29i230158

[145] Gilmore, R., & Hauert, R. (2001). Control of the tribological moisture sensitivity of diamond-like carbon films by alloying with F, ti or si. *Thin Solid Films*, *398-399*, 199–204. https://doi.org/10.1016/s0040-6090(01)01437-7

[146] Yoon, S., Kang, M., Kwon, S., & Kim, K. H. (2002). The influence of counterface materials and humidity on the tribological behavior of arc ion plated TiN films. *Surface and Coatings Technology, 157*(2-3), 144-150. doi:10.1016/s0257-8972(02)00145-7

[147] Wang, Q., Tu, J., Zhang, S., Lai, D., Peng, S., & Gu, B. (2006). Effect of AG content on microstructure and tribological performance of WS2–Ag Composite Films. *Surface and Coatings Technology*, *201*(3-4), 1666–1670. https://doi.org/10.1016/j.surfcoat.2006.02.039

[148] Briscoe, B. J., & Sinha, S. K. (2014). Tribology of polymeric solids and their composites. *Wear - Materials, Mechanisms and Practice*, 223–267. https://doi.org/10.1002/9780470017029.ch10

[149] Cohen, S. C. & Tabur, D. (1996). The friction and lubrication of polymers. *Proceedings of the Royal Society of London. Series A. Mathematical and Physical Sciences, 291*(1425), 186–207. https://doi.org/10.1098/rspa.1966.0088

[150] Khun, N. W., & Liu, E. (2012). Tribological behavior of polyurethane immersed in acidic solution. *Tribology Transactions*, *55*(4), 401–408. https://doi.org/10.1080/10402004.2012.656881

[151] Kosinskiy, M., Ahmed, S. I., Liu, Y., Schaefer, J.A., (2012) A compact reciprocating vacuum microtribometer. *Tribology International, 56*, 81-88. doi:10.1016/j.triboint.2012.06.019

[152] Kumar, D. D., Kumar, N., Kalaiselvam, S., Dash, S., Jayavel, R., (2015) Micro-tribo-mechanical properties of nanocrystalline TiN thin films for small scale device applications, *Tribology International, 88*, 25-30. doi:10.1016/j.triboint.2015.02.031.

[153] Achanta, S., Liskiewicz, T., Drees, D., & Celis, J.-P. (2009). Friction mechanisms at the micro-scale. *Tribology International*, *42*(11-12), 1792–1799. https://doi.org/10.1016/j.triboint.2009.04.018

[154] Heinrichs, J., Olsson, M., Jenei, I. Z., & Jacobson, S. (2014). Transfer of titanium in sliding contacts—new discoveries and insights revealed by in situ studies in the sem. *Wear*, *315*(1-2), 87–94. https://doi.org/10.1016/j.wear.2014.04.006

[155] Michler, J., Rabe, R., Bucaille, J.-L., Moser, B., Schwaller, P., & Breguet, J.-M. (2005). Investigation of wear mechanisms through in situ observation during microscratching

inside the scanning electron microscope. *Wear*, *259*(1-6), 18–26. https://doi.org/10.1016/j.wear.2005.02.111

[156] Heinrichs, J., Olsson, M., & Jacobson, S. (2012). New understanding of the initiation of material transfer and transfer layer build-up in metal forming—in situ studies in the sem. *Wear*, *292-293*, 61–73. https://doi.org/10.1016/j.wear.2012.05.032

[157] Heinrichs, J., Olsson, M., & Jacobson, S. (2012). Mechanisms of material transfer studied in situ in the sem: *Wear*, *292-293*, 49–60. https://doi.org/10.1016/j.wear.2012.05.033

[158] Gee, M., Kamps, T., Woolliams, P., Nunn, J., & Mingard, K. (2022). In situ real time observation of tribological behaviour of coatings. *Surface and Coatings Technology*, *442*, 128233. https://doi.org/10.1016/j.surfcoat.2022.128233

[159] Chen, C., Xue, P., Fan, X, Wang C., & Diao, D. (2018) Friction-induced rapid restructuring of graphene nanocrystallite cap layer at sliding surfaces: Short run-in period. *Carbon*, *130*, 215–221. https://doi.org/10.1016/j.carbon.2018.01.022

[160] Chromik, R.R., Winfrey, A.L., Lüning, J, Nemanich R.J., & Wahl, K.J., (2008) Run-in behavior of Nanocrystalline Diamond Coatings studied by in situ tribometry. *Wear*, *265*(3-4), 477–489. https://doi.org/10.1016/j.wear.2007.11.023

[161] Marino, M.J., Hsiao, E., Chen, Y., Eryilmaz, O.Y., Erdemir, A., & Kim, S. H. (2011) Understanding run-in behavior of diamond-like carbon friction and preventing diamond-like carbon wear in humid air. *Langmuir*, *27*(20), 12702–12708. https://doi.org/10.1021/la202927v

[162] Scharf, T. W., & Singer, I. L., (2009) Role of the transfer film on the friction and wear of metal carbide reinforced amorphous carbon coatings during run-in. *Tribology Letters*, *36*(1), 43–53. https://doi.org/10.1007/s11249-009-9457-z

[163] Michael, J., Prasad, S., Jungk, J., Cordill, M. J., Bammann, D., Battaile, C., Moody, N., Majumdar, B., (2016) Modeling of friction-induced deformation and microstructures, (2016) https://doi.org/10.2172/902880.

[164] Blau, P.J., (2005) On the nature of running-in. *Tribology International*, *38*(11-12), (2005), 1007–1012. https://doi.org/10.1016/j.triboint.2005.07.020

[165] Khonsari, M. M., Ghatrehsamani, S., & Akbarzadeh, S. (2021). On the running-in nature of metallic tribo-components: A Review. *Wear*, *474-475*, 203871. https://doi.org/10.1016/j.wear.2021.203871

3. MATERIALS AND METHODS

The substrates and the films deposited on them were introduced. Then, the analysis techniques were indicated to evaluate the corresponding film properties. In this point, microscopy and spectroscopy methods and tools were explained in addition to the methodologies for the analysis of electrical and mechanical properties. After that, the designed micro-tribometer and the methodology to perform the tribological test as well as to analyse the recorded results were stated in this chapter.

3. MATERIALS AND METHODS

The objective of this chapter is to describe the different materials that were investigated and the specific methods used for their study. Thin films, substrates, and the counter faces were defined, starting from the deposition process. After that, all the characterization methods for both *in situ* and *post mortem* analysis were used to determine the corresponding properties. Specifically, the thin films deposition process (magnetron sputtering), Microscopy (Scanning electron microscopy, transmission electron microscopy, light microscopy) and other spectroscopy techniques (Rutherford backscattering spectroscopy, X-ray photoelectron spectroscopy) are presented, in addition with X-Ray diffraction (XRD) and non-contact topographical interferometry. Moreover, the *in situ* small scale method which based on a reciprocating ball on disk system to be used for tribological analysis is presented in detail in this chapter.

3.1. Materials

3.1.1. Substrates

Films were deposited on different types of substrates, in relation with their targeted characterization. All the substrates (fused silica, glass and single crystal (100) silicon, NaCl, PET, steel) were prepared firstly by cleaning. Cleaning process was done either by an optical tissue and/or degreasing and rinsing with acetone and ethanol respectively. Even though this pre-cleaning step was varied based on the substrates, all the surfaces for each type of substrate were activated with Ar plasma. The “Zepto” plasma system was used (by Diener Electronic) which was equipped with a 40 kHz/100W generator with a 2.6 liters chamber volume. The power used was 90W under 80 Pa pressure. While fused silica and silicon substrates were designed for micro-mechanical deformation test (e.g. nanoindentation), silicon substrates were also used for the cross-section and density analysis of the films. Also fused silica substrates were specifically designed for high temperature analysis since they are heat resistant. Moreover, thanks to the solubility of NaCl in water, these were designed to extract the film over them easily to transfer onto TEM grids. Furthermore, while glass substrates were used for electrical measurements thanks to their insulative character, PET and steel substrates were prepared in specific dimensions to be used for tribological test. Here the surface state of steel substrates was considered to achieve high adhesion. Also, PET substrates were prepared to be used for

tribo-testing since PET is a commonly used material for biosensors. The characteristics of substrates used during analysis were indicated in detail below:

- Amorphous Insulating substrates

Rounded-shape fused silica specimens in 1 cm diameter were bought from Neyco company. They are transparent and resistant to high temperature. They were aimed to be used for XRD and XPS analyses. Other glass substrates are actually the materials which can be used as lames for analysis in optical microscope from labbox LBG company.They were prepared in different shapes and sizes were also used as substrates of Ti-Ag films to be tested for their electrical resistivity.

- Crystalline substrates

Silicon wafers are very commonly used substrates for the characterization of films prepared by Physical Vapor Deposition (PVD) processes. In the current work, they were used for microstructural characterization of top surface and cross-section of these films. These substrates were prepared also in various sizes and shapes as they were cut from a bigger wafer disc with a diamond tip pen.

Observation of films by transmission electron microscopy (TEM) requires very thin self-standing films. The easiest way to obtain such specimen is to deposit film directly on a NaCl single-crystal, which is then dissolved in deionized water, and transferred onto a TEM grid. The 1*1*10 cm^3 sodium chloride block samples are provided by Oxford Instruments SAS and they need to be cleaved before deposition.

- Substrates for the tribological study

Two types of substrate were used to represent the two families of contact considered: a hard contact, involving a steel-ceramic coated mild steel (12*50*2 mm^3) system on the one hand, and a soft contact with a soft ball rubbing onto a polyethylene terephthalate (PET) (12*50*2 mm^3) flat covered by a soft metallic film. For a homogeneity purpose and prior to deposition, mild steel (36CrNiMo16) was first mirror-polished, then cleaned with acetone and ethanol in ultrasonic bath for 10 minutes. For the polishing process, an automatic procedure was adopted on a Struers RotoPol-11 machine where the grinding paper or polishing tissues were placed while the samples to be polished were fixed on the Struers RotoForce-1 upper part. Polishing

process was started first with an abrasive grinding paper with 15 N of normal load and 300 rpm rotation speed for 8 minutes. For this step, de-ionized water was used for lubrication. Then finer polishing tissues were used (15 N load, 150 rpm, 4 minutes for each) with a 3 µm diamond particle solution and aerosol solution as lubricant.

For PET, initial surface state was good, and was only cleaned with heptane in ultrasonic bath (10 minutes).

- The counter-face

Two types of balls were used in the PhD, to mimic either a hard, or soft contact. Their diameter is 10 mm. However, upper part of the balls remains above of the sliding arm and this was causing a limitation to decrease working distance inside SEM chamber. Thus, they were cut by electro-erosion process or with a blade for polymeric balls to obtain a better resolution.

Steel balls (100Cr6) were produced by CIMAP company. Their hardness value is 210 GPa. And the roughness (Ra) is 0.02 µm. Before each test, balls were cleaned in ultrasonic bath with acetone and ethanol (10 minutes).

Polyurethane balls were used to mimic the friction occurring for soft stresses, since it is a proper material to be used for a biosensor in contact with the skin [1]. These balls were produced by Marteau & Lemaire company, and their Young's modulus is 360 MPa. Balls were cleaned in ultrasonic bath with heptane for 10 minutes before tests.

3.1.2. Thin Films

In order to investigate the reliability of our tribometer, different types of representative surfaces were tested. In this sense, several films, hard (ceramic-based) and soft (metallic-based), were deposited by PVD process.

3.1.2.1 TiN films

TiN films (2.3 µm thickness) were deposited onto mild steel substrates by cathodic arc (a Physical Vapor Deposition technique) by Ionbond company. These films were used for the preliminary tests to examine their tribological behavior in various environmental conditions, and to determine the protocol of coupling the tribometer with SEM. The characterization of the films has already been done by Mendibe et *al.* [2].

3.1.2.2 Ti-Ag films

Metallic Ti reference and Ti-Ag films with various Ag contents were deposited on different substrates *via* magnetron sputtering physical vapor deposition process. Their thickness was about 1 µm, except for the films deposited on NaCl substrates, for which the thickness was about 100 nanometers, in order to be suitable to perform TEM characterization. Anyway, their morphology, crystalline structure and overall response was the same as for the thicker ones. Two series of films were prepared in the University of Minho (Portugal). For the first series, the films were deposited directly of the substrates, while for the second one, a 100 nm-thick interlayer of the same composition of the film itself was added before the deposition of the main layer.

The Ti-Ag films were deposited by the magnetron sputtering (another Physical Vapor Deposition technique). Such a process is well-adapted for all types of thin films: metals, semiconductors and insulators. It provides an easy control of the deposition parameters, even for large surface areas, in addition to a good adhesion to most of the substrates normally used to coat. It can also provide the deposition of films with relatively high deposition rates, and alsp for low temperature with reduced surface defects.

The principle of magnetron sputtering PVD process is based on placing a closed magnetic field as parallel to the target to be deposited. With such a magnetic field, Ar^+ plasma is confined on the target surface, enhancing the ballistic effect of ions. With increasing ion density and energy, high sputtering rates are achieved from the target to substrates [3].

In this study, we used the deposition system from the Universidade do Minho - Physics department. The device is a custom-made chamber and the substrates were coated via DC magnetron sputtering inside this chamber.

The system is operated with a pumping system to provide high vacuum and thus allowing to deposit low-contaminated coatings. The reactor (a cylindrical stainless-steel chamber with a capacity of 60 dm^3, shown in Figure 3.1) is pumped by a turbomolecular pump, Adixen/Alcatel, model ATP 400 (pumping speed of 400 L/s), backed by a primary rotary pump AEG, model AMME 80ZCA4, in order to reach a base pressure before deposition, below 2.0 $x10^{-4}$ Pa. The operation pressure is measured by a Pfeiffer Vacuum pressure gauge, model Compact Full Range TM Gauge.

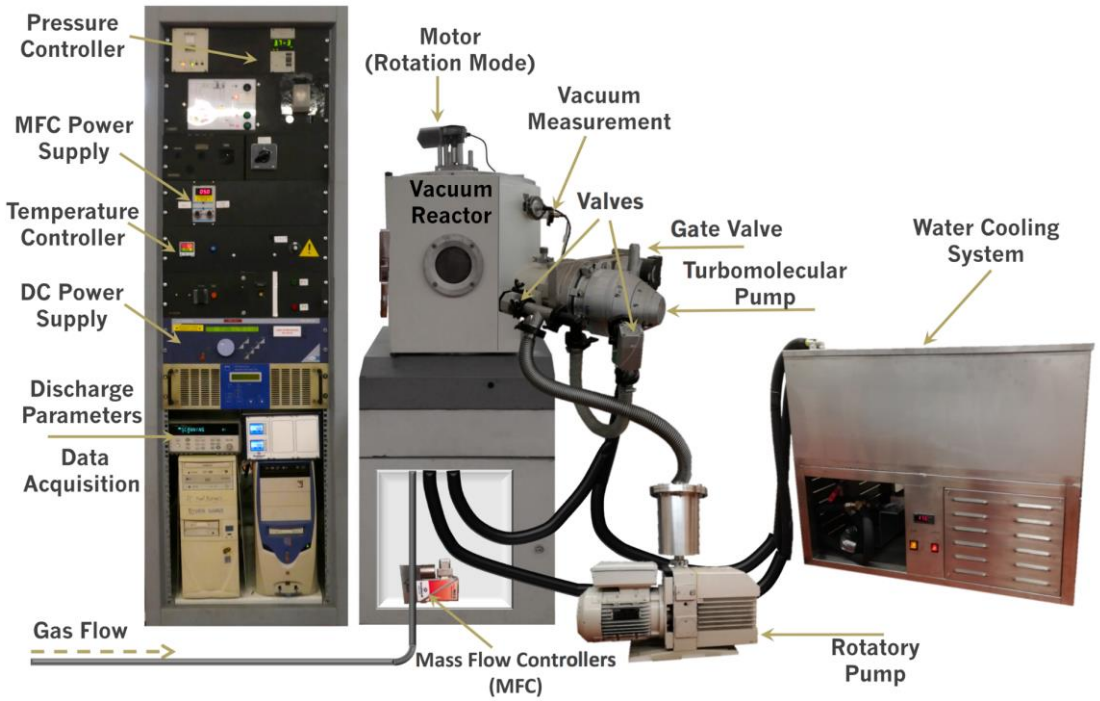

Figure 3.1: Custom-made deposition system used in the preparation of the Ti-Ag thin films.

The base pressure for the chamber has to be 10^{-6} mbar to deposit the films by avoiding any contamination. The chamber reaches this vacuum level in about 5-6 hours. The target is placed 7 cm away and parallel to the rotating substrate holder. The substrate holder has a hexagonal shape, composed of 6 rectangles to achieve a homogenous sputtering. Each rectangular face has a 100 cm^2 useful area, so the total deposition area is 600 cm^2. The rotation speed of the substrate holder can be modified according to the aimed thickness of the film and the deposition efficiency of the target. Reactive gases (oxygen, nitrogen, etc.) can be inserted inside the chamber if oxide- or nitride-based films are aimed to be deposited. Otherwise, only argon (working gas) is inserted to the chamber in order to sputter the target. Prior to the depositions, it is needed to clean the target to avoid any substrates surface contaminations and to create some micro-defects that will promote the enhancement of coating adhesion to the different substrates. For the target cleaning, a short pre-sputtering is done until the monitored voltage of the system becomes stable. Then, the substrate holder is placed inside the chamber, fixed, and the deposition starts.

In addition to the mechanical and chemical polishing, an ultimate plasma cleaning of substrates was applied in the PVD reactor after initial pumping. This cleaning process was performed

during 5 minutes with oxygen, 5 minutes with Ar (both at 0.8-1 mbar and 1.5 A current). The film thickness was targeted as 1 µm, and by considering the deposition rates, the deposition times for each composition were calculated (Table 3.1). First the prepared target and then the substrates were placed on the hexagonal substrate-holder, using double-sided kapton adhesive tape, fixed inside the PVD chamber (Figure 3.2).

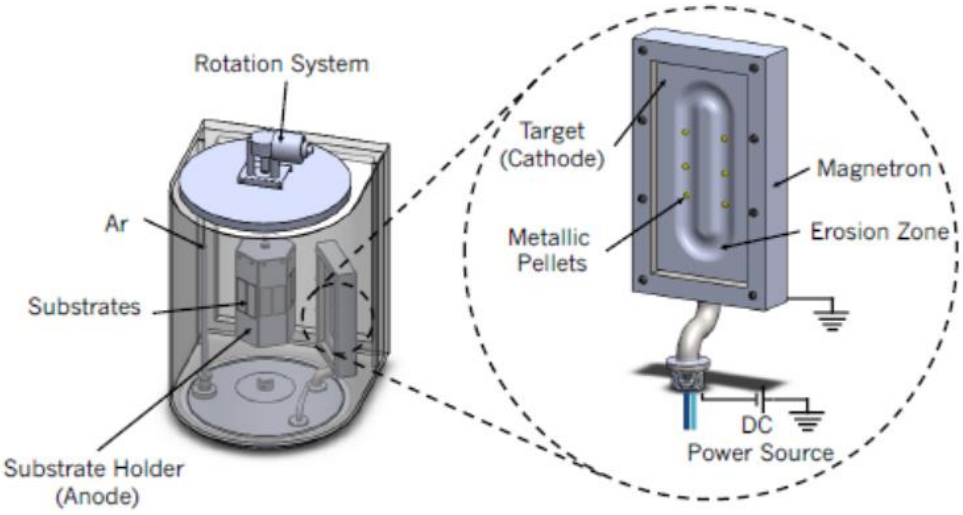

Figure 3.2: Detail of the vacuum chamber interior. Ag pellets were symmetrically distributed in the preferential erosion zone (racetrack) of the Ti target [4].

The Ti target was modified with different amounts of cylindrical Ag pellets (individual areas of about 16 mm^2). symmetrically distributed along its preferential erosion zone (glued with conductive silver paint), in order to change the amount of Ag in the coatings (Figure 3.3).

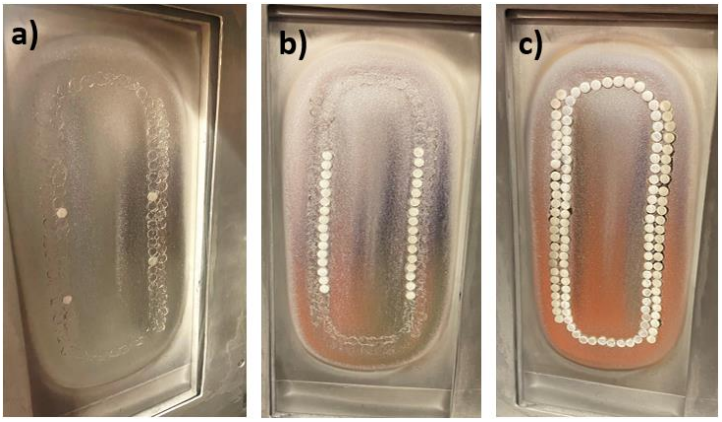

Figure 3.3: Targets with Ag pellets for deposition of different Ti-Ag film compositions: a) ~10-15%Ag expected, b) ~20-25%Ag expected, c) ~70-75%Ag expected

It is then expected that the resulting silver content in the film should reflect the Ti/Ag area ratio [5]. It was aimed to obtain four different film compositions, a pure titanium sample and three Ti-Ag film compositions, with various Ag contents (from low to high). Thus, it was decided to deposit the films first with pure Ti-target, and then by inserting 4, 32 and 120 Ag pellets on Ti-target by using a silver paint.

Table 3.1: Deposition process parameters for Ti-Ag films

Number of Ag pellets on Ti target	Deposition time (min)	Working pressure (mbar)	Working Potential (V)
0	85	$3.9*10^{-3}$	381
4	75	$3.6*10^{-3}$	352
32	55	$3.7*10^{-3}$	411
120	30	$3.3*10^{-3}$	426

Since some delamination problems occurred for the films deposited in a first series, the deposition of a 100nm-thick interlayer before depositing the 1 µm film was decided to enhance the adhesion strength of the coatings. For this second series, the chamber was pumped and plasma etching was performed. After the interlayer deposition, a second plasma treatment was performed to enhance the adhesion of the film (Figure 3.4).

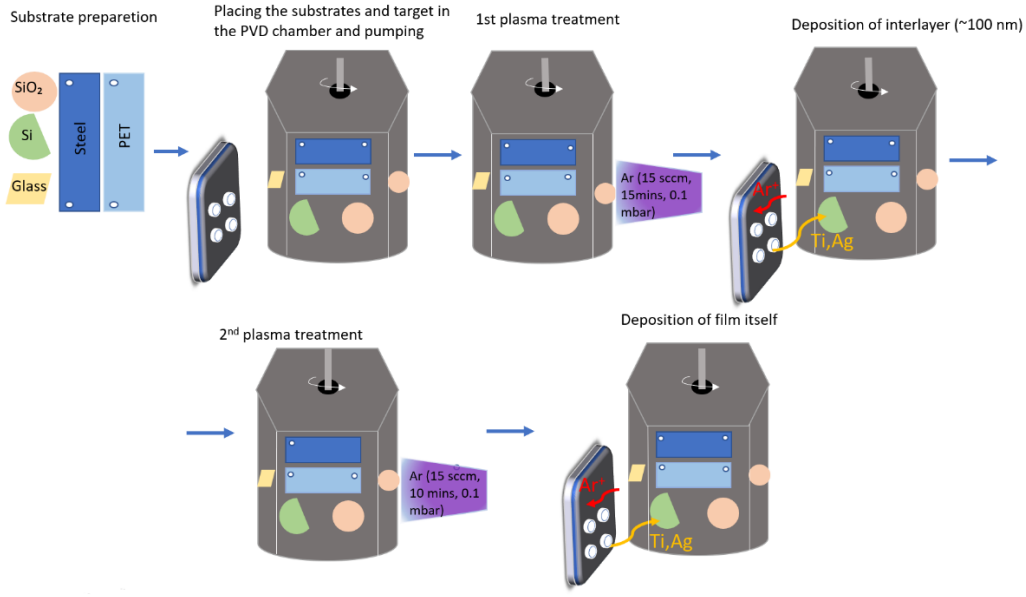

Figure 3.4: Schematic representation of deposition process with interlayer involving two plasma etching steps

The first series of films without interlayer was deposited with an Ar flow rate of 25 sccm (standard cubic centimeter per minute), corresponding to working pressure of about 3.10^{-3} mbar. A 1.5 A current was applied trough the DC power supply to the target and a rotation speed of 5 rpm (rotation per minute) of the substrate holder.

For the deposition of second series (with interlayer and double plasma etching), the parameters were kept the same as those used for the deposition of the first series. However, the ~100 nm interlayer was deposited before the deposition of ~1 µm film itself, for each composition. It was decided to deposit the interlayer with the same composition and parameters of the corresponding film itself.

3.2. Characterization methods

3.2.1. Microstructural Characterization

In order to correlate the tribological behaviour of coated flats with their microstructure and chemical nature, a multiscale approach of characterisation was required.

3.2.1.1. Light microscopy

We used a numerical light Keyence digital multi-scan microscope from LaMCoS laboratory, team TMI. It could provide a large-scale analysis in ambient air conditions. With the lens of this optical microscope, the analysis could be performed from x100 to x1000 magnifications. Thanks to its allowed large distance between the optical lens and the sample, the micro-tribometer could be put in this microscope stage. Therefore, the Keyence microscope was used for the preliminary surface analysis of samples, in addition to the *in situ* the analysis of the wear tracks on the samples and *post mortem* investigation of the ball tracks.

3.2.1.2. Scanning Electron Microscopy

The scanning electron microscopy (SEM) provides the analysis and characterization of variety of materials from nanometer to micrometer scale by obtaining 3D-like images in small scale (secondary electron signal). In SEM, the region to be analyzed is irradiated with an electron beam which is accurately focused on this specific area. Types of the signals obtained from this interaction can be secondary and/or back-scattered electrons, characteristic photons and some other photons based on different energies (e.g. Auger). Back-scattered electrons are the beam electrons which escape from the sample as the consequence of multiple elastic scattering, and

give a chemical information. Secondary electrons can be defined as the electrons of the sample which have a low kinetic energy based on inelastic collisions with the electrons of the beam. These signals could provide the characterization of surface topography, and morphology. SEM usually has two main components which are the electron column and the control unit. Electron column has an electron gun with at least two lenses which are effective on the direction of the electrons going down. Generally, below the gun, the pumps are placed to obtain the vacuum in desired levels. Electrons source of the two used microscopes was field emission gun (FEG), leading to high quality signals and good resolution.

Collection of electrons by specific detectors gives key-information about the irradiated sample.

Everhart-Thornley detector (ETD): Developed by Everhart and Thornley in 1960. It is the most commonly used SEM detector to collect secondary electrons (SE), and backscattered electrons (BSE) in a lesser extent. By considering the schema below (Figure 3.5), when the energized electrons hit to the scintillator, the light is emitted and transferred to the photo-multiplier (PM) with total internal reflection inside the light guide (LG). The light-formed signal passes through a quartz glass window and then through the first electrode of PM to be converted back to electrons. These electrons are accelerated to the following electrode in PM and continuously increasing cascade of electrons are produced until they reach the collector for imaging [6].

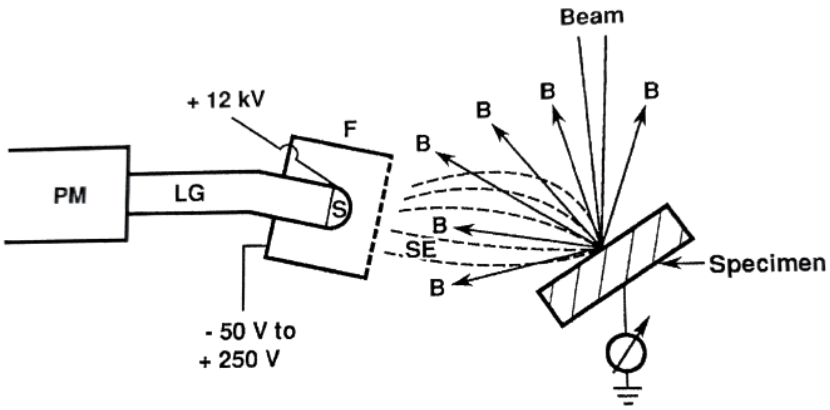

Figure 3.5: Schema of ETD detector [6]

Backscattered electron detector: Backscattered electrons are obtained by elastic scattering. Electrons moves in the primary electron beam and approaches to the nuclei of the atoms of the sample to be analyzed. Regarding the size of the nuclei, the number of backscattered electrons varies and this variation provides the color contrast in the image [7]. It provides to detect the backscattered electrons in high vacuum and low vacuum testing conditions [8].

Our analyses concerned an examination of surfaces either in "conventional" conditions, *i.e.* in high vacuum mode, or under a low controlled pressure of a gas.

- Vacuum characterization by SEM ZEISS Supra Gemini 55 VP

SEM Supra is a FEG scanning electron microscope, which we have used under vacuum. Its Gemini column is well adapted to low conductive, even insulating, materials, and give effective images at low accelerating voltages. It could be operated in secondary electron, back-scattering and in-lens modes and it can be used in the accelerated voltage range between 0.1 kV to 30 kV. Measurements can also be performed under various chamber pressures (2-133 Pa). Official resolution of the microscope is 1 nm at 15 keV and 4 nm at 0.1 keV. The magnification could be modified from x12 to x900000 and the chamber diameter is 270 mm [9] (Figure 3.6a).

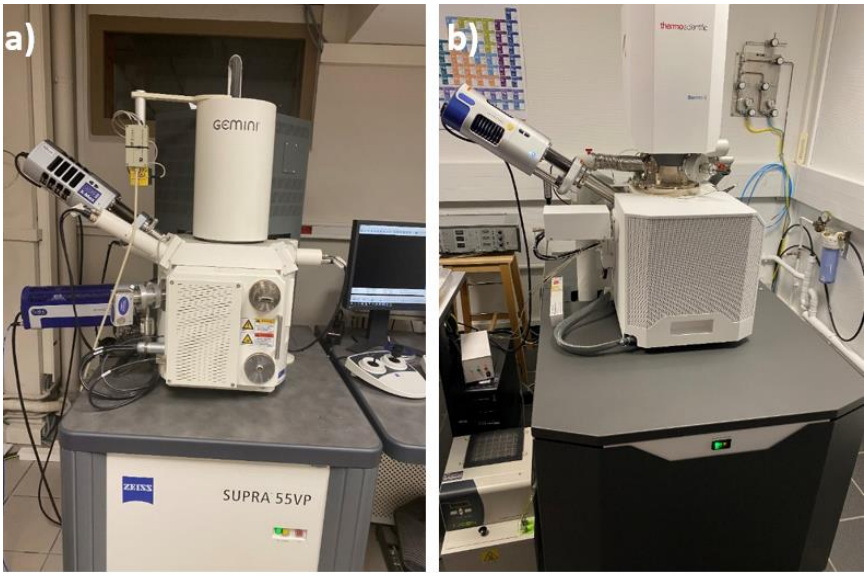

Figure 3.6: a) SEM Supra Gemini 55 VP, b) SEM Quattro by Thermo Fisher scientific

This microscope has been used for the top surface and cross section analysis of all films, in addition to the *post-mortem* wear track EDS analysis of both the coated flats and the. To investigate the cross-sections of samples, they were placed on a special stub for cross-section analysis with a carbon tape after ionic cross section polishing. Similarly, samples for the top surface analysis (for film morphology, wear track and the chemical analysis) were spaced on a standard circular stub with a carbon tape. In order to reduce the charging effect, to analyze the wear track of the poly-urethane balls in SEM Supra, they were covered with aluminum tape from the surroundings and coated with 2.8 nm of carbon layer.

Cross section analysis of thin films is always particularly difficult, owing to adhesion problems, brittleness/softness of the film in comparison to the substrate. In this sense, conventional mechanical preparations are most often inefficient. Therefore, we used a non-contact technic of preparation involving an ion polisher Ilion II^+ from GATAN. This apparatus provides slightly focalized ions of argon with the two guns inside which send Ar^+ ions onto zone of the sample to be polished (Figure 3.7). It is possible to prepare any kind of materials, their top surfaces (*e.g.* prior to EBSD characterization) and cross sections. It also has a cryogenic plate, thereby for sensitive samples, the system could provide the cooling down process during polishing. Rotation speed, voltage, angles of the guns, pressure, time for polishing and temperature can be adjusted.

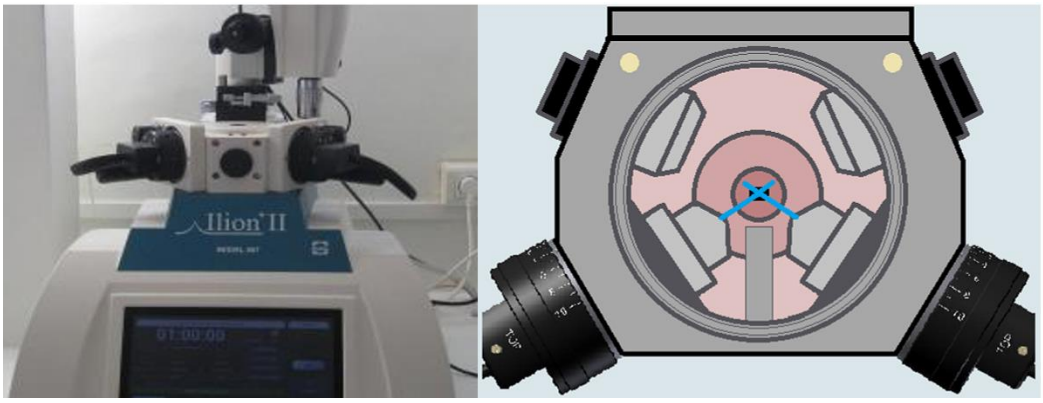

Figure 3.7: Ilion ionic polisher and two argon guns inside the chamber [10]

For the cross-section polishing, titanium masks are used. The sample has to be fixed on the mask with silver paint and the polishing depth is about 500 to 1800 µm depending on the sample [10] (Figure 3.8).

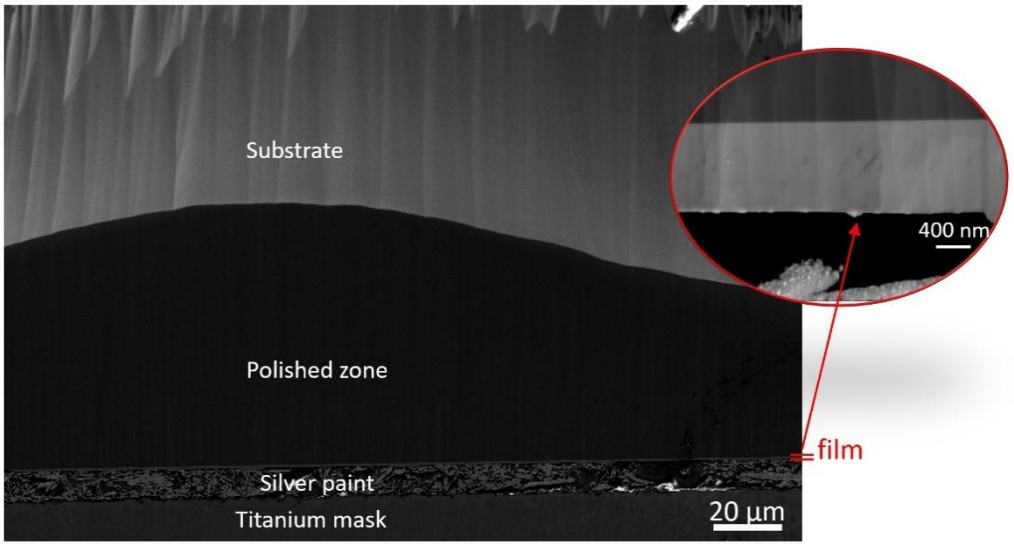

Figure 3.8: Sample cross section after ionic polishing

In our case, films were deposited onto Si wafer. Samples were cut with a diamond tip and then placed on titanium mask with silver paint. The polishing process was taken 4 hours as 3 hours in 5 keV and 1 hour in 3 keV at 3 rpm with 90° wedge at room temperature.

- Environmental characterization by eSEM Thermofisher Quattro

A dedicated electronic column with several compartments allowing different vacuum levels was built, thirty years ago, by the Philips company (now Thermofisher Scientific) (Figure 3.6b) [11]. It allows to work at different atmospheres up to 4700 Pa pressures. Detection is then done through specific detectors.

Low Vacuum Detector (LVD): Low vacuum detector placed in the SEM Quattro by Thermofisher Scientific, collects the signals from SE and BSE up to 200 Pa when the microscope is being operated in low vacuum mode (Figure 3.9a). For higher pressure levels, i.e. in environment mode, a dedicated detector, GSED, is required.

Gaseous Secondary Electron Detector (GSED): In hydrated or auxiliary conditions, this detector could gather only SE signals for the pressure up to 4700 Pa (Figure 3.9b).

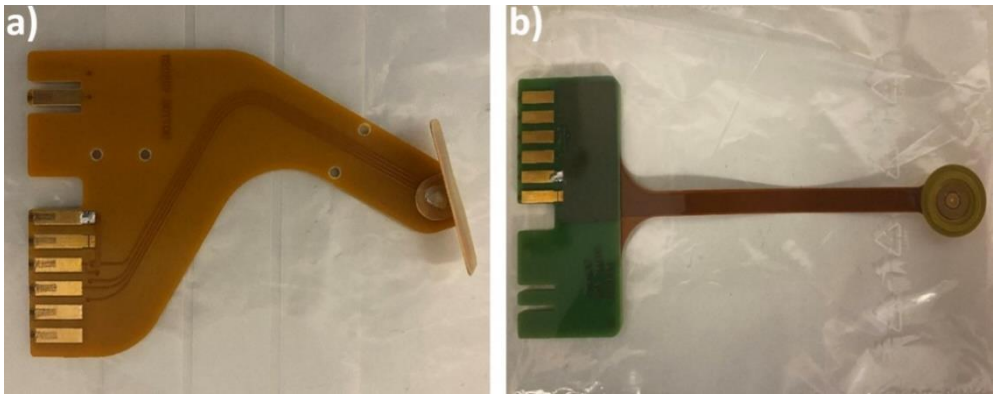

Figure 3.9: a) low vacuum, b) gaseous secondary electron detectors

In this work, SEM-Quattro of CLyM[1] was used for morphological characterization of films and wear debris during *in situ* tribological tests. It is a high-resolution scanning electron microscope which is operable in environmental mode (ESEM) in addition to high and low vacuum modes. The resolution of microscope is 1 nm at high vacuum (10^{-4} Pa), and 1.3 nm at low vacuum and ESEM modes at 30 keV and 3 nm for 1keV at each mode for secondary electrons. Everhart-Thornley detector (ETD) were used for high vacuum tests. Additionally, low vacuum secondary electron detector (LVD) can be used in low vacuum mode. While operating the SEM in low vacuum, the chamber pressure could be increased up to 2600 Pa for H_2O and 4000 Pa for N_2 insertion. Finally, gaseous secondary electron detector (GSED) is needed for the analysis while operating the microscope in ESEM mode. There is a five-axis motorized stage in 110x110 mm^2 and it provides 105° tilting. The sample weight to be tested could be up to 5 kg without tilting. The standard sample holder inside could provide fitting 18 samples with usual circular (Ø 12mm) stubs and the chamber width is 340 mm (Figure 7b). The microscope could provide *in situ* dynamic analysis during the experiments with the ability to modify the chamber pressure, gas nature or temperature [8].

The main purpose of eSEM Quattro was its coupling with the micro-tribometer to perform high resolution small scale *in situ* tribological analysis of the samples as a function of the controlled environment. Several specific media were tested: vacuum, 25% relative humidity (RH), 50% relative RH, 100% RH. To achieve these relative humidity levels, water vapor pressure and temperature were set as indicated in table 3.2.

[1] Clym: Consortium Lyon-Saint Etienne de Microscopie (FED 4092), www.clym.fr

Table 3.2: Environmental conditions for tribo-tests in SEM

Environmental condition	Pressure of chamber (Pa)	Temperature (°C)
High vacuum	10^{-3}	22
25% RH	200	4
50% RH	400.0	4
100% RH	813.3	4

- Focused Ion Beam (FIB)

Ion beams can provide focusing in very small diameters. Thus, with FIB, a piece of material, film or an implant can be removed in a very fine pattern without using any mask or resist as an advantage over lithography. Even though, it is quite a slow process, it helps to prepare thin samples in some nanometers to be analyzed in TEM. FIB system is based on several processes with three main components: ion source, column of ions and the sample displacement plate (Figure 3.10). The source emits ions from a single point and it can be either liquid metal or gaseous field source. However, liquid metal field sources are quite common usually the metal is tungsten. Today, several alloys are being used as the liquid source as well as gallium (Ga). The source is maintained with a sharp needed and the liquid metal gets it wet and flow down while there is a concentric round electrode creating an electric field. The sharper needle tip can provide a stronger electric field and liquid metal can be pulled down with following of emissions of the ions. Then, ion optics column provides the focusing and alignment of the ions to transfer through the sample surface to be exposed to cut with the excitement of electrons in the solid by the ions [12].

In this study, FIB system was used as coupled with SEM as in two columns. While one column is for Gemini 1 FEG SEM NVision 40, Carl Zeiss GmbH microscope, the other one is for SIINT zeta FIB from Seiko Instruments. Ga+ are used for the liquid source in this FIB system. The resolution of FIB is 4 nm at 30 keV and for 0.1 pA. The current range is between 1-45 pA at 3 keV and the accelerating voltage range is 1-30 kEV. Coupling the FIB column with SEM provided to examine the cut and sealing of the materials during the process. InLens detector is used for high resolution analysis. Also, when the SESI secondary electron detector provides to investigate the samples (lamellas) when they are thin enough.

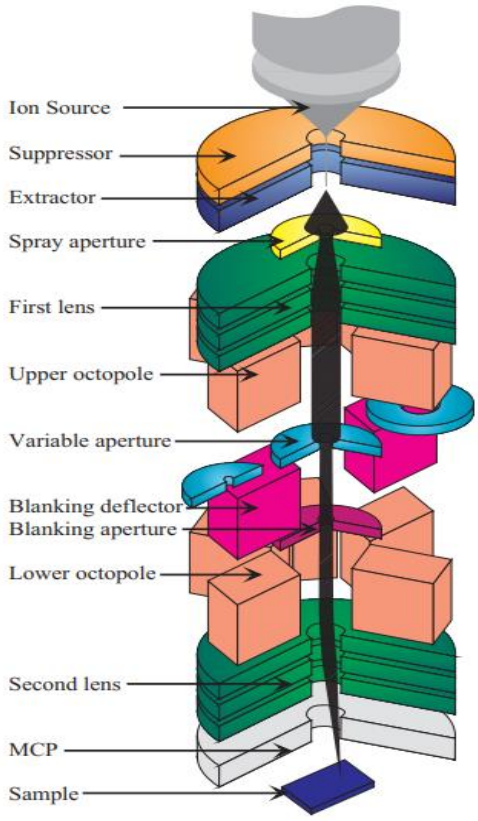

Figure 3.10: Focused ion beam schematics with components [12]

3.2.1.3. Transmission Electron Microscopy

Transmission electron microscopy (TEM) is one of the most efficient instruments for imaging materials at the nanometer-scale, and even beyond. It results from the focusing of the electron beam onto the specific zone of the specimen, which provides the appearing as the transmitted enlarged version of the sample on a fluorescent screen or camera. As many physical techniques, it is based on interaction between the energized electrons and the atoms of the specimen. Here, this high energy for the electrons is in the hundred keV range in the field of material science [13]. TEM can provide a sub-nanometer resolution for a very small-scale measurement. For this microscopy technique, samples have to be very thin to be electron-transparent. In our case, films are isolated from their NaCl substrate by water dissolution, their put on a grid. Grids is placed inside the column of the microscope and with the help of the digital cameras, imaging can be done with focusing, astigmatism correction and all the other settings [15]. Since it is a very high-resolution microscope, it could be used for analyzing the structure, chemistry, and morphology. Finally, the energy resolution could reach 0.01 eV which provides to perform imaging for variety of elements efficiently [16].

In this study, we have used a 200 kV FEG Jeol 2010F TEM of Clym, characterized by a resolution less than 1 Å (Figure 3.11).

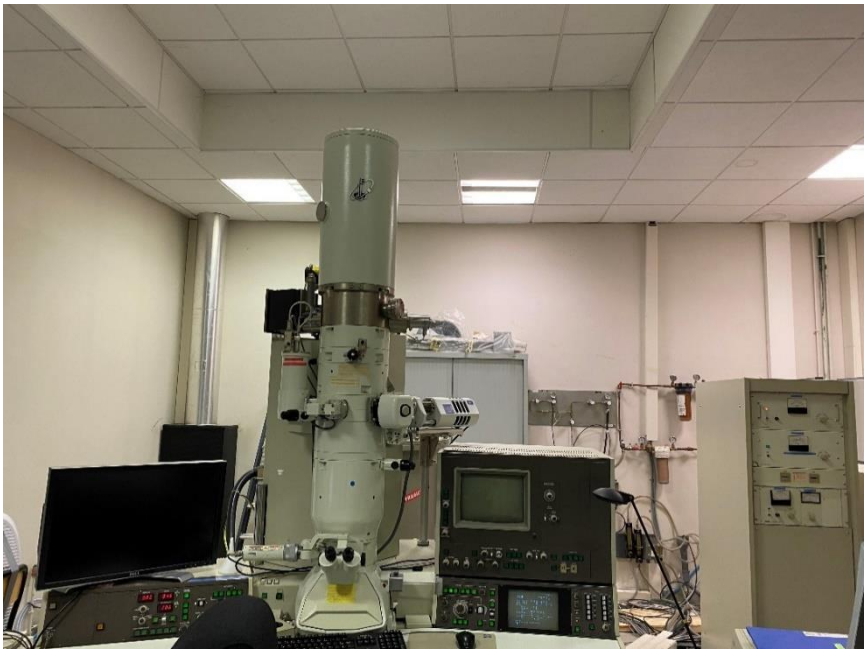

Figure 3.11: Transmission electron Microscope

3.2.2. Chemical characterization

To know the chemical nature of specimens is of prime importance. Its characterization may result from a direct chemical or indirect crystallographic analysis.

3.2.2.1 Energy Dispersive X-Ray Spectrometry

Atoms irradiated by a highly energetic electron beam emit X-photons characteristic of the atom [17]. Using Energy Dispersive X-ray Spectrometer (EDS), we can select and count these photons (for Z higher than 5) leading to the composition of the specimen (film, substrate, debris…).

In this work, Oxford Ultim Max 100 instrument was used as spectrometer. Its detection/recording speed is 1500000 counts per second (cps). However, for the accuracy of composition calculations it is more convenient to select the speed up to 400000 cps. X-ray lines could be identified down to 72 eV and it may provide live chemical imaging with large sensor size (up to 170 mm^2) [18]. Acquisition and interpretation of spectra is allowed by the Aztec software.

The purpose of using the EDS detector was to estimate the film composition for Ti-Ag films in terms of the atomic concentrations of the elements. Additionally, EDS analysis was performed for TiN films and ball counter faces during and after the tribo-tests.

While analyzing the wear tracks of the polymeric balls in SEM, the imagery was affected by charging effects related to the insulating nature of PU. Such undesirable effect is particularly limiting for EDS analyses, involving quite high acceleration voltages. An alternative consists in depositing a very thin layer (~2-3 nm) of carbon on the ball surface to increase its conductivity. This carbon deposition was done using a CCU-010 compact coating unit from Safematic company (Figure 3.12) which can provide very thin layer of coating and it has 10-100 mA current range during coating [19]. The deposition pressure was $4.8x10^{-5}$ torr and the deposition time was about 30 seconds.

Figure 3.12: CCU-010 Compact coating unit for carbon layer deposition

3.2.2.2. X-Ray Photoelectron Spectroscopy

X-Ray Photoelectron spectroscopy (XPS) is another widely preferred technique to do chemical analysis of surfaces. The system is based on irradiation of the surface to be analyzed with X-Rays with a controlled energy, and, in response of this excitation, to investigate the re-emitted electrons' energy. Usually, the photons of the X-rays can penetrate 1-10 µm depth from the sample surface to interact with the atoms of the sample and this causes the electron emission thanks to the photoelectric effect [20].

In this work, a special design XPS instrument developed from Ecole Centrale Lyon was used to perform XPS analysis on Ti-Ag films, which were deposited on SiO_2 and Si substrates (Figure 3.13). The XPS analysis were carried out on a PHI 5000 Versaprobe 2 apparatus from ULVAC-PHI Inc. A monochromatized AlKα source (1486.6 eV) was selected with a spot size of 200 µm. A dual beam (electron and Ar+ ion) charge neutralization system was used to limit the charging of the sample. For Ti-Ag films, spectra of Ag_{3d} and Ti_{2p} regions were obtained using a pass energy of 23.5 eV. All the peaks were fitted with the CasaXOS software using the Shirley background.

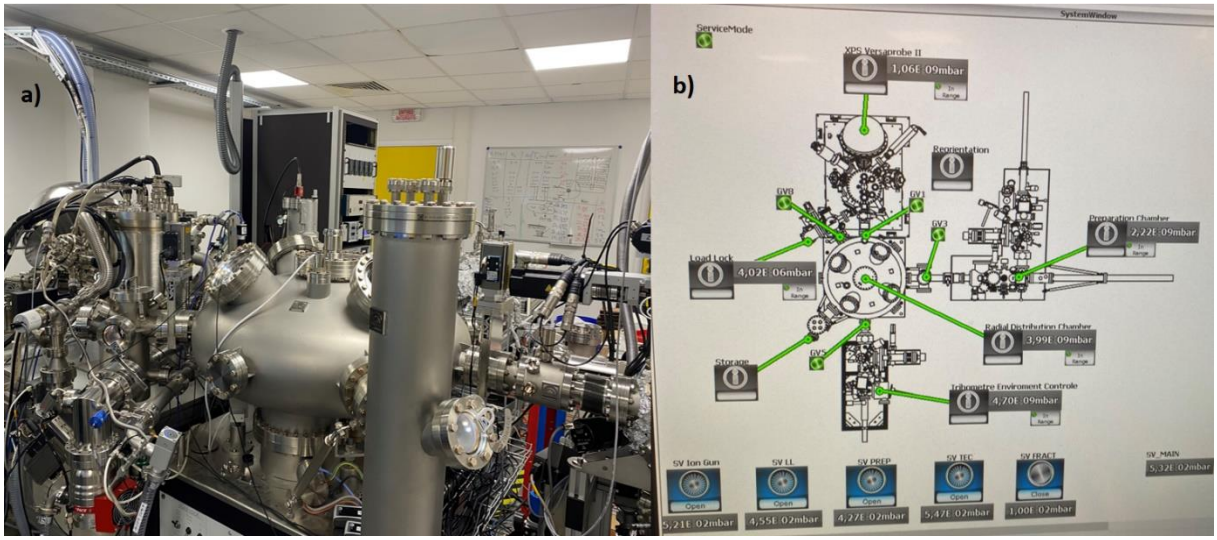

Figure 3.13: a) XPS instrument in Ecole Centrale Lyon, b) Schematic of the placing the samples and pumping mechanism inside the XPS chamber

3.2.2.3. Rutherford Backscattering Spectroscopy

Rutherford backscattering spectroscopy is a non-destructive analysis technique which could provide the examination of densities and chemical compositions of solid surfaces. In this method, charged particles ($^4He^+$) are used to obtain a depth profile of solids with a very high resolution (100-300 Å). The monoenergetic ion beam of $^4He^+$ is provided by an ion accelerator, the target is placed in this ion beam and so α-particle beams interact with the surface of the sample. In this point; some of the ions could be scattered elastically by the atoms of the surface and some others can penetrate into the target to be backscattered at various depths by losing some of their energy (Figure 3.14). These backscattered particles can be analyzed to acquire the Rutherford backscattering energy spectrum. By this spectrum, the nature of the elements which exist in target and their depth distribution could be investigated. As the main advantage

of the RBS, the atomic masses of elements adjacent to the target could be distinguished, so the chemical composition of solids could be identified [21]. Additionally, this spectroscopy technique provides to quantify the density of thin films in terms of area with a very high resolution. It also allows to identify the interdiffusion of elements through the thin film layers even if they have a very low-density contrast [22].

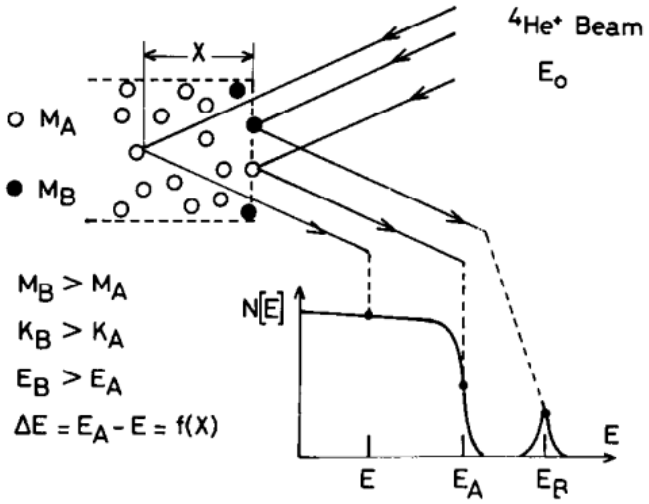

Figure 3.14: Schematic representation of RBS technique [20]

In this work, RBS analysis was performed by C^2TN Institute Superior Técnico Lisboa, to examine the film densities. Since the films have various Ag contents, it was aimed to investigate the role of Ag on the densification of film microstructure.

3.2.2.4. X-Ray Diffraction

X-Ray diffraction method can provide a non-destructive and versatile analysis of many material properties such as crystal structure and phases, chemical composition, and texture for variety of materials in powder form, surface or as bulk solid. Basically, x-rays could be defined as the electromagnetic waves (with wavelength (λ) 0.01-10 nm) or photon beams (with energy= 0.125-125 keV) The wavelength and energy values are proportional with each other. Phases could be defined by correlating the x-ray pattern with a reference database. The reflection positions could be calculated through the Bragg's law (Eq. 1). Here, λ is the wavelength, θ is the Bragg angle (θ_B), d is the interplanar spacing (d_{hkl}) and n is the order of the interference (n=1,2,3…) [23].

$$n\lambda = 2dsin\theta \text{ (Eq. 1) [23]}$$

In this work, it was required to use XRD for the investigation Ti-Ag film compositions. The instrument used for this analysis is θ-θ Bruker XRD D8 Advance system which uses Cu K_a radiation with l=0.1540 nm. The operating voltage of the device is 40 keV and the current used during working is 40mA. The linear detector (LynxEye) collects the data intensity in the determined 2θ range with the desired resolution. The accuracy of the instrument is less than 0.01° for 2θ and it can provide conventional x-ray powder diffraction, analysis of pair distribution function (PDF), small-, wide-angle x-ray scattering [24]. Here, the purpose to use XRD is to examine the intermetallic phases formed between Titanium and silver in the Ti-Ag system.

3.2.3. Mechanical characterization

By considering the substrate effect for thin films, it is often difficult to examine their superficial mechanical properties. Therefore, very small-scale measurements are needed regarding the thickness of the thin film. Nanoindentation is a convenient and easy method to estimate the hardness and Young's modulus of thin films. Usually, Berkovich indenter is used with a sharp diamond tip. It is driven into the film and moved up as loading and unloading respectively (Figure 3.15). The indentation load and displacement length are continuously recorded for hardness and Young's modulus determination.

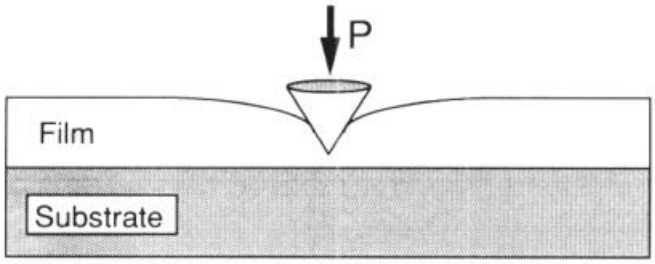

Figure 3.15: Nanoindentation schema [24]

In this study, mechanical properties of the thin films were assessed by nanoindentation by using G200 Aligent nanoindenter with a diamond Berkovich tip. Indents were performed using the continuous stiffness measurement mode with a 100 nm maximal depth (*e.g.* about 10% of the coatings thickness) to avoid substrate effect. The strain rate is 0.05 s^{-1} for 20 indentation tests. Hardness and Young's modulus of the films were calculated using Oliver and Pharr method [25]. Mean hardness and Young's modulus values were computed within the 160-220 nm range of indentation depth.

3.2.4. Electrical characterization

Four-point probe method is one of the most well-known technique for electrical resistivity measurements of surfaces. It was first developed by Wenner in 1916 to measure the resistivity of the earth. Even though it was mostly used by geophysicist those times, today it is widely used in thin film and semiconductor industries. In the classical arrangement, there are linearly placed four need-like electrodes touching to the samples surface (Figure 3.16). The outer two electrodes provide the current injection to the material whereas the inner two electrodes measure the electric potential distribution on the surface of the material. The purpose of using separated 2 electrodes for current supply and electrical potential measurement is avoiding from the showing up of the contact resistance between electrodes and tested material [26].

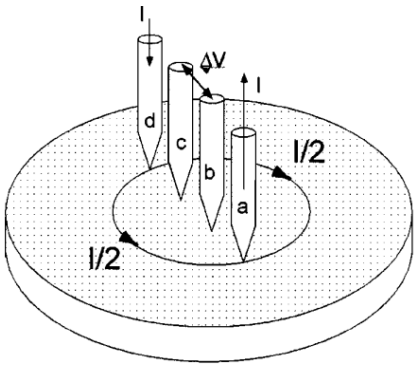

Figure 3.16: Schematic representation of four-point probe method [26]

In this work, electrical resistivity tests were carried out in Universidade do Minho, by Ossila four-point probe device from Sheffield. The probing system is based on spring-loading rather than using needle-like electrodes. The spacing between each electrode is 1.27 mm and their diameter is 0.48 mm. During the tests, 60 g of spring loading was applied to achieve an efficient measurement.

3.3. Tribological Experiments

3.3.1 Laboratory-made Microtribometer

Tribometers are used for the investigation of the friction and wear behaviour of surfaces under dry or lubricated conditions [27]. Nature of the contact is correlated with materials and geometry, the testing parameters such as normal load, stress and sliding speed. Also, the testing environment have a significant role on the tribological behaviour of materials [28].

Conventional tribometers can be classified based on the sliding motion of the tip head: rotational motion and reciprocating tribometers. Also based on the geometry of counter-face, they could be grouped as pin-on-disc or ball-on-disc system [29]. However, in this work, it is aimed to understand the *in situ* small scale tribological response of thin films by considering the effect of environmental conditions. Therefore, rather than a conventional tribometer, it was necessary to design a tribometer which has to be implemented inside the SEM. Additionally, the tribometer had to be operable in different atmospheric conditions (*e.g.* pressure, gas nature, and temperature) to investigate the effect of the environment. Lastly, it was needed to provide dynamic *in situ* examination to analyse the evaluation of the wear behaviour for every single cycle. For all these restrictive reasons, a dedicated laboratory-made mini-tribometer has been developed with the electronic team of MATEIS, based on a reciprocating ball-on-disk system. (Figure 3.17a, 3.17b). Note that the setup was designed to be also used with a Raman spectrometer, by selecting a transparent counter-face.

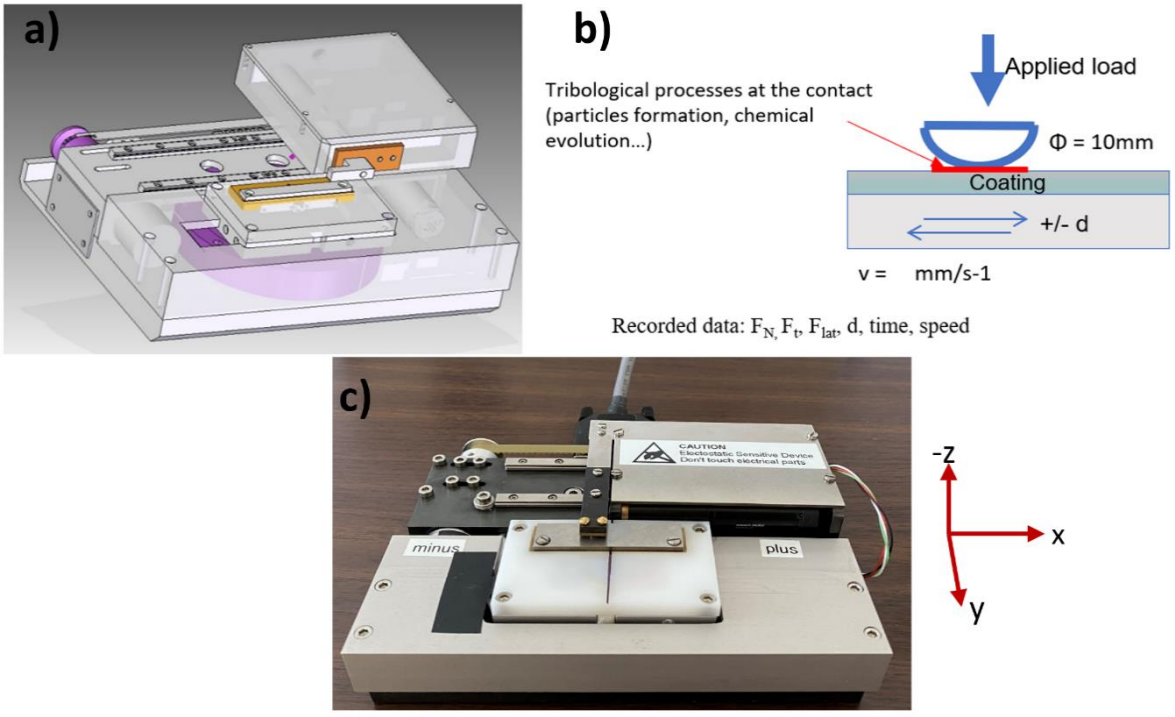

Figure 3.17: The laboratory-made tribometer: a) preliminary schema, b) dynamic of the contact and c) general view

Moreover, the device provides to set and control the system's temperature to the desired value thanks to its temperature sensor and Peltier stages. Such a thermal control combined with the

water pressure of the eSEM, could lead to a good definition of the humidity rate of the contact environment.

From a mechanical viewpoint, there is a 3-axis sensor for measuring the normal (z-axis), tangential (x-axis) and lateral forces (y-axis). Two motors control the position of the counter-face. While the main motor provides the sliding motion along the x-axis, the rotational one controls loading and unloading of the system by moving the sliding arm along the z-axis. 22755 elementary steps correspond to 1 mm for the main motor and 3183 steps correspond to 1° for the rotational one. The ball is inserted into the sliding arm which is placed on the upper part of the micro-tribometer. By reciprocating the arm along x-direction, the counter-face can move over the surface of the sample along ±20 mm. The position for displacement, normal load and all the other parameters are controlled with the home-made software (TRIBOMEB-MATEIS-LaMCoS-INSA Lyon) (Figure 3.18).

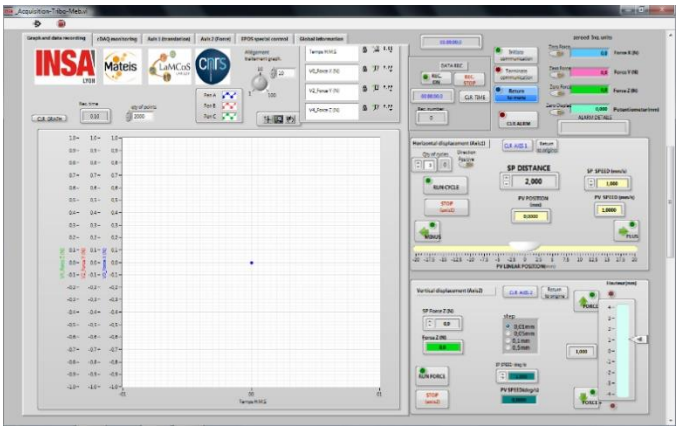

Figure 3.18: Drive and measure page of the TRIBOMEB software

By implementing the tribometer into SEM chamber, small scale dynamic characterizations can be performed. In addition to normal (F_z), tangential (F_x) and lateral force (F_y) values; time, displacement and the number of cycles could also be recorded by the system to obtain more detailed tribological information. The range for the applicable force on x and y axes is from -50N to 50 N while for z-axis the range is from 0N to 50N, and the sliding velocity range is 1-2 mm/s. Moreover, the device can be operated in the temperature range from 0 to 50°C for the tests in ambient air, high and low vacuum conditions. The micro-tribometer is 1.8 kg of weight and its dimensions are 16.4 x 13.3 x 5.0 cm (Figure 3.17c).

One objective of the PhD is to give a multiscale characterization of the friction. Therefore, the tribometer has been designed with the purpose to be adapted to different systems, light microscope as well as SEM.

First of all, the recording process was aimed to investigate in detail. To do that, the recording parameters (sampling rate, segment duration, recording time for segments) were adjusted from the corresponding interface in the software of the micro-tribometer (Figure 3.19).

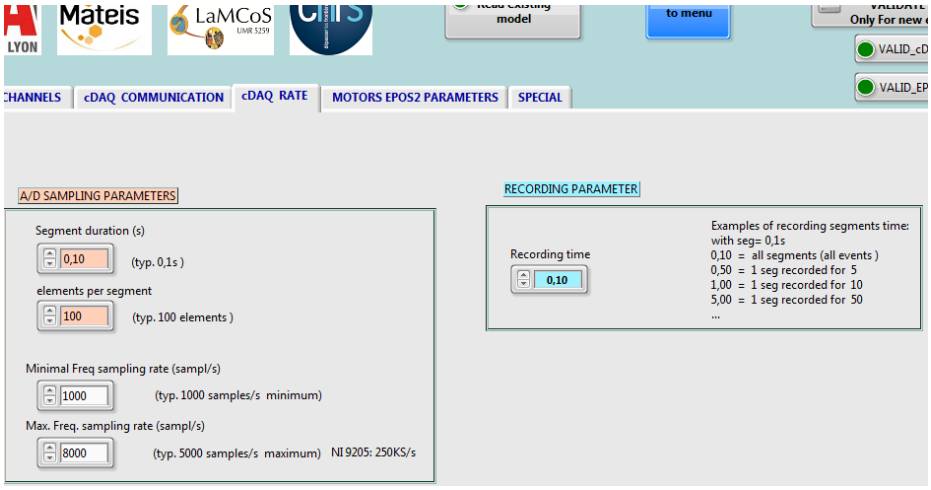

Figure 3.19: Data recording parameters interface in Tribo-MEB software

The number of data to be recorded per second and per segment was adjusted to interpret the data after the test easily and in a more reasonable way. To find the best data recording process, several trial tests were tried by using various parameters. Finally, it was decided to keep the segment duration as 0.1 with for 50 elements during 0.1 s recording time. For the other parameters, either very small amount of points was obtained and so some information was lost or excessive amount of data was recorded which was not complicated to analyse.

Before starting the tribological tests, calibration process was carried out to assure the measured force values by the sensors. Therefore, reference weights were used to apply force from 0.1 N to 10 N along 3 axes. This work is focused on the beginning of the run-in period. Therefore, a limited number of cycles was considered ($\leq$100). Tribological tests were performed with a determined normal load regarding the Hertzian pressure which was calculated by considering the elastic modulus, Poisson's ratio of both the film and the ball in addition to the diameter of the ball. For the tests performed with TiN film against steel ball, the normal load was selected as 6N and for Ti-Ag films, it was determined as 4N both against steel and polyurethane balls.

3.3.2. Mesoscale approach of friction

Before any local characterization, tribological tests were first performed under air at a global scale, using the light Keyence microscope (Figure 3.20). In order to correlate tribological measured parameters (tangential force in particular) with the wear track evolution, the system

was unloaded every 10 cycles to acquire images. Three representative regions are specifically considered: the central region and both extremities where the force is applied and the direction changed.

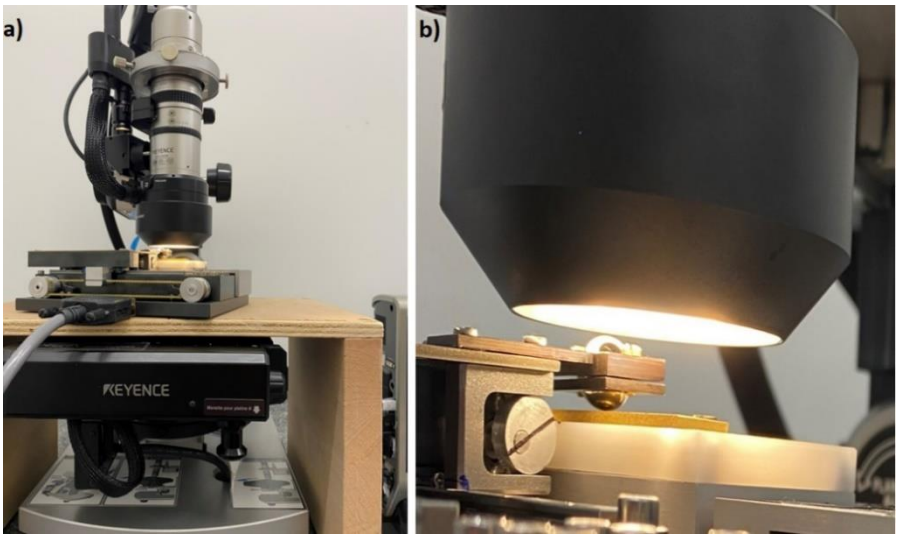

Figure 3.20: Keyence optical microscope as coupled with the micro-tribometer

3.3.3. Small-scale approach of friction

The micro-tribometer was developed to be implemented inside the SEM chamber (Figure 3.21) and *in situ* analysis of tribological behavior of samples could be performed for the same three regions of interest along the wear track. The micro-tribometer is placed on a specific polymeric insulating stage and connected to the electronic unit with a cable through the wall of the SEM chamber. When tests are performed under humidity, two further pipes of the cooling system have to be connected to ensure the cooling of Peltier elements.

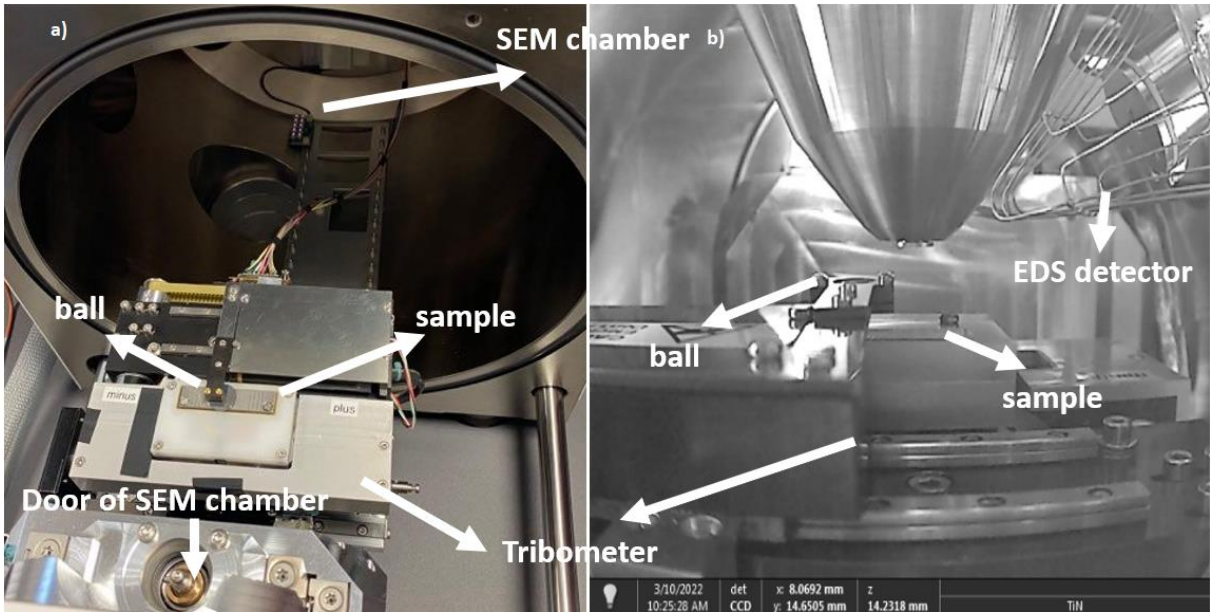

Figure 3.21: Tribometer as implemented into SEM a) from top view, b) inside the SEM chamber

The *in situ* analysis was performed after each cycle of sliding or after a certain number of cycles inside the microscope. In general, ten sliding cycles were applied as one set and then the contact was cut and the sliding arm was removed out below the beam to observe the wear track. The analyzed coordinates were recorded to investigate the modification after following cycles exactly on the same region. In addition to the *in situ* tests, 100 cycles were also applied in one single run and the *post mortem* analysis of the wear tracks was done to examine the effect of loading-unloading of the system.

Operating under environmental mode, tests were performed in various different controlled environmental conditions inside the chamber: in addition to vacuum, 25, 50, and 100% relative humidity levels were studied.

3.3.4. Data Processing for Tribological Tests

Since it was aimed to perform an *in situ* characterization, a specific procedure was determined and optimised for a proper tribological analysis. In the next chapter which is dedicated to proof of the concept, the test procedure and *in situ* analysis will be explained detailly. However, the data processing and the analysis of the interpreted data is needed to be indicated.

The wear tracks were analysed in three different regions of interest along the wear track by SEM: i) the region where the contact and sliding started (Figure 3.22a), ii) the region where the

sliding speed is constant (Figure 3.22b) and iii) the region where the sliding direction changed (Figure 3.22c).

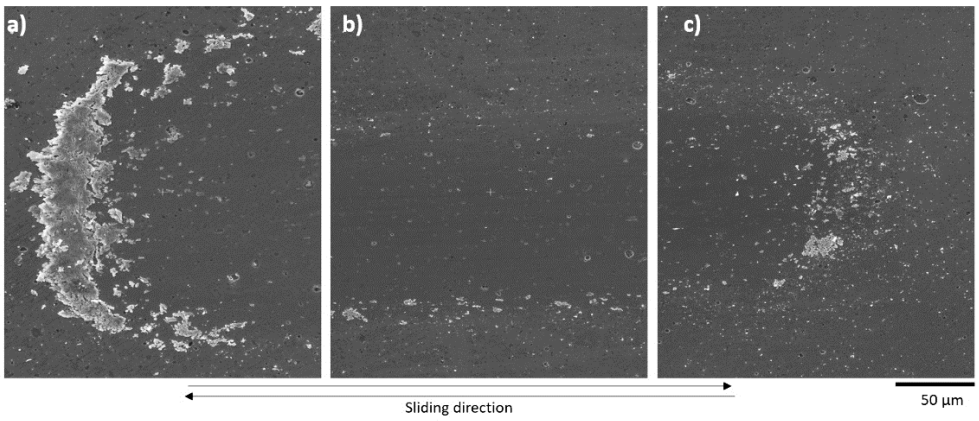

Figure 3.22: three regions of wear track as a) starting point of the contact, b) where the sliding speed is constant, c) where the sliding direction changed – Case of TiN film after 70 cycles at high vacuum as an example

These regions were investigated in every 10 cycles by unloading the system and removing the contact out from the wear track zone to evaluate the modifications on track morphology and debris formation and the recorded quantitative data were correlated with the SEM images of the during the *in situ* analysis. Here, in terms of quantitative data, normal (F_Z), tangential (F_X) and lateral forces (F_y) were considered as the first step for the analysis of each cycle.

The *in situ* evaluation of the wear track was aimed to be correlated by the quantitative results obtained from recorded data. In this point it was aimed to analyse the stability of the forces during the test and calculate the friction coefficient. To precisely calculate the friction coefficient, a cut-off procedure was applied for each cycle at each test, so only the region where the sliding speed is constant was investigated. Therefore, along 2 mm displacement, ~12.5% of the recorded data was eliminated from the beginning point of the contact and the point where the direction changed in both forward and backward direction.

After the cut-off process, mean coefficient of friction values were calculated for each cycle separately. Then the overall mean COF value for the corresponding test was calculating with the mean COF values of each cycle. The same process was considered as the error calculations. The standard deviation between the recorded values for each cycle was calculated. After that to calculate the error of the entire test, the standard deviation of the mean COF values of each cycle was considered.

The stability of normal, tangential and lateral forces during sliding was investigated. Here in the image below, tangential force evolution during sliding was indicated as an example for the test performed in high vacuum condition with TiN film and steel ball for the cycle 70 (Figure 3.23).

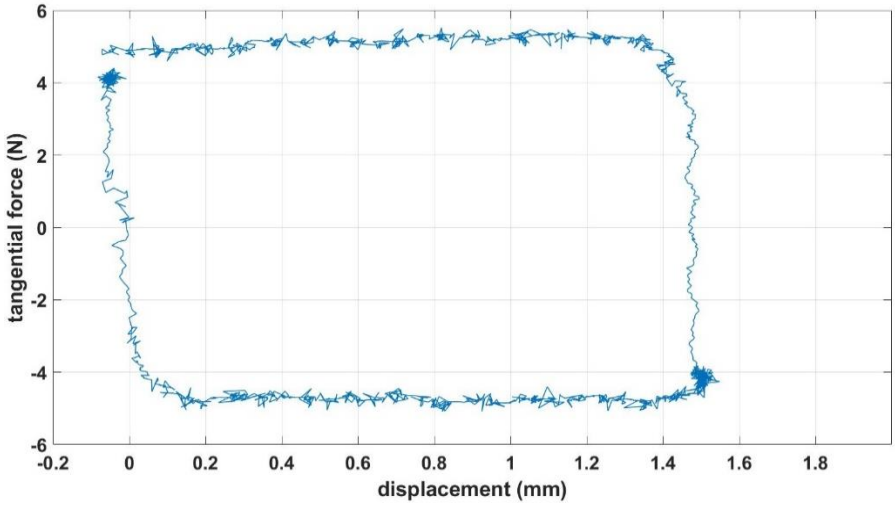

Figure 3.23: Displacement vs tangential force for cycle 70 of the test with TiN film against steel ball at high vacuum

These force values were investigated with respect to the displacement and the number of cycles (Figure 3.24). Then the mean friction coefficient was calculated by dividing mean absolute tangential force to the mean normal force (F_x/F_y). Here, it was aimed to observe the stability of normal force and the variations on the coefficient of friction values.

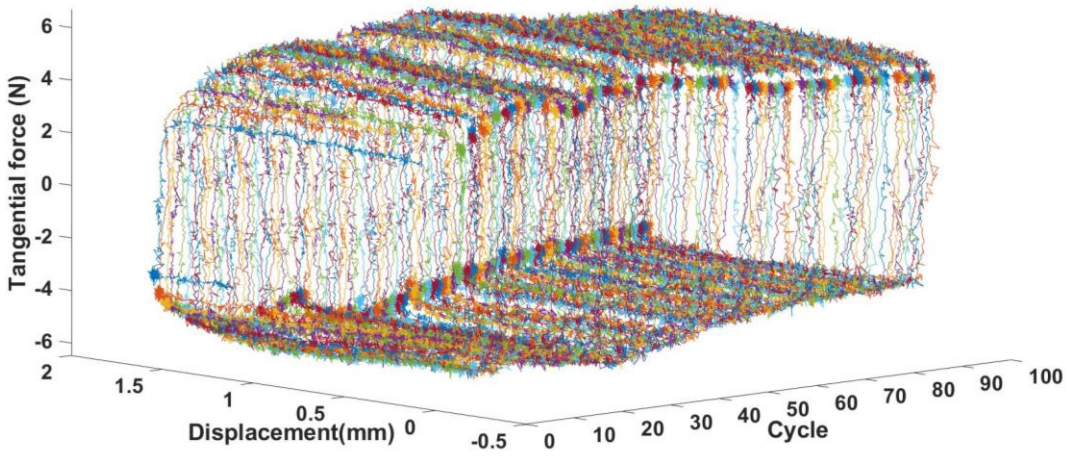

Figure 3.24: Tangential force vs cycle and displacement for TiN film-steel ball tests in high vacuum

To examine the change on the friction coefficient more in detail, friction maps were plotted and these maps were considered with the corresponding regions on the wear track as well as for the corresponding cycles (Figure 3.25). Thanks to the *in situ* investigation, the data shown in the friction map at any point for every 10 cycles, can be correlated with the microscopy images as it was demonstrated below.

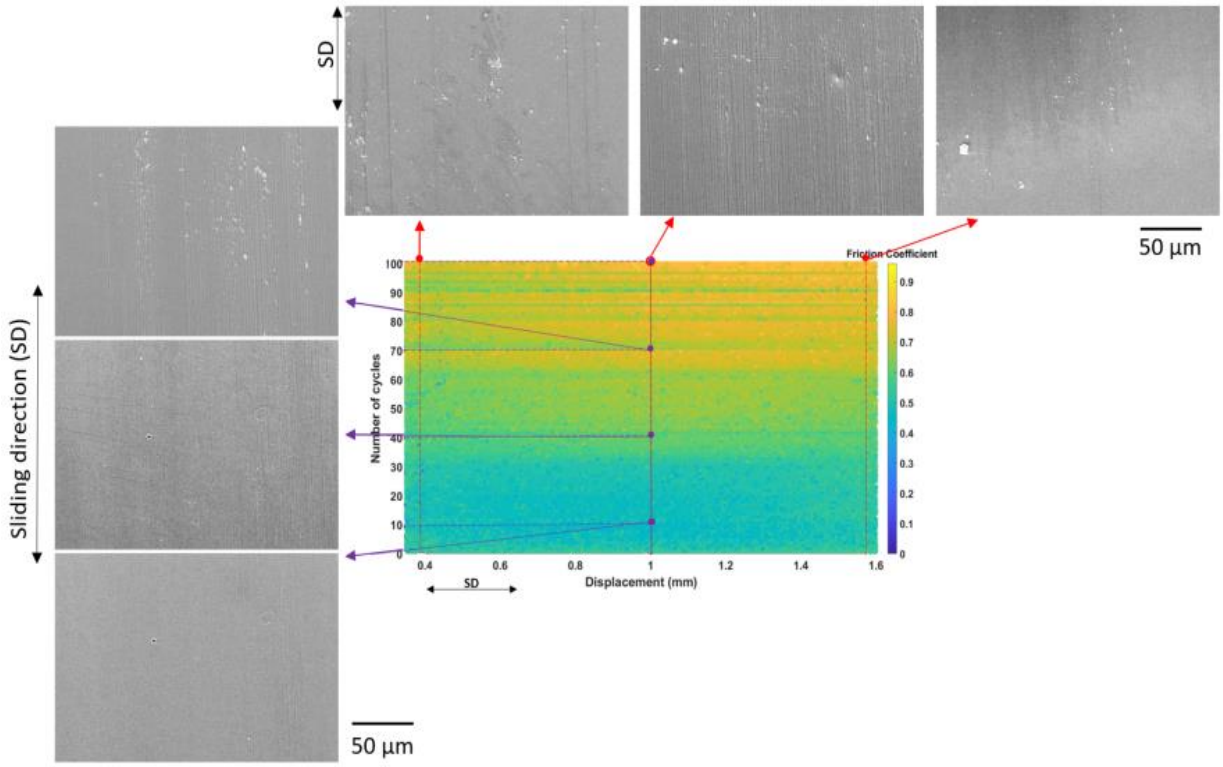

Figure 3.25: Friction map for Ti-reference film for the test at 50% RH with three region of interest analysis and for the *in situ* conditions at the centre of the track

It has to be noted that, with friction maps, the variation on the friction coefficient based on particle accumulation or trapping in contact, changes on the sliding speed can be observed. For example, in some tests, the friction coefficient seems lower through the extremities of the displacement length. This issue could be correlated by deceleration of the sliding speed and direction change. The friction maps shown below and in the following chapters were drawn by merging the forward and backward direction of sliding for all the cycles. However, by considering the material flow, acceleration and deceleration variations in both directions of the sliding, two different friction (forward and backward) maps can be drawn to better understand the friction behaviour of the films. Here in the figure 3.26, friction maps along the forward and backward directions of the same tribo-test were compared. It was seen that while the friction coefficient was remarkably lower at the beginning of the displacement in forward direction

especially after cycle 50, it was higher along the displacement length through the end of the test in backward direction. This weak scattering of values can be attributed to relative motion of the ball during sliding and flow of accumulated debris.

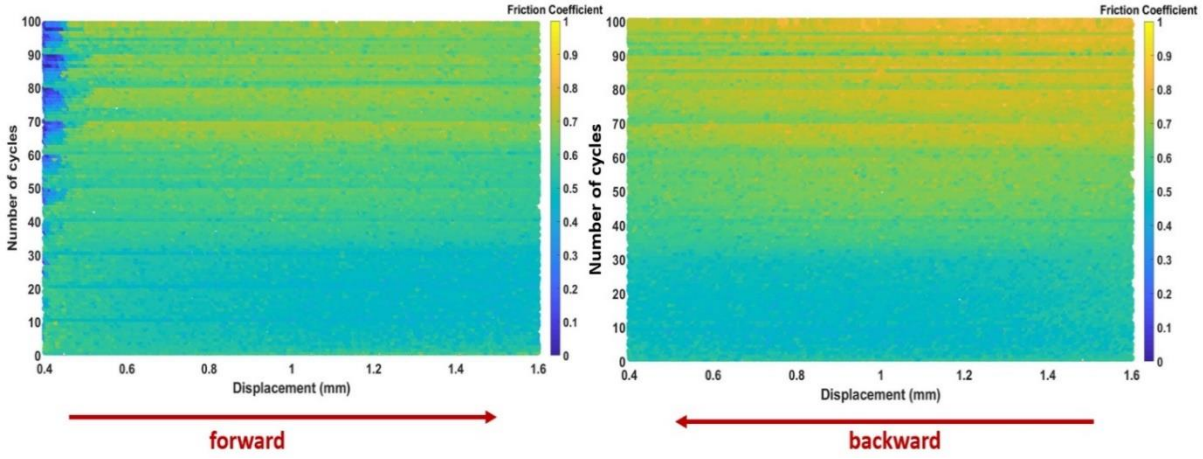

Figure 3.26: Friction maps in forward and backward directions for the Ti-reference film tribo-test against polyurethane ball at 50% RH

3.3.5. Post Mortem Characterization of Wear Tracks

After each test, both the wear track on the samples and on the ball surfaces were investigated in post mortem conditions by SEM and EDS. The morphological analysis with microscope is required to perform to examine the characteristics of debris and the wear track. The post-mortem analysis is quite crucial for the ball tracks because *in situ* investigation is achievable only for the flat sample but not for the ball. Also, the post-mortem EDS analysis was done after the tests in various environmental conditions to examine the chemical structure of the debris and to estimate if there is any material transfer, oxidation or contamination during sliding.

To investigate the surface profiles and the depth of the wear tracks on the films and the balls, the ZeGage Pro non-contact scanning interferometer was used (Figure 3.27). It is an interferometer which is able to perform analysis of different surfaces with high resolution and repeatability less than 3.5 nm for the topography of the surface. This device was developed by Zygo company and it is assisted with Mx^{TM} software [30]. The 3-dimension surface topography collected are analyzed with MountainsMap (DigitalSurf). In reference to the average plane (representing the initial surface, positive or negative volume are calculated). For that, ten profiles all along the wear track were scanned and a mean value of the volume was calculated.

Figure 3.27: ZeGage non-contact interferometer (a), and depth scans for the volume calculation

3.4. Conclusion

The Ti-based films were deposited by magnetron sputtering physical vapour deposition. For Ti-Ag films, magnetron sputtering technique was used and the film compositions were aimed to modify by changing number of Ag pellets inserted into Ti target. Various methods and devices were used to investigate their microstructural, mechanical and chemical structures. Here, microscopy techniques were specifically preferred to identify the microstructures of the Ti-Ag films by increasing Ag content by using SEM, e-SEM, TEM and light microscopy. Also, to investigate the chemical and crystal structure of these films numerous spectroscopy techniques were used such as EDS, RBS and XPS. Additionally, the crystal structures of these thin films were analysed with X-ray diffractometer. To prepare the samples for analysis, ionic polishing and focused ion beam were used. Finally, the tribological behaviours of these films were aimed to be investigated in various environments. Therefore, a laboratory-made novel design micro-tribometer was used by implementing it into e-SEM chamber. The parameters to record and interpret the data were adjusted from the software of the device accordingly. Moreover, with a home-made Matlab code, the friction maps were plotted in addition to the 3D force graphics and the graphics for mean friction coefficient with respect to number of cycles to properly analyse the data.

References (Chapter 3)

[1] Shin, J. H., Marxer, S. M., & Schoenfisch, M. H. (2004). Nitric oxide-releasing sol−gel particle/polyurethane glucose biosensors. *Analytical Chemistry*, *76*(15), 4543–4549. https://doi.org/10.1021/ac049776z

[2] Mendibide, C., Fontaine, J., Steyer, P., & Esnouf, C. (2004). Dry sliding wear model of nanometer scale multilayered tin/CRN PVD hard coatings. *Tribology Letters*, *17*(4), 779–789. https://doi.org/10.1007/s11249-004-8086-9

[3] Shi, F. (2018). Introductory chapter: Basic theory of magnetron sputtering. *Magnetron Sputtering*. https://doi.org/10.5772/intechopen.80550

[4] Baptista, A., Silva, F. J. G., Porteiro, J., Míguez, J. L., Pinto, G., & Fernandes, L. (2018). On the physical vapour deposition (PVD): Evolution of magnetron sputtering processes for industrial applications. *Procedia Manufacturing*, *17*, 746–757. https://doi.org/10.1016/j.promfg.2018.10.125

[5] Etiemble, A., Lopes, C., Nkou Bouala, G. I., Borges, J., Malchère, A., Langlois, C., Vaz, F., & Steyer, P. (2019). Fracture resistance of ti-ag thin films deposited on polymeric substrates for biosignal acquisition applications. *Surface and Coatings Technology*, *358*, 646–653. https://doi.org/10.1016/j.surfcoat.2018.11.078

[6] Goldstein, J., Newbury, D., Joy, D., Lyman, C., Echlin, P., Lifshin, E., Sawyer, L., & Micheal, J. (2003). *Scanning Electron Microscopy and X-Ray Microanalysis* (3rd ed.). Springer.

[7] *Backscattered Electron Imaging explained*. Thermo Fisher Scientific - US. (n.d.). Retrieved October 7, 2022, from https://www.thermofisher.com/fr/fr/home/global/forms/industrial/backscattered-electron-imaging.html

[8] Quattro-ESEM brochure, Ultra-versatile, high-resolution SEM with unique environmental capability, 2022, Thermo Fisher Scientific, https://assets.thermofisher.com/TFS-Assets/MSD/brochures/quattro-brochure-br0148-en.pdf

[9] *Physics microscopy*. Zeiss SUPRA 55-VP FEGSEM. (n.d.). Retrieved June 21, 2022, from https://warwick.ac.uk/fac/sci/physics/research/condensedmatt/microscopy/em-rtp/instruments/zeiss_supra_55/

[10] I*lion Polisher - Gatan*. CLYM. (n.d.). Retrieved June 21, 2022, from http://www.clym.fr/fr/node/334

[11] Danilatos, G. D., & Lewis, G. C. (1989, April 18). Integrated electron optical/differential pumping/imaging signal detection system for an environmental scanning electron microscope.

[12] Reyntjens, S., & Puers, R. (2001). A review of focused Ion Beam Applications in microsystem technology. *Journal of Micromechanics and Microengineering*, *11*(4), 287–300. https://doi.org/10.1088/0960-1317/11/4/301

[13] Winey, M., Meehl, J. B., O'Toole, E. T., & Giddings, T. H. (2014). Conventional transmission electron microscopy. *Molecular Biology of the Cell*, *25*(3), 319–323. https://doi.org/10.1091/mbc.e12-12-0863

[14] Ma, H., Shieh, K.J., Qiao, T.X., (2006). Study of Transmission Electron Microscopy (TEM) and Scanning Electron Microscopy (SEM). Nature and Science, 4(3), 14-15

[15] Yang, X., Luo, C., Tian, X., Liang, F., Xia, Y., Chen, X., Wang, C., Liang, S. X., Wu, X., & Chu, J. (2021). A review of in situ transmission electron microscopy study on the switching mechanism and packaging reliability in non-volatile memory. *Journal of Semiconductors*, *42*(1), 013102. https://doi.org/10.1088/1674-4926/42/1/013102

[16] Abd Mutalib, M., Rahman, M. A., Othman, M. H. D., Ismail, A. F., & Jaafar, J. (2017). Scanning electron microscopy (SEM) and energy-dispersive X-ray (EDX) spectroscopy. *Membrane Characterization*, 161–179. https://doi.org/10.1016/b978-0-444-63776-5.00009-7

[17] *Ultim Max - Nanoanalysis*. Oxford Instruments. (n.d.). Retrieved June 22, 2022, from https://nano.oxinst.com/products/ultim-max

[18] *Safematic CCU-010 coater family: CCU-010 HV high vacuum compact coating unit.* Safematic. Make it visible. Provider of high vacuum coating systems. (n.d.). Retrieved September 23, 2022, from https://www.safematic.ch/ccu-010-hv-sputter-coater-vacuum-coating-system-switzerland.php

[19] Zhang, Z., (2021), Determination and understanding of the role of alloying elements on the passive behaviour of Ni-based alloys by electrochemical investigation, p. 45, https://tel.archives-ouvertes.fr/tel-03394931

[20] Perrière, J. (1987). Rutherford backscattering spectrometry. *Vacuum*, *37*(5-6), 429–432. https://doi.org/10.1016/0042-207x(87)90327-7

[21] Kitahara, A., Yasuno, S., & Fujikawa, K. (2009). Study of thin-film thickness and density by high-resolution Rutherford backscattering spectrometry and X-ray reflectivity. *Transactions of the Materials Research Society of Japan*, *34*(4), 613–615. https://doi.org/10.14723/tmrsj.34.613

[22] Ermrich, M., & Opper, D. (2013). *Xrd for the analyst: Getting acquainted with the principles*. PANalytical.

[23] *D8 advance*. Bruker. (n.d.). Retrieved June 21, 2022, from https://www.bruker.com/en/products-and-solutions/diffractometers-and-scattering-systems/x-ray-diffractometers/d8-advance-family/d8-advance.html

[24] Pharr, G. M., & Oliver, W. C. (1992). Measurement of thin film mechanical properties using nanoindentation. *MRS Bulletin*, *17*(7), 28–33. https://doi.org/10.1557/s0883769400041634

[25] Schuetze, A. P., Lewis, W., Brown, C., & Geerts, W. J. (2004). A laboratory on the four-point probe technique. *American Journal of Physics*, *72*(2), 149–153. https://doi.org/10.1119/1.1629085

[26] Kapsa, P. (2001). Tribology at Different Scales. *Advanced Engineering Materials, 3*(8), 531. doi:10.1002/1527-2648(200108)3:8<531::aid-adem531>3.0.co;2-1

[27] Y.Berthier, Handbook of Materials Behavior Models, Acad.Press, Lemaître (2001) 676–699 (Chapter8).

[28] Kosinskiy, M., Ahmed, S. I., Liu, Y., & Schaefer, J. A. (2012). A compact reciprocating vacuum microtribometer. *Tribology International, 56*, 81-88. doi:10.1016/j.triboint.2012.06.019

[29] *Zegage Pro Optical Profiler*. Zygo. (n.d.). Retrieved July 31, 2022, from https://www.zygo.com/products/metrology-systems/3d-optical-profilers/zegage-pro

4. TRIBOLOGICAL ANALYSIS OF TIN FILM DURING RUN-IN PERIOD: AN *IN SITU* INVESTIGATION UNDER CONTROLLED ENVIRONMENT IN ESEM AS PROOF OF CONCEPT

The procedure used to perform the tribological tests was defined with the micro-tribometer in eSEM chamber as the proof of concept. The methodology developed for the evaluation of the effect of environment *in situ* conditions was indicated by using a commercial TiN CAE PVD film as the reference coating during the early stages of the contact. The results for were explained to better understand the role of environment in this stage in small scale both with *in situ* and post mortem analysis.

4. TRIBOLOGICAL ANALYSIS OF TiN FILM DURING RUN-IN PERIOD: AN *IN SITU* INVESTIGATION UNDER CONTROLLED ENVIRONMENT IN ESEM AS PROOF OF CONCEPT

(The work represented in this chapter is depending on my article which was titled as "Tribological analysis of TiN film during run-in period: An in situ investigation under controlled environment in eSEM" in the journal "Surface and Coatings Technology")

Tribology is a multidisciplinary science focused on the dynamic study of a system composed of two surfaces in contact [1]. The tribological system can be defined by three main components: i) the nature of the contact, depending on its geometry, on the different materials involved and on their surface properties, ii) the rubbing conditions, linked to the dynamic parameters (load, stress, time, speed…), and iii) the environment of the contact zone, associated with atmosphere, temperature and the stiffness of the device containing the contact [2, 3]. Therefore, many parameters may influence the wear behavior of materials, so that it is often complex to assess the tribological response of surfaces [3].

From a technological viewpoint, tribometer systems which have a pin or ball counter-face over a flat surface (pin-on-disk or ball-on disk system) are commonly used. They can be classified into two main different categories regarding their kinematics: rotational tribometers, which have a rotational actuator, and the reciprocating tribometers, which have an oscillating actuator. The selection of the proper type of tribometer is governed by the final targeted application [4].

Normally, the films on rigid substrates have a significant place in people's every-day lives as the coatings for numerous devices and applications. It is needed to consider that the functionality of these films in terms of their mechanical, electrical, magnetic properties are usually driven from the small dimensions [5]. Additionally, the wear procedure and the material response are mostly analyzed for lab duration tests at a large scale, through a conventional *post-mortem* comparative approach. However, for small-scale engineering devices such as MEMs and NEMs, an adapted small-scale analysis of the contact is required, which was on the basis of micro-tribology [6]. Additionally, Kumar et al. [7] pointed out the micrometer-sized phenomena which is linked to small-scale surface properties (*e.g.* surface energy, roughness). Also, the range of the normal load and the size of the contact have, in particular, to be adapted [8]. Recently, there is a considerable interest in examining the micro and nano-scale frictional contacts in the field of micro-and nano-sized devices, or to better understand the role of the

asperities in macro-scale [9]. Testing procedures in terms of both loads and contact sizes have to be adjusted, together with the investigation methods involving physical and chemical complementary analyses [9-11].

For a small-scale tribological characterization, two main types of tribometers are reported in the literature. It can be found nanotribometers, which derive from AFM-based systems. They are devoted to weakly defective surfaces such as in the electronics field [4]. AFMs with nano-tribometers can be used for the tribological analysis of small-scale engineering devices. To perform *in situ* tribological analysis in small-scale, AFM is an efficient choice regarding its high resolution and high precision on measurement abilities. Also, nano-tribometers can be used by coupling with electron microscopes to perform *in situ* analysis. For example, Deasi et *al.* [12] developed a nano-tribometer which provides dynamic investigation of tribological behavior of materials to be used for MEMs for the load range 1-100 nN. The second class of tribometers is called micro-tribometers, which are operable in vacuum or ambient air conditions with micro and milli-newton normal load ranges. Here, nano-indenters with AFM or FFM (friction for microscopy) could provide the tribological analysis from nano to micro scale load ranges [8]. Moreover, to better understand the complex surface/counter-face/environment interaction, *in situ* approaches of characterization are recommended, giving the access to a detailed evaluation of the friction nature throughout the phenomenon. It is then possible to follow the wear track and friction evolution at every cycle, during the entire process, and with well-defined contact conditions. Dynamic of the contact is then considered from a (micro)structural point of view by light, electron, or atomic force microscopes [13-20], and/or from a chemical point of view through Raman, XPS, AES spectroscopies [21-24]. For instance, Murarash et *al.* [25] examined the tribological behavior of biological surfaces by visual inspection *in situ* conditions by operating the tribometer in SEM chamber. Here, the developed tribometer for these particular surfaces has flat-on-flat contact to examine the pulling-off, shear and/or the peeling off the surfaces. Also, Naerheim [26] developed a tribometry system which is implementable into SEM chamber in addition coupling with XPS and AES. This system was based on having a cylinder and pin contact at the same time and tribometer could be operated in rolling or sliding mode for *in situ* analysis. In another research, to examine the role of environmental conditions, Meylan et *al.* [27] developed a ball-on-disk tribometer to couple with digital holographic microscope and to operate in high temperature and high vacuum conditions.

The long-term tribological behavior of materials is well-documented in general. [17, 28-31]. However, changes on the roughness, grain size or texture of the surface based on the frictional contact mostly occur during run-in period which affects the friction coefficient [32, 33]. The variations on friction coefficient at run-in period is based on contaminations on the film surface, formation of oxide layer, transferred material reaction of lubricants or reorientation of the sub-surface microstructure during the contact [30]. Thus, the presented approach in this chapter involves a dedicated home-made mini-tribometer, which was developed to examine the early stages of the contact. To prove the reliability of the tribometer, the system has been selected on a model hard surface: titanium nitride. TiN films are indeed well known for a long time for their enhanced tribo-chemical properties [22]. They are used in small-scale engineering applications such as ohmic contacts for Schottky barriers [23], solar cells, NEMs, MEMs [7], and anti-wear applications such as cutting tools, and orthopedic implants or bearings [22]. However, the performance of TiN films is sensitive to the tested atmosphere: vacuum environment [34, 35], water vapor [36-38], oxygen [39] or nitrogen [35]. For example, Yoon et *al.* [37] studied the wear character of TiN films against a steel ball from 2% to 25% and 85% relative humidity levels. It was pointed out that, for a long test (30000 cycles), the coefficient of friction decreased with the increasing relative humidity based on the formation of TiO_2 on the film surface. Besides, the structure of the worn coating was analyzed by Gant *et al.* [38] under different relative humidity environments with Raman spectroscopy. They demonstrated that high relative humidity promoted the rutile phase formation, whereas the anatase phase mostly predominated at lower humidity levels. In order to assess the effect of the atmosphere on the tribological behavior for the small-scale analysis of the contact, the presented mini-tribometer was designed to be implemented into the chamber of an environmental SEM (eSEM), in which atmosphere of the contact can be controlled, and chemical information can be obtained. In the current chapter, modification of the relative humidity will be the variable key-parameter. In this sense, the presented mini-tribometer represents a step ahead with respect to existing systems involving light microscopes or conventional SEMs [30].

This chapter proposes an *in situ* approach at the meso-scale, to investigate the tribological behavior of a material during the run-in period, highlighting the effect of the contact environment. The mini-tribometer, the TiN film, and the environmental SEM are first described. Both qualitative and quantitative results are then given by considering the coated flat

sample as well as the ball counterpart. Results are finally discussed in light of the debris dynamic on the one hand, and the effect of the humidity on the other hand.

4. 1. Materials and Methods for Proof of Concept

4.1.1. Mini-Tribometer in ESEM

The mini-tribometer is compact to be implementable in the eSEM chamber, and could be used under high vacuum as well as under different environmental conditions (*e.g.* different relative humidity, gas nature, and temperatures). By implementing the tribometer into the eSEM chamber, small-scale characterizations can be performed without modifying the atmosphere and containing the contact and with Everhart-Thornley detector (ETD). The used SEM-Quattro (Thermo Fisher Scientific) is a high-resolution scanning electron microscope, which is able to operate not only in high vacuum but also in controlled gaseous environments. Furthermore, the hygrometry surrounded the contact can be controlled by modifying the flat sample temperature (use of cooling Peltier elements) and the water vapor pressure P_{H_2O} inside the SEM chamber [41].

4.1.2. Materials and contact conditions

The TiN film deposited with 2.3 µm-thickness a mirror-polished mild steel substrate by the cathodic arc evaporation (CAE) process. As expected, the film presents the conventional fcc-TiN phase, with the classical heterogeneous microstructure obtained by CAE, gathering some pinholes pores, and droplets (Figure 4.2) [42-44]. More details on the film characteristics can be found in a previous dedicated paper [45].

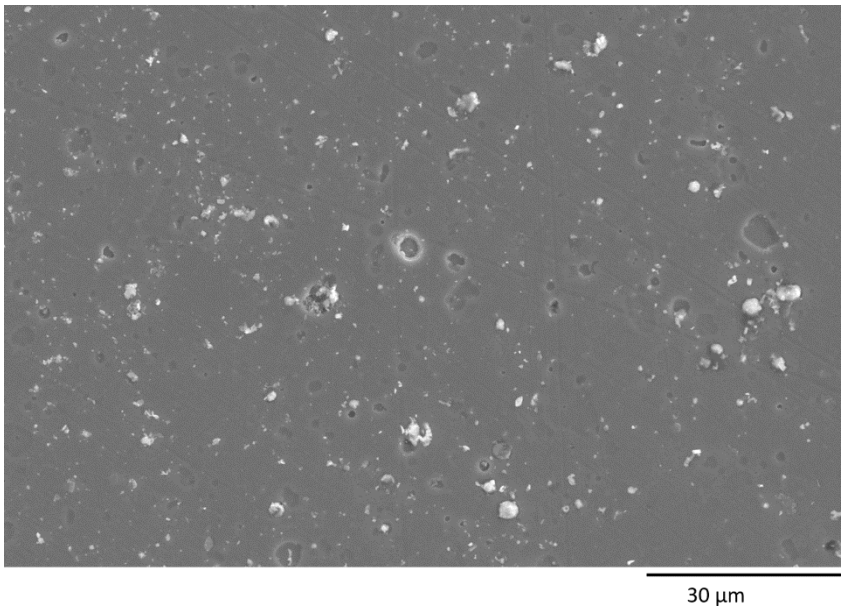

Figure 4.1: TiN film – SE image of the pristine surface

The applied normal load was 6 N and it was applied along 2 mm of displacement length, with a 1 mm/s sliding speed. The Young's modulus of TiN film was measured at 305 GPa [43], in good agreement with literature data [46, 47]. A steel ball (AISI52100) with a 10 mm diameter was selected as the counter-face. By considering the materials' mechanical properties and contact conditions, the maximum Hertz contact pressure was calculated as 1130 MPa.

4.1.3. *In situ* analysis

The whole tests were performed according to the procedure reported in Figure 4.2. A reduced number of cycles (100) was deliberately chosen to focus on the run-in period.

Preliminary tests were performed to select the best parameters (total number of cycles and periodicity of sets of cycles) leading to significant changes of the surface. To perform *in situ* analysis, sliding was interrupted and the contact was unloaded after every 10 cycles. That allows SEM captions of the worn zone, thus, to assess the wear track modifications. Two regions of interest were specifically monitored along the wear track: one edge of the track (turning point) and its center (where the sliding speed is constant). The unloading-loading edge was not analyzed during the *in situ* tests.

Tests were performed in two different environments: under high vacuum (10^{-4} Pa) and in water vapor environment (50% relative humidity). For the targeted 50% relative humidity, the

saturated water vapor pressure P_{H_2O} in the SEM chamber and the coated sample temperature were set to 400 Pa and 4°C respectively.

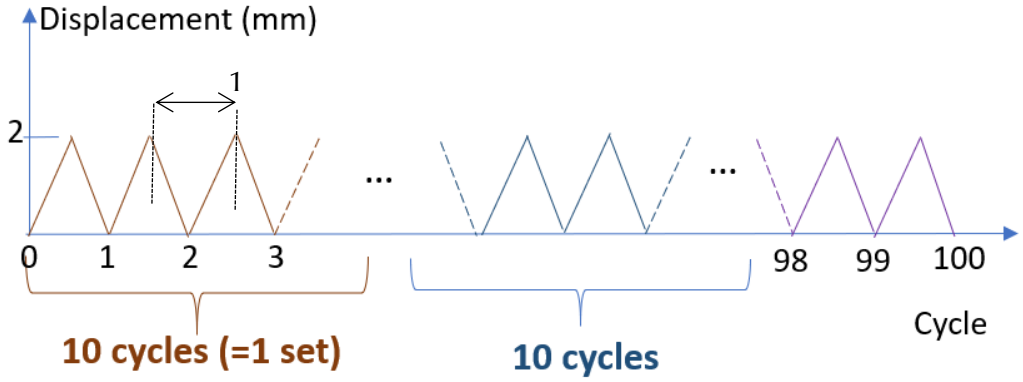

Figure 4.2: Protocol for *in situ* tribological tests

4.1.4. *Post mortem* analysis

The mini-tribometer as coupled with microscope could provide to perform *in situ* analysis on the flat; however, not for the ball surface. Thereby, it not possible to evaluate the wear tracks on the balls after every ten cycles without venting the chamber and since the tests were carried out in controlled environment, only *post-mortem* analysis was done on the ball surfaces.

Also, on the wear tracks TiN films, three regions of interests were investigated in *post mortem* conditions by energy dispersive x-ray spectroscopy (EDS). An Oxford Ultim max 100 spectrometer was used to analyse the debris and characterise the transferred film.

Surface profile analysis was performed both on the ball and on the TiN-coated steel to estimate their worn volumes. Surface morphologies of the wear tracks and balls were extracted using a ZeGage Pro non-contact scanning interferometer from Zygo company. Mx^{TM} software integrated with interferometer also provides 3D mapping. In this study, the Mountain software was used to extract the surface profiles and to calculate the wear volumes. The average wear volume was calculated by the integral method from ten profiles obtained from different regions along the whole wear track region.

4.2. Results

4.2.1. *In situ* analysis

Figure 4.3 shows examples of the tangential force evolution after different number of cycles. During each cycle the tangential force is constant for both atmospheres. The tangential force evolution for the forward and backward displacement is similar. The applied normal force is constant for each cycle and equal to the target value. The elasticity of the system and the stiffness of the arm allows a possible movement due to the interface evolution, *e.g.* the applied load might vary but in a very limited range.

An average friction coefficient was calculated for each reciprocating cycle (COF) when the speed is constant, *i.e.* the data from turning points are omitting (approximately 12 % at each track end). The friction coefficient is defined as the ratio between the tangential force to the applied normal force.

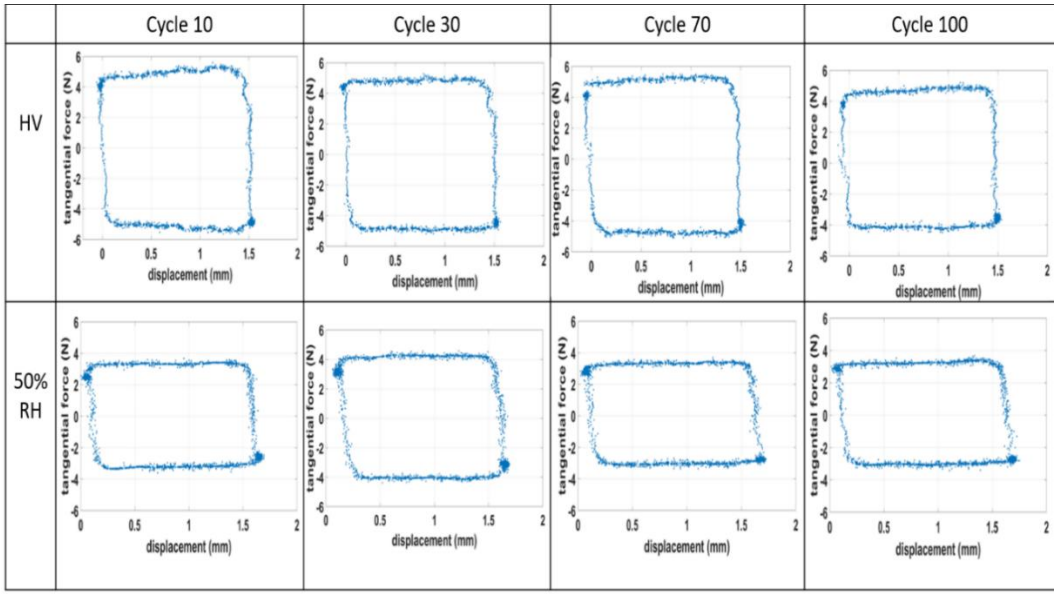

Figure 4.3: Tangential force *vs* displacement at different cycle (a) under high vacuum, (b) under RH 50%

Friction tests were monitored by plotting COF as a function of the cycle number (Figure 4.4) for both high vacuum and humid environment. A general interpretation of curves allows concluding that the COF evolutions are similar whatever the environments, with an increase during the first 30 cycles with a higher amplitude at high vacuum (0.90) than for humid

conditions (0.55). Then, a similar slow decrease of the COF is recorded down to 0.67 and 0.47 for the high vacuum test and humid test respectively.

It is seen that the first cycle of each set systematically presents a lower coefficient of friction with respect to the other following 9 cycles in the same set. When the contact was reloaded and the sliding was restarted, there was a sharp drop of COF values, phenomenon met every 10 cycles.

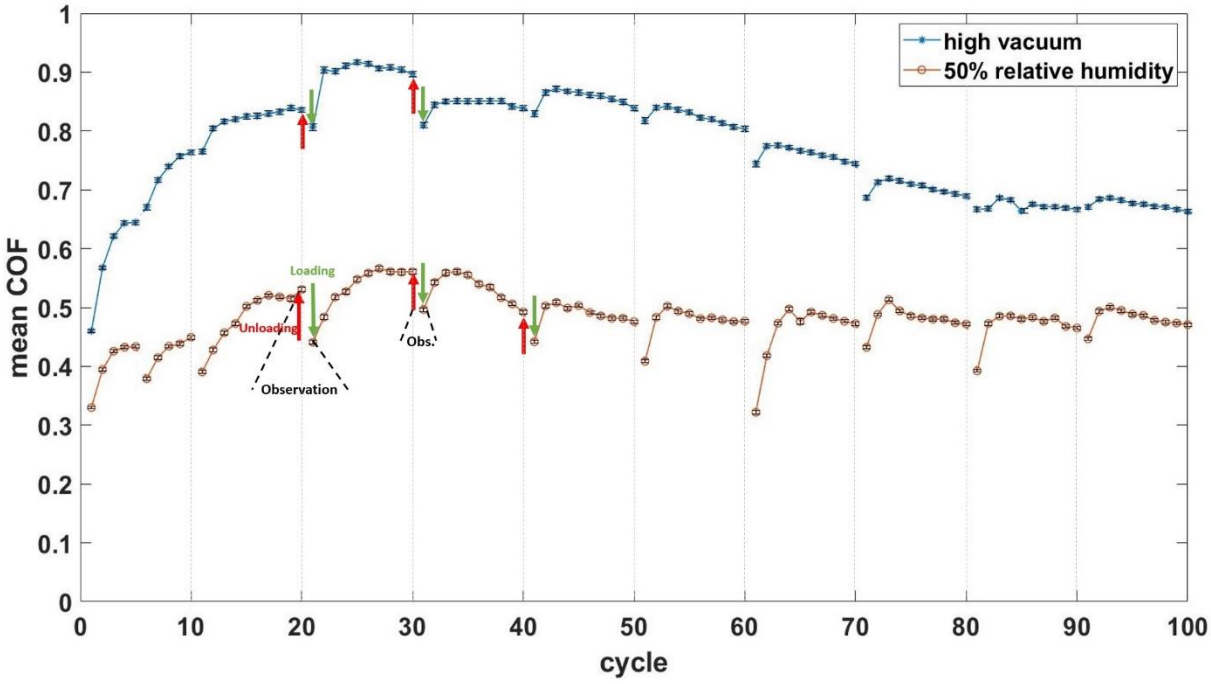

Figure 4.4: Mean coefficient of friction per cycle for the tests performed at high vacuum and 50% relative humidity

In addition to quantitative evaluation of the sliding via COF analysis, a complementary observation of the surface throughout the test was performed. SEM images were analyzed at low magnification in two specific regions of interest which are the center and the end of the wear track (Figure 4.5). It appears that whatever the environment, tracks are mainly identified by the debris left at its edges.

In both atmospheres, it is worth to mention that there was not a significant change observed between cycle 30 and cycle 40. In this sense, the highest COF value revealed after 30 cycles could be a consequence of particles sticking between the ball and the film surface.

In comparison with powder-like debris encountered under vacuum, the dynamic of debris generated under humidity seemed strongly changed, with a smoother track, in addition to fine

and aligned debris. Moreover, the amount of debris observed at the edges is increasing with the test duration in humid environment.

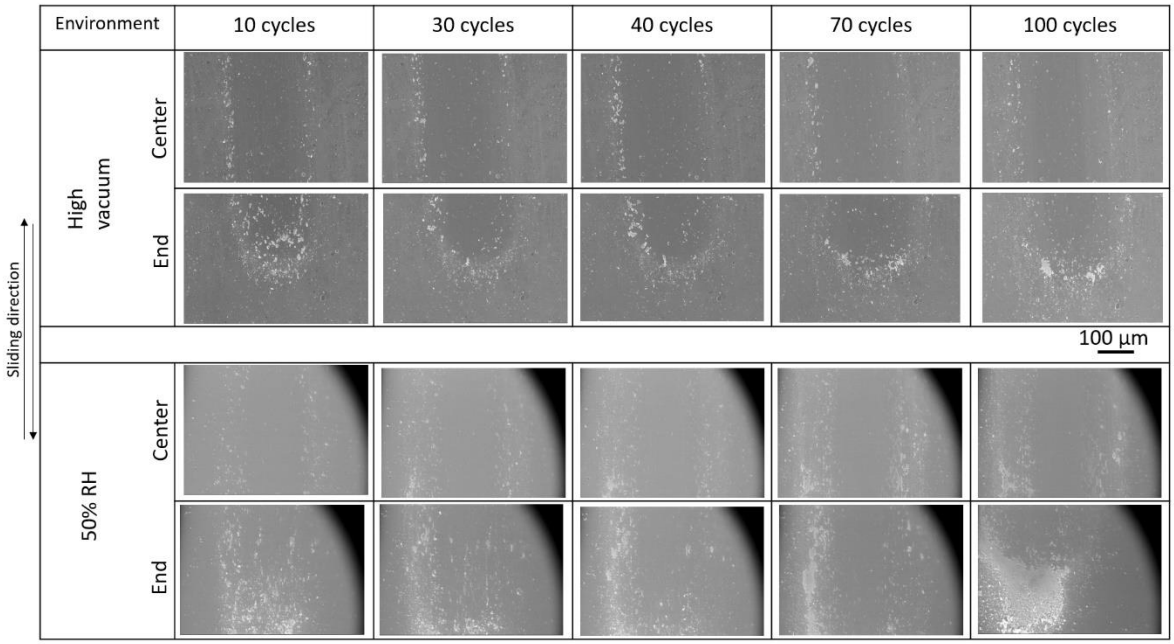

Figure 4.5: Images of wear tracks (center and end) at several numbers of cycles for the two environments (*NB*: *due to the gaseous secondary electron detector used for the humid mode, the aperture appears in images (top right) at low magnification*)

At higher magnification, in the case of high vacuum, the pores observed on the pristine surface (Figure 4.1) were still visible in the center of the friction track, after each 10 cycles set (red arrows in figure 4.6). After 10 cycles the flow of particles was detected (*e.g.* highlighted by yellow arrows or circled by a dotted line), but some of those particles tends not to be visible afterwards. On the contrary, at 50% of relative humidity, the pores were gradually "disappearing" (red arrows on figure 4.7). On the same time, one can note that third body spread on the surface together with the formation of agglomerates between 70 and 100 cycles in humid environment (yellow arrows and dotted ellipse).

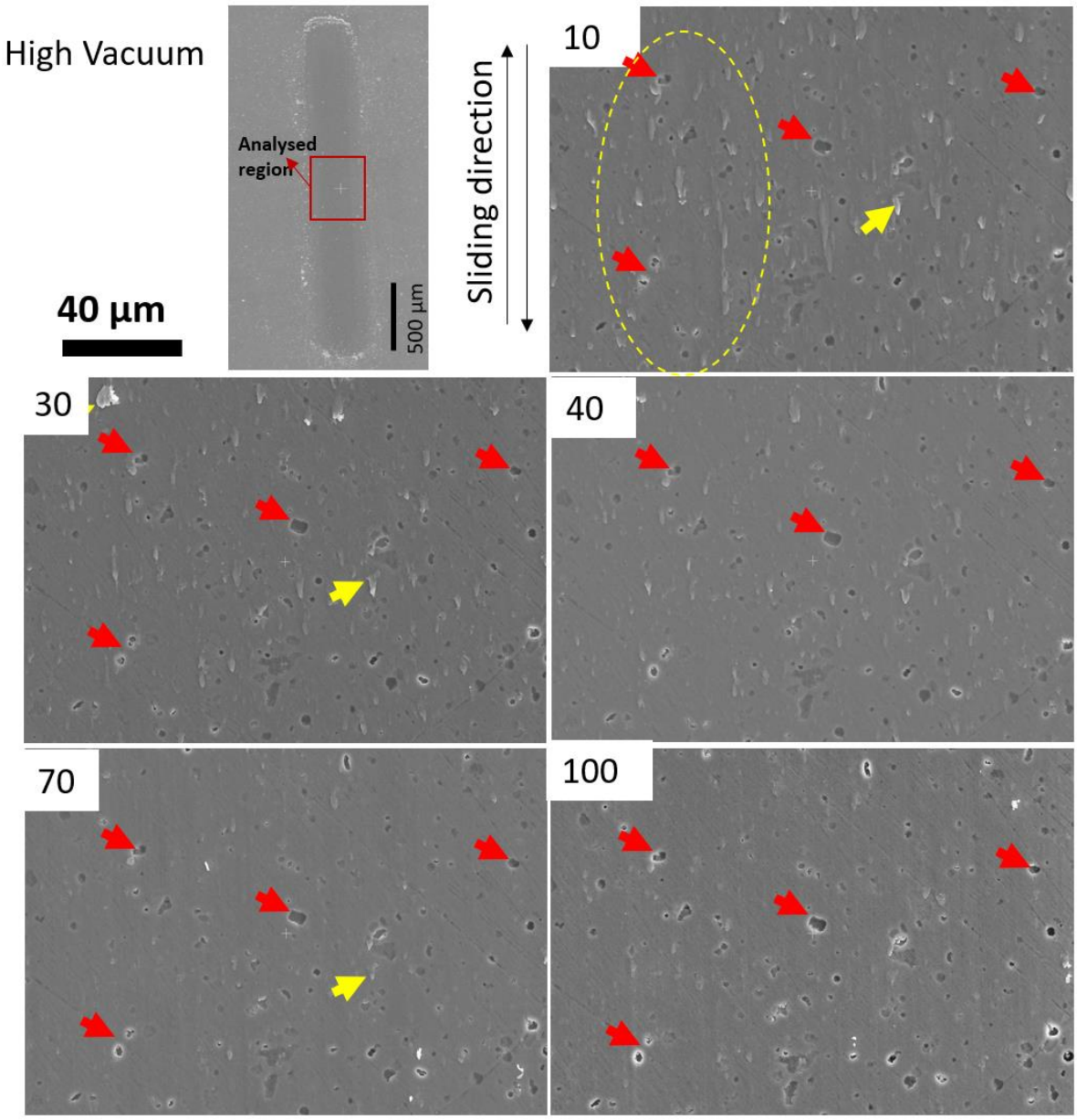

Figure 4.6: Center of the wear track after cycle 10, 30, 40, 70 and 100 in high vacuum tests

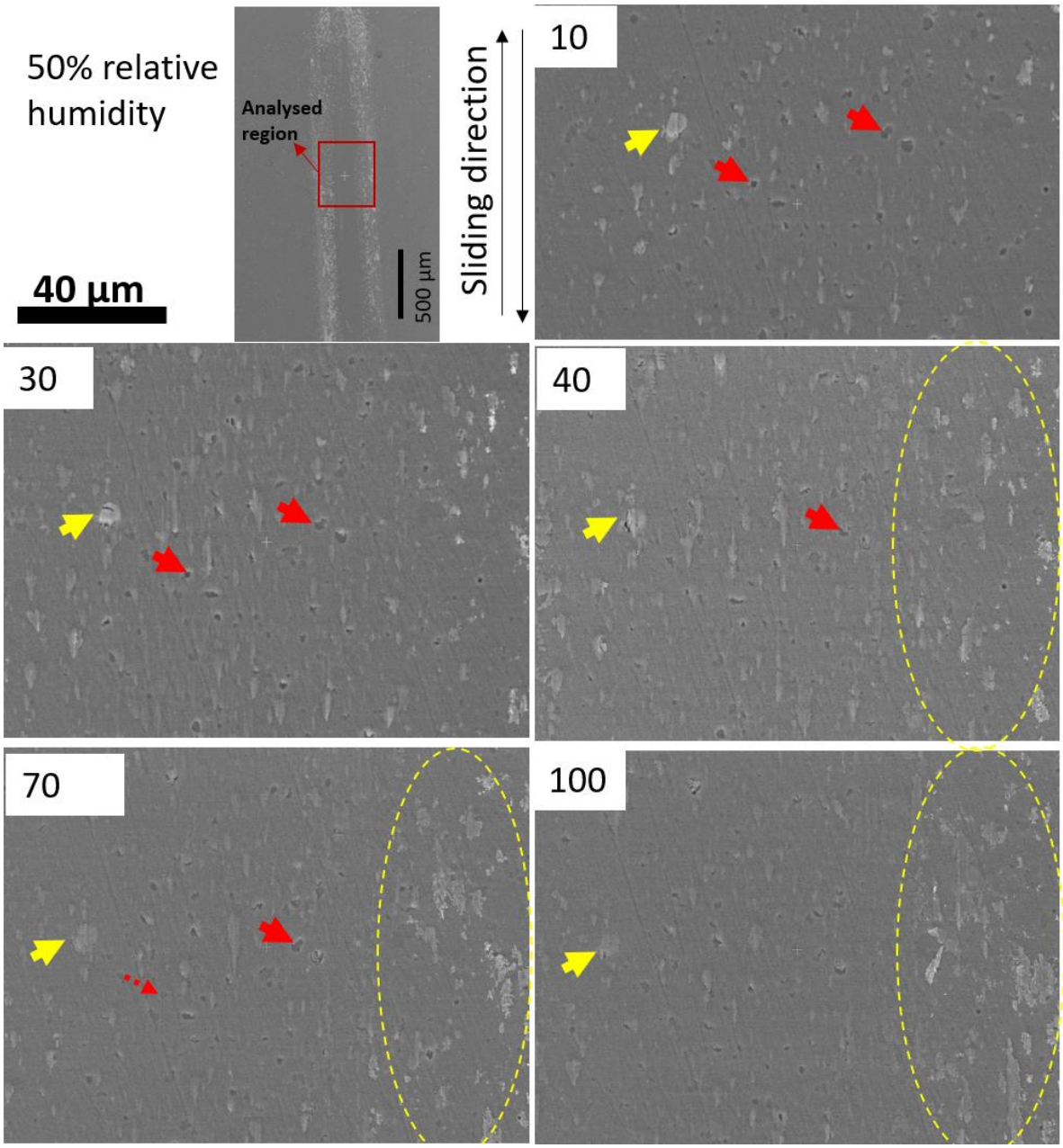

Figure 4.7: Center of the wear track after cycle 10, 30, 40, 70 and 100 in 50% RH tests

The mean friction coefficients of 100 cycles were compared with the evaluated wear tracks of TiN film both under high vacuum and 50% relative humidity by considering the SEM images. The difference of friction behavior observed in these two environments can be associated with differential arrangements of the particles, and different loss of debris. As a quantitative clue, it was seen that the mean friction coefficient varied from 0.65 to 0.49 for high vacuum to humid environment.

4.2.2. *Post mortem* analysis

After 100 cycles, a microstructural characterization of wear tracks for the TiN film and the ball counter-face were investigated by SEM and EDS. Since the *in situ* analysis on the ball was not possible after venting the chamber, the ball was removed from the system for SEM observations leading to its superficial oxidation. SEM images report different ball track dimensions depending on the test environment, in agreement with the width of the films' wear tracks (Figure 4.8).

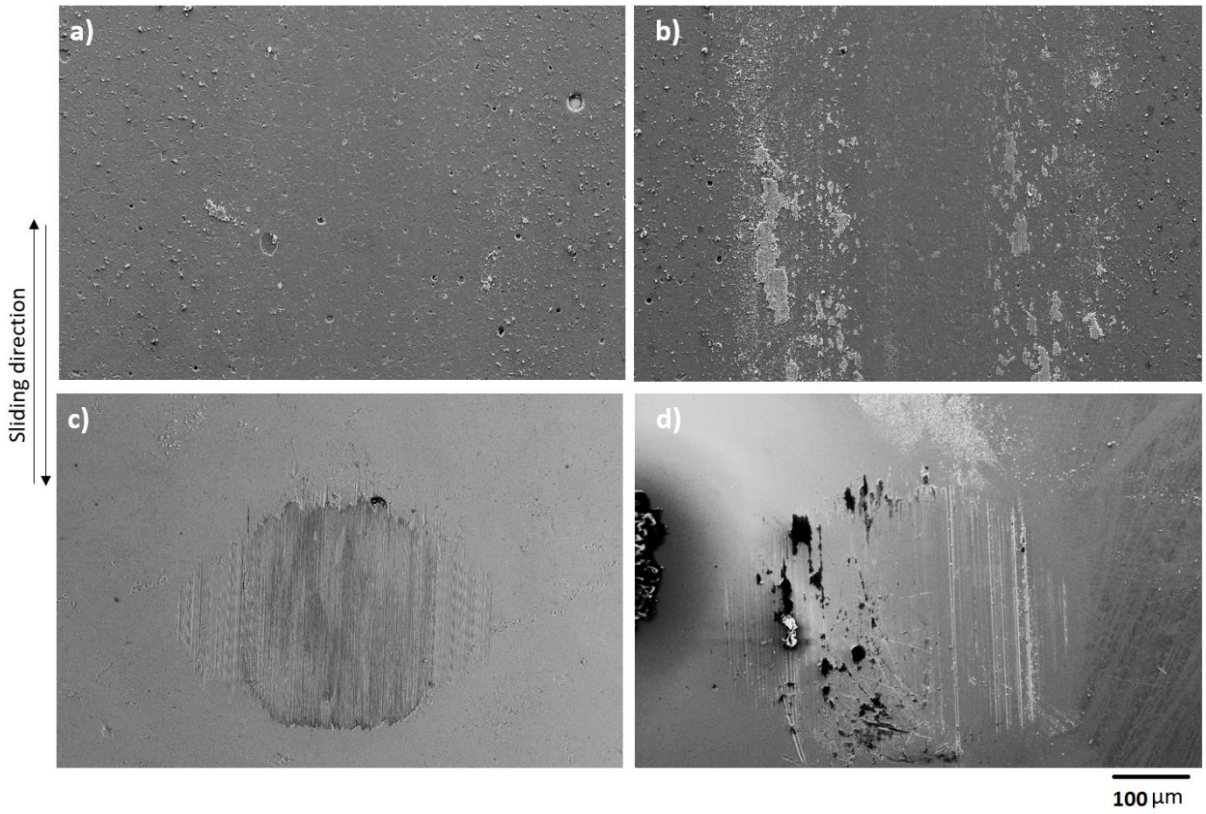

Figure 4.8: Comparison of wear tracks after 100 cycles for TiN film at a) high vacuum, b) 50% relative humidity, and balls tracks rubbed to TiN film at c) high vacuum, d) 50% relative humidity

After 100 cycles, wear tracks are well-defined, but show a strong heterogeneity. To have a global view of the wear track morphology, three characteristics zones were again more specifically considered: both the extremities and the central area (Figure 4.9). Such specific points were selected to qualify the different regions of contact where the load is applied, where the sliding speed is constant, and where the sliding direction was changed. It appears quite compacted particles at the starting point of the contact in high vacuum conditions. On the other

hand, in 50% relative humidity, particles seemed partially spread along the contact-starting region. There were also some debris along the track length. In addition, a large amount of third body particles are strongly compacted and formed a ductile film at the finishing point of the displacement length at humid environment by comparison with the high vacuum mode.

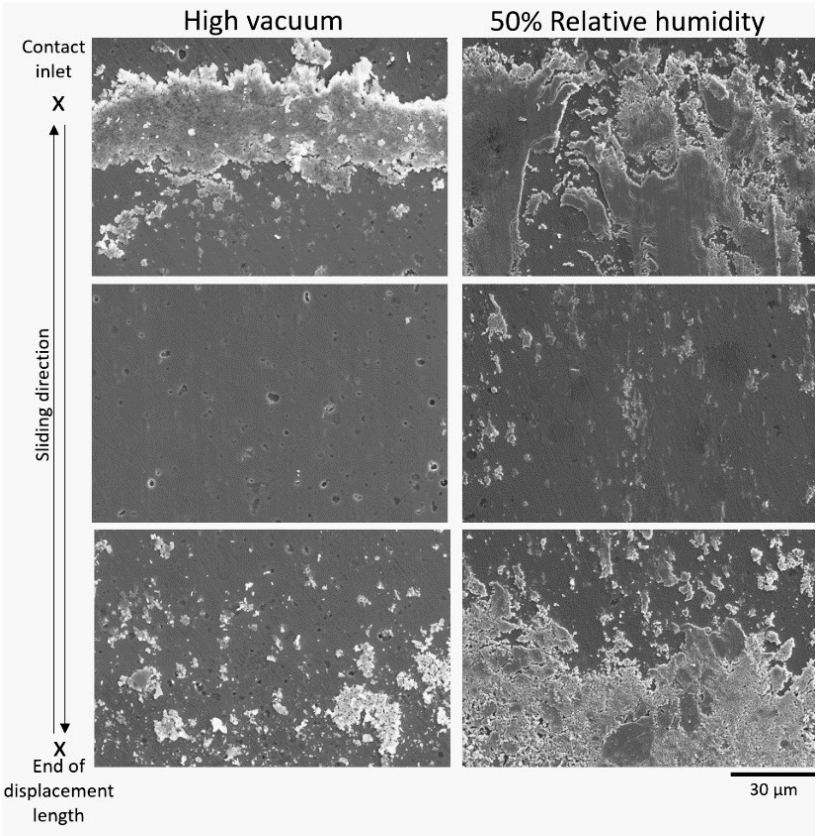

Figure 4.9: Wear track for 3 regions of interest after 100 cycles under high vacuum and 50% relative humidity

A complementary chemical analysis of the worn parts was carried by EDS for the coated flat sample after 100 cycles at the unloading-loading zone and at the center of the wear track (Figure 4.10). Titanium, iron, and oxygen were specifically analyzed: titanium signal reveals the nitride coating, while iron and oxygen indicate debris of the ball counter-part.

Whatever the environment, Ti distribution is inverted with Fe and O signals. Thus, at the tips of the wear track, debris are composed of iron oxide coming from the ball, compacted in the high vacuum test. In presence of relative humidity, the transferred material appeared more ductile and homogeneously distributed, as it is shown in the EDS maps. Also, when the centers of the wear tracks were investigated, small iron particles were detected at high vacuum (Figure 4.10b). However, these particles could come from the ball since there is no significant film

removal on this zone. On the other hand, there is a strong oxide signal in addition to detected iron on the frontiers of the wear track for the test performed in 50% relative humidity (Figure 4.10d). It could be stated that the iron oxide was spread over wear track in the humid environment.

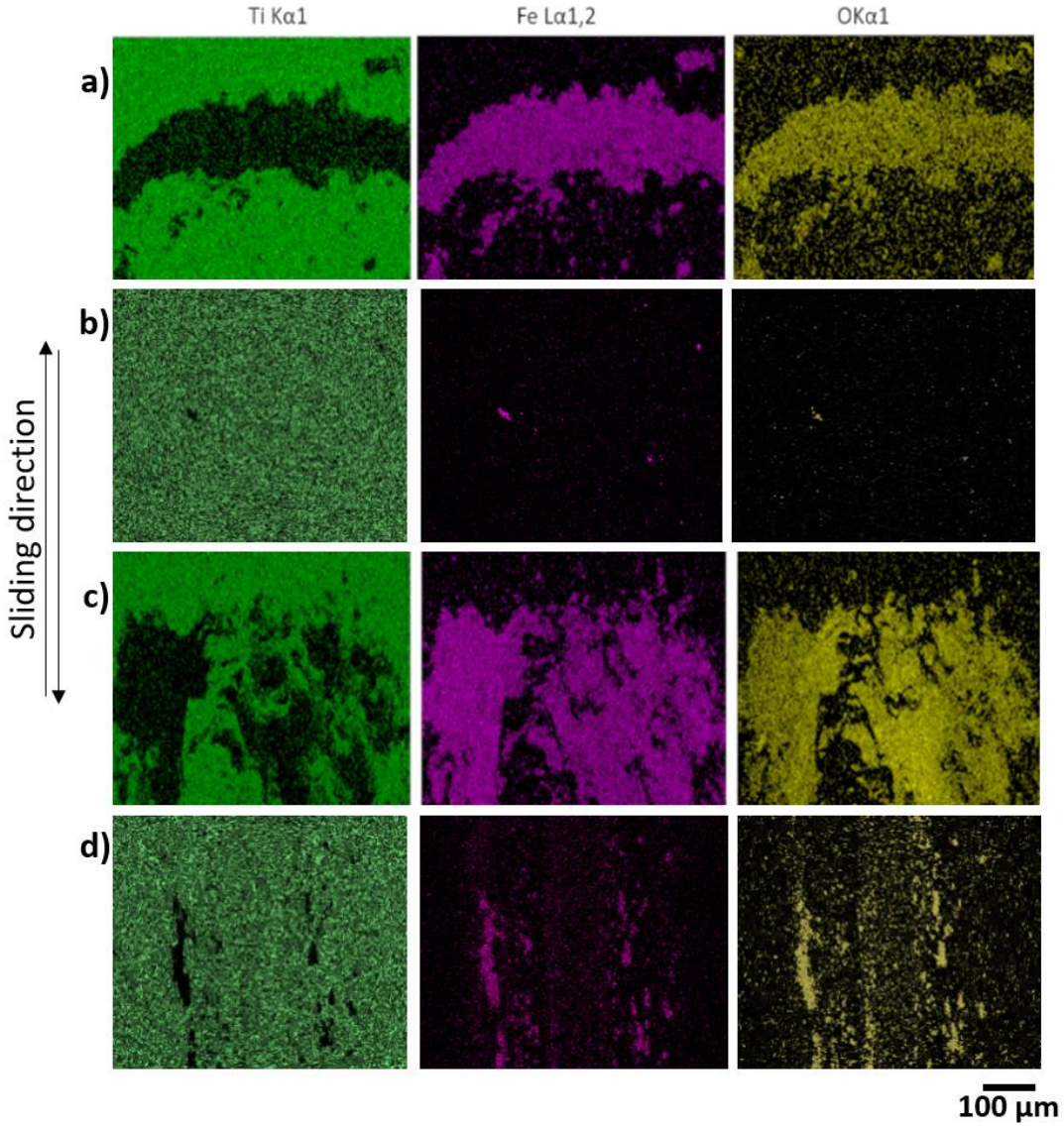

Figure 4.10: EDS maps of the worn TiN film after 100 cycles under at high vacuum from a) the starting of contact, b) center of the contact and at 50% relative humidity from c) starting of the contact, d) center of the contact

In addition to the previous phenomenological approach, a complementary quantitative study was also performed regarding topographic measurements. The damaged surface topography of the wear tracks of TiN film was scanned with a non-contact interferometer. Figure 4.11 shows 3D cross-sectional topographies and the surface profiles of the wear track after the test carried

out in the two environments. The differences in the wear tracks could be seen in the 3D images extracted from the profile analysis.

Wear volumes were calculated as the average of 10 profiles indicated as the lines on the cross-section topographies in Figure 4.11. The reference unworn film surface has been defined as the 0 µm level. Thereby, the volume below the reference surface was considered as the worn material, while the volume above the reference surface was accepted as the accumulated particles along the frontiers of the wear track. When the gained volume was subtracted from the worn volume, the absolute wear volume was calculated. It was seen that the wear volumes were dependent on the atmosphere: it was higher for the wear track which has been generated in 50% of relative humidity (12762±41µm^3) than in high vacuum (9929±23 µm^3) test. It could be stated that even though the oxide layer formed on the wear track of the film caused a decrease of the friction coefficient, it leads to a higher wear volume.

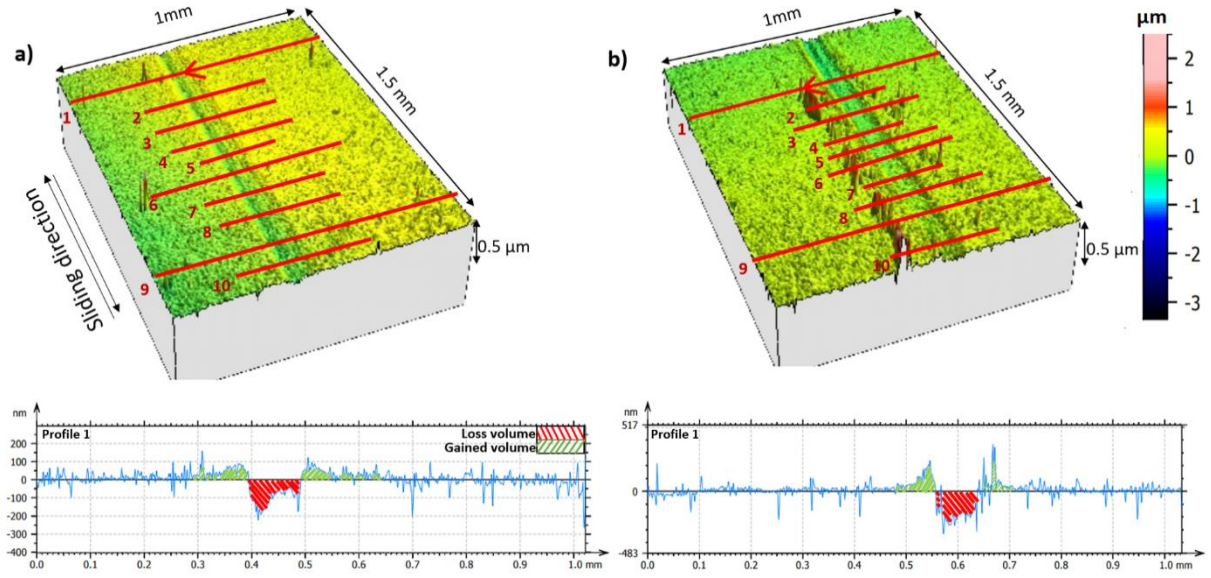

Figure 4.11: Wear track profiles from the beginning of the contact of TiN film with schema of wear volume calculation at a) high vacuum, b) 50% relative humidity

The same microstructural characterization was performed to the ball counter-face (Figure 4.12). Titanium was detected over the wear track on the ball surface at vacuum test, whereas almost no film material was detected on the surface of the ball used in humid mode. However, for the high deformed region of the ball surface, more oxidation was evidenced due to the existence of water vapor at 50% humidity. The iron oxide seemed slightly higher in worn region for ball used in high vacuum test. Since the chamber had to be vented and the ball exposed to ambient air atmosphere, this higher oxidation in the worn zone could be related to an enhanced surface

reactivity due to the fresh exposed worn metallic area. Such a local unexpected reactivity is often reported in tribo-corrosion experiments of passive materials [48]. On the other hand, in humid conditions, a more localized oxidation of the ball is detected on its extremities, without any traces of film transfer.

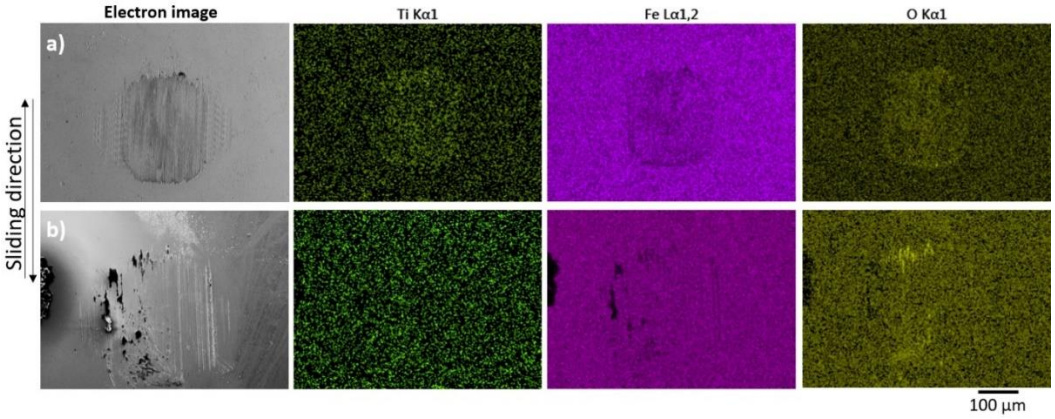

Figure 4.12: Electronic images and EDS maps acquired of the worn steel ball rubbed to TiN film for 100 cycles under a) high vacuum, b) 50% relative humidity

Moreover, profiles of the ball tracks were also characterized by non-contact interferometry (Figure 4.13). The surface of the ball rubbed to TiN film at 50% relative humidity-exhibits a slight visible flattening on the top. It has a rougher topography than high vacuum tests. This result is convenient with the wear tracks topographies and wear volumes calculated for respective environments.

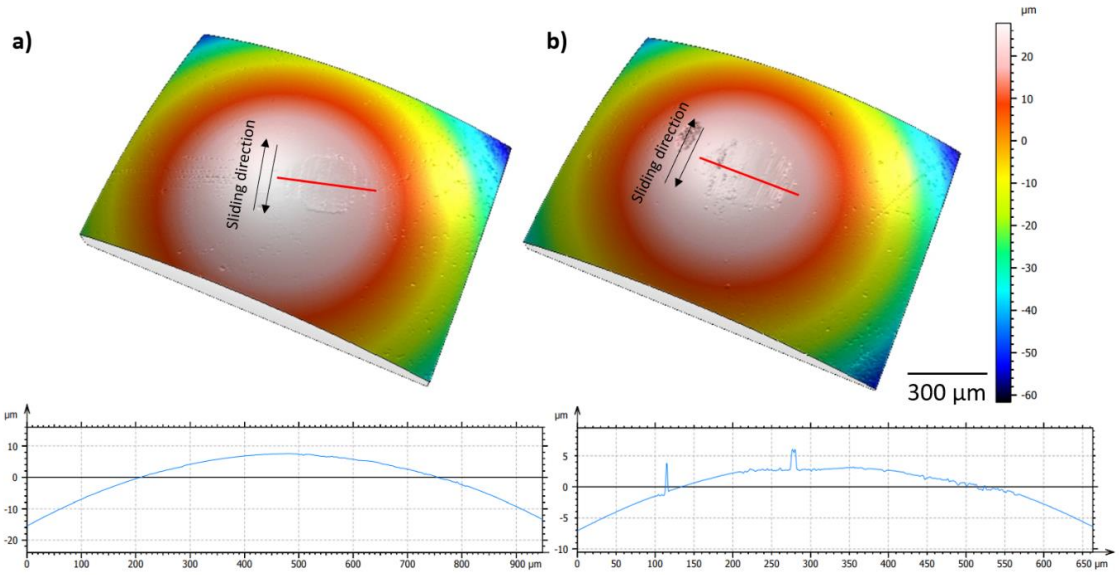

Figure 4.13: Wear tracks on balls rubbed to TiN film after 100 cycles at a) high vacuum, b) 50% relative humidity

4.3. Discussion

4.3.1. Role of a superficial TiN oxidation

The tribological behavior of thin TiN coating against a steel ball was studied at the mesoscale in different environments focusing on the run-in period. It was shown that the tribological behavior of materials involved in the contact and so their friction coefficients were influenced by the atmosphere. Moreover, the particles formed during the humid environment test were more spread and tend to be in crumbled form on the two turning points of the wear track. Under vacuum, particles were more localized and compact on the starting point of the contact of the wear track. Such a particles distribution could be correlated with the soft oxide layer formed on the wear track in humid environment, which was attested by the presence of oxygen by EDS analysis.

The role of humidity on the tribological behavior of TiN coatings has been highlighted in the literature. Yoon et *al.* [27] performed the tests on TiN films where the relative humidity was tuned from 2% to 25% to 85% with steel balls. For the beginning of the tests, it was stated that while the friction coefficient was ~0.25 for the first 100 cycles at 2% and 25% relative humidity, it increased almost up to ~0.35 in 85% relative humidity test. However, with increasing number of cycles, lower friction coefficient was exhibited at 85% relative humidity than the rests performed in 2% and 25% humidity levels. The role of the titanium oxide corroborates the study of Zhang et *al.* on TiN films in dry and lubricated conditions. They indeed showed that the passive layer formed in humid environment on the contact area played the role of a solid lubrication film, decreasing the coefficient of friction [26]. As a confirmation, under high vacuum, the coefficient of friction was higher than under humidity, which can be interpreted by the impossibility for TiN to maintain and feed its superficial passive layer. It is worth mentioning that, there are only few studies about the friction behavior of TiN films under high vacuum. Chen et *al.* [29] have for instance reported a lower mean coefficient of friction as 0.31 under vacuum (0.005 Pa) than in ambient air conditions which was 0.58 (at room temperature, 22-25% RH). Whereas, in our tests, the mean coefficient of friction was 0.75 in vacuum and it decreased to 0.49 for the test performed in 50% RH. These results were defined as unusual also in their study and it was explained by the mechanical polishing of the film surface during the sliding process, which caused a reduction of the surface roughness lowering the coefficient of friction. Nevertheless, their films were unusually thick (10.3 µm) and much higher than ours

(2.3 µm) in addition to the longer displacement length that they selected for their procedure. This difference in thickness and displacement may affect also the final surface roughness of TiN films between two studies, which may contribute to explain the two differential sliding regimes.

4.3.2. Effect of unloading-reloading process: Role of debris dynamics

To perform *in situ* analyses, a procedure involving successive loading and unloading of the system was required. This procedure caused a relatively lowered mean COF for the first cycle of each set, with an increasing trend for the following cycles in the same set (Figure 4.4). This issue explains why the both extremities of the wear track, where particles accumulate, is dissymmetric, highlighting by the different distribution and volume of the particles.

In order to estimate influence of the transitory loading-unloading steps, a 100-cycles test was performed in a single run without any opening of the contact. Evolution of the mean COF with respect to the cycle number appears in figure 4.14. The COF in humid conditions is quite stable around 0.40 which is very close to the value of the contact-interrupted *in situ* test (Figure 4.4). However, the tribological response recorded under high vacuum is much more complex, with a continuous increase of the COF from 0.45 to 0.90 for the 35 first cycles, strictly similar to the one reported in Figure 4.4. Then, from 40 to 60 cycles, the evolution is drastically changed with a slight decrease of the COF, which can be attributed to trapping of debris and then ejection of them after cycle 60. Finally, a scattered regime is initiated, with fluctuating values reaching 1.0 to 1.10. Such an evolution suggests a modification of the nature of the contact during the test, reaching a steel-steel contact.

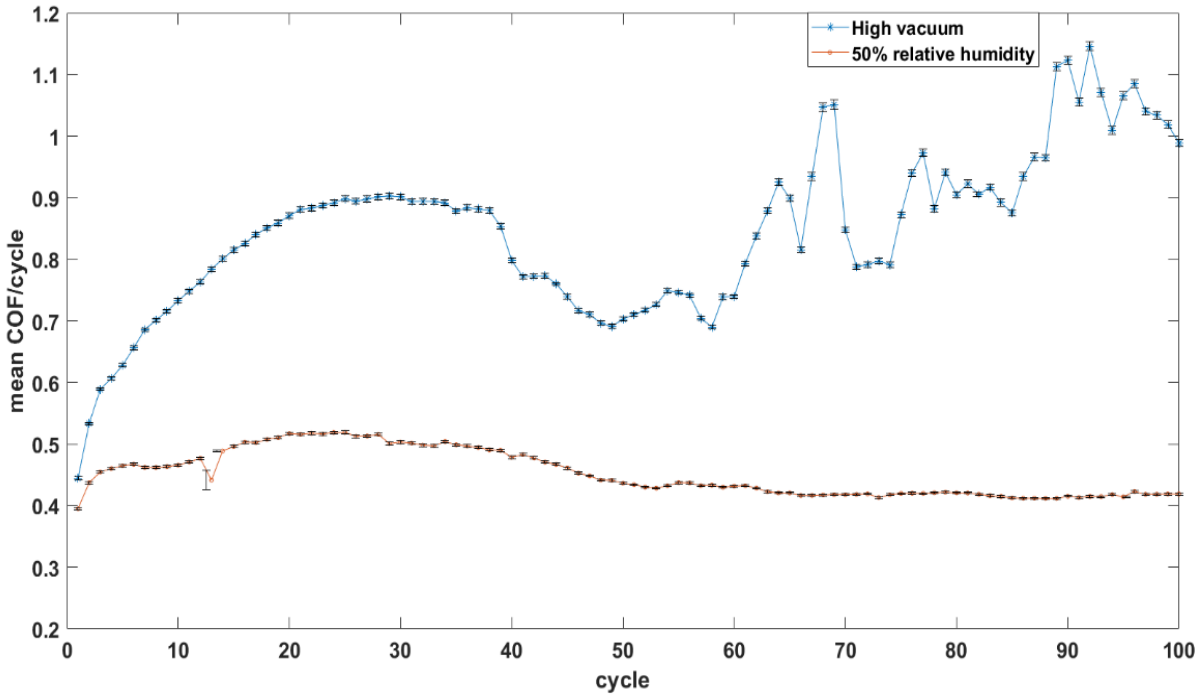

Figure 4.14: Evolution of the mean coefficient of friction for the tests carried out in a single run (without successive opening of the contact) for 100 cycles at high vacuum and 50% relative humidity tests.

Under vacuum, the EDX analysis of the wear track (figure 4.15a) confirmed that the uninterrupted test has led to the total removing of the nitride coating, and the underlying steel substrate appearing. On ball track, an important transfer of TiN and large amount of particles or agglomerates of TiN were also highlighted in the center (figure 4.15c). These debris are accumulated at edges of the track, but also stacked to the ball center, which highlighted that some TiN debris were trapped in the contact. In the loading-unloading configuration, each successive unloading of the contact led to a significant loss of released debris, resulting in an under-estimated reduced wear. In opposite, in the case of the uninterrupted test under vacuum, debris are emitted during the first 35 cycles and are trapped in the contact area, leading to a higher damage of the coating until its total consumption.

For the test conducted under 50% relative humidity, the film remained whatever the protocol adopted: with or without contact opening. Traces of iron oxides are detected all along the track coming from the ball (figure 4.15b). Chemical analysis of the ball track has highlighted a local oxidation of the ball contact region under humid environment (Figure 4.15d). The beneficial effect of the humidity on the sliding conditions, already revealed in the loading-unloading

configuration, is confirmed. That confirms the protective role of the passive layer formed under relative humidity.

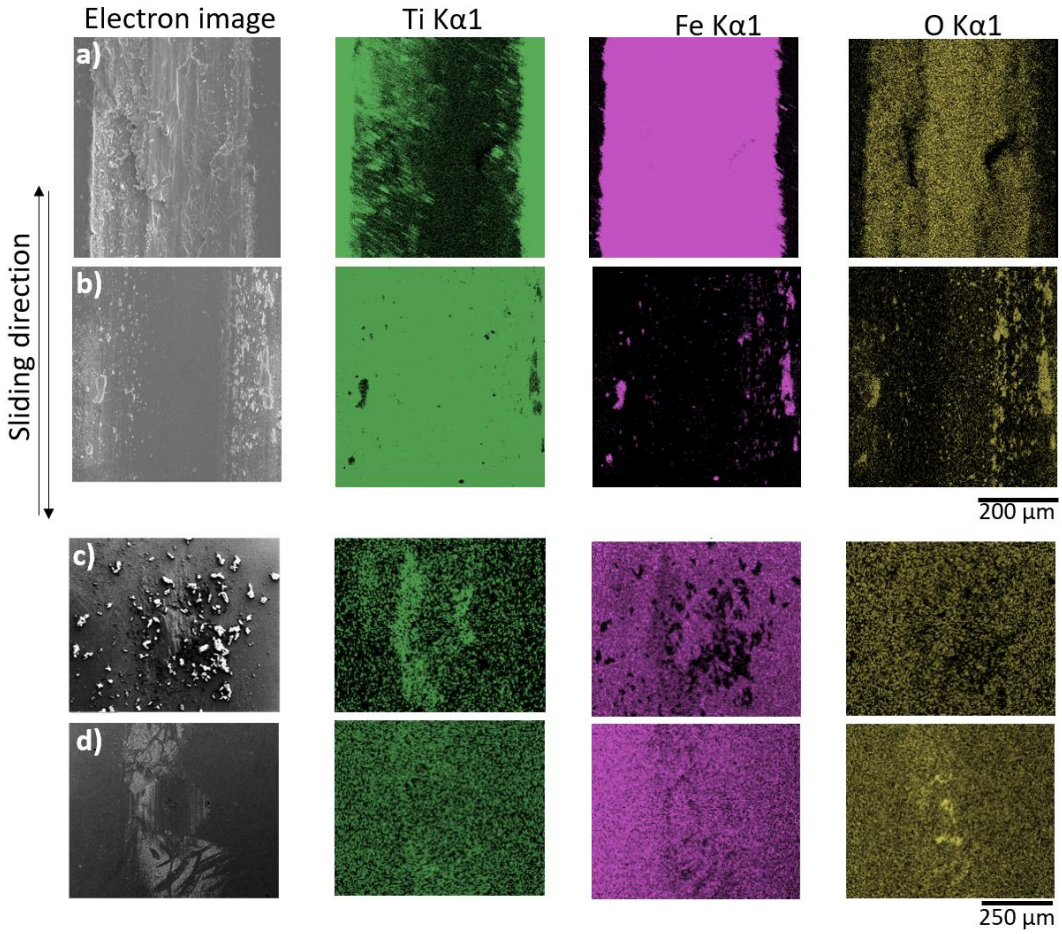

Figure 4.15: EDS Maps after uninterrupted test. Wear track under a) high vacuum, b) 50% relative humidity and ball track under c) high vacuum, d) 50% relative humidity

4.3.3. Towards a mechanism of degradation

Combining the evolution of COF in both configurations, with contact opening (Figure 4.4) or as uninterrupted (Figure 4.14), the morphology and the chemical nature of wear tracks, it is possible to propose a degradation mechanism highlighting the role of environment on the one hand, and the dynamics of debris on the other hand. The results can be revisited in the light of the tribological circuit [16] which describes the different third body flows that may take place in a contact. The source flow (Qs) corresponds to the detachment of particles due to tribological transformations of the structure or damage mechanisms such as cracking, abrasion… It leads to the formation of the third body. The internal flow is the flow of the third body circulating inside the contact. The recirculation flow (Qr) is composed of the third body escapes from the contact

and reintroduced into the contact. Wear flow (Qw), is composed of the third body (wear debris) that has been definitively ejected from the contact and can no longer participate in velocity accommodation. The wear rate is defined through a balance between the particles formation flow (Qs) and the particles ejection flow (Qe) from the contact [49]. Schemas presented in Figure 4.16 illustrates the evolution of the contact area throughout the continuous test, highlighting the nature of interfaces involved in the contact.

Under vacuum, the debris at the edges of the wear track are constituted from iron and titanium, meaning that source flow of particles come from the ball and the coating. The accumulation of those debris at the edges, *e.g.* outside of the contact, highlighted that wear flow has been activated. The particles trapped in the contact contributed to the internal flow and caused changes on the friction response of the film. Such hard debris would act as abrasive matter. In the loading-unloading configuration, those debris can be lost for the contact because of the opening procedure and a new contact steel – TiN is occurred without such debris (the coating is still visible after each 10 cycles (Figure 4.5)). Even if the source flow is reactivated to form new debris, the ejection of debris at next opening (wear flow) prevent the abrasion. In the single run configuration, debris were trapped, preventing this cyclic phenomenon but allowing abrasion by activation of the internal flow, causing a dramatic wear of the coating (Figure 4.16c), until reaching the substrate itself (Figure 4.16d).

At 50% relative humidity, a plastic deformation was observed on the film and ball surfaces. Besides, the film was preserved throughout the 100 cycles. Under humidity, the nature of the coating surface is different than under vacuum, and present an initial passive titanium oxide layer. Such top layer, in contact with the ball, is soft. Source flow is constituted by particles detached from the coating (presence of Ti) and thus of this passive layer and by particles detached from the ball (presence of iron). The accumulation of particles at the edges and some debris along the track length, *e.g.* outside the contact, highlighted that wear flow has been activated. The third body present in the contact spread on the surface, and contributed to the internal flow. Its ductility facilitates is entrapment whatever the configuration. The wear flow is not increased between the two configurations. Furthermore, the water vapor environment is prone to continuously feed and renew the passive layer, which would be on the basis of the stable and lower COF values with time compared to those under vacuum.

The small-scale tribological investigation adopted in this study was then able to explain the beneficial solid-lubricant role of titanium oxide reported in the literature, and in this sense has validated our approach together with the mini-tribometer.

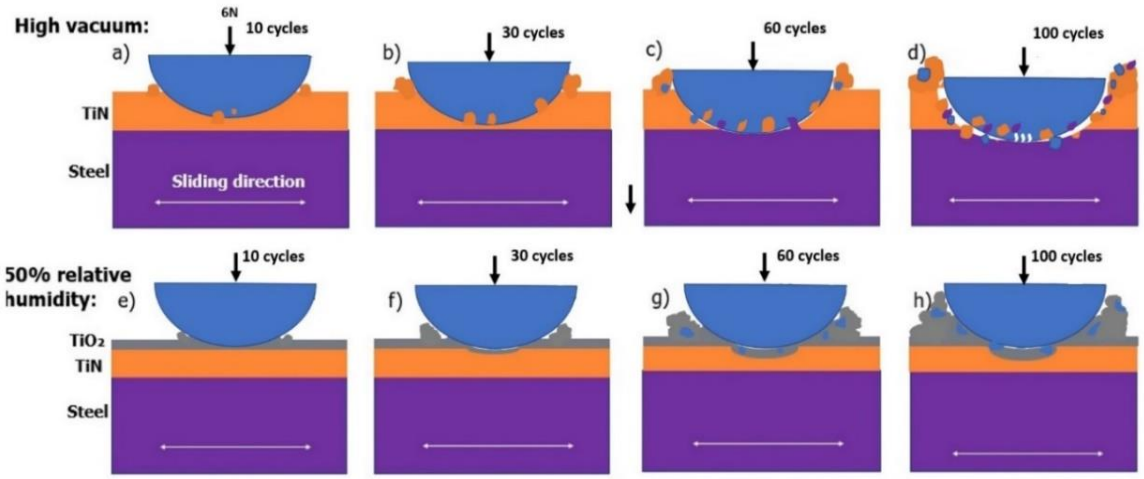

Figure 4.16: Schematic representation of the damaging mechanism of TiN-coated steel under a-d) high vacuum, or e-h) 50% relative humidity.

(The scale of balls and films thickness are not adapted to emphasize the deformation on both film and ball surfaces clearly)

4.4. Conclusion

To sum up, *in situ* characterization of a model-TiN film was performed during the run-in period with a home-made reciprocating mini-tribometer. This device can be introduced into the chamber of an environmental SEM, to analyze the effect of the environment on the tribological behavior of materials at small scale. The main experimental parameters; loading, displacement characteristics and nature of the environment are controlled, while the COF is continuously measured. Morphology of the film wear track is recorded *in situ* throughout the tribo-test. A *post mortem* evaluation of the worn damaged volume was also done on both counterparts, together with a morphological and chemical characterization of wear tracks.

To validate this device, a model-contact was investigated as a proof-of-concept: a PVD micrometric TiN film rubbing onto a hard steel ball and the relevance, repeatability and efficiency of the mini-tribometer were demonstrated.

It was shown that degradation mechanisms of TiN were strongly dependent on its use environment: the role of humidity, which allowed a continuous growth of oxide layer favoring the sliding was confirmed, while it was demonstrated that the wear of TiN under vacuum was rather governed by the dynamic of abrasive debris (third body flows).

Unfortunately, a real-time chemical characterization of the wear track was not possible with the current configuration. This next step can be achieved either by performing EDX analysis *in situ* in SEM, or by using a transparent ball, allowing a continuous analysis of the contact by Raman spectroscopy.

References (Chapter 4)

[1] P. Kapsa, Tribology at Different Scales, *Advanced Engineering Materials. 3*(8) (2001) 531. doi:10.1002/1527-2648(200108)3:8<531:aid-adem531>3.0.co;2-1.

[2] Y. Berthier, Handbook of Materials Behavior Models, Acad.Press, Lemaître, 2001, pp. 676–699.

[3] W. G. Sawyer, K. J. Wahl, Accessing Inaccessible Interfaces: In Situ Approaches to Materials Tribology, *MRS Bulletin, 33*(12), 1145-1150. (2008) doi:10.1557/mrs2008.244.

[4] M. Kosinskiy, S. I. Ahmed, Y. Liu, J. A. Schaefer A compact reciprocating vacuum microtribometer. *Tribology International, 56*, (2012) 81-88. doi:10.1016/j.triboint.2012.06.019.

[5] M. J. Cordill, P. Kreiml, C. Mitterer, Materials Engineering for Flexible metallic thin film applications, *Materials*, *15*(3), (2022) 926. https://doi.org/10.3390/ma15030926.

[6] P. Stoyanov, R. Chromik, Scaling Effects on Materials Tribology: From Macro to Micro Scale, *Materials, 10*(5), (2017) 550. doi:10.3390/ma10050550.

[7] D. D. Kumar, N. Kumar, S. Kalaiselvam., S. Dash, R. Jayavel, Micro-tribo-mechanical properties of nanocrystalline TiN thin films for small scale device applications, *Tribology International, 88*, (2015) 25-30. doi:10.1016/j.triboint.2015.02.031.

[8] B. Bhushan, Tribology on the macroscale to nano-scale of microelectromechanical system materials: A review, *Proceedings of the Institution of Mechanical Engineers, Part J: Journal of Engineering Tribology, 215*(1), (2001) 1-18. doi:10.1243/1350650011541657.

[9] M. Gee, J. Nunn, A. Muniz-Piniella, L. Orkney, Micro-tribology experiments on engineering coatings, *Wear, 271*(9-10), (2011) 2673-2680. doi:10.1016/j.wear.2011.02.031.

[10] C. C. Schmitt, J. R. Elings, M. Serry, Nanoindenting, Scratching and Wear Testing with the Atomic Force Microscopy, Bruker (2010).

[11] Y. G. Gogotsi, A. Kailer, K. G. Nickel, Phase transformations in materials studied by micro-raman spectroscopy of indentations, *Materials Research Innovations*, *1*(1), (1997) 3–9. https://doi.org/10.1007/s100190050011.

[12] A. V. Desai & M. A. Haque, A novel MEMS nano-tribometer for dynamic testing in-situ in Sem and Tem. *Tribology Letters*, *18*(1), (2005), 13–19. https://doi.org/10.1007/s11249-004-1700-z

[13] T. D. Jacobs, C. Greiner, K. J. Wahl, R. W. Carpick, Insights into tribology from in situ nano-scale experiments, *MRS Bulletin*, *44*(06), (2019) 478-486. doi:10.1557/mrs.2019.122.

[14] J. Heinrichs,, M. Olsson, I. Z. Jenei, S. Jacobson, Transfer of titanium in sliding contacts—New discoveries and insights revealed by in situ studies in the SEM, *Wear, 315*(1-2), (2014) 87-94. doi:10.1016/j.wear.2014.04.006.

[15] J. Heinrichs, M. Olsson, S. Jacobson, Mechanisms of material transfer studied in situ in the SEM, *Wear, 292-293*, (2012) 49-60. doi:10.1016/j.wear.2012.05.033.

[16] W. Federle, T. Endlein, Locomotion and adhesion: Dynamic control of adhesive surface contact in ants, *Arthropod Structure & Development, 33*(1), (2004) 67-75. doi:10.1016/j.asd.2003.11.001.

[17] J. Heinrichs, M. Olsson, S. Jacobson, Influence of tool steel microstructure on initial material transfer in metal forming—In situ studies in the SEM, *Wear, 302*(1-2), (2013) 1249-1256. doi:10.1016/j.wear.2013.01.114.

[18] A. P. Merkle, L. D. Marks, Liquid-like tribology of gold studied by in situ TEM, *Wear, 265*(11-12), (2008) 1864-1869. doi:10.1016/j.wear.2008.04.032.

[19] S. Descartes, Y. Berthier, Rheology and flows of solid third bodies: Background and application to an MoS1.6 coating, *Wear, 252*(7-8), (2002) 546-556. doi:10.1016/s0043-1648(02)00008-x.

[20] J. Martin, T. L. Mogne, M. Boehm, C. Grossiord, Tribochemistry in the analytical UHV tribometer, *Tribology International, 32*(11), (1999) 617-626. doi:10.1016/s0301-679x(99)00090-0.

[21] J. M. Shockley, S. Descartes, P. Vo, E. Irissou, R. R. Chromik, The influence of al2o3 particle morphology on the coating formation and dry sliding wear behavior of cold sprayed al–al2o3 composites, *Surface and Coatings Technology*, *270*, (2015) 324–333. https://doi.org/10.1016/j.surfcoat.2015.01.057 .

[22] S. Descartes, L. Courtieux, Y. Berthier, F. Peditto, Tribological study of Oral Care Silica, *Tribology International*, *82*, (2015) 551–560. https://doi.org/10.1016/j.triboint.2014.02.023.

[23] J. R. Waldrop, Titanium nitride schottky-barrier contacts to gaas. *Applied Physics Letters*, *43*(1), (1983) 87–89. https://doi.org/10.1063/1.94131.

[24] C. Muratore, J. E. Bultman, S. M. Aouadi, A. A. Voevodin, In situ raman spectroscopy for examination of high temperature tribological processes, *Wear*, *270*(3-4), (2011) 140–145. https://doi.org/10.1016/j.wear.2010.07.012.

[25] B. Murarash & M. Varenberg, Tribometer for in situ scanning electron microscopy of microstructured contacts. *Tribology Letters*, *41*(2), (2010), 319–323. https://doi.org/10.1007/s11249-010-9717-y

[26] Y. Naerheim, A SEM/AES/XPS tribometer for rolling and sliding contacts. *Wear*, *162-164*, (1993), 593–596. https://doi.org/10.1016/0043-1648(93)90547-y

[27] B. Meylan, D. Ciani, B. Zhang, E. Cuche & K. Wasmer, A new ball-on-disk vacuum tribometer with *in situ* measurement of the wear track by Digital Holographic Microscopy. *Surface Topography: Metrology and Properties*, *5*(4), (2017), 044004. https://doi.org/10.1088/2051-672x/aa854a

[28] C. Chen, P. Xue, X. Fan, C. Wang & D. Diao, Friction-induced rapid restructuring of graphene nanocrystallite cap layer at sliding surfaces: Short run-in period. *Carbon*, *130*, (2018) 215–221. https://doi.org/10.1016/j.carbon.2018.01.022

[29] R. R. Chromik, A. L. Winfrey, J. Lüning, R. J. Nemanich & K. J. Wahl, Run-in behavior of Nanocrystalline Diamond Coatings studied by in situ tribometry. *Wear*, *265*(3-4), (2008), 477–489. https://doi.org/10.1016/j.wear.2007.11.023

[30] M. J. Marino, E. Hsiao, Y. Chen, O. L. Eryilmaz, A. Erdemir & S. H. Kim, Understanding run-in behavior of diamond-like carbon friction and preventing diamond-like carbon wear in humid air. *Langmuir*, *27*(20), (2011), 12702–12708. https://doi.org/10.1021/la202927v

[31] T. W. Scharf, & I. L. Singer, Rolce of the transfer film on the friction and wear of metal carbide reinforced amorphous carbon coatings during run-in. *Tribology Letters*, *36*(1), (2009), 43–53. https://doi.org/10.1007/s11249-009-9457-z

[32] J. Michael, S. Prasad, J. Jungk, M. J. Cordill, D. Bammann, C. Battaile, N. Moody, B. Majumdar, Modeling of friction-induced deformation and microstructures, (2016) https://doi.org/10.2172/902880.

[33] P.J. Blau, On the nature of running-in. *Tribology International*, *38*(11-12), (2005), 1007–1012. https://doi.org/10.1016/j.triboint.2005.07.020

[34] M. Sasaki, I. Nakamura, I. Takano, Y. Sawada, Vacuum pressure dependence of the tribological properties of Ti, TiO2, and TiN thin films, *Electrical Engineering in Japan*, *149*(3), (2004) 1-7. doi:10.1002/eej.20020.

[35] Q. Chen, A. Li, G. Wu, Z. Lu, G. Zhang, G. Tian, Structure vs chemistry: Tribological behavior of TiN films in the nitrogen atmosphere, *Ceramics International*, *46*(18), (2020) 28053-28063. doi:10.1016/j.ceramint.2020.07.300.

[36] L. Zhang, H. Yang, X. Pang, K. Gao, H. T. Tran, A. A. Volinsky, TiN-Coating Effects on Stainless Steel Tribological Behavior Under Dry and Lubricated Conditions, *Journal of Materials Engineering and Performance*, *23*(4), (2014) 1263-1269. doi:10.1007/s11665-014-0904-0.

[37] S. Yoon, M. Kang, S. Kwon, K. H. Kim, The influence of counterface materials and humidity on the tribological behavior of arc ion plated TiN films, *Surface and Coatings Technology*, *157*(2-3), (2002) 144-150. doi:10.1016/s0257-8972(02)00145-7.

[38] A. Gant, M. Gee, L. Orkney, The wear and friction behaviour of engineering coatings in ambient air and dry nitrogen, *Wear*, *271*(9-10), (2011), 2164-2175. doi:10.1016/j.wear.2011.02.032.

[39] Q. Chen, G. Wu, D. Li, A. Li, L. Shang, Z. Lu, Z. Zhang, Z. Wu, G. Tian, Understanding the unusual friction behavior of TiN films in vacuum, *Tribology International*, *137*, (2019) 379-386. doi:10.1016/j.triboint.2019.05.024.

[40] M. Gee, T. Kamps, P. Woolliams, J. Nunn, K. Mingard, In situ real time observation of tribological behaviour of coatings, *Surface and Coatings Technology*, *442*, (2022) 128233. https://doi.org/10.1016/j.surfcoat.2022.128233.

[41] D. J. Stokes, Characterisation of soft condensed matter and delicate materials using environmental scanning electron microscopy (ESEM), *Advanced Engineering Materials*, *3*(3), (2001) 126–130. https://doi.org/10.1002/1527-2648(200103)3:3<126::aid-adem126>3.0.co;2-b.

[42] L. F. Lu, H. Y. Chen, Characterization of titanium nitride films deposited by cathodic arc plasma technique on copper substrates, *Surface and Coatings Technology*, *130*(2-3), (2000) 290–296. https://doi.org/10.1016/s0257-8972(00)00710-6.

[43] M. A. Hussein, A. Y. Adesina, A. M. Kumar, A. A. Sorour, N. Ankah, N. Al-Aqeeli, Mechanical, in-vitro corrosion, and tribological characteristics of TiN coating produced by cathodic arc physical vapor deposition on Ti20nb13zr alloy for biomedical applications, *Thin Solid Films*, *709*, (2020) 138183. https://doi.org/10.1016/j.tsf.2020.138183.

[44] A. Mège-Revil, P. Steyer, G. Thollet, R. Chiriac, C. Sigala, J. C. Sanchéz-Lopéz, C. Esnouf, Thermogravimetric and in situ sem characterisation of the oxidation phenomena of protective nanocomposite nitride films deposited on steel, *Surface and Coatings Technology*, *204*(6-7), (2004) 893–901. https://doi.org/10.1016/j.surfcoat.2009.06.040.

[45] P. Steyer, A. Mege, D. Pech, C. Mendibide, J. Fontaine, J. F. Pierson, C. Esnouf, P. Goudeau, Influence of the nanostructuration of PVD Hard Tin-based films on the durability of Coated Steel, *Surface and Coatings Technology*, *202*(11), (2008) 2268–2277. https://doi.org/10.1016/j.surfcoat.2007.08.073.

[46] V. Chawla, R. Jayaganthan, R. Chandra, Microstructural characteristics and mechanical properties of magnetron sputtered nanocrystalline tin films on glass substrate, *Bulletin of Materials Science*, *32*(2), (2009) 117–123. https://doi.org/10.1007/s12034-009-0018-8.

[47] T. Namazu, S. Inoue, H. Takemoto, K. Koterazawa, Mechanical properties of polycrystalline titanium nitride films measured by XRD tensile testing, *IEEJ Transactions on Sensors and Micromachines*, *125*(9), (2005) 374–379. https://doi.org/10.1541/ieejsmas.125.374.

[48] K. Kim, J. Geringer, J. Pellier, D. D. Macdonald, Fretting corrosion damage of total hip prosthesis: Friction coefficient and damage rate constant approach, *Tribology International*, *60*, (2013) 10–18. https://doi.org/10.1016/j.triboint.2012.10.008.

[49] N. Fillot, I. Iordanoff, Y. Berthier, Modelling third body flows with a discrete element method—a tool for understanding wear with adhesive particles, *Tribology International*, 40, (2007) 973–981. doi:10.1016/j.triboint.2006.02.056.

5. FUNCTIONAL CHARACTERIZATION OF Ti-Ag MAGNETRON SPUTTERED THIN FILMS – PRELIMINARY TRIBOLOGICAL STUDY

The deposition parameters for the Ti-Ag films and the details about the deposition process were indicated. Then the film characteristics were evaluated in terms of the chemical compositions and the microstructural properties. Effect of Ag content on the mechanical and electrical properties were explained in addition to the film densities. Moreover, the preliminary tribological tests results were discussed in terms of the role of the silver content and the environmental conditions.

5. FUNCTIONAL CHARACTERIZATION OF Ti-Ag MAGNETRON SPUTTERED THIN FILMS – PRELIMINARY TRIBOLOGICAL STUDY

5.1 Introduction

In modern medicine, it is necessary to accurately monitor the biopotential generated by human body. Electrocardiography (ECG), electroencephalography (EEG) and electromyography (EMG) are common examples for which these system electrodes are needed. With the exponential interest of the use of bio-sensors for variety of applications, the surface of the electrodes was functionalized by conductive films which were formed via PVD processes in most of the studies [1-10].

Titanium with its high corrosion resistance, self-cleaning and bio-compatible character, was considered as a suitable material for the thin films to be used in bio-sensor applications [4]. Besides, it could be deposited with various alloying elements to enhance the performance of the film. As the external element, silver is a good candidate to incorporate with titanium regarding its antibacterial nature. It also tends to form intermetallic compounds with titanium and improves the film properties [5].

In previous studies, several properties of Ti-Ag PVD thin films have been investigated. For example, to examine the anti-bacterial character of Ti-Ag films, Wojcieszak et *al.* observed how several bacteria and fungi species do evolve on the surface of these coatings and in 24 hours all the microbes were dead owing the strong biocide effect of the films [6]. Moreover, to analyse the durability of Ti-Ag films, Lopes at *el.* studied the mechanical properties of them and it was seen that these films had good combination of high mechanical strength and low Young's modulus which made them suitable for biosensing [7]. Also, Marques et *al.* performed strain analysis of Ti-Ag films and indicated that, up to 5% of strain, these films could be an efficient choice for the piezoresistive sensors [8]. In another study, Lopes et *al.* investigated the tuning of the electrical properties by depositing Ti-Ag films with glancing angle deposition in various angles and heat treatment to provide the better signal acquisition. It was seen that with increasing temperature, electrical properties were enhanced; however, with increasing angle of the flux, the film microstructure became too porous and the electrical resistivity increased [9].

Moreover, Etiemble et *al*. examined the effect of Ag content on the fracture resistance and continuous bio-signal acquisition of these films with an *in situ* fracture test. It was seen that with increasing Ag content crack density and electrical resistivity decreased. Also, the pathway of electrical conduction was preserved for the film with the highest Ag content [10].

Regarding all the aspects mentioned above, it could be stated that Ti-Ag PVD films are good candidates for bio-sensor applications and changing Ag content can provide modification on the performance of these coatings. Therefore, in this chapter the microstructural, electrical, mechanical properties of films will be analysed regarding the role of Ag content. Even though there are several studies about the characterization of Ti-Ag PVD coatings as expressed above, their tribological behaviour has never been investigated. Thereby, as another goal of this chapter, the tribological behaviour of these films were examined considering not only the effect of Ag content, but also the influence of the environment.

5.2. Static Analysis of Ti-Ag films

A multi-scale characterization was performed on a first series of films, not really optimised for their sliding properties. The aim of this chapter is to better understand how silver does influence properties of films. In a second part, preliminary tribological test will be conducted in order to assess their behaviour in terms of friction.

Four different films were deposited onto several different substrates. Firstly, pure-Ti target was used for deposition of the film without any silver addition. Binary films were also deposited by placing 4, 32 and 120 Ag pellets along the erosion zone of the Ti target to achieve various film compositions in terms of Ag/Ti ratio.

5.2.1 Microstructural characterization of Ti-Ag films

5.2.1.1 SEM analysis

It was aimed to deposit Ti-Ag films with PVD technique in ~1 µm of thickness. The target preparation was done specifically for each composition before the deposition process. While Ti-reference film was deposited with pure Ti target, films containing silver were deposited by placing certain number of Ag pellets along the erosion zone of Ti target via silver paint. The number of Ag pellets inserted on target surface were selected regarding the expected composition of the film. In SEM, the films deposited on silicon wafer substrate were analysed

for their both cross sections and top surfaces. Since the deposition efficiency of Ag is higher than Ti, the deposition time decreased with increasing number of Ag pellets used during the deposition to reach ~1 µm of thickness.

After the deposition process, the chemical composition of each film was investigated. Based on the EDS analysis, as expected, Ag content in the final film composition increased with increasing number of Ag pellets on Ti target (Figure 5.1).

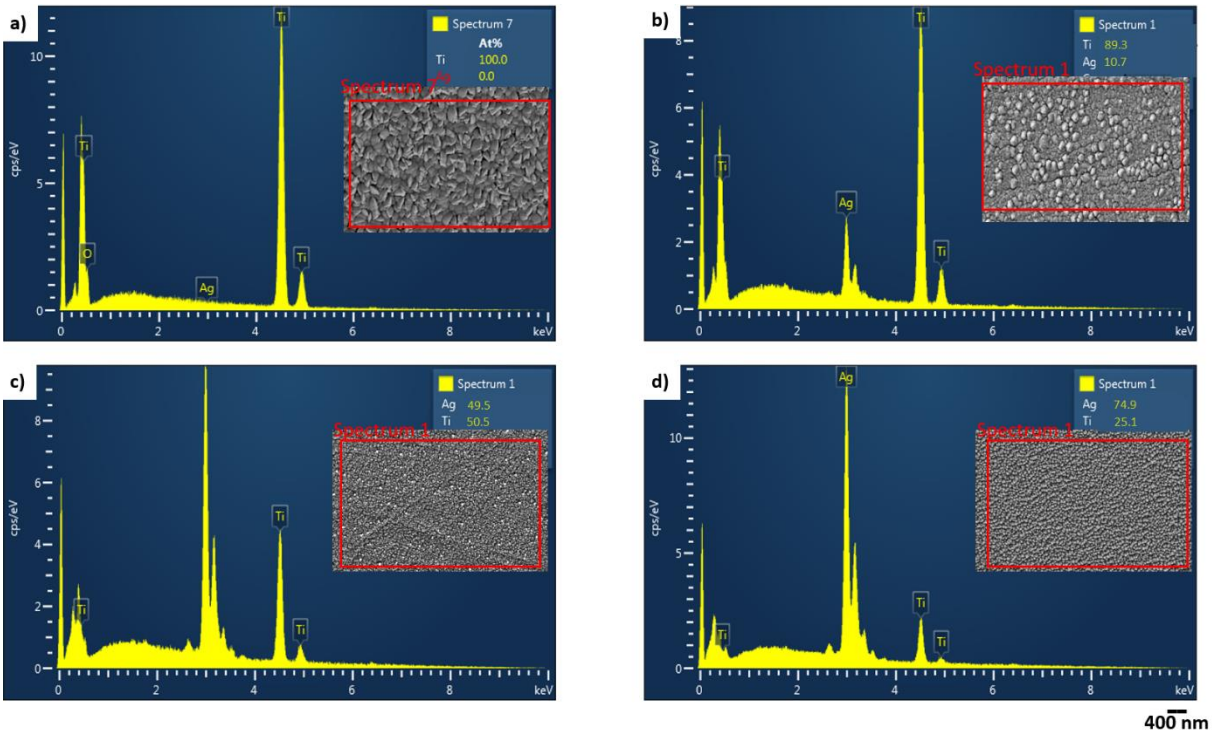

Figure 5.1: EDS analysis of the compositions for Ti-Ag films deposited with a) 0, b) 4, c) 32, d) 120 Ag pellets on Ti target.

It was seen that for the Ti-Ag film deposited with 4 Ag pellets on Ti-target, Ag content in final film composition is 9-10 (at.) % while it is about 48.5-5(at.) % for the film deposited with 32 pellets and 71.2-73.4% for the film deposited with 120 pellets. Based on these values the atomic ratio of Ag to Ti was calculated for each composition as it is shown in table 5.1.

Table 5.1: Films composition and thicknesses regarding the number of Ag pellets inserted on Ti target during deposition

Film/Deposition parameters	Ag/Ti (at%)	Ag (at.%)	Ti (at.%)	Thickness (µm)
Ti-reference	0	0	100	1.05
Ti-Ag with 4 Ag pellets	0.12	10.7	89.3	1.14

Ti-Ag with 32 Ag pellets	0.98	49.5	50.5	1.10
Ti-Ag with 120 Ag pellets	3.14	75.8	24.2	1.25

As asserted by Lopes [11], silver addition in the film drastically modifies its morphology, in terms of plan-view as well as in cross section (Fig. 5.2, 5.3).

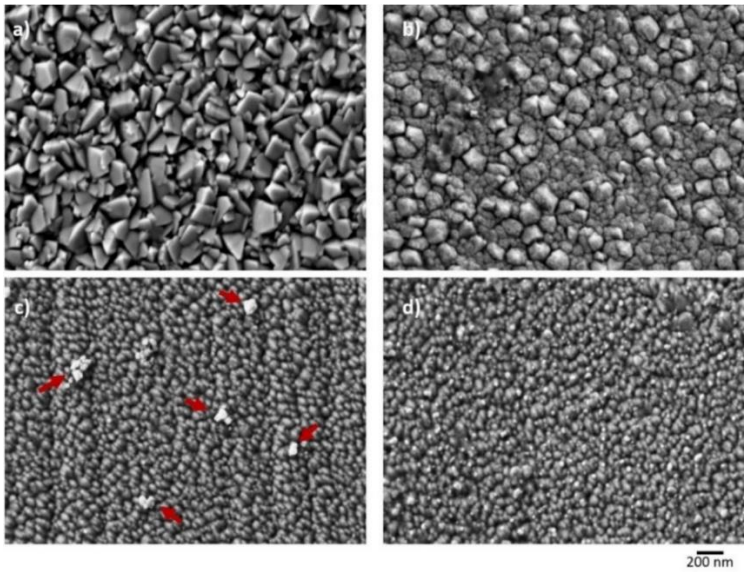

Figure 5.2: Top surfaces of Ti-Ag films with Ag/Ti= a) 0, b) 0.12, c) 0.98, d) 3.14

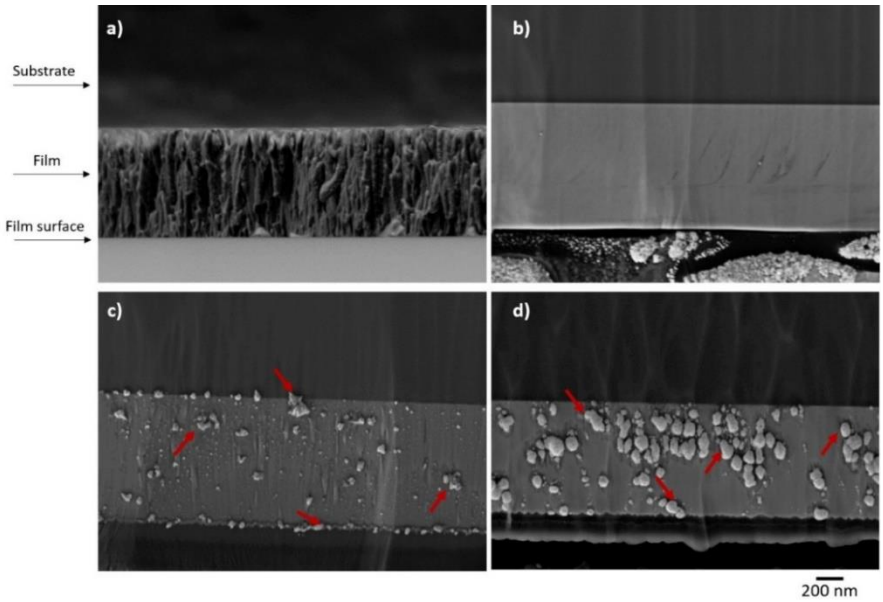

Figure 5.3: Cross section morphology for Ti-Ag films with Ag/Ti= a) 0, b) 0.12, c) 0.98, d) 3.14

In this work, different number of Ag pellets were used and so different Ag/Ti ratios were obtained than the previous studies. It was seen that while the Ti grains could be easily seen for Ti reference film with a more pinned microstructure on the film surface; increasing Ag content caused disappearing of these surface microstructures and refined the grains. Additionally, for the film has Ag/Ti=0.98, brighter spots appeared (arrowed in Figure 5.2c) similarly as its cross section (Figure 5.3c).

It was examined that along cross section, while the film has a columnar microstructure for Ti-reference composition, Ag/Ti=0.12 film has a more compact microstructure (Figure 3a, 3b). Additionally, for Ag/Ti=0.98, some clusters appeared (shown with arrows in figure 3c) and for the Ag-richest film (Ag/Ti=3.14), these clusters become larger (Figure 3d). Previously, Benelmekki et *al.* also asserted the inhomogeneous distribution of Ag clusters based on PVD process for the deposition of Ag:TiO_x films [12]. Here also, it could be noted that a gradient presents on the distribution of the Ag-based particles along the cross section of the film. While there are more clusters close to the film-substrate interface, the number of clusters seems decreasing through the surface of the film. Such a gradient could be correlated with decreasing size of Ag pellets on Ti-target with sputtering, whereas there was higher deposition efficiency of Ag at the beginning of the deposition process based on the larger surface area of Ag pellets to be sputtered.

When the EDS analysis was performed on the clusters detected in the film with Ag/Ti=0.98, it was seen that they are richer in Ag (Figure 5.4). Thus, it could be stated that, while small amount of Ag is infilling the titanium grains, increasing Ag content caused the silver-richer clusters along the film thickness.

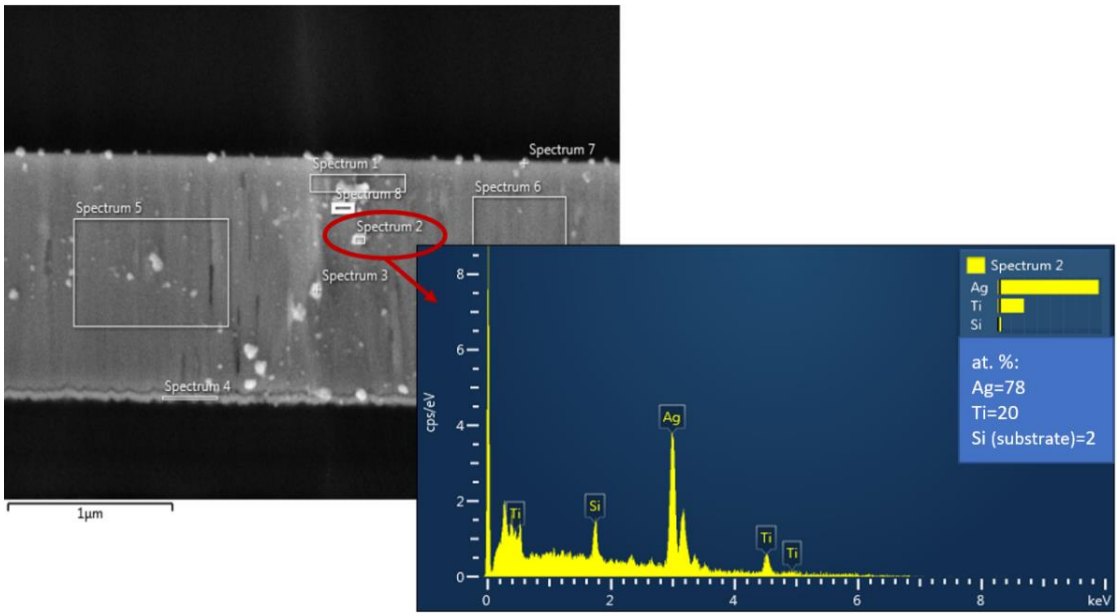

Figure 5.4: EDS analysis of clusters for film Ag/Ti=3.14

5.2.1.2 RBS Analysis

It was obvious from the SEM analysis that, increasing Ag content into Ti-film composition caused morphological changes and also Ag tends to segregate to generate clusters. To investigate these modifications more in detail, film densities were also identified with Rutherford Backscattering Spectroscopy (RBS) by C^{2}TN Instituto Superior Técnico Lisbon. For this analysis, the films deposited on the silicon wafer substrates were used. As it was assumed by the qualitative microstructural SEM examination, it was quantitatively proved that, increasing Ag content into the film, increases the film density (Table 5.2).

Table 5.2: Film densities

Film composition	Density (x10^{22} at/cm^3)
Ti-reference	6.63
Ag/Ti=0.12	7.93
Ag/Ti=0.98	8.39
Ag/Ti=3.14	8.88

RBS analysis provided to explain the variations on the microstructure of the films with increasing Ag content. Indeed, while SEM showed qualitatively (Fig. 3) that grains size was

decreasing with the silver content making denser the microstructure, RBS analysis proved this fact quantitatively.

5.2.1.3 TEM Analysis

A deeper characterization of films at the TEM-scale was carried to explain the role of silver on their microstructure. Indeed, by considering the SEM, EDS and RBS analyses, it was aimed to identify how Ag was able to densify films. Moreover, Ag-rich clusters were observed by SEM. Their architecture at small scale has indeed to be analysed, since they may significantly influence properties of the surface, *e.g.* electric conductivity in particular, as already reported by Etiemble et *al.* [10].

Since there is no Ag in the Ti-reference film, only the three binary Ti-Ag films were investigated. TEM characterization was conducted on 100nm-thick films deposited onto NaCl substrates then dissolved and put on a TEM grid. It was examined that for the film with Ag/Ti=0.12, Ag filled the surroundings of the grains of titanium as brighter lines (Figure 5.5a), which could explain the more compact cross section appearance from SEM images and higher film density measured by RBS analyses. Additionally, segregation of Ag in the form of clusters was confirmed for Ag-richer films. Their chemical nature, very rich in silver, as it was corroborated by EDS analysis. Such dense microstructure confirms Lopes' study [11] which stated that, Ag fills the Ti-grains and segregates Ti-Ag clusters there. For the film with Ag/Ti=0.98, there are smaller clusters and some silver accumulated in the grains of Ti matrix (figure 5.5b); however, for the film with Ag/Ti=3.14, there are larger Ag-based clusters (Figure 5.5c).

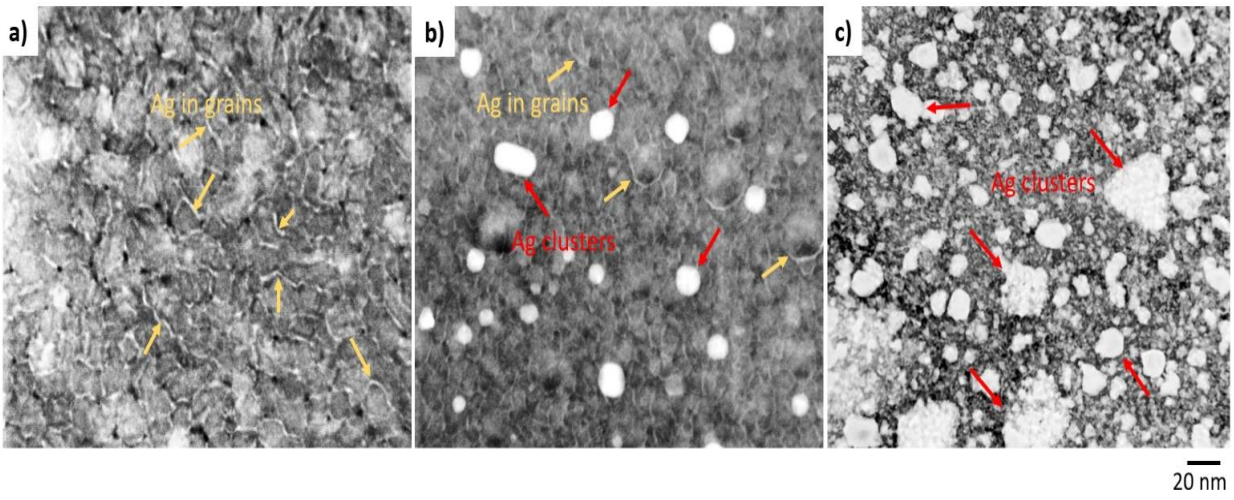

Figure 5.5: TEM analysis of Ti-Ag films with Ag/Ti= a) 0.12, b) 0.98, c) 3.14

When the Ag placing in the titanium matrix and segregation of Ag clusters were investigated detailly with TEM analysis for the three Ti-Ag compositions, the film densification and morphology change could be clearly explained based on increasing Ag content. The role of the clusters and their increasing size for the highest Ag containing film could help to enhance mechanical, electrical and tribological properties. Therefore, after examining such a microstructure with TEM analysis, it was crucial to identify the formed phases to define how these properties could be tuned for corresponded microstructures and compositions.

5.2.2 Crystal Structure Analysis

5.2.2.1 XRD Analysis

The solubility of Ti and Ag between each other and formation of their intermetallic phases in films were discussed in several studies. Murray et *al.* [13] stated that, a bcc (βTi) solid solution can be formed for films up to Ag/Ti=0.18 (*i.e.* 15.5 at.% Ag). The hcp (αTi) solid solution can be also achieved with up to Ag/Ti=0.05 (4.7 at.% Ag). Additionally, until Ag/Ti=1 (50% of Ag (in at.)) intermetallic phases can be achieved above 600°C as it was shown in the phase diagram (Figure 5.6). Therefore, to obtain both solid solution and intermetallic phases is possible for our Ti-Ag alloys.

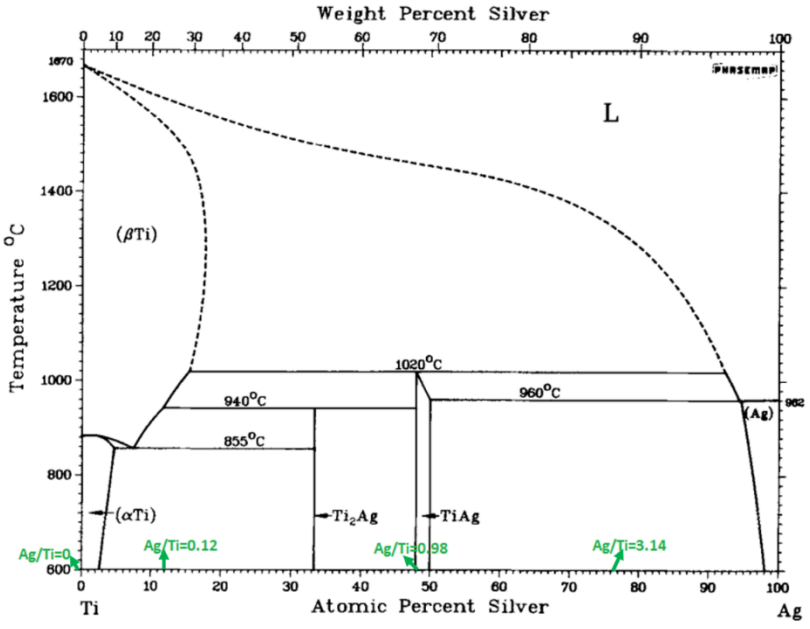

Figure 5.6: Ti-Ag phase diagram [12]

The XRD analysis was performed with θ-2θ Bruker XRD D8 advanced diffractometer and the computations were done with PDF data base by using EVA and TOPAS software. The samples analysed with XRD are the films deposited on the fused silica (SiO_2) substrate. Here the purpose was to investigate which crystal phases were formed for the corresponding compositions. It was aimed to define the solid solution and/or intermetallic compounds forming with increasing Ag content.

Figure 5.7 presents the diffractograms for Ti reference and Ag/Ti=0.12 films. Ti-reference film present the expected hexagonal closed packed (hcp) Ti phase (with space group P63/mmc 194). However, regarding the bright lines estimated in TEM analysis, it was thought that there could be pure Ag phase which was placed surroundings of the Ti grains. Therefore, the fcc-cubic phase and the intermetallic tetragonal Ti-Ag phase were also considered for the peaks of this composition. However, even though peak intensities varied, it was seen that Ag/Ti=0.12 film has the quite similar diffractogram pattern as Ti-reference film. Thus, for this composition, hcp (αTi) solid solution phase with similar peaks as pure Ti even if a slight shift towards lower angles is recorded. This shift is consistent with the weak enlargement of the lattice induced by the bigger silver insertion (atomic radius of elements: 140 and 160pm for Ti and Ag respectively).

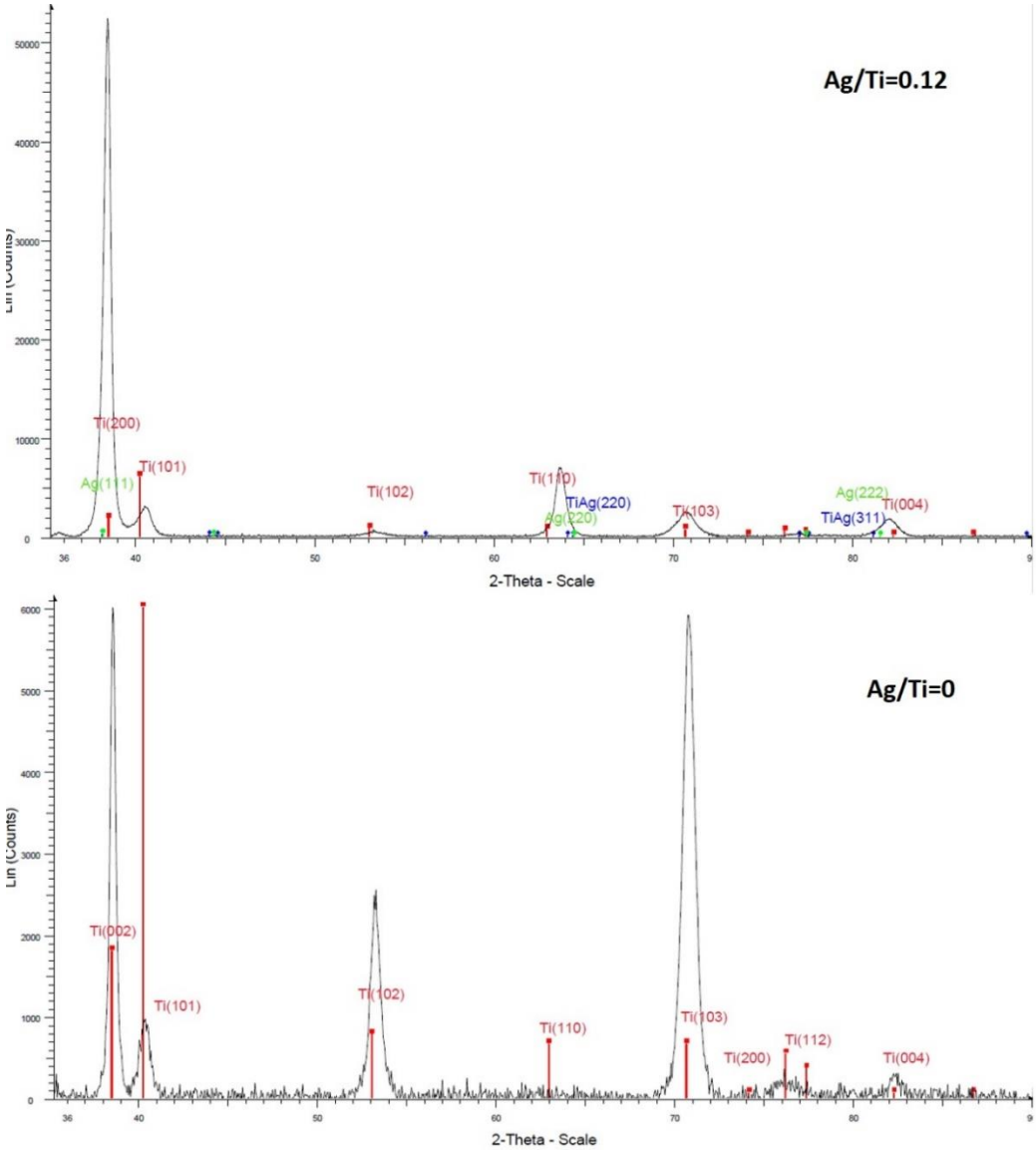

Figure 5.7: XRD analysis for the Ti reference and Ag/Ti=0.12 films

Additionally, with the further increase in Ag content, Lopes [1], indicated that the structure changes to intermetallic phases. It was expected also by considering the phase diagram of Ti-Ag (Figure 5.6). Two intermetallic different phases were considered for the films with Ag/Ti= 0.98 and =3.14 compositions: tetragonal Ti_2Ag (I4/nmm or 139) and tetragonal TiAg (P4/nmm or 129). Furthermore, since there are Ag-based clusters for Ag/Ti=0.98 composition and they are enlarging with increasing Ag content for the film with Ag/Ti=3.14, it was expected that, face-centred cubic (fcc) Ag metallic phase could also be achieved. Nevertheless, it has to be noted that the peaks for intermetallic phases and cubic Ag phase are very close to each other. As it was shown in Figure 5.8, the peak positions at 2θ=38° and 81.5°, fcc-Ag phase and TiAg intermetallic phase are overlapped.

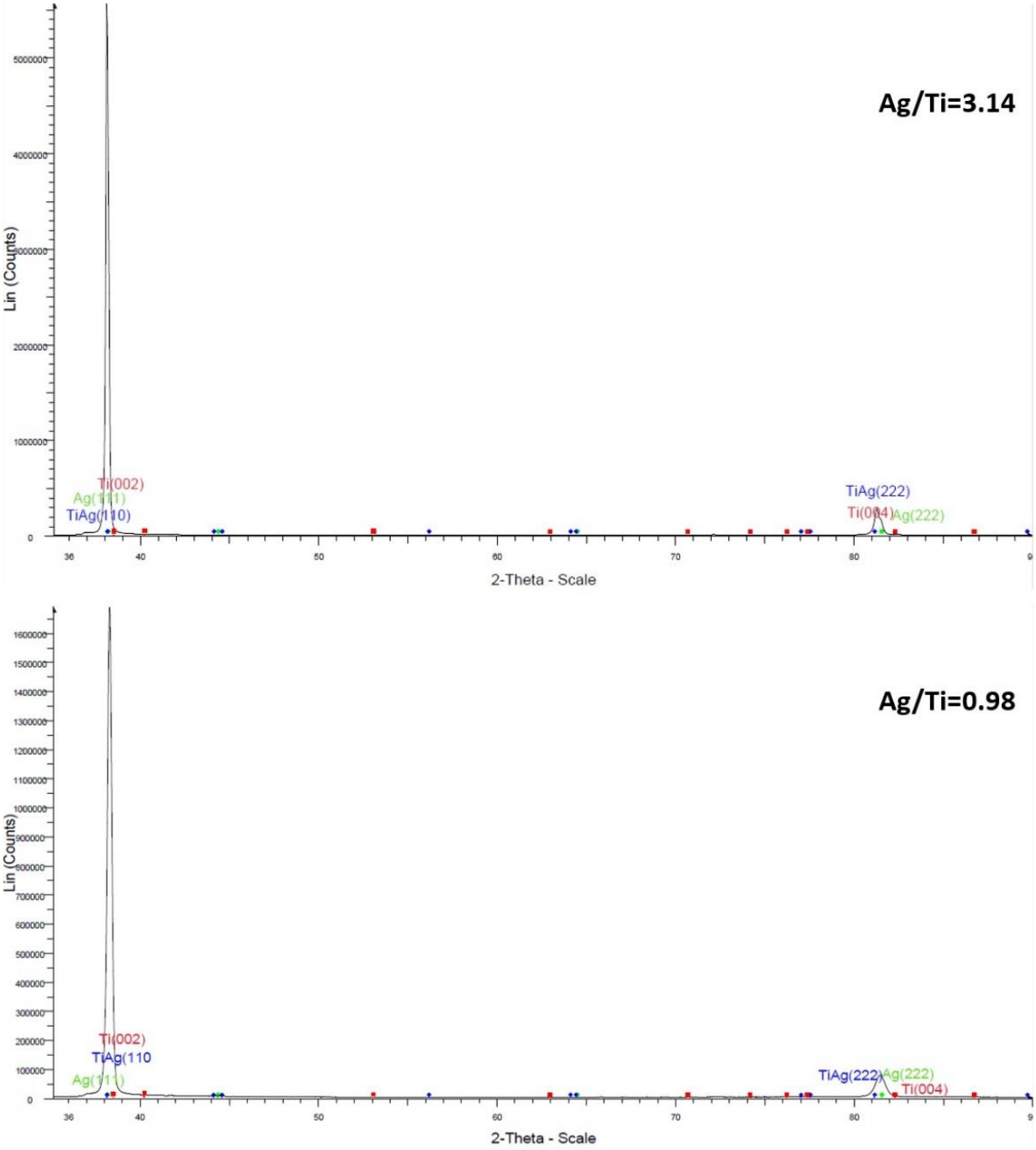

Figure 5.8: Crystal phases for the Ag/TI=0.98 and =3.14 films

Even though there are two intermetallic phases (tetragonal TiAg P4/nmm or tetragonal Ti_2Ag I4/nmm) could be achieved for these two Ag richer compositions, in the currently used PDF database, only TiAg P4/nmm phase exists. However, in previous study, Lopes examined the Ti_2Ag phase for the composition with Ag/Ti=0.5. Also, it is was considered that the films with

Ag/Ti=3.14 has TiAg phase by considering the same previous study for the XRD pattern of the film with Ag/Ti=2.42 (Figure 5.9) [11].

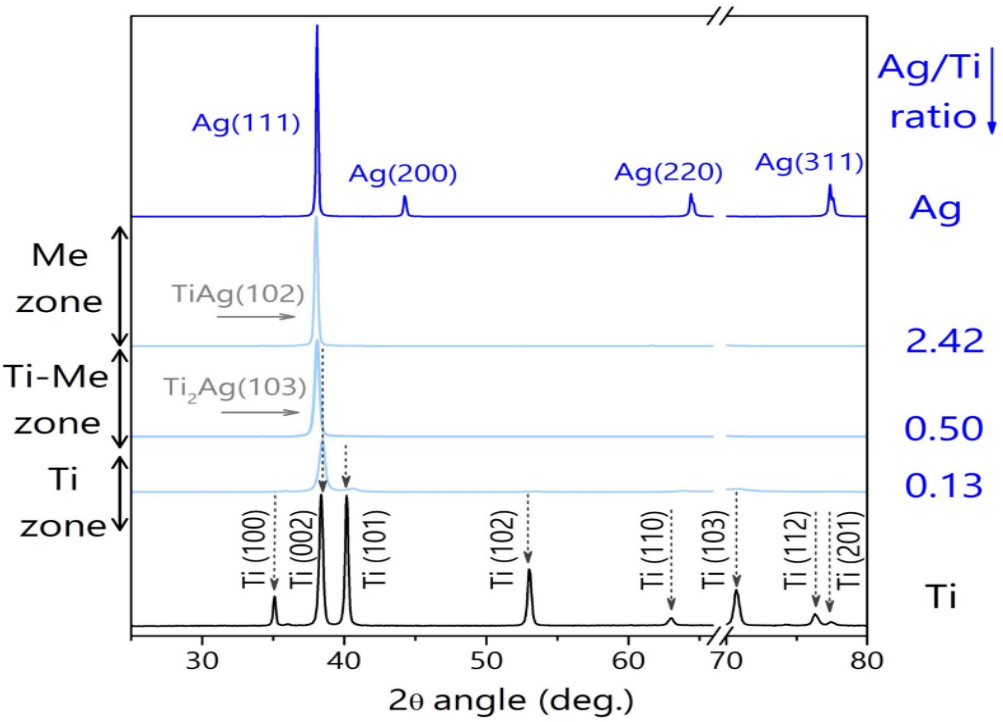

Figure 5.9: Crystal phase analysis for Ti-Ag films with different compositions from a previous research to compare [11]

To sum up, by considering the Ti-Ag phase diagram and the XRD analysis, it could be stated that the film with Ag/Ti=0.12 is in hcp (αTi) solid solution with Ag traces. However, the existence of pure Ag phases for this composition or the intermetallic phases as well as the pure fcc-Ag phase for Ag-richer compositions cannot be perfectly defined with XPS analysis. Therefore, a further analysis technique (XPS) was aimed to perform.

5.2.2.2 XPS Analysis

To investigate the change of metal-metal environment detailly with increasing Ag content in the film and to discuss any potential Ti-Ag intermetallic phases for the corresponding film compositions, X-ray photoelectron spectroscopy (XPS) was used.

Before starting to the analysis, to avoid from the quantification of extra oxides or other pollutants over the surfaces of the films, they were exposed to Ar+ etching at 3 kV for 5 minutes. Samples analysed with XPS are the films deposited on both silicon wafer and fused silica

substrates. By considering the XRD analysis, three more compositions were deposited. Here, it was aimed to investigate the solubility limits of Ag in Ti matrix and the ranges of the Ag content to achieve the intermetallic phases in the film. These extra three compositions can be defined as extremely Ti-rich (Ag/Ti (at.) = 0.08, deposited with 2 Ag pellets on Ti target), extremely Ag rich (Ag/Ti (at.) = 24, deposited with 4 Ti pellets on Ag target) and Ag-reference film (deposited with pure Ag target). The films with Ag/Ti=24 and Ag-reference film were aimed to better understand the transition from intermetallic Ti-Ag phase to solid solution of fcc-Ag with Ti in it and then to pure Ag phase.

Films deposited on SiO_2 substrates were investigated and it was seen that the Ti peaks were slightly disappeared with increasing Ag content. However, for the films with Ag/Ti=0.08 and Ag/Ti=0.12, Ag peaks were barely detected. Even though for the film with Ag/Ti=0.08, the intensity of Ag peak is quite small, it became easily recognisable for the Ag/Ti=0.12 film composition which confirms the co-existing of Ag phase in addition to the hexagonal Ti phase. Moreover, the intensity of Ti peaks decreased while the intensities of Ag peaks were increasing for the films having higher Ag content (Figure 5.10).

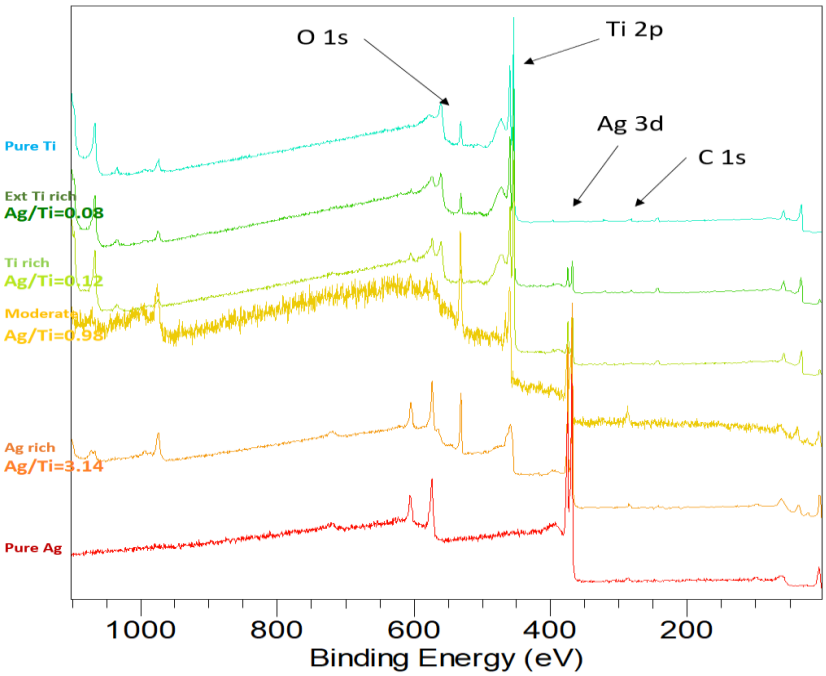

Figure 5.10: XPS analysis of Ti-Ag films on SiO_2 substrate

When the films on Si substrates were investigated, it was seen that the film compositions are the same as they were estimated with EDS. However, there is a considerable amount of oxidation along the film thicknesses which was correlated with the placing of Ag in Ti grains

as it was confirmed with TEM, since both Ti and Ag are highly tend to oxidise. Even though there is no continuous trend on the oxidation tendencies with increasing Ag content in the films, the highest oxidation was observed for the film with Ag/Ti=3.14 in addition to a strong noise for Ti content for the same composition.

Consequently, while the Ti-reference and Ti-Ag films with Ag/Ti=0.08 and =0.12 behaved similarly as pure titanium (with small amount of Ag contamination for Ti-Ag films); transition was seen with high noise of Ti2p peaks for the film with Ag/Ti=0.98. For three Ag-richer compositions Ag peaks detected so intermetallic Ti-Ag and/or pure fcc-Ag phases are existing for these compositions. However, also XPS could not provide the exact information on the structure of phases existing in these compositions.

5.2.3 Mechanical and Electrical Properties

5.2.3.1 Nano-indentation Test

To investigate the mechanical properties of Ti-Ag films, nanoindentation tests were performed with a Berkovich nano-indenter tip. The indentation frequency was set as 45 Hz and the penetration depth limit was 500 nm. For this analysis, samples deposited on fused silica substrates were tested. It was seen that with increasing Ag content, both hardness and Young's modulus are slightly increasing. Even though there is not a continuous increment, the films could be grouped as Ti richer ones (Ag/Ti= 0 and 0.12) and Ag richer ones (Ag/Ti=0.98 and 3.12) in terms of their mechanical properties (Table 5.3). The small amount of increase on mechanical properties can be correlated with increasing oxide content which was estimated by XPS analysis. It was seen that the brittle metal oxides helped to achieve higher modulus and hardness. The slight decrease of the mechanical properties for the composition with Ag/Ti=3.14 could be explained with the increasing pure Ag phase (large Ag clusters as fcc-Ag) and so increasing ductility of the film. This point could be explained as the indents are covering not only the titanium phase but also the clusters.

Table 5.3: Mechanical properties of Ti-Ag films

Films for Ag/Ti (at.)	Young's modulus (GPa)	Hardness (GPa)
0	89.97 (±9.06)	3.47 (±0.70)
0.12	91.13 (±10.55)	3.54 (±0.73)
0.98	103.5 (±1.44)	4.78 (±0.10)

3.14	98.92 (±1.73)	4.20 (±0.14)

It could be expressed that increasing Ag content helped to slightly enhanced the mechanical properties of Ti-Ag films regarding the nanoindentation test. However, larger standard deviation on the measurement for two Ti-richer compositions can be explained with the columnar nature of Ti along the indentation depth, whereas there are denser microstructures and ductile clusters for Ag-richer films.

5.2.3.2 Four Point Probe Test

The electrical properties were investigated with four-point-probe electrical resistivity technique in Universidade do Minho (Portugal). The sheet resistivity values for each composition were multiplied with the film thicknesses. The purpose of this analysis is to investigate the effect of Ag content on the electrical conductivity of these films, since it was aimed to use them for biosensor applications.

The similar behaviour was observed for the electrical resistivity as the mechanical properties (Table 5.4). While it was increasing with Ag content in the film, there is a decrease for the composition with the Ag/Ti=3.14. Here the resistivity increase with increasing Ag content could be explained with the presence of intermetallic phases which were assumed with the XRD analysis. However, it can be stated that there is a maximum level of resistivity increase with increasing Ag content which is lower than Ag/Ti=3.14. This issue could be based on enlarging of Ag richer clusters and formation of pure Ag phase which is highly ductile and conductive. Therefore, the film with Ag/Ti=3.14 was performed higher conductivity since resistivity is inversely proportional with conductivity [14].

Table 5.4: Electrical resistivities of Ti-Ag films

Films for Ag/Ti (at.)	Electrical resistivity (Ωm ($*10^{-6}$))
0	1.17 (±0.10)
0.12	2.13 (±0.02)
0.98	2.34 (±0.04)

3.14	1.33 (±0.01)

It could be concluded as in addition to the increased ductility to provide discontinuous crack propagation for a longer signal acquisition as it was expressed in previous study [10], increasing Ag content also helped to achieve higher film conductivity. This characteristic makes the film with Ag/Ti=3.14 quite suitable material for bio-sensor application.

5.2.4. Preliminary Tribological Analysis

The tribological tests were applied with the laboratory-made micro-tribometer which was validated with the preliminary tests carried with TiN film. It was aimed to investigate the tribological behaviour of Ti-Ag films, in early stages since they can expose to sliding motion at joints and against human skin or clothes. To perform the tribological test in small scale *in situ* conditions, the micro-tribometer was operated by coupling it with a light microscope and also once it was implemented into SEM chamber (SEM Quattro). First tests in SEM were performed in high vacuum conditions (10^{-3} Pa). Additionally, for the first tests, steel balls (AISI52100, Ø10mm) were used as the sliding counter-face. The hardness of Ti-Ag films is ~210 GPa with Poisson's ratio is 0.27 [15], giving a maximum contact pressure calculated with the Hertzian theory of 0.55-0.60 GPa for 4N of normal load.

The tribological tests were performed on the films deposited on the steel substrates with 2mm of wear track to achieve a region where the sliding speed is constant. Finally, the sliding speed was fixed as 1 mm/s. The normal, tangential and lateral forces in addition to time and displacement were recorded for the further data analysis by the TRIBOMEB software to calculate the friction coefficient for each cycle.

When the first tests were performed with steel ball, strong delamination issue was examined for most of the compositions. Additionally, debris formation and particle accumulation occurred at the frontiers of the wear track in both ambient air (Figure 5.11) and high vacuum conditions (Figure 5.12). During the test performed in ambient air conditions, the film removed along the sliding distance for Ti-reference composition. Also, for the compositions with Ag/Ti=0.12 and 0.98, the film was delaminated around the sides of the wear track. It can be noted that the delamination was larger along the wear track for the composition with Ag/Ti=0.98. Since this large amount of delamination and film removal was seen with optical microscope only after 3

cycles, the tests were stopped at this point. However, no film removal or delamination was detected after three cycles for the film with Ag/Ti=3.14. This enhanced wear character can be correlated with the formed Ag-rich clusters which might help the sliding of the coating.

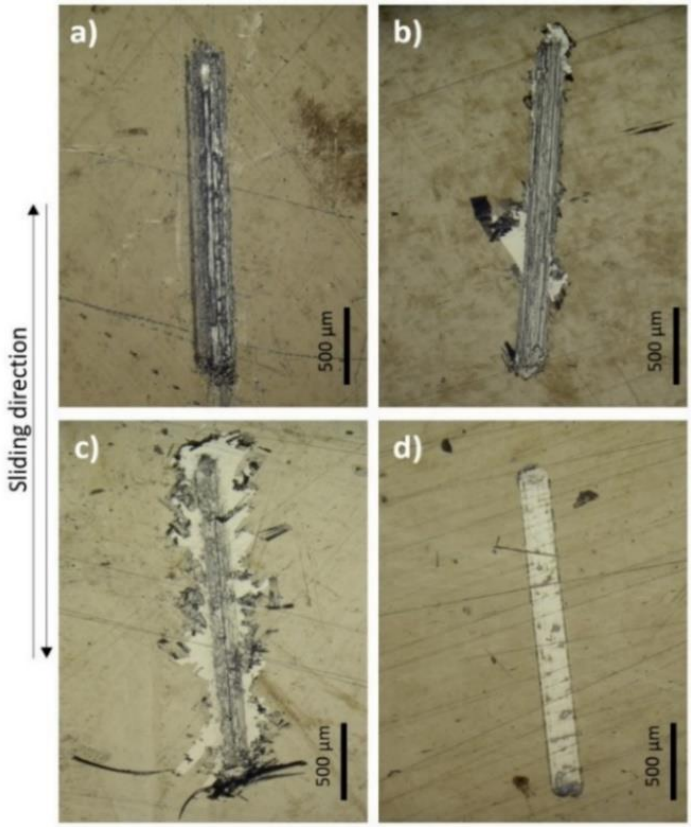

Figure 5.11: Wear tracks of a) Ti reference film and the Ti-Ag films with Ag/Ti= b)0.07, c)0.98, d)3.14

Furthermore, the tests were performed in high vacuum conditions inside the SEM chamber. Similar behavior was examined on the corresponding compositions with the tests carried out in ambient air conditions. Debris formations and film delamination were detected for the first three compositions after 3 cycles, whereas there was no delamination on the film with the Ag/Ti=3.14.

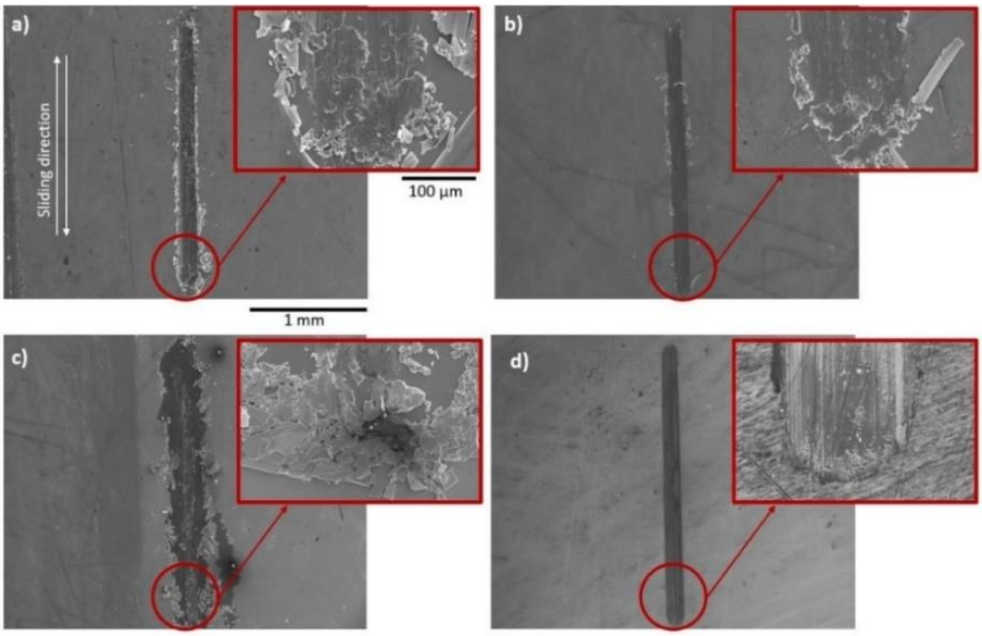

Figure 5.12: Wear tracks after 3 cycles for Ti-Ag films with Ag/Ti= a) 0, b) 0.12, c) 0.98, d) 3.14

It was seen that Ti-reference film as well as the films with Ag/Ti=0.12 and 0.98, the film was almost totally removed even only after 3 cycles. However, the situation was completely different for the Ag richest composition (Figure 5.11d and 5.12d). There was no film removal, debris or particle accumulation at the edges or along the length of the wear track for this composition.

Additionally, friction coefficients were calculated. The friction coefficient of the Ti-Ag film with Ag/Ti=3.14 was remarkably lower than the friction coefficients of the other three compositions. There is no trend on the decrease of the friction coefficient with increasing Ag content but from the Ti-reference film, to Ag-richest Ti-Ag film, there is almost one order of magnitude decrease on friction coefficient values (Table 5.5).

Table 5.5: Friction coefficients of Ti-Ag films

Film for Ag/Ti (at.)	COF at ambient air	COF at high vacuum
0	0.78 (±0.29)	0.83 (±0.31)
0.12	0.31 (±0.14)	0.43 (±0.27)
0.98	0.45 (±0.10)	0.60 (±0.28)
3.14	0.08 (±0.04)	0.08 (±0.02)

The smoother wear track appearance without any debris and delamination in addition to the smallest friction coefficient in both environmental conditions for the film with Ag/Ti=3.14 could be explained by a solid lubricant effect of ductile Ag-based clusters. Here, the clusters were appeared in nanoparticle form. It is worth mentioning that, Ag nanoparticles have already been used as an additive solid lubricant to enhance the tribological behavior of various materials [16-19].

In addition to the analysis of the effect of film composition on tribological behaviors of Ti-Ag films, the effect of environmental conditions on tribological susceptibility of these films were also investigated. As it was seen in table 5 above, there is an increase on friction coefficient from ambient air to high vacuum conditions for the first three compositions. Additionally, the composition with Ag/Ti=0.98 was tested also in low vacuum conditions. Here the purpose was to better understand the role of clusters with humidity since the Ag richer clusters was firstly detected in this composition. The first tests were performed in ambient air condition (~23% relative humidity) with an optical microscope and also in both low (173 Pa) and high vacuum (10^{-3} Pa) conditions in SEM. When the wear tracks were compared for the film in two controlled environments in SEM, it was seen that the wear track of the film has larger delamination and more removed film particles at high vacuum (Figure 5.13e) than at low vacuum (Figure 5.13c). Also, Figure 5.13d and 5.13e shows that the particles on the ball surface was more spread at low vacuum test whereas, there is a larger track with more compact particles on the ball used at high vacuum. On the other hand, at ambient air atmosphere, even though the ball has a wear track showing more compact debris, it was clearly seen that there is large amount of delamination on the surroundings of the wear track of the film (Figure 5.13).

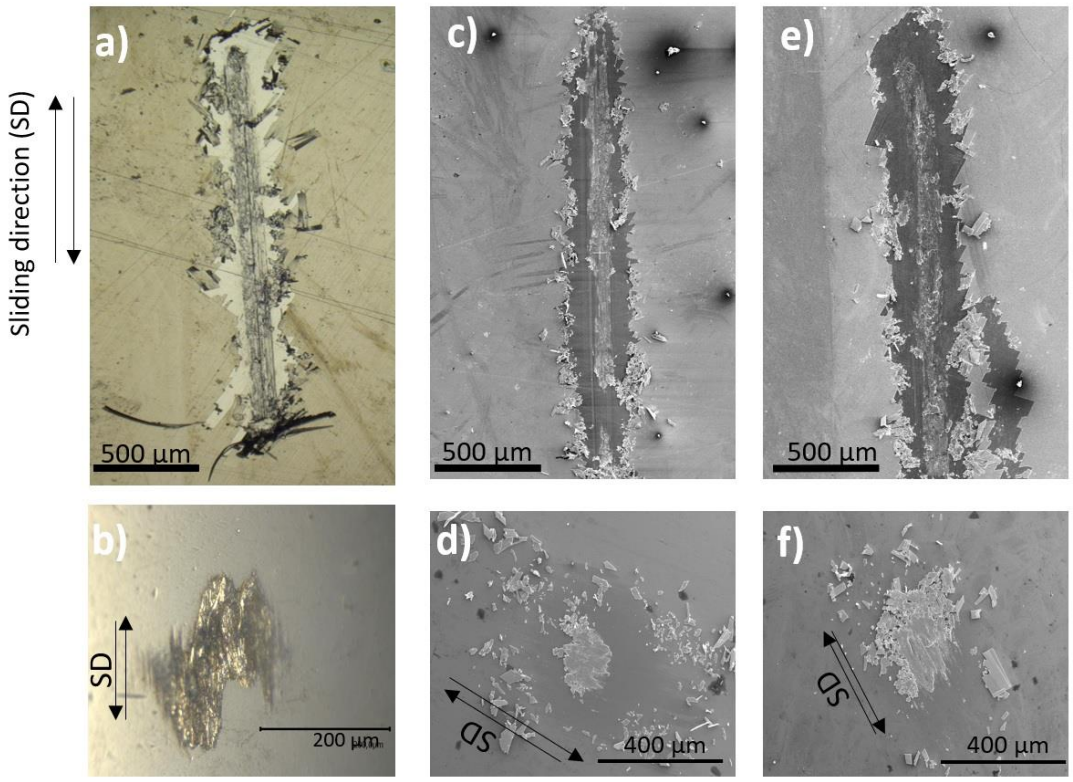

Figure 5.13: Wear tracks of the Ti-Ag (Ag/Ti=0.98) film after tribo-test with 3 cycles at ambient air a) on film, b) on ball; at low vacuum c) on film, d) on ball; at high vacuum e) on film, f) on ball

Furthermore, it was seen that from ambient air to increasing vacuum, the friction coefficient was slightly increased (Table 5.6). The tuning of the friction coefficient with increasing vacuum could be explained with the tendency of oxidation of the metals in ambient air atmosphere (both for Ti and Ag). It was confirmed by XPS analysis that, the Ti-Ag (Ag/Ti=0.98) film has high tendency to be oxidized. Also, as it was explained in the previous studies that continuously forming oxide layer of titanium provides a solid lubricant effect along the wear track for Ti-based films [20-25]. Therefore, the oxide layer formed along the wear track based on the existence of humidity could be at the origin of the measured friction coefficient decreases.

Table 5.6: Comparison of friction coefficients for Ti-Ag film (Ag/Ti=0.98) at different environmental conditions

Testing environment	Ambient air	Low vacuum	High vacuum
Friction coefficient	0.45 (±0.08)	0.58 (±0.05)	0.60 (±0.07)

Moreover, since there was strong delamination detected on the films surfaces except the composition with Ag/Ti=3.14, it was aimed to investigate the change on the mean friction coefficient from one cycle to another. Therefore, the COF values of the films tested in high vacuum conditions were analyzed. It was seen that for the first three compositions there is a clearer increase or decrease at cycle 2; nevertheless, the friction coefficient was relatively stable for the film with Ag/Ti=3.14. Even though there is a variation on the cycle 2 for the first three compositions, there is not a strong jump which actually shows that film removal occurred at the very beginning of the contact (Figure 5.14). Thereby, improvement of the adhesion of these films was a significant requirement to be able to analyze their tribological susceptibility.

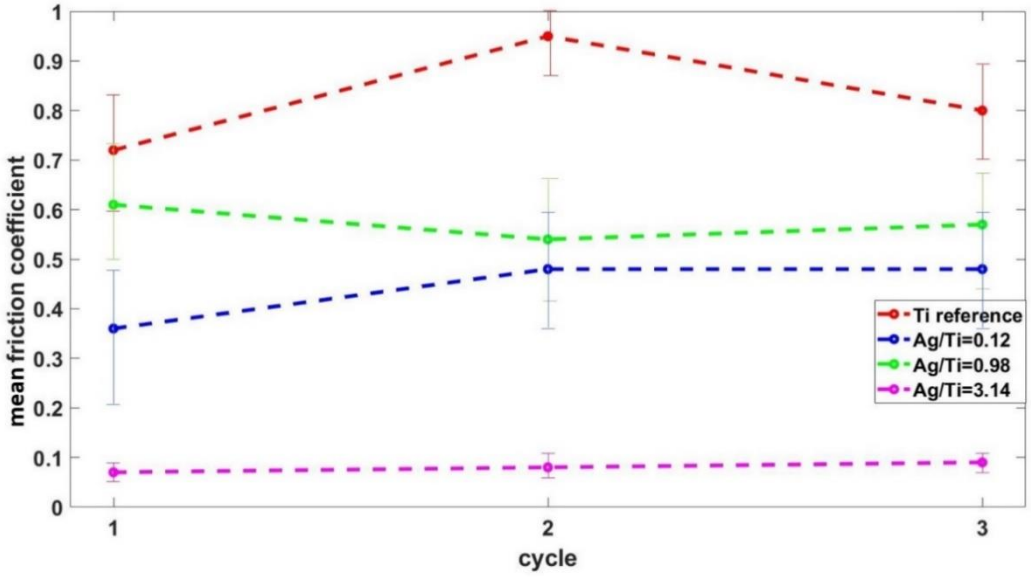

Figure 5.14: Mean friction coefficients of Ti-Ag films for 3 cycles at high vacuum

Lastly, Ag-richer clusters helped to enhance the tribological behavior of Ti-Ag films by acting the role as a solid lubricant for the Ag/Ti=3.14 film composition. Also, increasing humidity caused a slight decrease in friction coefficient of the film with Ag/Ti=0.98 based on the formation of continuous oxide layer of titanium with the existence of the water vapor in the environment. However, the films were mostly delaminated as large particles over the substrate surface only after 3 cycles. Thus, it was aimed to enhance their adhesion character and the tests repeated to achieve with more adherent films to deeply investigate their tribological behavior in early stages.

5.3. Conclusion

Four different compositions were deposited with varying number of Ag pellets on Ti-target via magnetron sputtering PVD technique. The film behaviors were analyzed to examine the effect of Ag content. It was seen that mechanical and electrical properties are slightly enhanced in addition to the densification of the film microstructure. Regarding the TEM analysis, firstly Ag filled the Ti-grains and then accumulated in nanocluster form in the film matrix with its increasing content. When the tribological behaviors of these films were analyzed with laboratory-made ball-on-disk micro-tribometer, it was seen that only the film with Ag/Ti=3.14 had a good resistance against friction. While the other compositions were almost totally removed, the enlarged Ag-based clusters for the film with Ag/Ti=3.14 provided a solid lubrication effect and enhanced the wear resistance of the film for the tests performed both in high vacuum and ambient air atmosphere. Moreover, slight effect of humidity on the friction coefficient of these films were detected, yet the films removed only after three cycles. Therefore, regarding the outcomes of this chapter, it was aimed to enhance their adhesion character to analyze the *in situ* tribological behaviors in early stages of the contact and to investigate the role of contact environment more in detail for Ti-Ag films.

References (Chapter 5)

[1] Batista, P. P. E. T. (2015). *Conductive thin film-coated flexible polymers a new materials approach for designing biomedical electrodes* (thesis).

[2] Marques, S. M. S. (2016). *Development of multifunctional coatings deposited on polymers based sensors for biomedical applications* (thesis).

[3] Lopes, C., Gonçalves, C., Borges, J., Polcar, T., Rodrigues, M. S., Barradas, N. P., Alves, E., Le Bourhis, E., Couto, F. M., Macedo, F., Fonseca, C., & Vaz, F. (2015). Evolution of the functional properties of titanium–silver thin films for biomedical applications: Influence of in-vacuum annealing. *Surface and Coatings Technology*, *261*, 262–271. https://doi.org/10.1016/j.surfcoat.2014.11.020

[4] Choi, J.-Y., Chung, C. J., Oh, K.-T., Choi, Y.-J., & Kim, K.-H. (2009). Photocatalytic antibacterial effect of tio2 film of TiAg on streptococcus mutans. *The Angle Orthodontist*, *79*(3), 528. https://doi.org/10.2319/0003-3219(2009)079[0528:paeotf]2.0.co;2

[5] Ewald, A., Glückermann, S. K., Thull, R., & Gbureck, U. (2006). Antimicrobial titanium/silver PVD coatings on Titanium. *BioMedical Engineering OnLine*, *5*(1). https://doi.org/10.1186/1475-925x-5-22

[6] Wojcieszak, D., Mazur, M., Kaczmarek, D., Mazur, P., Szponar, B., Domaradzki, J., & Kepinski, L. (2016). Influence of the surface properties on bactericidal and fungicidal activity of magnetron sputtered ti–ag and Nb–Ag Thin Films. *Materials Science and Engineering: C*, *62*, 86–95. https://doi.org/10.1016/j.msec.2016.01.029

[7] Lopes, C., Gabor, C., Cristea, D., Costa, R., Domingues, R. P., Rodrigues, M. S., Borges, J., Alves, E., Barradas, N. P., Munteanu, D., & Vaz, F. (2020). Evolution of the mechanical properties of TI-based intermetallic thin films doped with different metals to be used as biomedical devices. *Applied Surface Science*, *505*, 144617. https://doi.org/10.1016/j.apsusc.2019.144617

[8] Marques, S. M., Costa, P., Lanceros-Mendez, S., & Carvalho, S. (2016). Strain analysis on ti1−xagx and Ag–TiNx electrodes deposited on polymer based sensors. *Thin Solid Films*, *604*, 55–62. https://doi.org/10.1016/j.tsf.2016.03.016

[9] Lopes, C., Pedrosa, P., Martin, N., Barradas, N. P., Alves, E., & Vaz, F. (2015). Study of the electrical behavior of nanostructured ti–ag thin films, prepared by glancing angle deposition. *Materials Letters*, *157*, 188–192. https://doi.org/10.1016/j.matlet.2015.05.067

[10] Etiemble, A., Lopes, C., Nkou Bouala, G. I., Borges, J., Malchère, A., Langlois, C., Vaz, F., & Steyer, P. (2019). Fracture resistance of ti-ag thin films deposited on polymeric substrates for biosignal acquisition applications. *Surface and Coatings Technology*, *358*, 646–653. https://doi.org/10.1016/j.surfcoat.2018.11.078

[11] Lopes, C. J. R. (2018). *Development of Ti-based intermetallic thin films for enhanced biomedical sensing performance* (thesis).

[12] Benelmekki, M., Torrell, M., Xuriguera, E., Vaz, F., & Teixeira, V. (2012). Structure and properties of silver clusters implanted in pet by PVD sputtering for active packaging applications. *Journal of Nano Research*, *18-19*, 105–116. https://doi.org/10.4028/www.scientific.net/jnanor.18-19.105

[13] Murray, J. L., & Bhansali, K. J. (1983). The ag−ti (silver-titanium) system. *Bulletin of Alloy Phase Diagrams*, *4*(2), 178–183. https://doi.org/10.1007/bf02884876

[14] Heaney, M. (2003). Electrical conductivity and resistivity. *Electrical Measurement, Signal Processing, and Displays*. https://doi.org/10.1201/9780203009406.ch7, p.1

[15] Guo, Y. B., & Liu, C. R. (2001). Mechanical properties of hardened AISI 52100 steel in hard machining processes. *Journal of Manufacturing Science and Engineering*, *124*(1), 1–9. https://doi.org/10.1115/1.1413775

[16] Estrada-Ruiz, R. H., Flores-Campos, R., Treviño-Rodríguez, G. A., Herrera-Ramírez, J. M., & Martínez-Sánchez, R. (2016). Wear resistance analysis of the aluminum 7075 alloy and the nanostructured aluminum 7075 - silver nanoparticles composites. *Journal of Mining and Metallurgy, Section B: Metallurgy*, *52*(2), 163–170. https://doi.org/10.2298/jmmb150103011e

[17] Ghaednia, H., Hossain, M. S., & Jackson, R. L. (2016). Tribological performance of silver nanoparticle–Enhanced Polyethylene Glycol Lubricants. *Tribology Transactions*, *59*(4), 585–592. https://doi.org/10.1080/10402004.2015.1092623

[18] Ma, J., Mo, Y., & Bai, M. (2009). Effect of ag nanoparticles additive on the tribological behavior of multialkylated cyclopentanes (macs). *Wear*, *266*(7-8), 627–631. https://doi.org/10.1016/j.wear.2008.08.006

[19] Zhang, W., Demydov, D., Jahan, M. P., Mistry, K., Erdemir, A., & Malshe, A. P. (2012). Fundamental understanding of the tribological and thermal behavior of ag–mos2 nanoparticle-based multi-component lubricating system. *Wear*, *288*, 9–16. https://doi.org/10.1016/j.wear.2012.03.003

[20] Dong, H., Bloyce, A., Morton, P. H., & Bell, T. (1997). Surface Engineering to improve tribological performance of ti–6al–4v. *Surface Engineering*, *13*(5), 402–406. https://doi.org/10.1179/sur.1997.13.5.402

[21] Siva Rama Krishna, D., Brama, Y. L., & Sun, Y. (2007). Thick rutile layer on titanium for tribological applications. *Tribology International*, *40*(2), 329–334. https://doi.org/10.1016/j.triboint.2005.08.004

[22] Aniołek, K., Kupka, M., & Barylski, A. (2016). Sliding wear resistance of oxide layers formed on a titanium surface during thermal oxidation. *Wear*, *356-357*, 23–29. https://doi.org/10.1016/j.wear.2016.03.007

[23] Dong, H. (2010). *Surface Engineering of light alloys: Aluminium, magnesium and titanium alloys*. Woodhead.

[24] Zhang, L., Yang, H., Pang, X., Gao, K., Tran, H. T., Volinsky, A. A. (2014). TiN-Coating Effects on Stainless Steel Tribological Behavior Under Dry and Lubricated Conditions, *Journal of Materials Engineering and Performance*, *23*(4), 1263-1269. doi:10.1007/s11665-014-0904-0.

[25] Sasaki, M., Nakamura, I., Takano, I., & Sawada, Y. (2004). Vacuum pressure dependence of the tribological properties of Ti, TiO2, and TiN thin films. *Electrical Engineering in Japan*, *149*(3), 1-7. doi:10.1002/eej.20020

6. DYNAMIC ANALYSIS OF TRIBOLOGICAL BEHAVIOUR OF Ti-Ag FILMS

The 2nd series of Ti-Ag films (with interlayer) and their properties were indicated. Then, their tribological behaviours were examined by rubbing against a polyurethane ball. First the role of the testing procedure at high humidity level was explained. After the selection of the proper procedure, the effect of the environment was evaluated on the tribological behaviour of the films with the highest Ag content. Finally, the effect of films composition on the friction and wear behaviour of these films were asserted in terms of increasing Ag content.

6. DYNAMIC ANALYSIS OF TRIBOLOGICAL BEHAVIOUR of Ti-Ag FILMS

6.1. Introduction

Thin film for biosensor applications have some specific requirements. First of all, it is significant to choose the proper substrate and counter-face selection by considering the possible friction [1, 2, 3]. For most of the bio-sensors, polymeric materials are being used based on their light weight, flexibility and durability [4]. Also, to provide the electrical acquisition, conductive polymers are the preliminary choice as the substrate materials [1, 3, 5].

As well as the substrate, the selection of the counter-face material is also crucial. In addition to the use of polymers for the substrate of the film, use of polymeric counter-part is also convenient for a bio mimicking system [3,6].

Normally, the relative motion like on pulse or cardiographic measurements [7], or movements on joint prosthesis of knees or hips, are endlessly repeating during the lifetime [8, 9]. Even though the amount of the normal load varies at different body parts, it is necessary to investigate the damaging mechanism in early stages of the contact of the sensors and/or body-prosthesis which are exposing a repeating sliding motion.

Furthermore, friction of the counterparts has a vital importance for a bio-system [6]. In this case, the counter-face was selected as a polymeric ball (polyurethane- PU) in 10 mm diameter to mimic the bio-contact [11, 12]. In addition to the material choice, the contact pressure also has a significant role. There is a commonly used model (Greenwood-Williamson) for contact area calculation of the rigid solid surfaces but for polymers this calculation is not easily adaptable. Therefore, the contact pressure can be roughly calculated but it is also needed to consider the molecular interactions between surfaces for the case of polymeric contact [5].

In previous studies polyurethane have been used both as substrate for a film [10] and/or as in a functionalised form for bio-sensor applications [11, 12, 13]. In addition to bio-sensors, polyurethane is a commonly selected material for polymeric catheters [14], artificial joints [8], or foot soles [15] in biomedical applications regarding its low friction character [10].

Previously, *in situ* tensile behaviour of Ti-Ag films on PET substrates for biosensors were studied in terms of the effect of Ag content for the data acquisition [16]. Furthermore, Ti, TiO_2 [15,17] and TiN [18,19] films deposited on PET substrate to be used for bio-sensor application and their tribological performance analysed against metallic balls were tested. However, metal-polymer contact is quite different than metal-ceramic or metal-metal contact because the polymeric system is mainly elastic [3]. In this point the interaction of dynamic contact is significant for polymers because, contact pressure, sliding temperature and speed has an important role on friction [4]. When the roles of these parameters were investigated, it could be stated that:

- Normal load and sliding speed: Friction coefficient is normally independent than these values; however, it decreases with increasing normal load or relative velocity within the deformation limit of polymer and the contact temperature.
- Temperature and glass transition temperature (T_g): The melting point of polymers is lower than metals and ceramics. Here the normal load and sliding speed have to be considered for contact temperature. Also, even though the variation of friction coefficient from the semi-crystalline to amorphous phase is often neglected, it might be quite different above and below of T_g [3].

In this chapter firstly, the static analysis of the Ti-Ag films deposited with interlayer (2^{nd} series of films) were investigated in terms of their microstructural, chemical, mechanical and electrical behaviours. Then, the methodology of the dynamic analysis of tribological behaviour of Ti-Ag films was described with a reference test (Ag/Ti=0.72, at 50% relative humidity). Finally, the *in situ* small scale characterization was performed considering three main factors: i) testing procedure, ii) environment, iii) effect of film composition.

6.2. Static Analysis of Ti-Ag films with interlayer

To enhance the adhesion, multilayer deposition was performed with a ~100 nm interlayer between the substrate and film itself. Here, the same target was used for the deposition of the interlayer and film itself. So, for each of the four compositions, the interlayers have the same chemical composition as each film itself deposited over them. It was though that, as well as the adhesion behavior, all the other characteristics of the films could be modified in comparison with the previous Ti-Ag film series because of the interlayer. Therefore, these behaviors were investigated thoroughly.

6.2.1. Microstructural and Chemical Analysis

6.2.1.1. SEM & EDS Analysis

The microstructural and chemical analysis for the 2nd series of films (deposited with ~100 nm interlayer), were performed with SEM and EDS and the film compositions and thicknesses were examined (Table 6.1).

Table 6.1: Composition of 2nd series of Ti-Ag films deposited

Films (with number of Ag pellets used during deposition)	Ti (at.%)	Ag (at.%)	Thickness (µm)
Ti reference with 0 Ag pellets	100	0	1.07
Ti-Ag with 4 Ag pellets	93.56	6.44	1.33
Ti-Ag with 32 Ag pellets	67.44	32.56	1.04
Ti-Ag with 120 Ag pellets	58.62	41.38	0.89

A variation was noticed on the film composition of the second series, compared with the first series (chapter 5), as it was seen in table 6.2, even though both series of films were deposited with the same parameters (voltage, current, pressure, deposition time, number of Ag pellets).

Table 6.2: Comparison of film compositions in terms of Ag/Ti (at.) ratios of 1st and 2nd series

	Ag/Ti (at.)	
Films (with number of Ag pellets used during deposition)	1st series (no interlayer)	2nd series (~100 nm interlayer)
Ti reference with 0 Ag pellets	0	0
Ti-Ag with 4 Ag pellets	0.12	0.07
Ti-Ag with 32 Ag pellets	0.98	0.48
Ti-Ag with 120 Ag pellets	3.14	0.72

The variation on the film compositions could be explained by modification of deposition efficiencies of metals (Ti and Ag) based on the erosion rate of the target. During the sputtering process, the target erodes and a ring shaped “race track” forms on target surface. Therefore, the deposit quality changes with changing depth of this race track. Even though the PVD method

is quite reproducible, the depth of the erosion ring on target surface has a crucial role to modify the deposition rate [20]. To explain the effect of target erosion on sputtering yield, Schoff [21] investigated the time-evolution of target consuming by using a copper target. With that study, it was seen that by increasing erosion depth of the target, both the sputtering yield and coating rate decreases based on the reducing of the gun voltage. Also, since the target geometry changes with the erosion, the power of the felt magnetic field changes as well, which may affect the sputtering yield. Thus, the decrease on the silver amount for the second series explained with two reasons:

- In the first series, an already eroded Ti target was used. For the deposition of the second series, a brand new Ti target was used without any erosion. Therefore, it had higher sputtering yield for titanium.
- Secondly, it is significant to place the Ag pellets precisely along the erosion zone of the target. However, because the Ti-target was not eroded for the second set of deposition, Ag pellets were placed regarding the estimated erosion zone of the target. Thereby, the small variations on their location caused to have a difference on the final film composition.

Additionally, the film microstructures were investigated for these 2nd series of films with SEM. The grain refinement with increasing Ag content in the film composition was clearly seen (Figure 6.1).

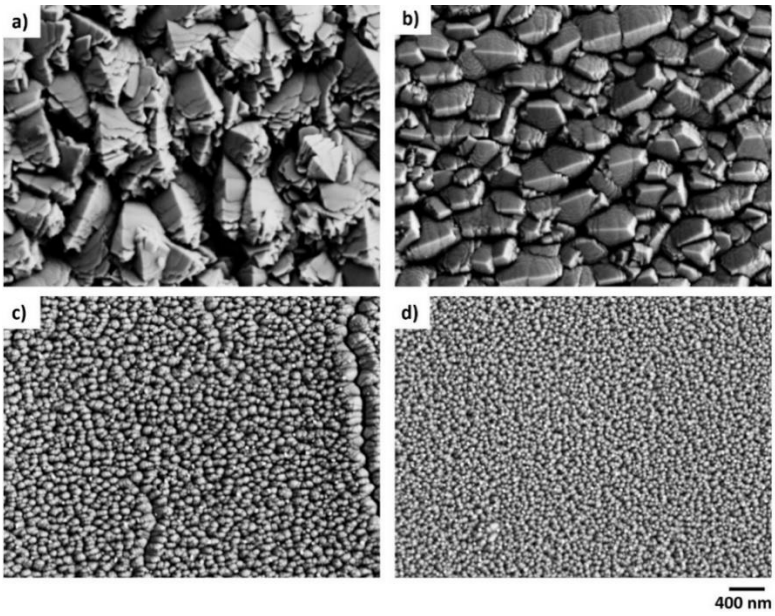

Figure 6.1: Top surface of the films with Ag/Ti= a) 0, b) 0.07, c) 0.48, d) 0.72

The cross sections of the 2nd series films with interlayer were also investigated. It has to be noted that, the Ag-richer clusters were appeared along the cross section of the films both with Ag/Ti=0.48 and =0.72 (Figure 6.2). However, these clusters were quite small for the film with Ag/Ti=0.48. It was also seen that in the first series of films, the ionic polishing had an artifact on the density for the cross-section appearance. Thus, the samples were aimed to be analyzed only by breaking with a diamond tip. The columnar microstructure was noticed not only for Ti-reference film but also for the films with Ag/Ti=0.07 and Ag/Ti=0.48. For the film with Ag/Ti=0.72, to reach a clear cross-section appearance by breaking the sample on the Si substrate was a challenge based on the ductility of the film with high Ag content. Therefore, ionic polishing was done to detect the distribution and size of the Ag-based clusters with this sample. Yet, it was aimed to investigate the cross-section microstructure of this film with further TEM analysis. Also, it is worthy to mention that the size and distribution of clusters have a gradient along the cross section of the film with Ag/Ti=0.72.

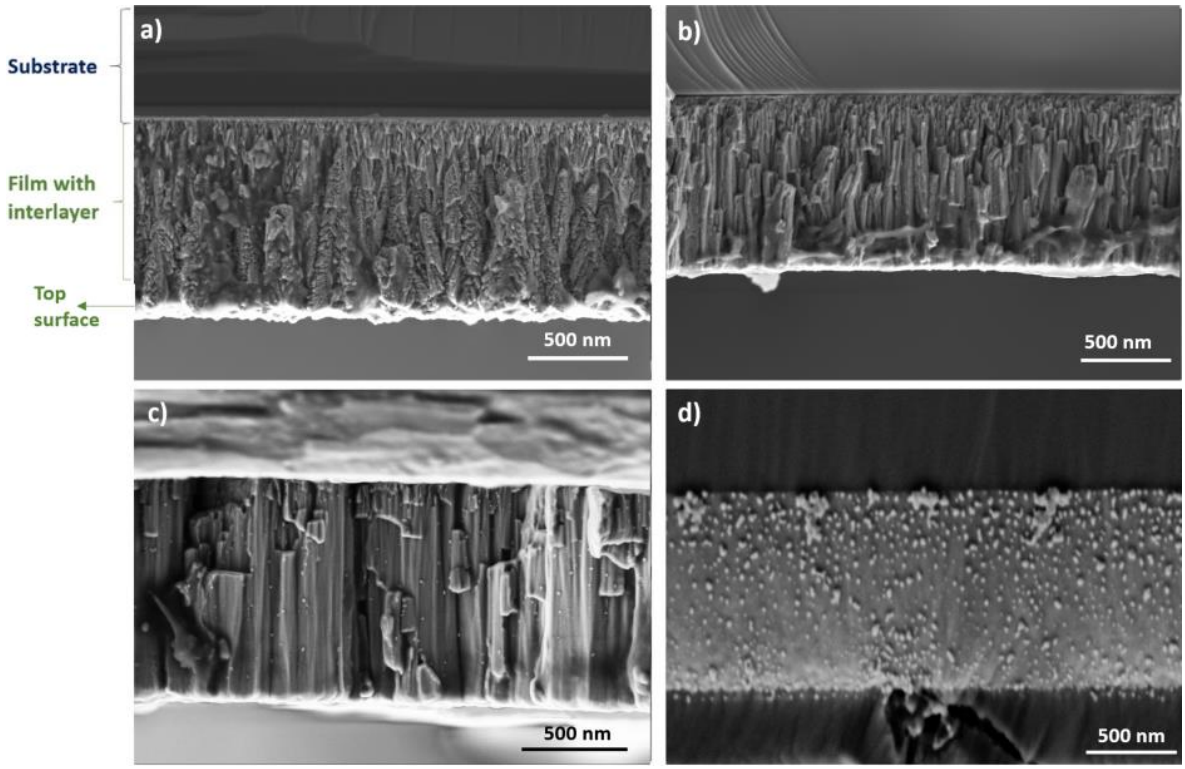

Figure 6.2: Cross sections of the films with Ag/Ti= a) 0, b) 0.07, c) 0.48, d) 0.72

Furthermore, according to the EDS analysis, it was seen that some of the clusters formed along the cross section of the film with Ag/Ti=0.72, could be purely Ag (Figure 6.3).

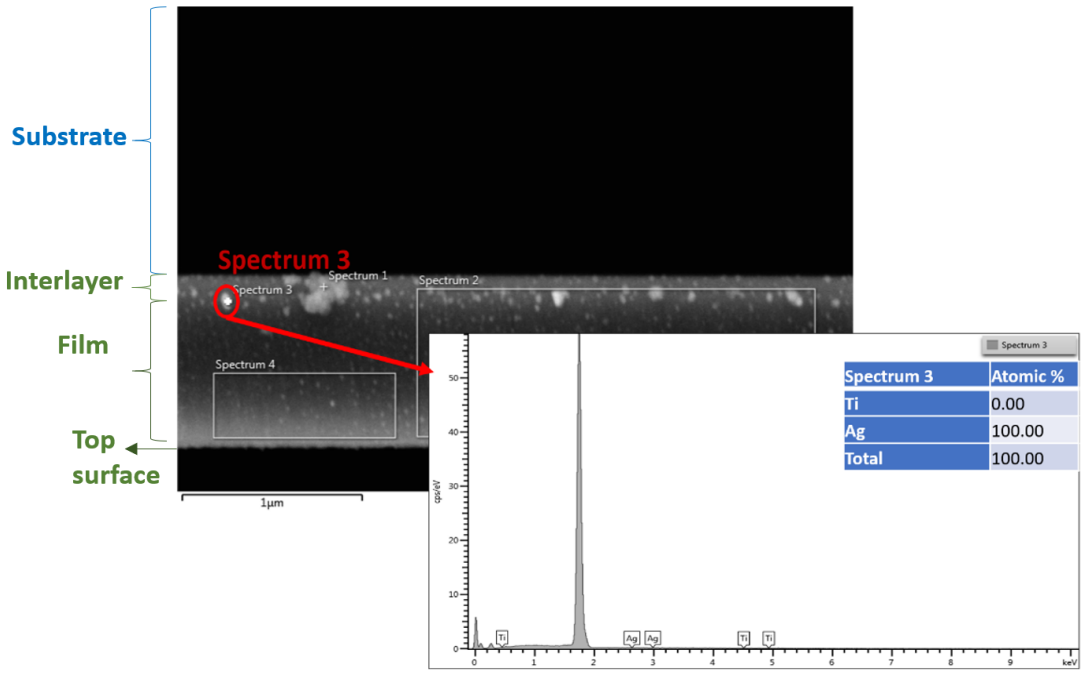

Figure 6.3: EDS analysis of the clusters for the Ti-Ag film with Ag/Ti=0.72

To sum up, it was seen that, Ag richer clusters were present along the cross section of the film with Ag/Ti=0.72. Grain refinement was seen with increasing Ag content as expected. Additionally, while the Ti-reference film has a quite columnar microstructure, an obvious densification was achieved with increasing Ag content. On the other hand, since a new Ti-target was used during the deposition process, film composition of the 2nd series was different from the 1st series in terms of Ag/Ti ratio.

6.2.1.2. RBS Analysis

It was seen that the distribution of Ag-based clusters for the Ag-richest film was not uniform in the film thickness (Figure 6.2.d and 6.3). In order to quantify such a distribution RBS analysis was done (Figure 6.4). It was observed that there is a gradient on the distribution of the Ag-based nanoclusters along the film thickness and this gradient causes a variation on the film density as well as on the composition along the thickness. The gradient of the Ag content appeared more clearly for the Ag richest composition as five layers (the film with Ag/Ti=0.72).

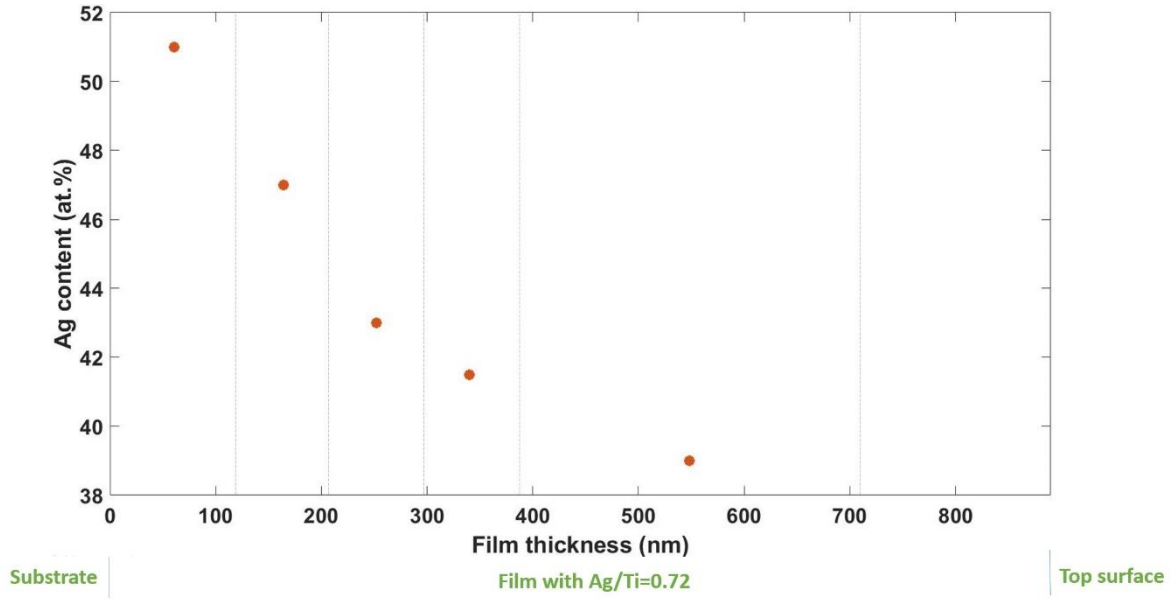

Figure 6.4: Distribution of Ag content along the thickness of the film with Ag/Ti=0.72

Furthermore, the effect of Ag content on the densification of the film was analysed for this second series for all the Ti-Ag films. It was confirmed that increasing Ag content helps to slightly densify the film microstructure (Table 6.3).

Table 6.3: Film Densities of 2nd series

Film composition	Density (x10^{22} at/cm^3)
Ag/Ti=0.07	5.59
Ag/Ti=0.48	5.71
Ag/Ti=0.72	5.76

6.2.1.3. TEM Analysis

For the second set of deposition, it was aimed to investigate the film microstructure in detail in addition to the location of Ag-richer nanoparticles along the thickness of the film. Another purpose of the microstructural analysis with TEM was to investigate the interlayer which was deposited to enhance the adhesion since it was not detected with SEM analysis. Therefore, the cross sections of the films which were deposited on Si substrate were examined after cutting them with FIB. Only the films with Ag/Ti=0.48 and =0.72 were investigated since they have higher Ag content and possibly have clusters.

The columnar microstructure was still clearly visible for both compositions. However, columns were more appeared for the film with Ag/Ti=0.48 (Figure 6.5a) whereas Ag-richer clusters stuck in the direction of film growth were easily detectable along the cross section of the film with Ag/Ti=0.72 (Red circles in figure 6.5b).

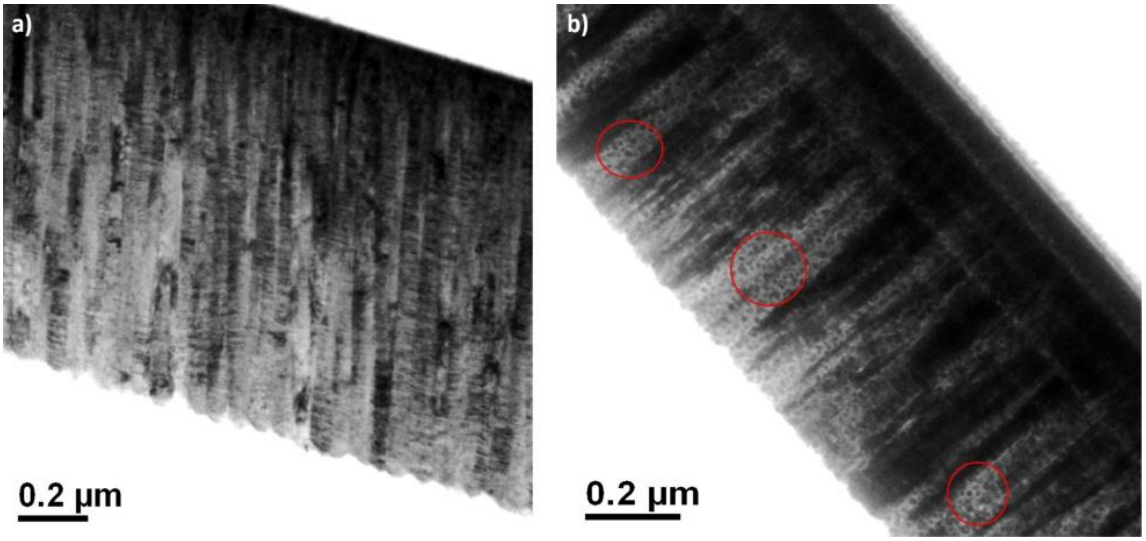

Figure 6.5: TEM analysis of the cross section of 2nd set of film series for the films with Ag/Ti a) =0.48 and b) =0.72

Some Ag-based nanoparticles were seen also in the film matrix for the film with Ag/Ti=0.48. Additionally, bigger clusters were appeared on the top surface of the film with Ag/Ti=0.72 (Figure 6.6).

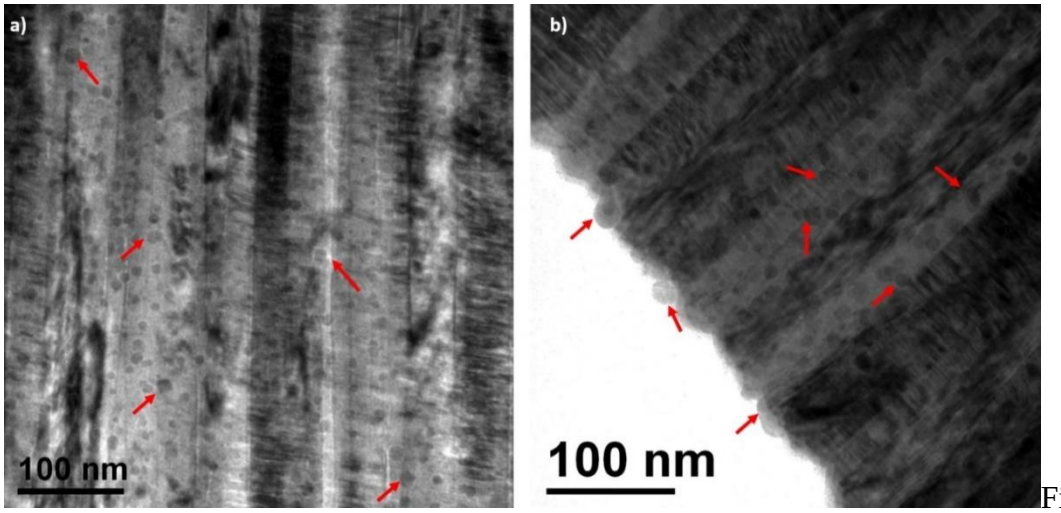

Figure 6.6: Ag-richer nano-clusters with TEM in films with Ag/Ti a) =0.48, b) =0.72

Finally, the deposited interlayer to improve the film adhesion was detected with TEM analysis and the interlayer thicknesses were measured as ~83-87 nm (Figure 6.7).

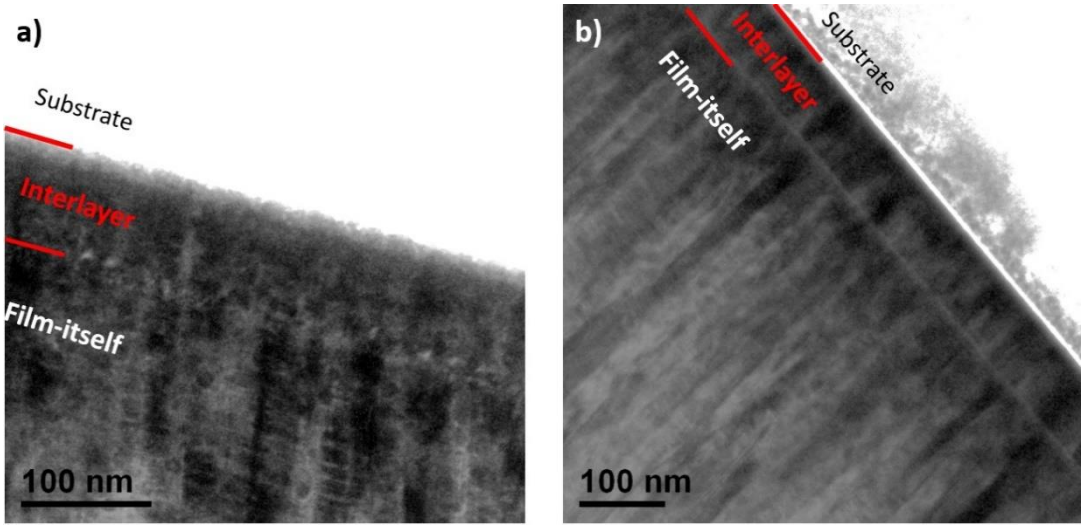

Figure 6.7: Film interlayers detected with SEM for the films with Ag/Ti a) =0.48, b) =0.72

In summary, with TEM analysis it was examined that the columnar micro-structure was protected even for the film with the highest Ag content (Ag/Ti=0.72). Moreover, interlayers were detected for both compositions, with a thickness of ~83-87 nm. TEM analysis confirmed the cluster formation for both compositions.

6.2.2. Crystal Structure Analysis

The crystal structures of the 2nd set of films were investigated with XRD technique. The film deposited with 4 Ag pellets has the similar pattern of peaks as Ti-reference film (Figure 6.8). By considering the solubility of Ag into Ti, the film with Ag/Ti=0.07 evidenced the hcp(αTi) structure with Ag atoms probably in substitution regarding their respective radii (r_{Ti}=187 pm, r_{Ag}=172 pm).

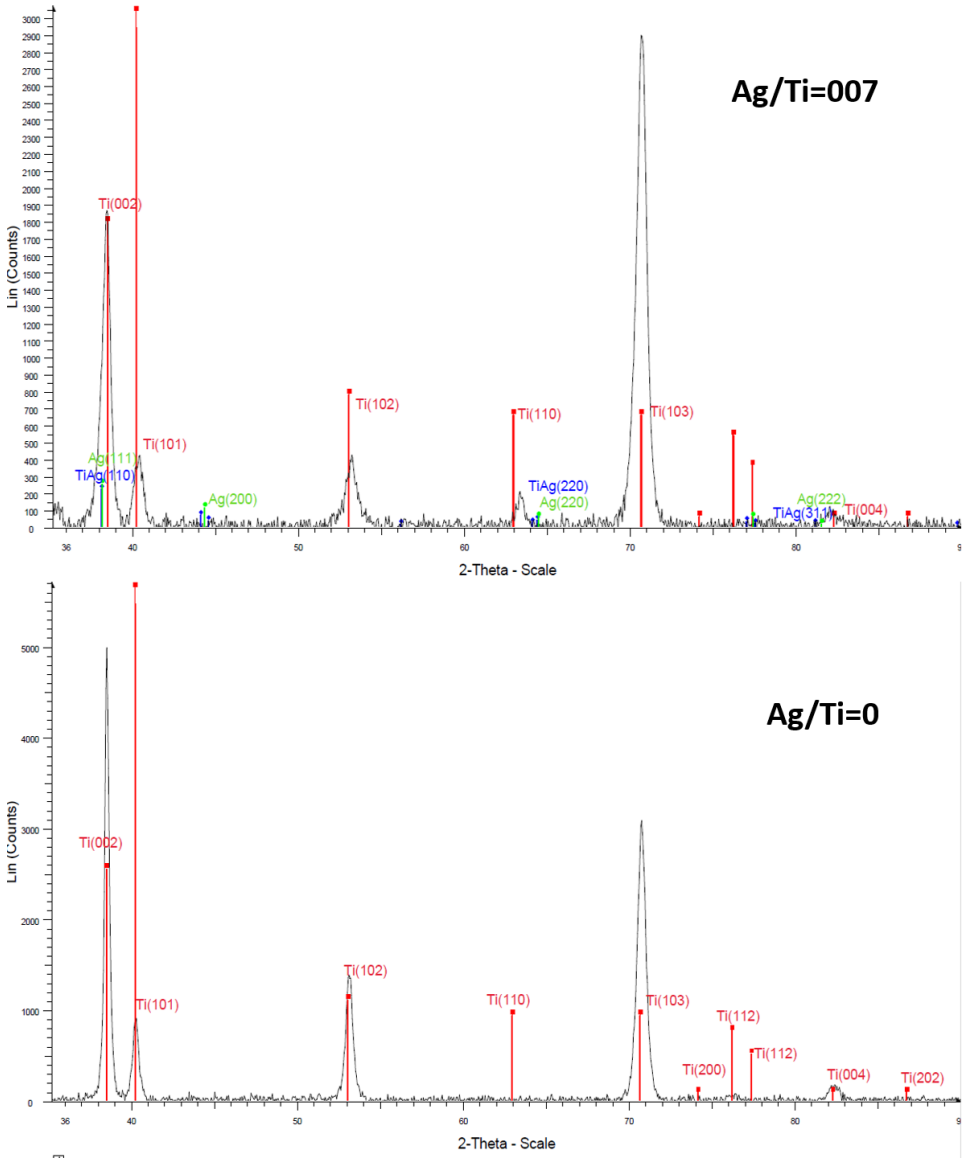

Figure 6.8: XRD analysis of Ti-reference and Ag/Ti=0.07 films with interlayer

For the two other compositions which have higher Ag content, both intermetallic Ti-Ag phases and pure fcc-Ag phase were considered to be co-existing (Figure 6.9). However, since the peaks of both phases are overlapping, it was again challenging to identified them for corresponding compositions.

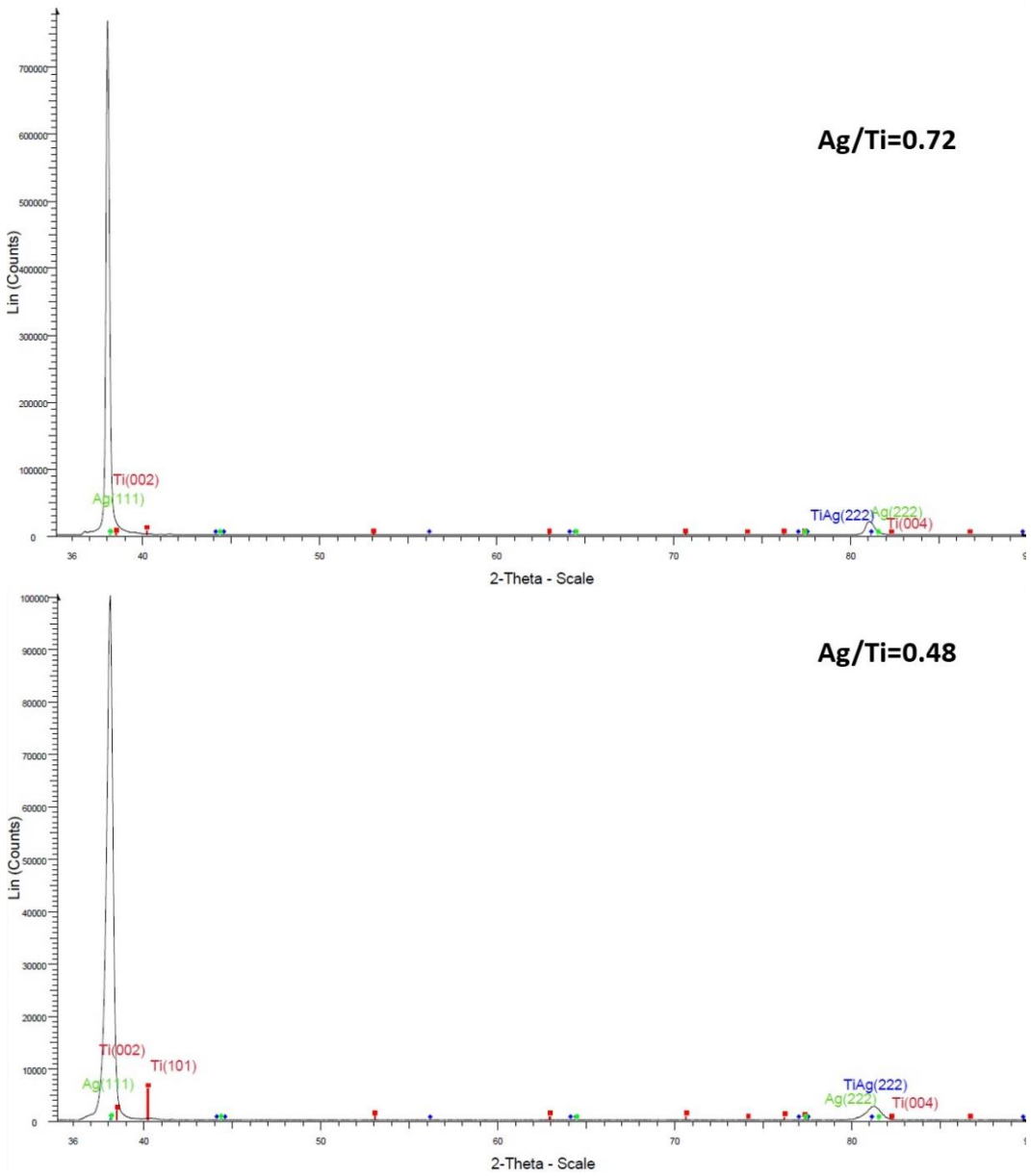

Figure 6.9: XRD Analysis of Ag/Ti=0.48 and =0.72 films with interlayer

In conclusion, also for the second set of films the crystal phases were not exactly detected with XRD analysis, since the peaks are very close to each other. However, the first two Ti-richer compositions (Ti-reference and Ag/Ti=0.07) and the last two Ag-richer compositions (Ag/Ti= 0.48, =0.72) have the similar diffraction patterns.

6.2.3. Mechanical and Electrical Properties

6.2.3.1. Nano-indentation

To estimate the mechanical properties of 2nd series, nanoindentation test was performed. It was seen that, even though there is not a continuous trend with increasing Ag content in the film composition, the highest elastic modulus was reached for the film with Ag/Ti=0.48. This film is the first composition which has intermetallic phase in addition to tiny Ag-based clusters as it was expressed in XRD and TEM analysis. On the other hand, the second film which has intermetallic phase with higher Ag content (Ag/Ti=0.72) reached the highest hardness value even though it has the lowest elastic modulus within these four compositions (Table 6.4). However, this lowest modulus could be correlated with the formation of the pure fcc-Ag phase in larger clusters in the film composition.

Table 6.4: Mechanical properties of 2nd set of deposition Ti-Ag films

Films for Ag/Ti (at.)	Young's modulus (GPa)	Hardness (GPa)
0	106.67 (±9.87)	4.66 (±0.72)
0.07	106.47 (±8.16)	3.69 (±0.50)
0.48	120.5 (±8.71)	5.58 (±0.74)
0.72	102.27 (±3.3)	6.4 (±0.38)

6.2.3.2. Four-Point Probe Test

Before to perform the tribological analysis *in situ* conditions in small scale, also the electrical properties of these films were aimed to analyze. It was noted that while the resistivity firstly increases with the small amount of Ag addition, it decreased for the film with the highest Ag content (Table 6.5).

Table 6.5: Electrical resistivities of 2nd set of deposition Ti-Ag films

Film for Ag/Ti (at.)	Electrical Resistivity (Ωm (*10^{-6}))
0	0.38 (±0.02)
0.07	2.18 (±0.08)
0.48	2.03 (±0.90)

0.72	0.28 (±0.07)

The higher resistivity for the films which contain less Ag could was attributed to the columnar microstructure of the film. Since the Ti grains were surrounded by Ag along the film thickness, the conductivity was more on the vertical direction. However, for the film with Ag/Ti=0,72 the lowest resistivity value was reached which could be correlated with the densification of the film and the formation of pure Ag phase (Ag-clusters). Thus, more uniform and higher electrical conductivity was achieved for this composition.

6.3. Methodology of *in situ* Tribological Analysis

During the tribological tests for the Ti-Ag films with interlayer, by rubbing against PU ball, the applied normal force was 4 N, the sliding distance was 2 mm and the sliding speed was 1 mm/s. Since the Young's modulus of polyurethane ball was indicated as 360 MPa by the provider (Marteau & Lemaire company) and the Young's modulus of Ti-Ag films was calculated with nanoindentation test as in the range between 102-120 GPa, the maximum Hertzian contact pressure was calculated as ~ 20 MPa. The microscope images were investigated in the same way as the protocol defined previously (Chapter 4, section 4.1.3), after every 10 cycles for three different regions of interest in various magnifications. Here below, images with high magnification were shown from these three regions of interest (Figure 6.10). As it was seen, while the contact point for the reference test is clearly visible after 100 cycles, the wear track on the region where the sliding speed was constant has a smoother appearance and some particle accumulation was detected on the region while direction changed.

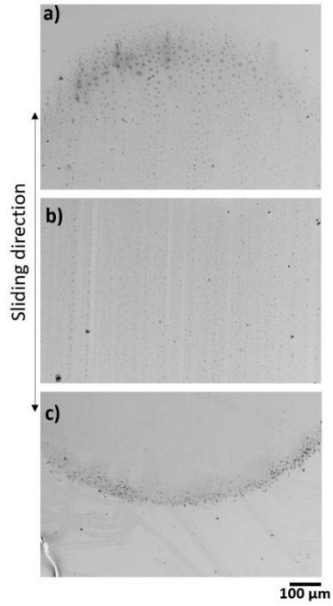

Figure 6.10: Film with Ag/Ti=072 - Wear track after 100 cycles, a) starting region of the contact, b) the region where the sliding speed is constant, c) the region where the sliding direction changed

The *in situ* analysis was performed on these three regions every 10 cycles. Since the clearer changes were seen on the region where the sliding direction changed, this region is shown as an example. With increasing number of cycles, more debris accumulation was detected on this region. (Figure 6.11).

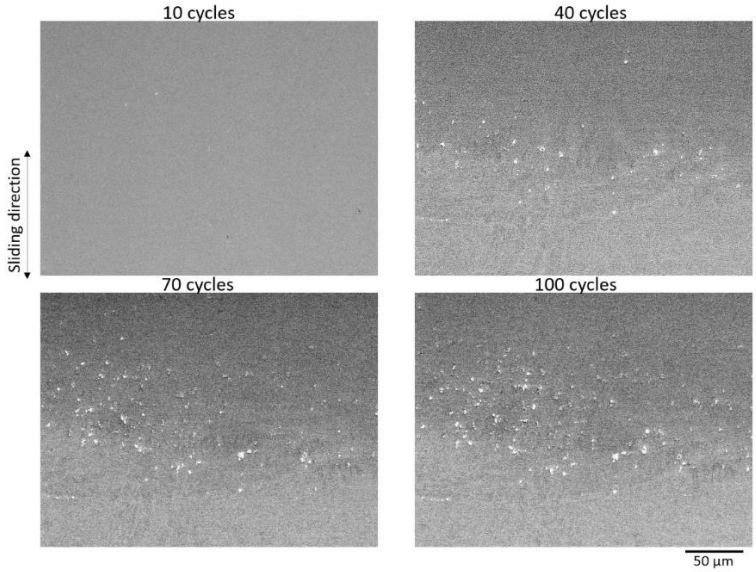

Figure 6.11: *In situ* analysis of the film with Ag/Ti=0.72 from the region where the sliding direction changed after 10, 40, 70, 100 number of cycles at 50% RH

Also, the recorded normal and tangential forces and the friction coefficients were measured for each cycle from the recorded data. The tangential forces were indicated for a reference test which was performed at 50% RH for the film with Ag/Ti=0.78 during *in situ* analysis (Figure 6.12). It was seen that the tangential force was lower at the beginning of the test. The increase on the further cycles could be correlated with the third body formation and material flow along the sliding distance with the effect of oxidation of the freshly worn zone in humid environment.

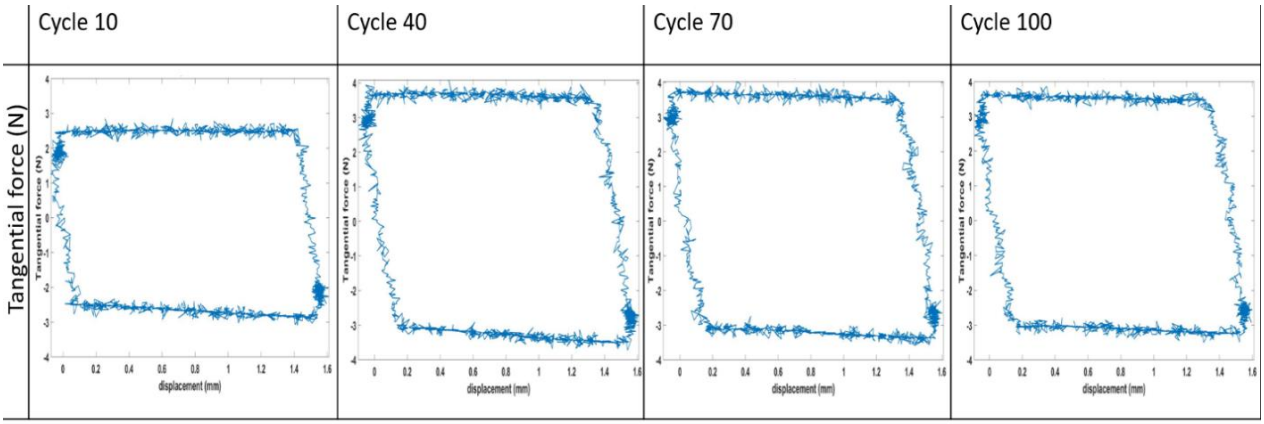

Figure 6.12: Tangential force (from -4 to 4 N) along displacement length (from 0 to 16 mm) for the film with Ag/Ti=0.72 at 50% RH

During the *in situ* analysis of the tribological behaviour of Ti-Ag films, the film with Ag/Ti=0.72 was tested in various environmental conditions inside the eSEM chamber to evaluate the effect of humidity with high Ag amount of Ag. Finally, the role of Ag content on the tribological behaviour of Ti-Ag films was studied since it was examined in chapter five that increasing Ag content may enhance the friction and wear character of these coatings.

6.4. *In Situ* Tribological Analysis

6.4.1. Effect of Environment

All the films were analysed in ambient air conditions (22±2°C, 25±2% RH), in addition to the controlled environment in eSEM chamber at 50% relative humidity (4°C, 400 Pa). Here it is worthy to note that both titanium and silver tend to oxidise in the existence of humidity. Therefore, tribological behaviour of the film with Ag/Ti=0.72 was investigated under these two

environmental conditions. Figure 6.13 presents the evolution of the COF throughout the 100-cycle test.

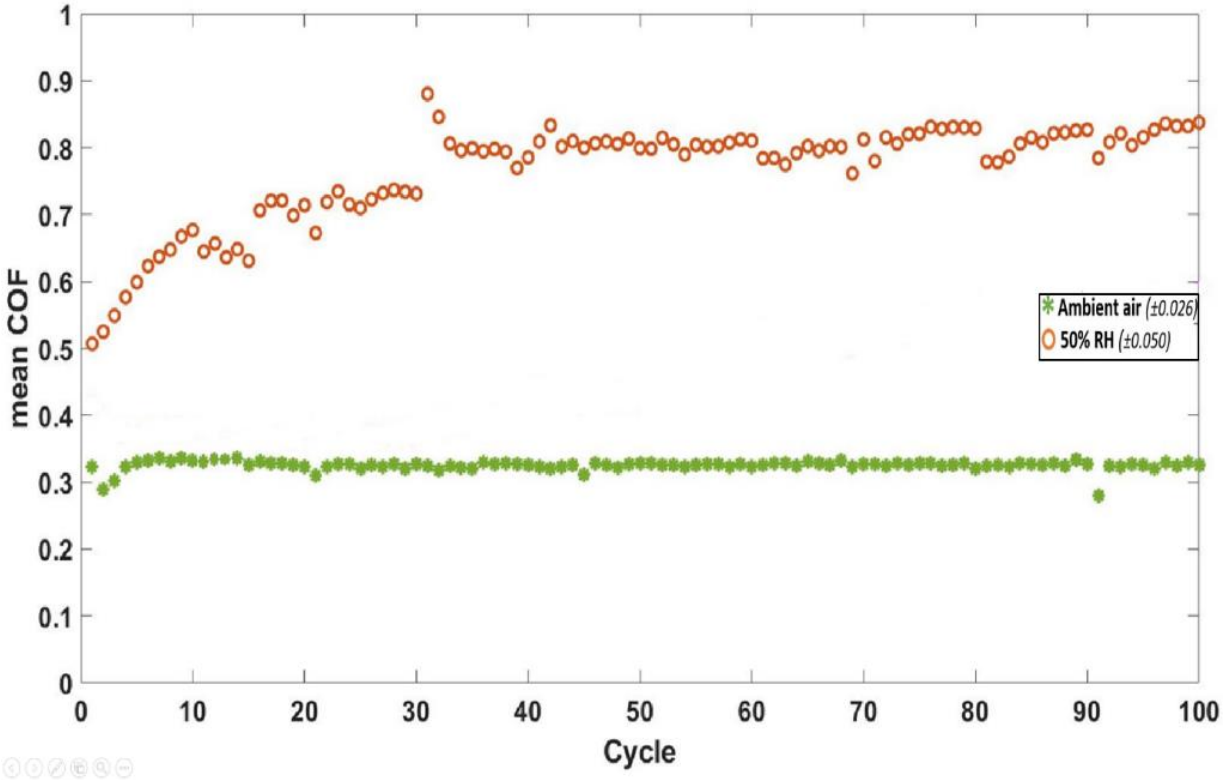

Figure 6.13: Mean COF for the films with Ag/Ti=0.72 in two different environments

Even though there are slight variations on the curve, the lower and well-stable mean COF values were achieved in ambient air. At 50% RH, the mean COF values increased and became remarkably unstable for every ten cycles. Here, while the overall mean COF value for the test performed in ambient air was 0.33 (±0.026), it was 0.77 (±0.05) for the test performed in 50% RH. Especially for the first 30 cycles, significant variations were detected on mean COF values in 50% RH test, while they are relatively more stable for the higher number of cycles in this condition. Therefore, the first 30 cycles were deeply investigated by considering the *in situ* images for both testing conditions (Figure 6.14).

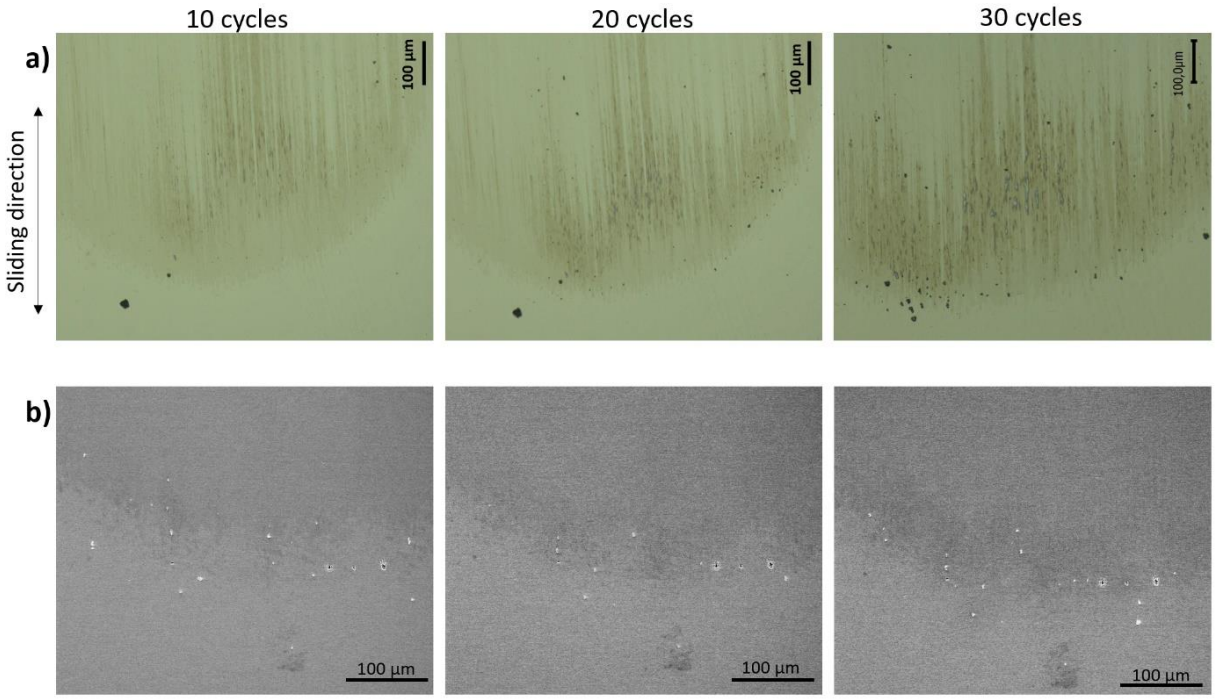

Figure 6.14: Wear track from the turning point of sliding for the first 30 cycles for the tests performed at a) ambient air (light microscope images), b) 50% RH (SEM images) for the film with Ag/Ti=0.72

Regarding the *in situ* recorded images from the turning point of the sliding for the first 30 cycles, the deformation of the film slightly increased from 10 to 30 cycles for the ambient air test while the mean COF values are more stable. At 50% RH, some small debris were detected at the very early stage of the contact and the deformation of film increased with increasing number of cycles. After the cycle 40, the friction coefficient was relatively stabilized which could be attributed with the staying of the debris at the contact region. To confirm this, a *post mortem* analysis was required, and Figure 6.15 shows the two rubbing surfaces after the test.

When the wear tracks of the films (their respective widths are indicated by red arrows) and the balls were investigated in *post mortem* conditions, it was seen that both the film and the ball rubbed in ambient air atmosphere displayed less deformation with respect to 50% RH test. No debris were appeared on the center of the film surface while the wear track was barely appeared as a darker zone of the ball surface. On the other hand, for the tests performed in 50% RH, the wear tracks of the film and the ball were clearly seen with some debris.

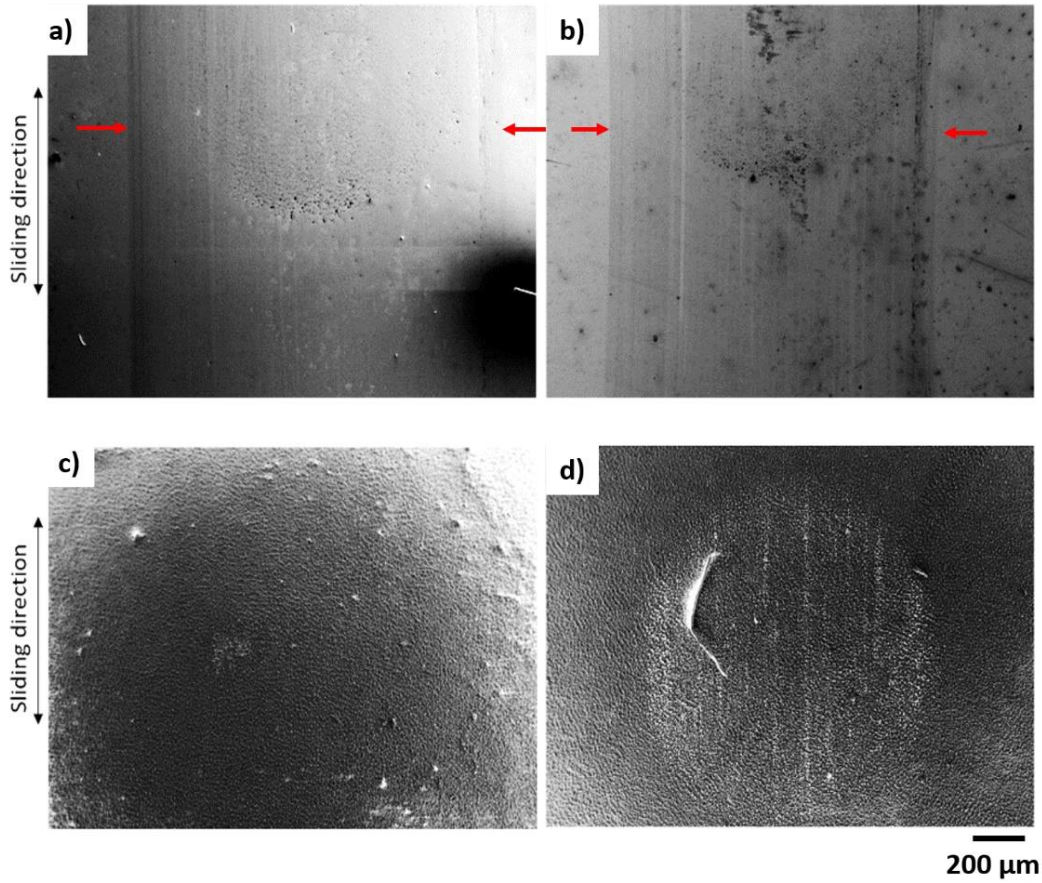

Figure 6.15: Wear tracks from the center of the film with Ag/Ti=0.72 a) in ambient air, b)50% RH and ball tracks c) in ambient air, d)50%RH

Besides, a further chemical analysis of the tracks was performed by EDS (Figure 6.16). This analysis did not conclude on significant differences between both environments, but has confirmed that the film integrity was preserved, without any traces of iron. In order to quantitively estimate the effects of wear, a 3D profile for each track was performed (Figure 6.17).

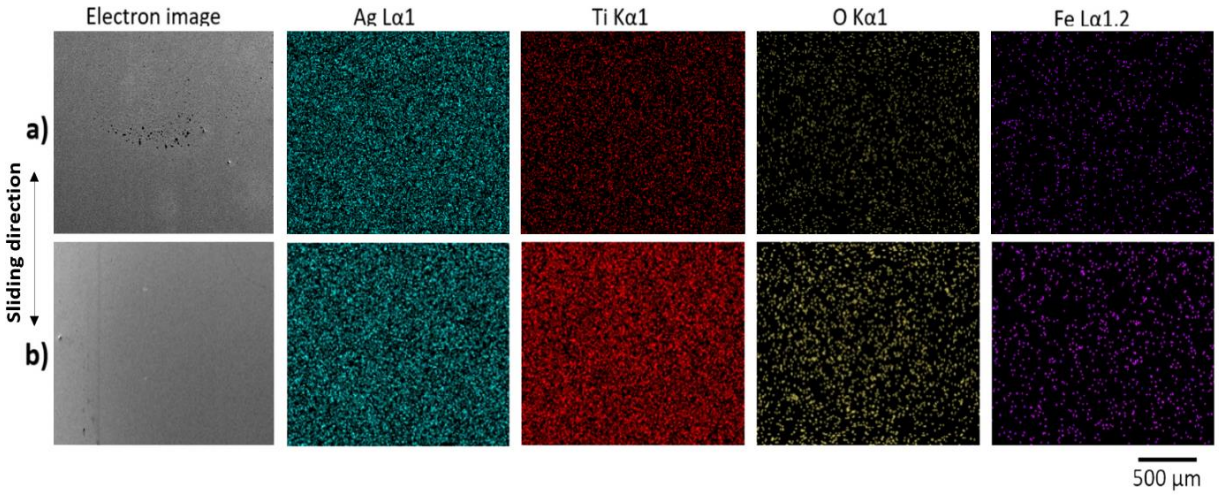

Figure 6.16: EDS analysis of the center of wear tracks of the film with Ag/Ti=0.72 a) in ambient air, b) in 50% RH

As already qualitatively suggested in electronic images of the worn surface (Figures 6.15 a,b), the wear track resulting from the ambient air appears very smooth, whereas under 50% humidity the wear profile is more complex, indicating a more important wear on both edges of the track.

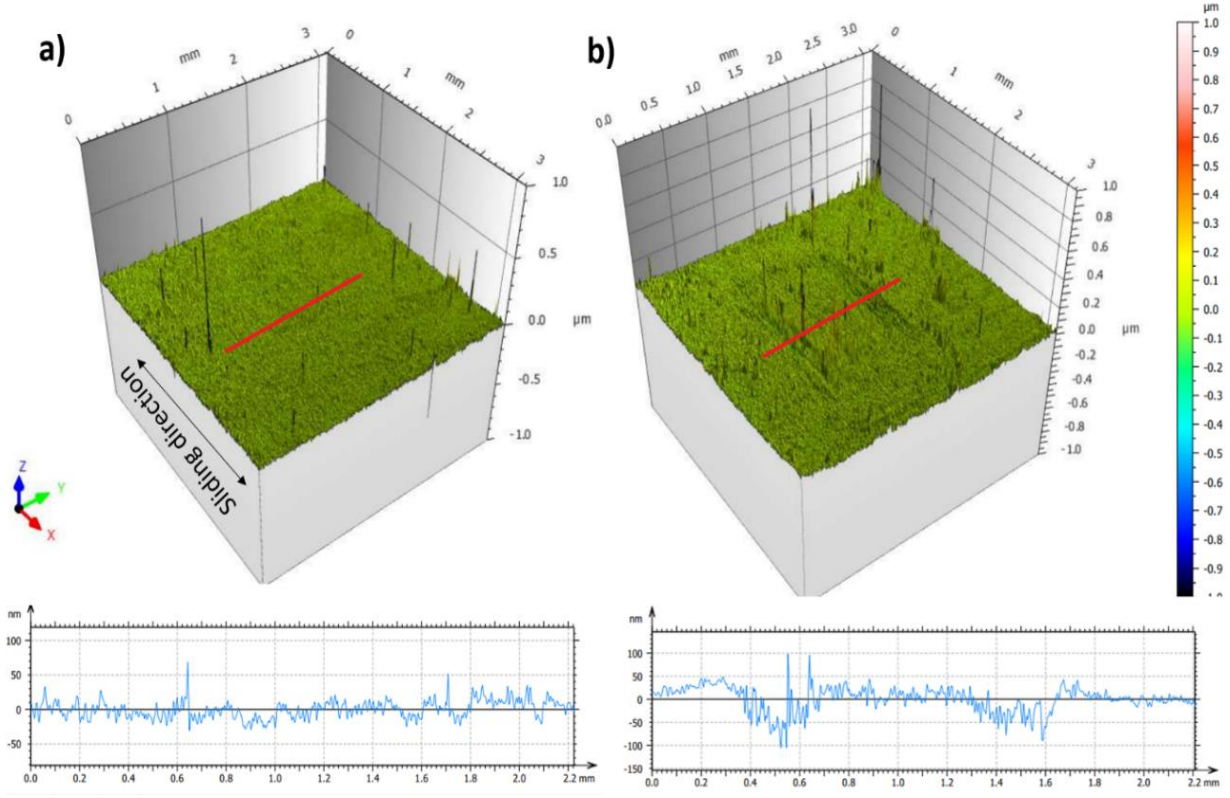

Figure 6.17: 3D profiles of the wear tracks for the tests performed a) in ambient air, b) at 50% RH for the film with Ag/Ti=0.72

To determine the potential role of the counter-face on the wear behaviour, both balls were analysed. Their electronic and X-ray maps appear Figure 6.18.

For the ball used in 50% RH test, distribution of silver and titanium is quite homogeneous and at a very low level. In opposite, rubbing under humidity reveals a strong localised enrichment of metals, aligned in the sliding direction, associated with an accumulation of debris constituting to a film transfer.

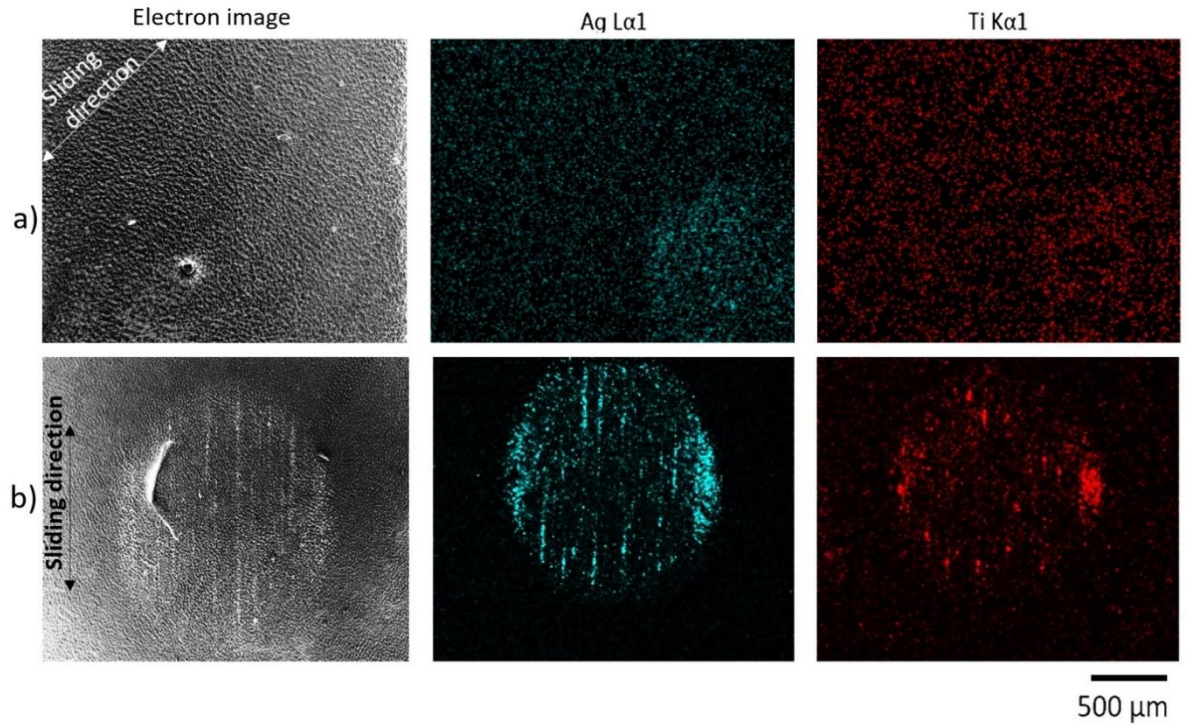

Figure 6.18: EDS analysis of the material transfer on ball track for the test performed at a) in ambient air, b) at 50% RH rubbed against the film with Ag/Ti=0.72 after 100 cycles

To verify this assumption at a deeper scale, a deeper characterisation by TEM was conducted. Thin foils were then extracted from the wear tracks by FIB, observed by TEM (STEM HAADF mode, Figure 6.19), and analysed by EDS (Figure 6.20). Thus, the centres of the wear tracks were compared under *post mortem* conditions. Here, while neither debris nor large amount of deformation was detected along width of the wear track for the test performed in ambient air (25%RH, 25°C), dispersed bright debris as a discontinuous thin layer was detected as spread over the surface of the wear track at 50% RH test. It has to be noted that, except the debris formed on the contact region, the film itself and its columnar structure was seen as undeformed.

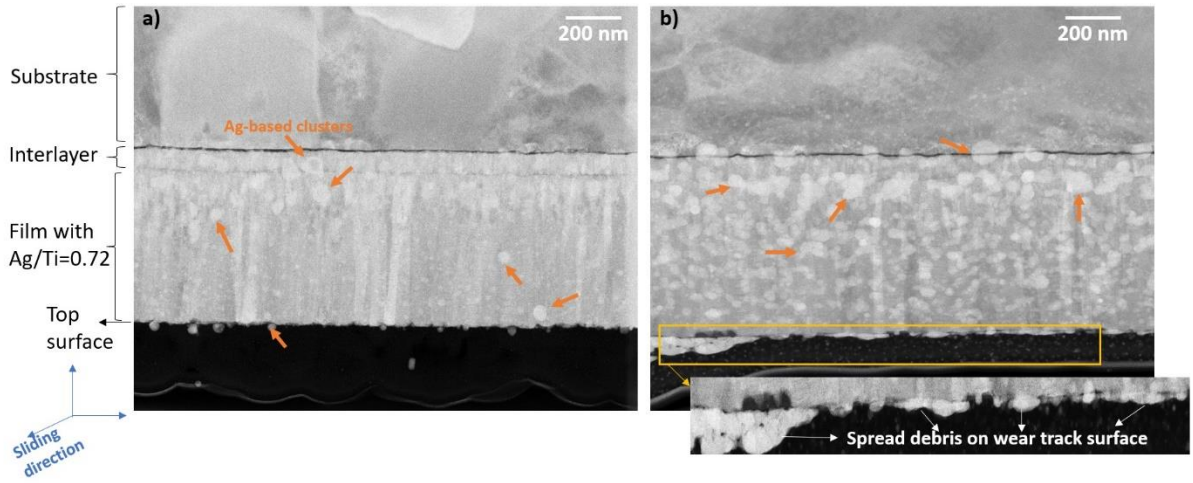

Figure 6.19: Cross section analysis of the wear tracks of the film with Ag/Ti=0.72 for the tests performed at a) ambient air, b) 50% RH in *post mortem* conditions

When an EDS analysis was performed for the cross section of the wear track from the test performed at 50% RH, it was seen that the debris formed and stuck on the contact zone is mostly composed of silver without significant traces of neither titanium, nor oxygen.

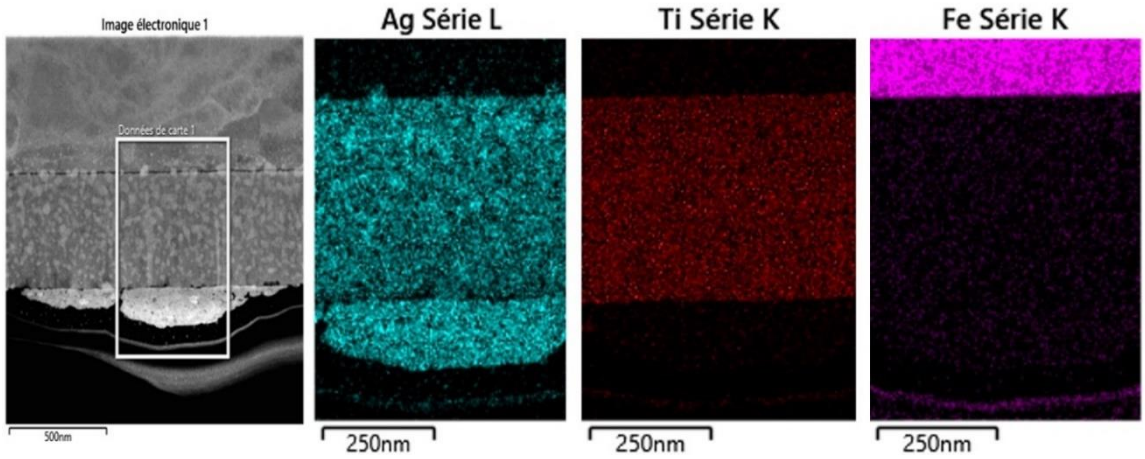

Figure 6.20: EDS maps of the cross section wear track of the film with Ag/Ti=0.72 for the test performed at 50% RH.

Considering previous chemical and topographical information, a scenario for the surface damaging has to be built. The increase of the Ag-based debris at the contact interface with increasing number of sliding was aimed to be shown. It is important to note that the accumulation of debris in the contact region, their chemistry and their effect on wear mechanism was modified with increase of humidity. Likewise, it is also important to remind that the controlled humidity rate into the SEM chamber results from an imposed (Water

pressure, temperature) couple. Therefore, not only the humidity level, but also the temperature parameter, are changing between the two test conditions: ambient air: 22°C, 50% RH: 4°C. Surely such an indirect difference was also met for the preliminary tests conducted with TiN deposited onto steel (see Chapter 4), but without any functional effect considering the intrinsic thermal stability of both film and substrate. In our case, the problem is different because the contact involves two thermal sensitive material: silver on the one hand and PU on the other hand.

The effect of humidity on the tribological behaviour of silver added to WS_2 films has already been studied by Wang *et al.* [23]. They attested best performance for the film containing 41% of Ag and for tests performed both under vacuum and at 60% RH, but at the room temperature. However, Logan et *al.* [25] showed that silver can be considered as a thermal sensitive material, for which the mechanical properties (flow stress) strongly change with temperature in the [77°K-473°K] range (Figure 6.21a) and also with strain rate. It was seen that while the stress decreases, a brittle to ductile transition occurs with increasing temperature. Therefore, in our case it could be stated that Ag-based nanoclusters in Ti-Ag films could show a more brittle/rigid character at 4°C for the test performed in 50% RH and these harder particles, behaving as abrasive particles. The interfacial film formed is different and it may explain the difference in the mean COF values. Additionally, these clusters adopted a more ductile nature at room temperature for the test performed in ambient air, and so they behaved like solid lubricant providing a lower and more stable mean COF values. Such thermal modification on the silver mechanical properties was also confirmed by Wakamoto et *al.* [24] stated that both the elastic modulus and the ultimate tensile strength decreased continuously with increasing temperature for pure Ag film (10µm of thickness).

As well as the silver, it is also necessary to consider the effect of the environmental conditions on the counter-face. The mechanical properties and crystallinity of polyurethane are known to change with the temperature [26, 27]. Tobushi et *al.* [26] analysed the mechanical properties of polyurethane below and above its glass transition temperature (Figure 6.21b). It was seen that above the glass transition temperature of PU (318°K) the deformation resistance increases with increasing cyclic motion.

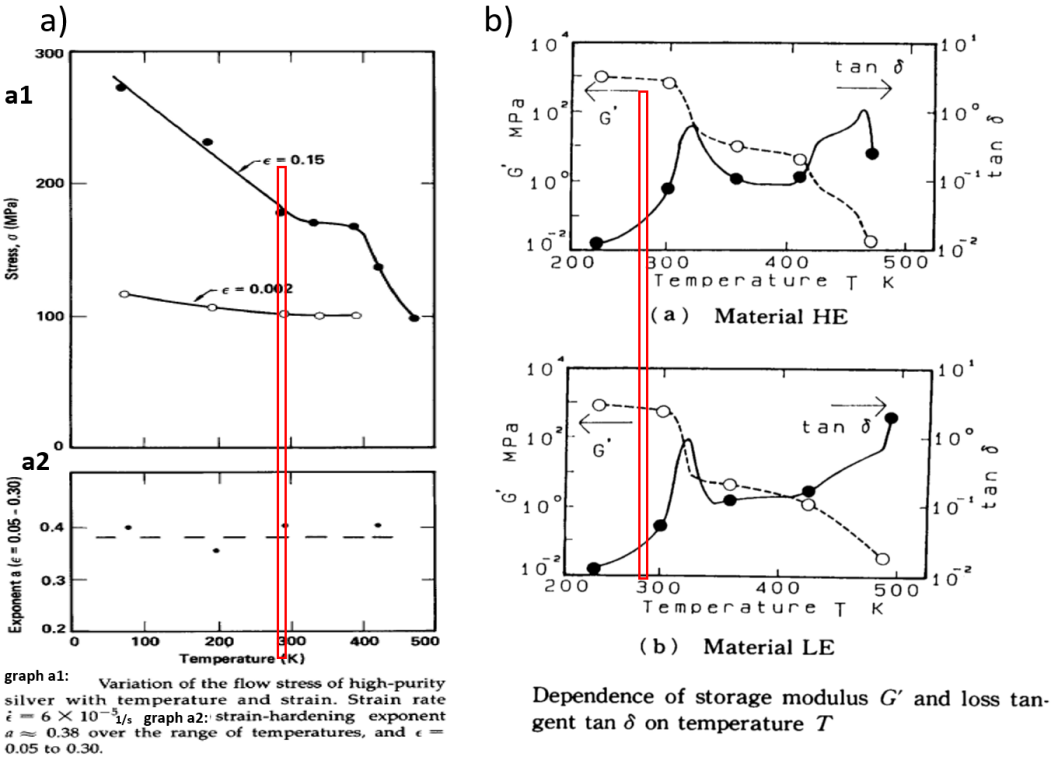

Figure 6.21: Temperature dependence on mechanical properties from literature, a) for silver [25] and b) for PU [26]

Also, Huh et *al.* [27] investigated the changes on the mechanical properties of PU dynamically from -150 to 200 °C and it was seen that the elastic modulus of the two types of tested polyurethanes decreased with increasing temperature in addition to several relaxation states. Therefore, from 4°C to 22°C, the mechanical properties and crystallinity of PU ball could be different and this may cause a change on the stress and wear behaviour of the ball.

Considering such thermal effect of both Ag-containing film and ball, a scenario is proposed to explain damaging (Figure 6.21). In this "damaging model", PU should have a rather soft character at room temperature, and would change towards a more rigid one at 4°C. Similarly, silver mechanical behaviour would change, respectively, from a ductile to more rigid behaviour.

Therefore, in ambient air (*i.e.* at room temperature), application of the load to the soft PU ball leads to its deformation, accommodating a part of the shear. The contact is then made less severe. Besides, superficial silver clusters are ductile, prone to be deformed in the contact area, without propensity to stick to the counter-face (Figure 6.22a). Resulting debris are rare and not really aggressive for the rubbed surface.

In opposite, under 50% RH conditions, *i.e.*at 4°C, mechanical properties of both PU ball, and silver clusters are changing, becoming harder and more rigid. Affinity of the ball to stick silver is by far higher than at room temperature, giving rise, quite early, to an accumulation of silver-based debris on the ball and on the film track (Figure 6.22b). The silver debris formed may behave as an abrasive material. Thus, the interfacial material observed at the end of the test is composed of silver (see the tracks on figure 6.16 and 6.18) and titanium (see silver + titanium on the ball on figure 6.18). It has a lower ductility at 4°C than at 22°C. This interfacial layer sheared during the test in SEM, leading to a high friction coefficient.

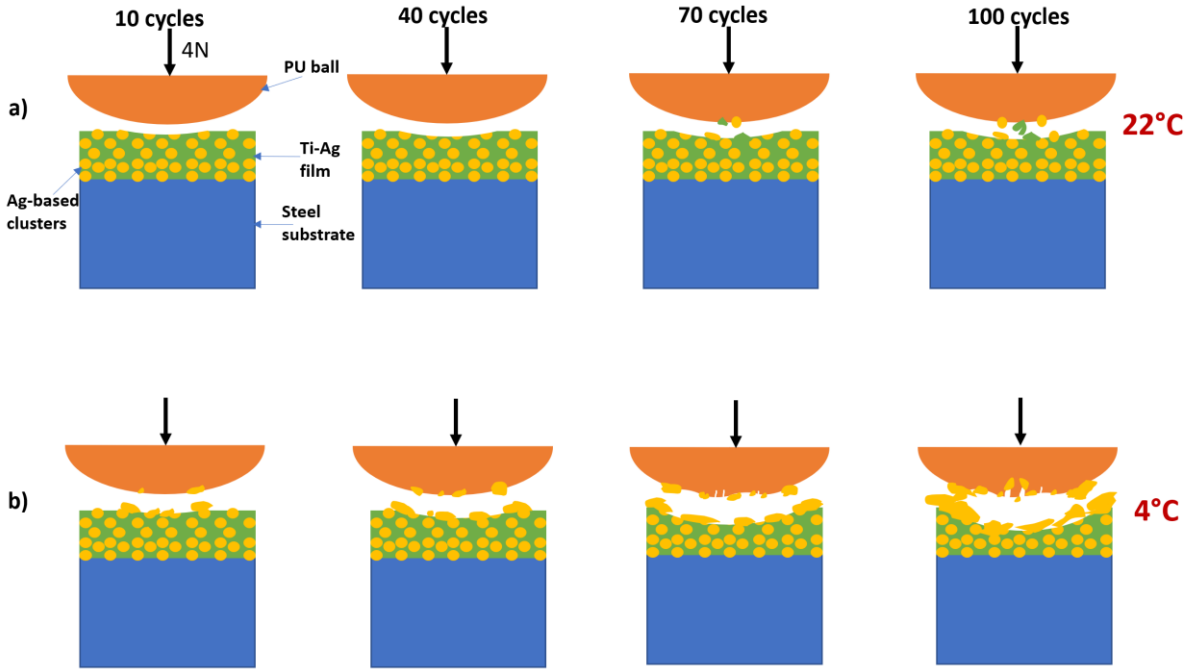

Figure 6.22 Schema of damaging mechanism of the film with Ag/Ti=0.72 for the test performed at a) ambient air, b) 50% RH

6.4.2. Effect of Film Composition

The role of the film composition on tribological behaviour of Ti-Ag films was considered in terms of varying Ag content. Three previously defined Ti-Ag films (the compositions with Ag/Ti=0.07, =0.48, =0.72) were used for the tribo-tests. Here, it is important to remind that in previous set of series, Ag-richest composition had performed the best wear resistance by comparison to the others in ambient air and vacuum conditions. Considering the role of humidity on Ag as it was explained in section 6.4.1, it was also aimed to examine the role of increasing Ag content under 50% RH.

NB: The reason for selecting 50% RH is to perform the analysis in the range of the relative humidity standards for thermal comfort of the environment which was determined by ASHRAE (American Society of Heating, Refrigerating, and Air Conditioning Engineers, Inc) [28].

All the other test parameters (normal load, sliding speed and sliding distance) were kept same as before. It was seen that, on the contrary of the literature [22, 23, 29] for the tests performed in lower humidity levels, the tribological behaviours of the films are strictly different with increasing Ag content, for 50% relative humidity level in controlled environments.

Figure 6.23 shows the friction maps obtained for the three compositions for a comparison purpose. Both the beginning and end of the displacement distance (corresponding to a 0.4 mm length) were cut off to use the values only where the sliding speed is constant. Comparing maps, we can easily conclude that the film where Ag is incorporated as a solid solution present a stable and good tribological behaviour with a low coefficient of friction, whatever the cycle type (inward, backward) and time. For a moderate silver content (Ag/Ti=0.48), two regions can be discriminated: below 20 cycles sliding is quite low then COF continuously increases until 30 cycles, from which a steady state is reached. For the film with Ag/Ti=0.72, except in the region where sliding direction changed (in blue), the COF evolution is similar, with a higher level for the stable final reached COF values.

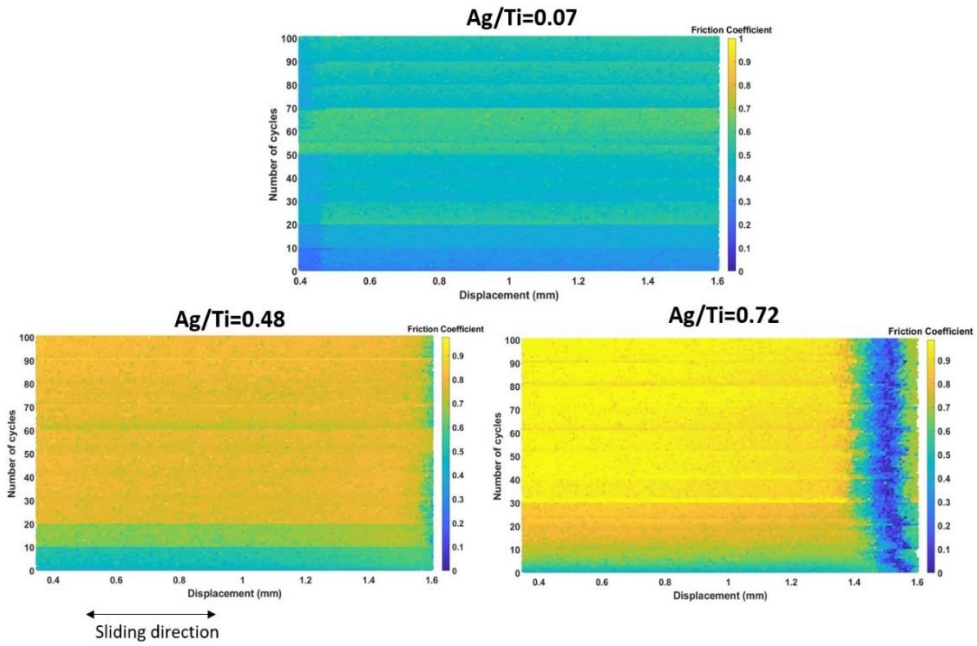

Figure 6.23: Friction maps of the different films performed in 50% RH

The same tendencies display more quantitatively Figure 6.24, where the mean values of COF for each cycle was calculated, and reported for the different films. The lowest and well-stable

COF values are obtained for the solid solution film at 0.52 (±0.05). Films attesting Ag/Ti ratios =0.48 or 0,72 indicate mean COF at 0.62 (±0.04) and 0.77(±0.50) respectively.

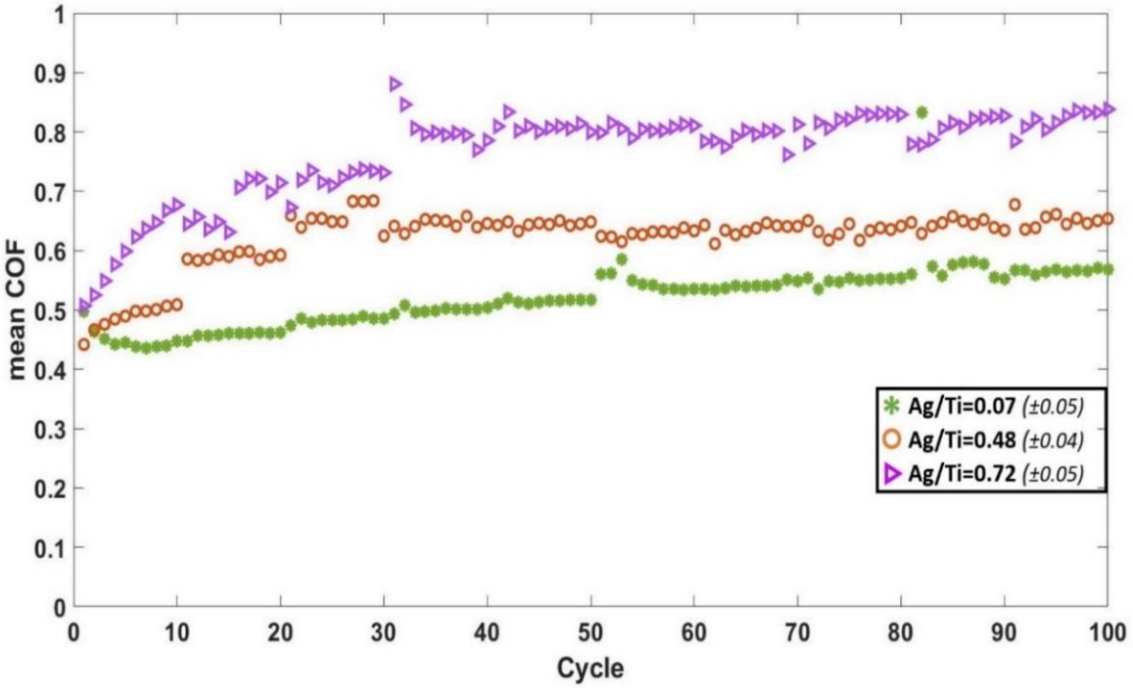

Figure 6.24: Effect of the film composition on mean COFs of Ti-Ag films in 50% RH

To consider the effect of wear on the rubbed surface, the resulting worn track was *in situ* observed throughout the test (Figure 6.25-27). The film with Ag/Ti=0.07 shows several scratch marks detected on the wear track with a smooth appereance (Figure 6.25). For the film with Ag/Ti=0.48, a plastic deformation on the turning point of the sliding was seen for the early stages, highlighted by some white bright particles appearing through the end of the test (after 100 cycles) on the same region of the wear track (Figure 6.26). For the highest silver content, these white bright debris appeared even from the first cycles (after 10 cycles) of sliding process (Figure 6.27).

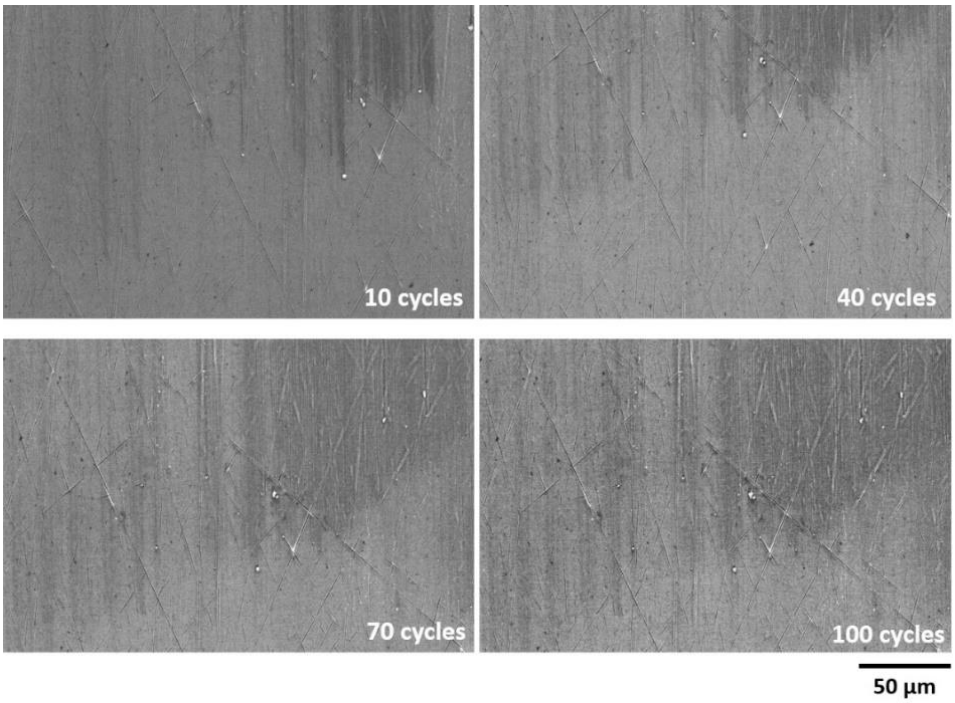

Figure 6.25: *In situ* analysis of the turning point of the wear tracks for the tests at 50% RH of the Ti-Ag films with Ag/Ti= 0.07

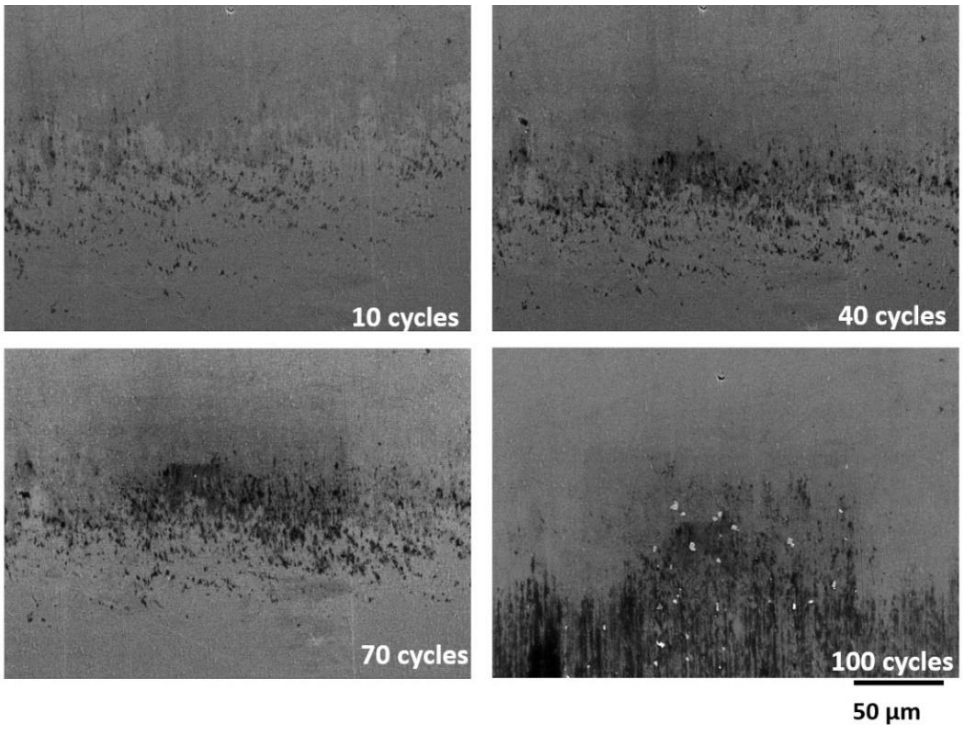

Figure 6.26: *In situ* analysis of the turning point of the wear tracks for the tests at 50% RH of the Ti-Ag films with Ag/Ti= 0.48

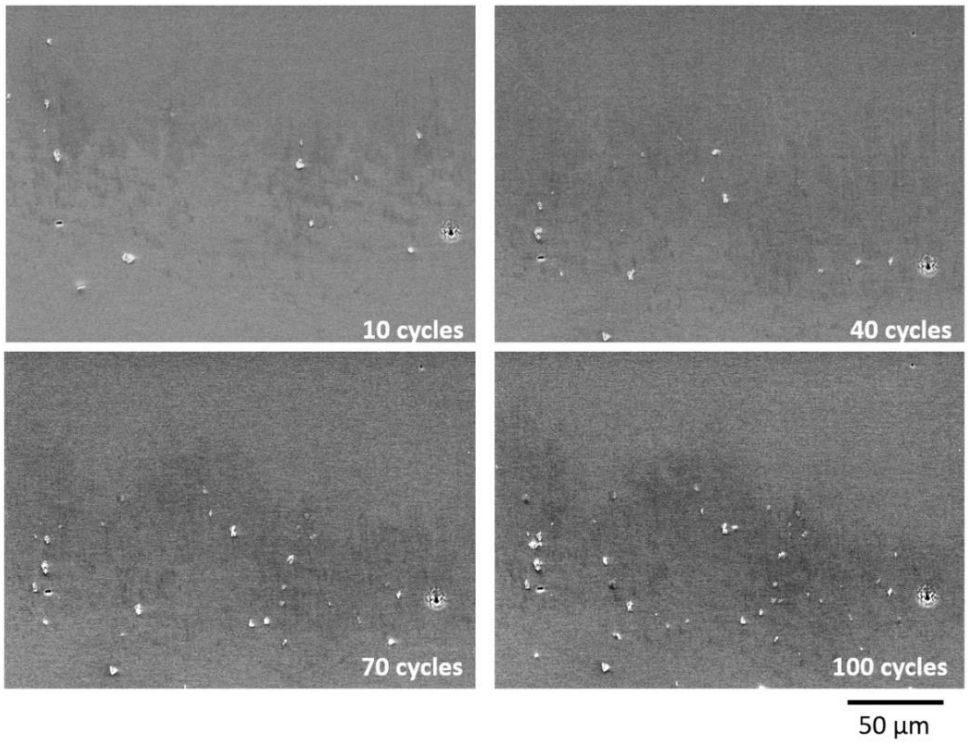

Figure 6.27: *In situ* analysis of the turning point of the wear tracks for the tests at 50% RH of the Ti-Ag films with Ag/Ti= 0.72

A further chemical analysis by EDS was performed, leading to elemental map (Figure 6.28). They did not reveal a significant difference of the different wear tracks composition. Nevertheless, iron X-ray map, again, indicate the film preservation without traces of the substrate, independently on the film silver content.

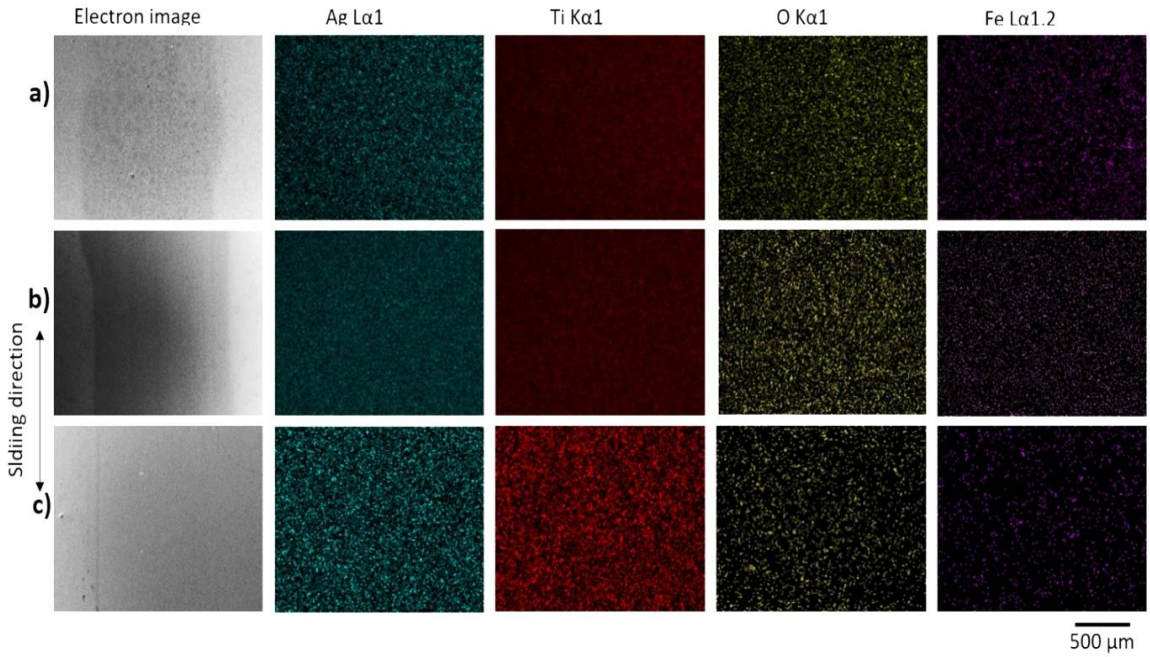

Figure 6.28: EDS analysis of film surfaces of Ti-Ag films with a) Ag/Ti=0.07, b) Ag/Ti=0.48, c) Ag/Ti=0.72 films at 50% RH after 100 cycles

Thus, chemistry of the worn film cannot explain the different tribological behaviours. What about the counter-face? Figure 6.29 presents then analysis of the ball, after the test. Balls revealed strict differences after rubbing against the three different compositions. In particular, a large amount of film material was detected on the surface of the ball which rubbed to the Ag-richest film. The strong material transfer is in line with the highest friction coefficient for this composition. Also, several localised film particles were detected on the ball surfaces which were rubbed to the films with Ag/Ti=0.07 and =0.48. This small amount of material transfer and the slight deformation on the surface of the balls can explain their relatively lower and more stable mean COF values.

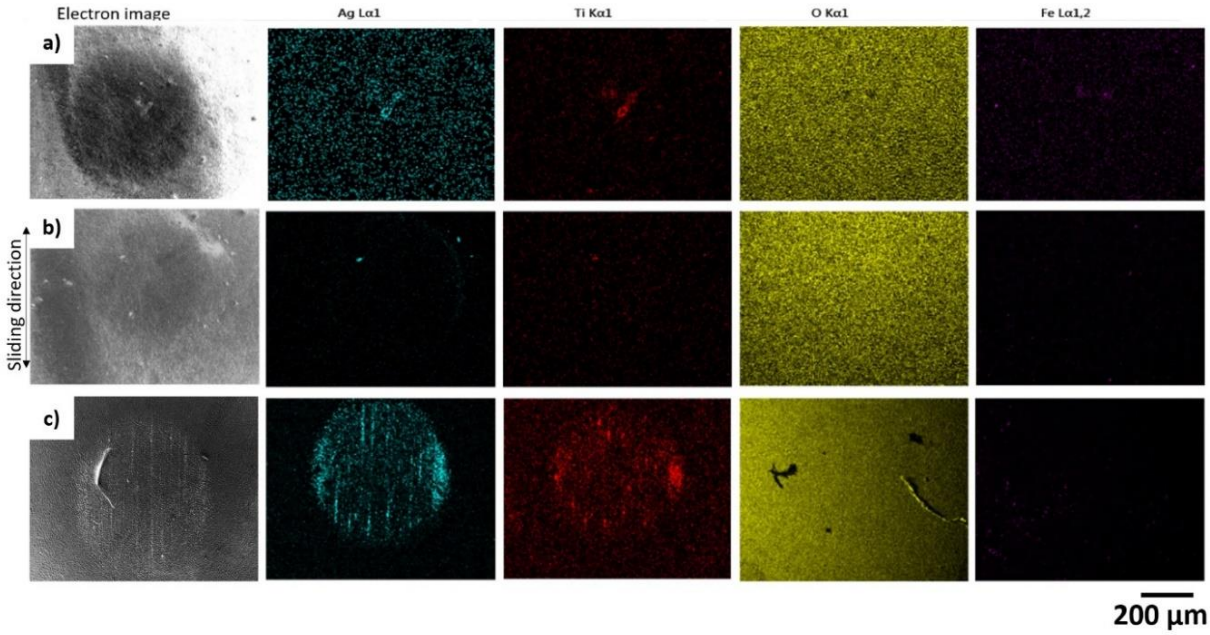

Figure 6.29: EDS analysis of PU balls surfaces after rubbing to the Ti-Ag films with a) Ag/Ti=0.07, b) Ag/Ti=0.48, c) Ag/Ti=0.72 films at 50% RH

The role of Ag content at 50% relative humidity can be summarised through a scenario representing the state of the contact area as a function of the test progression.

The literature reports most often a positive effect of silver on tribology of silver-containing films. Such beneficial influence would be based, for instance, on good sliding properties of Ag-based added particles [22, 23], or on an Ag-induced smoothing effect [30]. In our case, such a positive effect was not evidenced, but, as mentioned above, tests were not done in conventional conditions regarding the tested temperature, susceptible to modify mechanical properties of materials involved in the contact. Indeed, at 50%RH, the contact is hold at a 4°C temperature, which makes PU ball and silver clusters more rigid. Such a combination of stickable hard silver debris would be on the basis of the important wear met for the silver richest film (Figure 6.30c). In this sense, the better tribological behaviour in terms of lower mean COF and wear can be explained by the smaller amount and size of silver clusters (Figure 6.30b). Finally, the best stable sliding behaviour is given by the film devoid from particles, where silver is present as a solid solution (Figure 6.30a). Such titanium matrix is prone to be oxidized, giving rise to a continuous passive layer, able to behave as a solid lubricant layer.

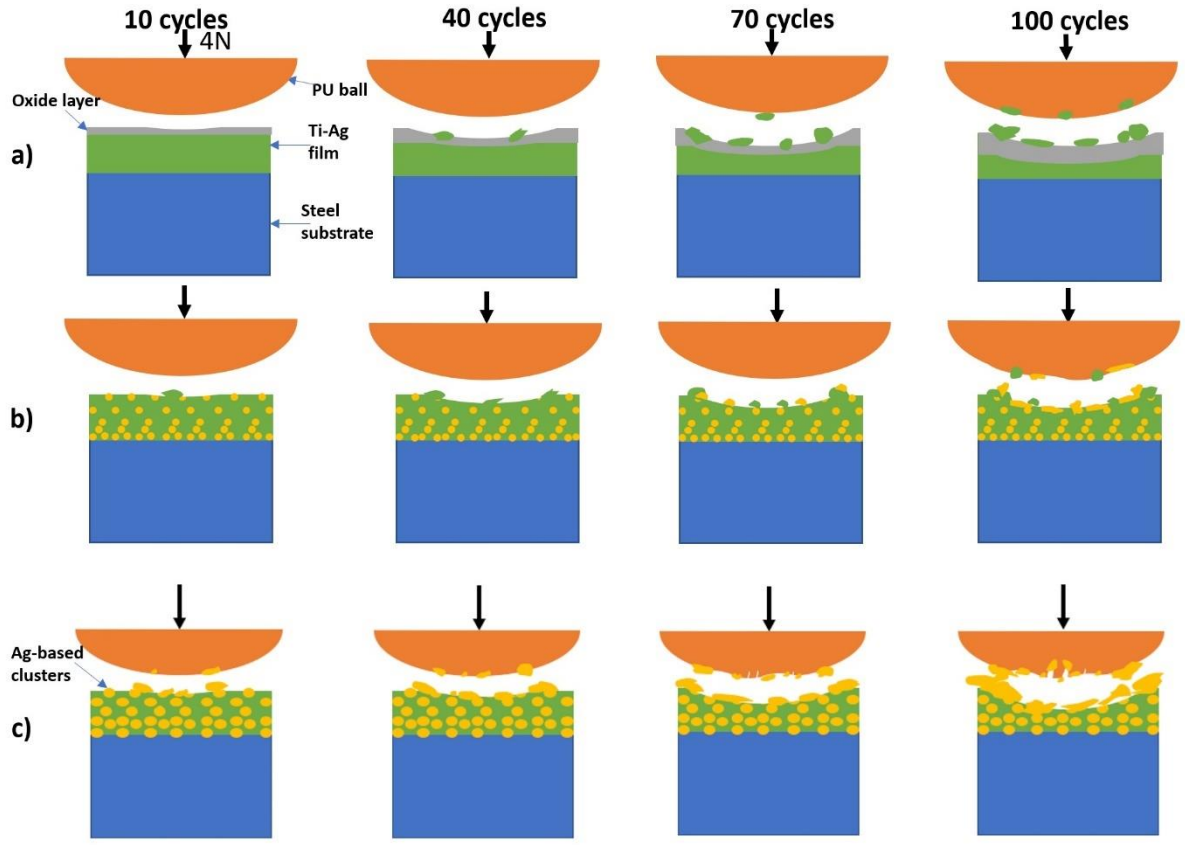

Figure 6.30: Schematics of *in situ* damaging mechanism of Ti-Ag films at 50% RH for the compositions with Ag/Ti= a)0.07, b)0.48, c)0.72.

6.5. Conclusion

To conclude, Ti-Ag films were deposited with a further interlayer to enhance their adhesion character. Their chemical compositions, microstructures, densities, electrical and mechanical properties were investigated to evaluate the effect of Ag content on film properties. The tribological behaviour of Ti-Ag films deposited on steel substrates were analysed by rubbing against PU balls.

The role of the environment (ambient air or 50%RH) was investigated for the silver-richest film (Ag/Ti=0.72). The wear behaviour was discussed in light of the affinity for the surface to "catch" Ag-based debris coming from the clusters. Such a sticking characteristic could be an indirect consequence of a change in mechanical properties of the contact materials induced by

the temperature difference of both environments. Indeed, based on the literature the PU ball as well as silver clusters present a soft, ductile behaviour at 22°C, and become more rigid at 4°C. In the later condition, silver-based debris stick to the PU counter-face, accumulate on its surface, and finally constitute abrasive materials with a detrimental influence on wear.

The effect of Ag content was also investigated on tribological behaviour of Ti-Ag films in humid conditions (50%RH). As reminded above, in constant temperature (4°C) condition, the combination of a rigid PU ball and hard silver clusters lead to activate the wear flow. Silver clusters can be then considered as harmful for the sliding. In this sense, the cluster-free film (Ag/Ti=0.07) took profit of its intrinsic passive-ability to form a protective lubricant-like layer in those conditions.

Finally, from a pragmatic viewpoint and considering the bio-sensor targeted application, it is worth mentioning that Ag cluster are required for increasing the electric conductivity. In this sense, we can recommend the use of the moderately enriched-Ag film (Ag/Ti= 0.48), combining good electric properties with an enhanced tribological behaviour.

References (Chapter 6)

[1] Arya, S. K., Saha, S., Ramirez-Vick, J. E., Gupta, V., Bhansali, S., & Singh, S. P. (2012). Recent advances in zno nanostructures and thin films for biosensor applications: Review. *Analytica Chimica Acta*, *737*, 1–21. https://doi.org/10.1016/j.aca.2012.05.048

[2] Friedrich, K. (2018). Polymer composites for Tribological Applications. *Advanced Industrial and Engineering Polymer Research*, *1*(1), 3–39. https://doi.org/10.1016/j.aiepr.2018.05.001

[3] Teles, F. R. R., & Fonseca, L. P. (2008). Applications of polymers for biomolecule immobilization in electrochemical biosensors. *Materials Science and Engineering: C*, *28*(8), 1530–1543. https://doi.org/10.1016/j.msec.2008.04.010

[4] Myshkin, N., & Kovalev, A. (2018). Adhesion and surface forces in polymer tribology—a review. *Friction*, *6*(2), 143–155. https://doi.org/10.1007/s40544-018-0203-0

[5] Hesketh, P. J., Zivanovic, S., Pak, S., Ilic, B., & Clair, L. S. T. et al. (1998). Biosensors and Microfluidic Systems. In B. Bhushan (Ed.), *Tribology Issues and Opportunities In Mems* (Pp. 85–94). Essay, Kluwer Academic Publishers.

[6] Miao, X., Li, Z., Liu, S., Wang, J., & Yang, S. (2022). MXenes in tribology: Current status and Perspectives. *Advanced Powder Materials*, 100092. https://doi.org/10.1016/j.apmate.2022.100092

[7] Pu, X., An, S., Tang, Q., Guo, H., & Hu, C. (2021). Wearable triboelectric sensors for Biomedical Monitoring and human-machine interface. *IScience*, *24*(1), 102027. https://doi.org/10.1016/j.isci.2020.102027

[8] Scholes, S. C., Unsworth, A., & Jones, E. (2006). Polyurethane unicondylar knee prostheses: Simulator wear tests and lubrication studies. *Physics in Medicine and Biology*, *52*(1), 197–212. https://doi.org/10.1088/0031-9155/52/1/013

[9] Gardner, J. W., & Bartlett, P. N. (1996). Application of conducting polymer technology in Microsystems. *Small Scale Structures*, 57–66. https://doi.org/10.1016/b978-0-444-82312-0.50022-0

[10] Lackner, J. M., Waldhauser, W., Major, L., Teichert, C., & Hartmann, P. (2013). Tribology of bio-inspired nanowrinkled films on Ultrasoft substrates. *Computational and Structural Biotechnology Journal*, *6*(7). https://doi.org/10.5936/csbj.201303002

[11] Soto, R. J., Schofield, J. B., Walter, S. E., Malone-Povolny, M. J., & Schoenfisch, M. H. (2016). Design considerations for silica-particle-doped nitric-oxide-releasing polyurethane glucose biosensor membranes. *ACS Sensors*, *2*(1), 140–150. https://doi.org/10.1021/acssensors.6b00623

[12] Ahmadi, Y., & Kim, K.-H. (2020). Functionalization and customization of Polyurethanes for Biosensing Applications: A state-of-the-art review. *TrAC Trends in Analytical Chemistry*, *126*, 115881. https://doi.org/10.1016/j.trac.2020.115881

[13] Wang, N., Burugapalli, K., Song, W., Halls, J., Moussy, F., Ray, A., & Zheng, Y. (2013). Electrospun fibro-porous polyurethane coatings for implantable glucose biosensors. *Biomaterials*, *34*(4), 888–901. https://doi.org/10.1016/j.biomaterials.2012.10.049

[14] Wan, H., Lin, C., Kaper, H. J., & Sharma, P. K. (2020). A polyethylene glycol functionalized hyaluronic acid coating for cardiovascular catheter lubrication. *Materials & Design*, *196*, 109080. https://doi.org/10.1016/j.matdes.2020.109080

[15] Chou, J.-C., Wu, C.-Y., Lin, S.-H., Kuo, P.-Y., Lai, C.-H., Nien, Y.-H., Wu, Y.-X., & Lai, T.-Y. (2019). The analysis of the urea biosensors using different sensing matrices via wireless measurement system & Microfluidic Measurement System. *Sensors*, *19*(13), 3004. https://doi.org/10.3390/s19133004

[16] Etiemble, A., Lopes, C., Nkou Bouala, G. I., Borges, J., Malchère, A., Langlois, C., Vaz, F., & Steyer, P. (2019). Fracture resistance of ti-ag thin films deposited on polymeric substrates for biosignal acquisition applications. *Surface and Coatings Technology*, *358*, 646–653. https://doi.org/10.1016/j.surfcoat.2018.11.078

[17] Lu, M., Choi, S. S., & Cunningham, B. T. (2008). Plastic distributed feedback laser biosensor. *LEOS 2008 - 21st Annual Meeting of the IEEE Lasers and Electro-Optics Society*. https://doi.org/10.1109/leos.2008.4688542

[18] Negm, A., Howlader, M. M., Belyakov, I., Bakr, M., Ali, S., Irannejad, M., & Yavuz, M. (2022). Materials Perspectives of Integrated Plasmonic Biosensors. *Materials*, *15*(20), 7289. https://doi.org/10.3390/ma15207289

[19] Qiu, G., Thakur, A., Xu, C., Ng, S. P., Lee, Y., & Wu, C. M. L. (2018). Detection of glioma-derived exosomes with the biotinylated antibody-functionalized titanium nitride plasmonic biosensor. *Advanced Functional Materials*, *29*(9), 1806761. https://doi.org/10.1002/adfm.201806761

[20] Madsen, N. D., Christensen, B. H., Louring, S., Berthelsen, A. N., Almtoft, K. P., Nielsen, L. P., & Bøttiger, J. (2012). Controlling the deposition rate during target erosion in reactive pulsed DC magnetron sputter deposition of alumina. *Surface and Coatings Technology*, *206*(23), 4850–4854. https://doi.org/10.1016/j.surfcoat.2012.05.070

[21] Schoff, M. E. (2009). *Sputter target erosion and its effects on long duration Dc magnetron sputter coating* (thesis). University of California, San Diego, La Jolla.

[22] Şevik, H. (2014). The effect of silver on wear behaviour of zinc–aluminium-based ZA-12 alloy produced by gravity casting. *Materials Characterization*, *89*, 81–87. https://doi.org/10.1016/j.matchar.2013.12.015

[23] Wang, Q., Tu, J., Zhang, S., Lai, D., Peng, S., & Gu, B. (2006). Effect of AG content on microstructure and tribological performance of WS2–Ag Composite Films. *Surface and Coatings Technology*, *201*(3-4), 1666–1670. https://doi.org/10.1016/j.surfcoat.2006.02.039

[24] Wakamoto, K., Mochizuki, Y., Otsuka, T., Nakahara, K., & Namazu, T. (2020). Temperature dependence on tensile mechanical properties of sintered silver film. *Materials*, *13*(18), 4061. https://doi.org/10.3390/ma13184061

[25] Logan, R. W., Castro, R. G., & Mukherjee, A. K. (1983). Mechanical properties of silver at low temperatures. *Scripta Metallurgica*, *17*(1), 63–66. https://doi.org/10.1016/0036-9748(83)90071-6

[26] Tobushi, H., Hayashi, S., & Kojima, S. (1992). Mechanical properties of shape memory polymer of polyurethane series: Basic characteristics of stress-strain-temperature relationship. *JSME International Journal. Ser. 1, Solid Mechanics, Strength of Materials*, *35*(3), 296–302. https://doi.org/10.1299/jsmea1988.35.3_296

[27] Huh, D. S., & Cooper, S. L. (1971). Dynamic mechanical properties of polyurethane block polymers. *Polymer Engineering and Science*, *11*(5), 369–376. https://doi.org/10.1002/pen.760110504

[28] Turner, S. *(chair)* et al. (2010). (rep.). *ASHRAE STANDARD Thermal Environmental Conditions for Human Occupancy 55-2010*. Atlanta.

[29] Zhang, M., Wang, X., Fu, X., & Liu, W. (2009). Investigation of electrical contact resistance of ag nanoparticles as additives added to peg 300. *Tribology Transactions*, *52*(2), 157–164. https://doi.org/10.1080/10402000802167695

[30] Arslan, E., Totik, Y., Demirci, E., & Alsaran, A. (2009). Influence of surface roughness on corrosion and tribological behavior of CP-ti after thermal oxidation treatment. *Journal of Materials Engineering and Performance*, *19*(3), 428–433. https://doi.org/10.1007/s11665-009-9504-9

[31] Xu, Y., Qi, J., Nutter, J., Sharp, J., Bai, M., Ma, L., & Rainforth, W. M. (2021). Correlation between the formation of tribofilm and repassivation in biomedical titanium alloys during tribocorrosion. *Tribology International*, *163*, 107147. https://doi.org/10.1016/j.triboint.2021.107147

[32] Goto, H., & Buckley, D. H. (1985). The influence of water vapour in air on the friction behaviour of pure metals during fretting. *Tribology International*, *18*(4), 237–245. https://doi.org/10.1016/0301-679x(85)90069-6

7. CONCLUSIONS AND PERSPECTIVES

The verification of the developed system and the procedure was indicated. The final comments and discussions were explained according to the obtained results after the tribological tests. The future plans for the project and the upcoming tests were stated.

7. CONCLUSIONS AND PERSPECTIVES

In this research, it was aimed to better understand the tribological behaviour of titanium based PVD films in small scale *in situ* conditions. In this framework, the effect of the contact environment was investigated in terms of tribological susceptibility of thin films with a laboratory-made ball-on-disk micro-tribometer which is implementable into eSEM chamber. The testing protocol as well as the analysing strategy was determined with preliminary tests performed with conventional TiN hard film prepared with CAE PVD technique against steel ball during run-in period for 100 cycles. The modifications on the wear track were analysed after each sliding and, there was no significant change observed. Thus, to perform the test *in situ* conditions, the system was unloaded after every 10 cycles and the wear track on the film was evaluated in three specific regions of interest (starting point of the contact, constant sliding speed zone and turning point of sliding direction). With this set-up, it is possible to measure and quantify the recorded information (normal force, tangential force friction coefficient…) for any region of the wear track at any cycle. Also, the effect of various environmental conditions can be tested on the wear behaviour of thin films in the eSEM chamber (high vacuum, low vacuum, humid conditions, nitrogen atmosphere, synthesized air…)

Tests were performed both in high vacuum and humid conditions to test the operability of the micro-tribometer in different environments and to examine the effect of contact environment on tribological behaviour of TiN film. From this study it was proven that, the novel developed system is qualified for *in situ* small scale tribological tests under various environmental conditions. Also 50% RH has a positive effect on tribological response of TiN films. As a consequence, in humid conditions, an oxide layer formed on freshly worn film surface in addition to the oxidised particle formation which behaved as solid lubricant by reducing the friction coefficient.

Ti-Ag films were previously selected for biosensor applications since titanium is bio-adaptable and silver is anti-bacterial. The mechanical and electrical behaviour of these films were investigated, and it was shown that increasing Ag content provides a higher fracture resistance and longer signal acquisition for Ti-Ag films which makes them suitable for bio-sensors. However, their tribological character was not studied although this parameter may have a significant role by considering their exposing to relative motion at joints or against skin or

clothes. Therefore, in this study, 1 µm thick Ti-Ag films were deposited with varying Ag content by magnetron sputtering PVD technique in Universidade do Minho. First, to ensure the effect of Ag content on the film properties, various tests were performed and their microstructural, chemical, mechanical and electrical properties were investigated. While the columnar microstructure of titanium film densifies by filling of its grains with Ag, further increase in Ag content might enhancing Ag-based nanocluster in the film matrix. Furthermore, both electrical and mechanical properties of these films were slightly enhanced with increasing Ag content. Lastly, the first tribological tests were applied with steel ball in ambient air and high vacuum conditions and it was seen that the films were almost totally removed with poor adhesion even after 3 cycles except the film with Ag/Ti=3.14. On the other hand, this Ag richest composition performed higher wear resistance without any film removal or debris formation and with the lowest friction coefficient in both of the environmental conditions. This study verified that Ag addition enhances the mechanical and electrical behaviour of titanium films. Also grain refinement, reduced film roughness and solid lubricant effect of Ag-based nanocluster with increasing Ag content, provides enhanced tribological character to these thin films.

As the next step, a new (2^{nd}) series of films were prepared with an interlayer which has the same composition as film itself to improve their adhesion. Before the tribological tests, the characteristics of these films were also identified and then their tribological behaviour were tested by considering the effect of environment and Ag content. To better mimic the bio-contact conditions poly-urethane ball was used as the counter-face.

Firstly, since both Ti and Ag tend to oxidise, the effect of humidity on the tribological response of these films was investigated. Here, the film with Ag/Ti=0.72 was examined in ambient air, and 50% RH. Ag based clusters performed negative effect for the wear character of the film based on the effect of temperature change of the mechanical properties of silver. Also, the effect of temperature was considered for the friction resistance of the counter-face since PU ball would be more rigid at 4°C than at room temperature based on the literature. The modifications on the mechanical properties of both Ag and PU ball caused catching of the Ag-based debris by PU ball and increase the friction coefficient in 4°C (at 50%RH).

Lastly, three Ti-Ag film compositions were investigated in terms of their tribological behaviour: Ag/Ti=0.07, =0.48, =0.72. It was verified that at lower humidity levels (ambient air condition with 25% RH) increasing Ag content significantly reduces the friction coefficient and the debris

formation. Here, while it is well known that increasing Ag content in ambient air enhances the tribological behaviour of films; Ag based clusters performed different sliding character by interacting with water vapour in controlled environment in eSEM chamber. The mean COF values increased with increasing Ag content regarding the formation of more Ag-based debris as a thin layer in contact region based on the existence of more Ag-based nanoclusters. On the other hand, the cluster free film took the profit of forming the titanium based passive oxide layer with the existence of humidity as a solid lubricant over the film surface and achieving the lower mean COF.

In this research work, there are numerous perspectives which can prolongate this PhD. Mainly, they could be gathered into two categories: the first ones are already planned while in progress, and the second ones could be considered for the future experiments. As the first on-going perspective, it was aimed to define a code, which could perform the image analysis of the wear track. Here, since the tribometer was implemented inside the eSEM chamber, a small-scale dynamic analysis can be performed to investigate the formation of the particles and the evolution of the track texture (surface, morphology, materials flow) during the running-in period under different environmental conditions (vacuum, gas nature, gas pressure, relative humidity). The particle distribution and the morphology of the wear track aimed to analyse. This part of the work is still going on and the analysis are being performed with steel-steel contact (Figure 7.1) in collaboration with Alizée Bouchot (LaMCoS-LGF PhD student, EUR Manutech Sleight). Different descriptors have been established during A. Bouchot's thesis which is still ongoing [1]. In this joint work the effect of detectors used (*i.e.* the contrast obtained) for a specific environment have to be studied on the results. The objective is to correlate relevant quantitative indicators, characteristic to the rheological behaviour of solid interfaces formed *in situ* and to tribological properties.

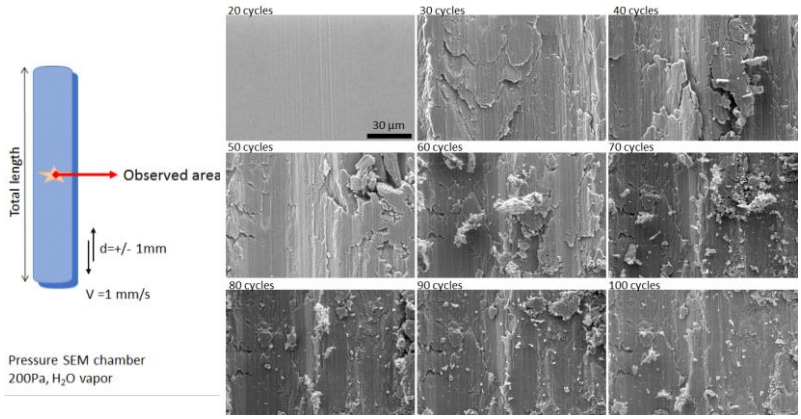

Figure 7.1: Steel-steel contact, contact pressure of 800 MPa (normal force 4N)-Morphology evolution in the centre of the track

In addition to the thin films or bare steel surfaces, many different types of surfaces could be analysed with this novel system by implementing the laboratory-made micro-tribometer inside the eSEM chamber. Thereby, as the second continuing perspective, it is targeted to mimic the friction of snake skin against sand with this current set-up to better understand the deformation on the skin surface based on sliding direction and contact conditions.

Material architecture and surface structure of the skin influence the details of material failure. The abrasion pattern and material failure strongly differ between the species tested (Figure 7.2) correlating with the native wear observed. The biologists do not know much about the exact snake skin performance in vivo [2, 3].

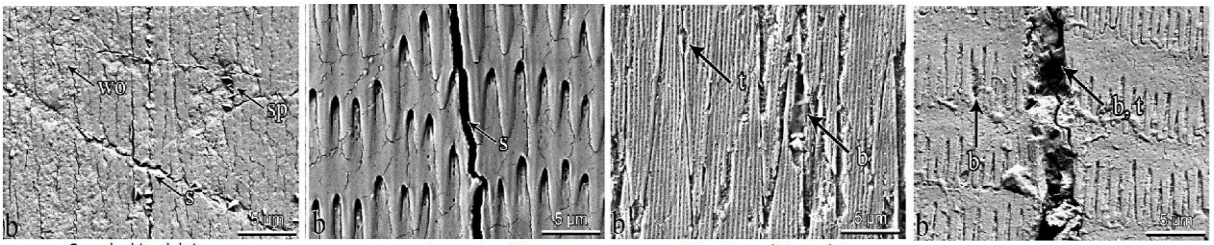

Figure 7.2: SEM images of the wear appearance of the ventral scales exuvium from different snakes [4]

The tests are aimed to be carried out under various environmental conditions in directions of the skin flakes and/or the orientation of the sliding in x-y direction. This work is in progress by

collaborating with Prof. Stanislav GORB from Kiel university-Germany (team "Functional Morphology and Biomechanics").

As another future work a real-time tribo-chemical analysis can be performed by coupling the micro-tribometer with Raman spectrometer. Here, to provide the fully transmission of the laser beam from spectrometer to sample surface, it is necessary to use a transparent counter-part such as glass. During this study, it was aimed to perform this kind of analysis but unfortunately, a totally transparent glass ball could not be supplied from the conventional bearing companies; however, it could be specifically designed for an order. Then, a perfectly *in situ* investigation can be achieved at every point along the wear track during the contact and sliding.

Additionally, when the films were deposited on polymeric substrate, based on the low melting temperature of PET, the film had a textured surface after cooling down of the sample and shrinkage of the substrate. Nevertheless, the films could be deposited on a more thermally resistant substrate or the targeted film thickness could be reduced by decreasing the deposition time, so the PVD chamber would heat up less. These parameters, could help to provide better adhesion and uniformity of Ti-Ag films on polymeric substrate. Then, by using a polymer counter-face as well, a bio-mechanical system could be simulated in a better condition for the future tests. In this way, more precise tribological analysis could be achieved with the proper contact conditions.

Also, further tests could be performed by modifying the recording parameters, such as sampling rate, segment duration and elements per segment from the software of the system. These changes could provide to do interpretation in a more precise or easier way. Here, it is important to deeply understand these parameters and their relation with each other to find the optimum recording conditions.

To conclude, since the system is quite new, many forecasts are possible for the feature works. The image analysis and the experiments with various materials such as snake skin as the flat are already aimed. Also, real-time investigation of the wear track, setting the software parameters for better interpretation of the results and changes on mechanical components of the device more developed *in situ* small scale examinations can be performed.

References (Chapter 7)

[1] A. Bouchot, A. Ferrieux-Paquet, G. Mollon, S. Descartes, J. Debayle, Segmentation and morphological analysis of wear track/particles images using machine learning, Journal of Electronic Imaging 31 (5), (2022) 051605. (doi : 10.1117/1.JEI.31.5.051605)

[2] S N. Gorb, E. V. Gorb, Snake Skin Tribology, Material, Surface Structure, Frictional Properties, and Biomimetic Implications, chapter 7 in book "Progress in Lubrication and Nano- and Biotribology", 2021, DOI: 10.1201/9781003096443-7

[3] M.-C.G. Klein, S.N. Gorb, Scratch resistance of the ventral skin surface in four snake species (Squamata, Serpentes), Zoology 119 (2016) 81–96

[4] M.-C.G. Klein, S.N. Gorb, Ultrastructure and wear patterns of the ventral epidermis of foursnake species (Squamata, Serpentes), Zoology 117 (2014) 295–314

APPENDIX

Calibration of 3-Axes Sensor of Micro-Tribometer

The calibration process was carried out with universal calibration weighs starting from 10 g to 1000 g. When the weighs were started to place (or hang), the data was recorded to evaluate the precision of the applied load with gradually increasing load. During this process, the applied load was also fellow from the interface of the TRIBOMEB software as it was shown in the red circle below (Figure 1).

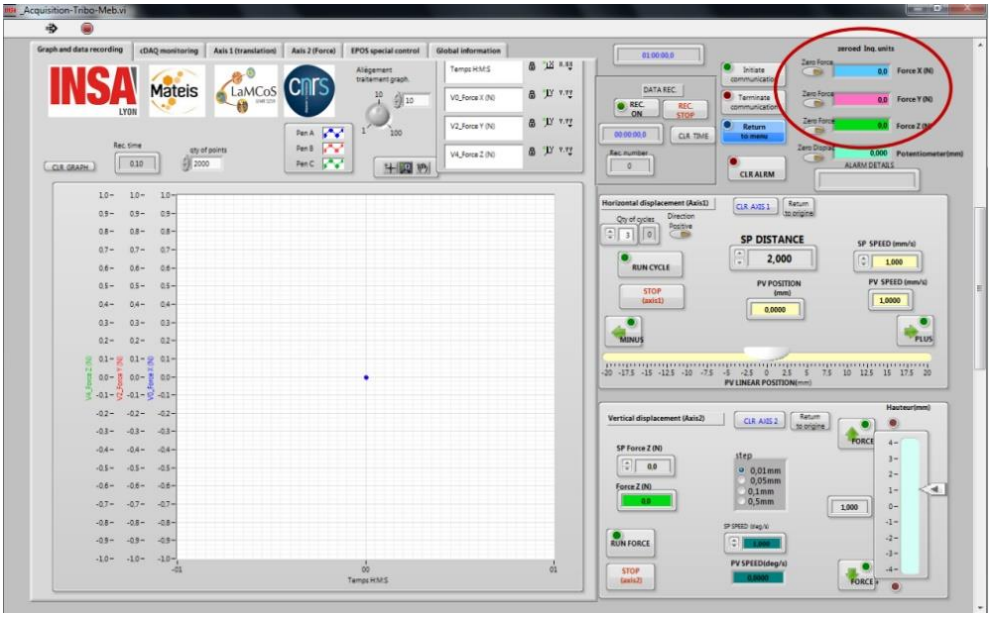

Figure 1: Controlling the applied load during calibration

Since the loads applied separately in three different direction, finally three files of recorded data were evaluated for i) normal force (z-direction), ii) tangential force (x-direction), iii) lateral force (y-direction). After that, the slopes of the time versus force graphics were calculated and they were indicated in TRIBOMEB software as a particular model (orange rectangles in figure 2) to be used for the following tribo-tests.

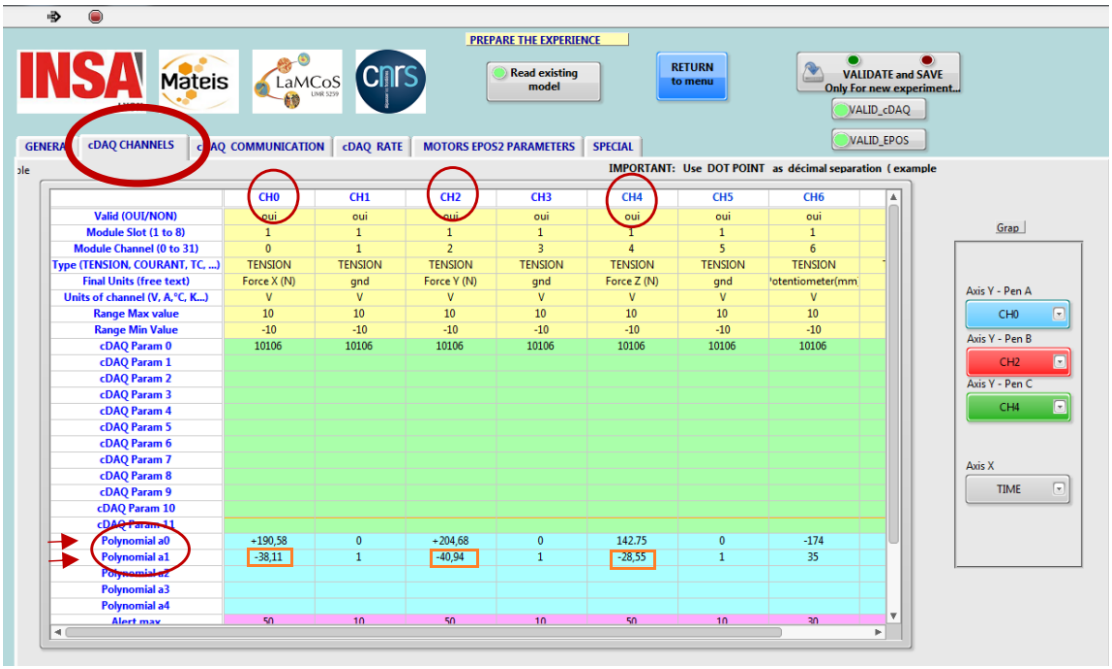

Figure 2: Model definition after calibration

Optimising Data Recording Process of Micro-tribometer

In the TRIBOMEB software, number of recorded data as in segments, recording frequency and recording time could be modified. This characteristic can provide to optimise the recording process both to achieve reliable results and to reduce the noise in the recorded data. There are certain number of elements can be determined as in one segment. The duration of one segment can be also changed which can be correlated with the recording time. As well as the settings based on segments, frequency of the sampling rate per second can be modified. Regarding these aspects the overall file of the recorded data during the sliding process could be improved. Tests were performed with steel-steel contact and the 8 N of normal load was applied along 3 cycles for 2 mm of displacement. Several changes were done on the recording parameters and the data was analysed in terms of displacement with respect to real time. Firstly, segment duration was considered as 0.1 s for 10 elements per segment. Then the recording time set as 0.1and 0.2 to examine its effect. Here the sliding speed was kept constant as 1 mm/s for both of the test. When the test performed with 0.2 seconds of recording time, it was seen that the number of recorded segments decreased to half (Figure 3)

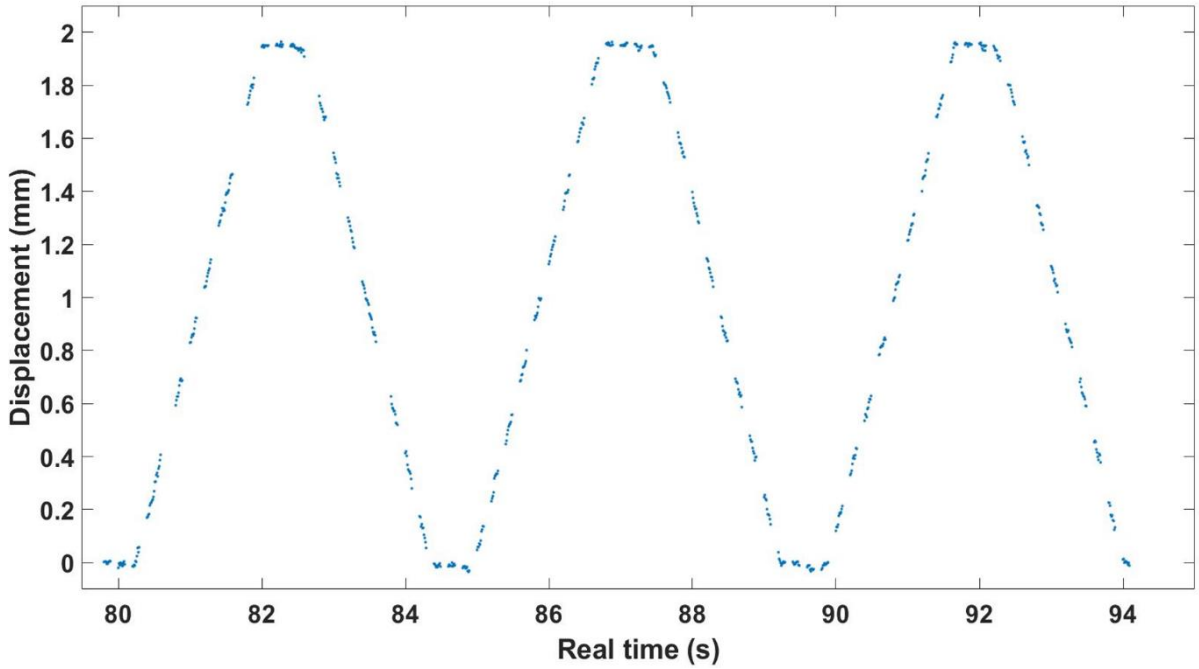

Figure 3: Tribo-test performed with 0.1s segment duration, 10 elements and 0.2s recording time.

Then, the recording time was set as 0.1 which is equal to segment duration. In this case it was seen that all the segments were recorded (Figure 4).

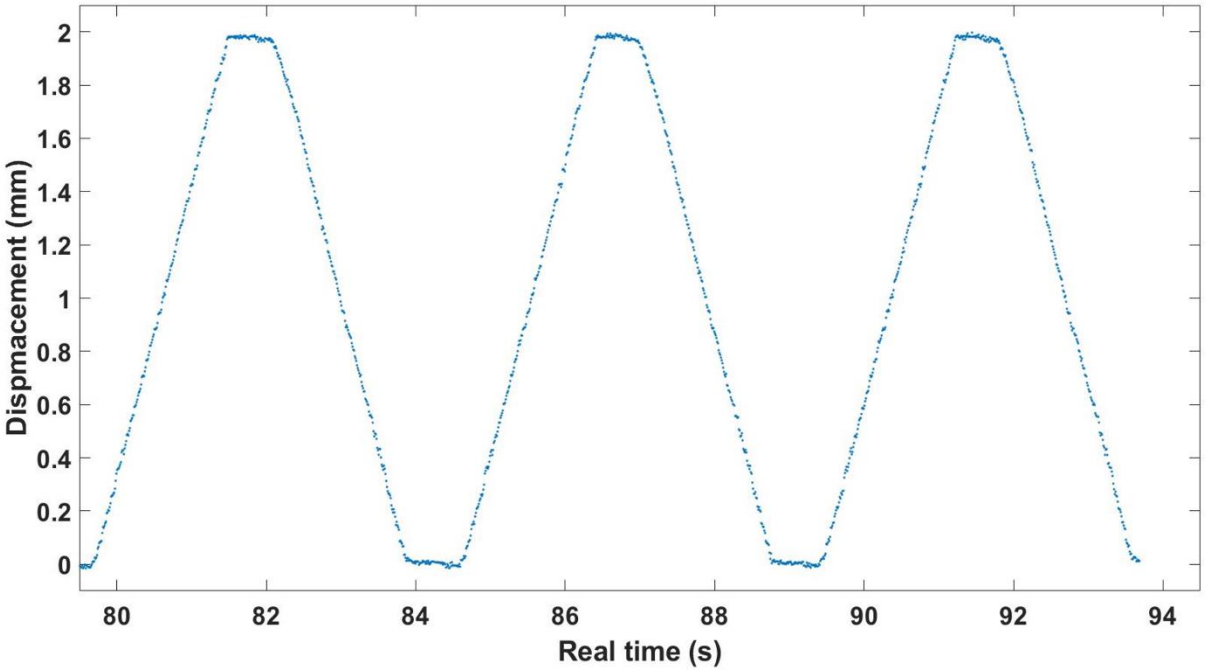

Figure 4: Tribo-test performed with 0.1s segment duration, 10 elements and 0.1s recording time.

However, even though the segments were equally distributed along displacement, the recorded number of data was still not enough for the precise calculations of the friction coefficient since there was significant gaps between each point along the sliding. Therefore, number of elements were increased from 10 to 50. Finally, the recorded data points achieved a more continuous distribution (Figure 5) and these recording parameters were used for the entire tests. It was not tried for the higher number of elements to be recorded to avoid from obtaining noisy results.

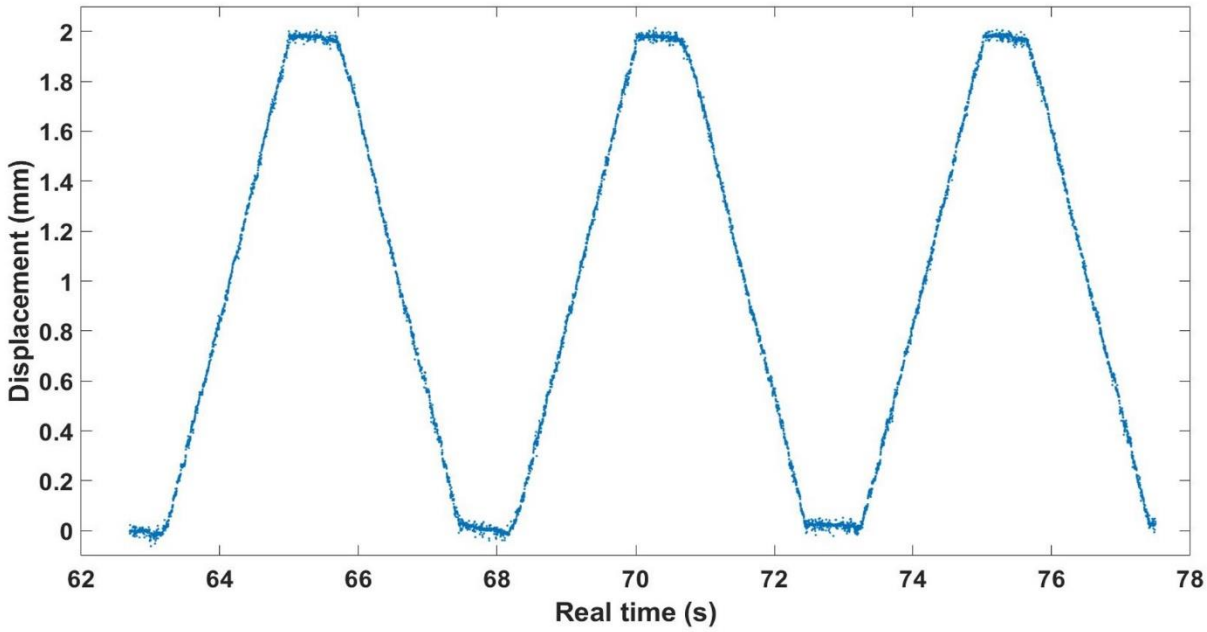

Figure 5: Tribo-test performed with 0.1 segment duration, 50 elements and 0.1 recording time.

Effect of Testing Procedure

The testing procedure has a great importance on tribological susceptibility of Ti-Ag films. Here it was aimed to investigate its role at 100% relative humidity because several different procedures can be fellow to examine the wear tracks in this humidity level.

Ag richest composition was selected particularly because (Ag/Ti=0.72) at 100% relative humidity, it was noticed that there is a large deformation on the film surface with the highest mean friction coefficient by comparison to other compositions. This characteristic was not expected since the corresponding film composition has Ag-clusters and these clusters have a good sliding behaviour as it was confirmed with the tests performed against steel ball. In addition to the solid lubrication effect of these Ag-based clusters, it was also expected to have a titanium-oxide film formed on the freshly formed wear track which helps to reduce the friction

coefficient as it was seen in chapter 4. To lighten this issue, as it was stated before, Wang et *al.* expressed that Ag is very sensitive to environment and this sensitivity causes an increase on friction coefficient for higher humidity levels. However, this behaviour of Ag richest film composition was aimed to investigate more in detail since the modification is quite remarkable.

Unfortunately, decreasing the chamber pressure is the only way to perform the *in situ* analysis on the wear track in 100% RH. Because with increasing humidity, based on the higher chamber pressure, some water droplets condensate on the wear track surface which cover the wear track and made impossible to analyse it *in situ* conditions. Additionally, as it was seen for the tribological analysis of TiN films previously that, loading and unloading of the system may have a role on the tribological responses of the materials Therefore, three testing procedures were considered (Table 1).

The first test was almost the same than the one described in chapter 4, section 4.2.1, but the observation step is different. The pressure was first increased to 813 Pa while the temperature was 4°C to reach 100% relative humidity. This step provided the condensation of water droplets on the film surface (Figure 6). After that, the sliding for 10 cycles were performed.

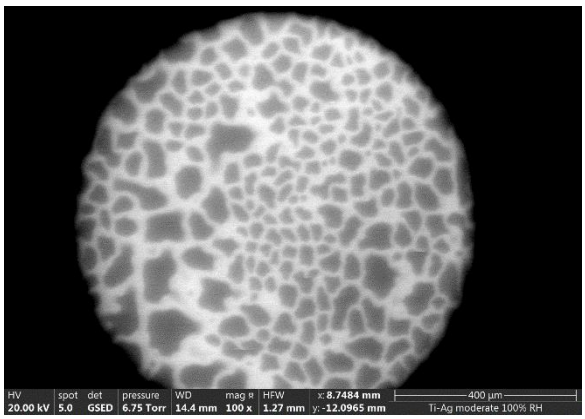

Figure 6: Water droplets on Ti-Ag (Ag/Ti=0.48) film surface at 100% RH

When the sliding process was finished and the system was totally unloaded, the water vapour pressure decreased to 400Pa so the humidity level decreased to 50%. The purpose here was to evaporate the water to be able to examine the wear track in microscope, and to perform *in situ* analysis. Basically, it could be stated that the sliding was performed at 100% RH, whereas the observation was performed at 50% RH. Yet, the change on the water vapour pressure may cause variation on the oxidation process of both Ti and Ag.

Therefore, a second procedure was performed by following exactly the same procedure (by interrupting the contact after every 10 cycles) but without changing the water pressure. No *in situ* observations were done for this test. And the third procedure was done as a single run without any opening of the contact, at 100% RH.

Table 1: Parameters to investigate the effect of testing procedure for the film with Ag/Ti=0.72 in 100% RH

# test	Chamber pressure	Contact condition	*In situ* imaging
1	813 Pa during sliding, 400 Pa during imaging	Interrupted in 10 cycles	Yes
2	813 Pa (constant)	Interrupted in 10 cycles	No
3	813 Pa (constant)	No interruption	No

It was examined that for three different procedures, the tribological responses of the film are strictly different. Since only *ex situ* analysis was performed for the last two tests, the wear tracks were analysed after 100 cycles. However, the mean COF was calculated for each cycle for the tests performed in these three different conditions (Figure 7).

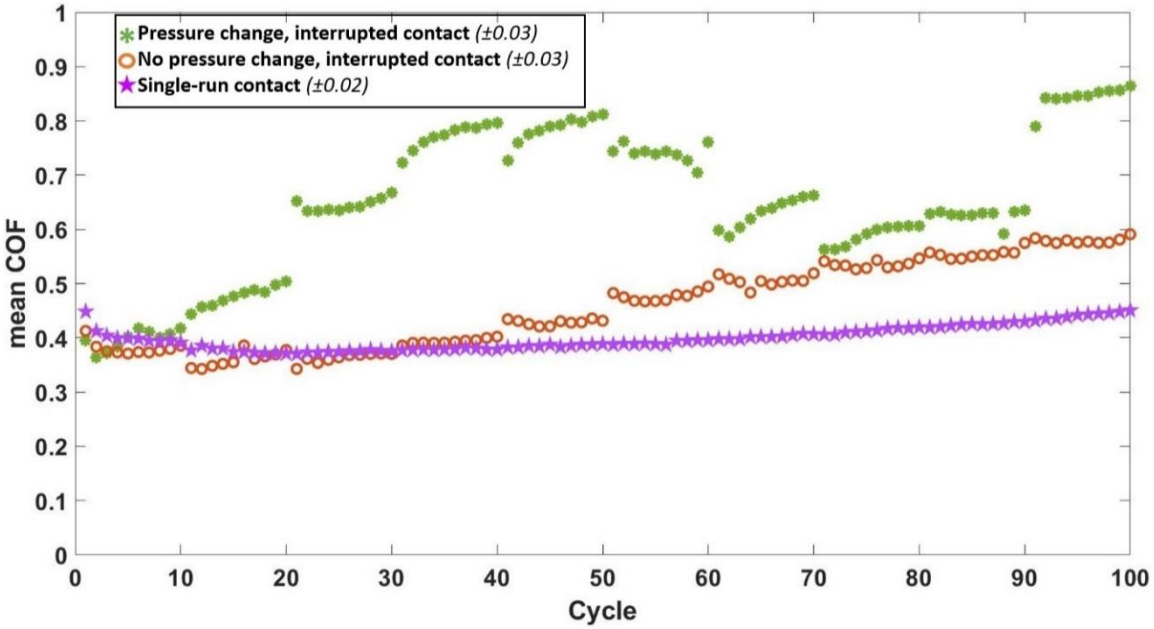

Figure 7: Mean COF values per cycle for the with Ag/Ti=0.72 at 100% RH based on different testing procedures

First of all, the effect of the pressure change in the chamber was clearly seen with a higher mean COF and instable trend of the curve during the test #1 with increasing cycle number. Even though it was aimed to decrease the pressure gradually and precisely for a more uniform evaporation of water droplets over the surface of the wear track, the pressure change time was not perfectly the same after every set of sliding with 10 cycles. Thereby, variations were quite possible on the rate of the oxidation reaction of the particles and worn film surface.

On the other hand, the mean COF (over the 100 cycles) was 0.46 (±0.03) for the test performed without changing the pressure (test #2) and it was quite lower than the previous pressure-changed test (test #1) which was 0.65 (±0.03).

Additionally, the effect of loading & unloading of the system was less clear but still exist for the test performed under the constant pressure at 100% RH (test #2).

Finally, for the test performed in single run (test #3), without loading & unloading, it was seen that the mean COF was even lower (0.40 (±0.02)) but still quite close to test #2 and it is following a more stable trend with increasing number of cycles. Thus, it could be stated that the test procedure has a significant effect on the quantitative tribological analysis.

When the strong variation on the friction coefficient values were seen based on test procedure, the friction maps were plotted and both the difference on friction coefficient along the length of the wear track and effect of loading & unloading the system were identified clearly (Figure 8).

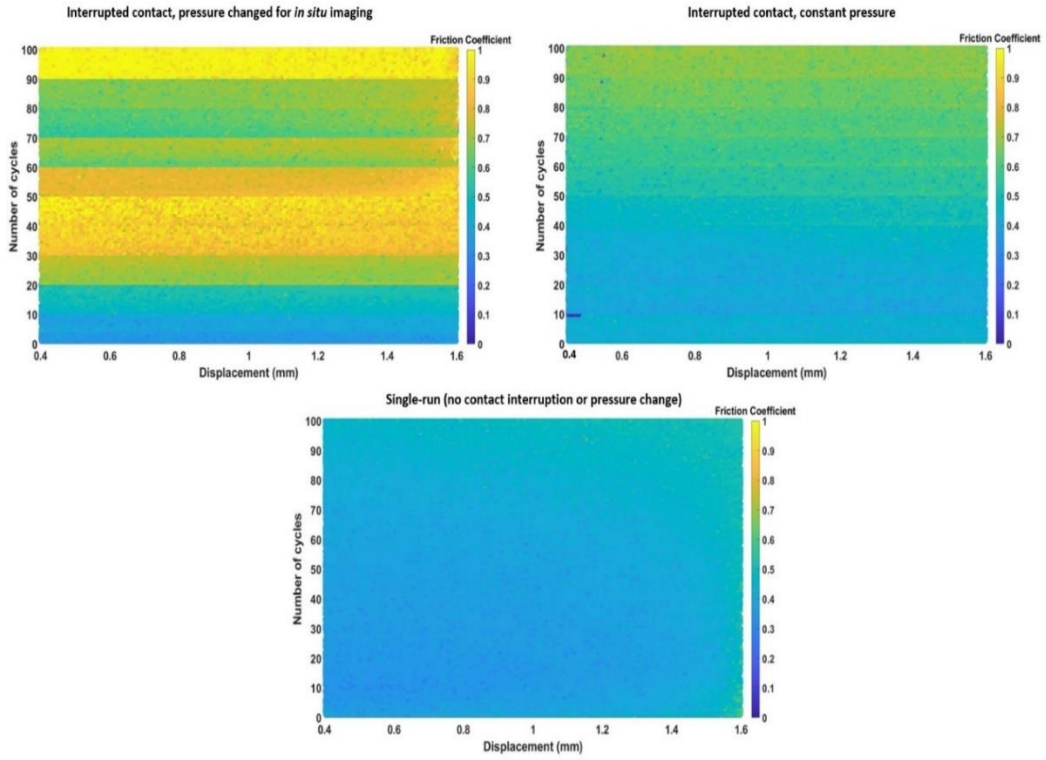

Figure 8: Friction maps for Ti-Ag film (Ag/Ti=0.072) in 100% RH for 3 different testing procedures

In addition to the higher friction coefficient values for *in situ* test (based on pressure change), the friction coefficient is quite constant for each set with 10 cycles along the displacement. On the other hand, for the test #2 (by interrupting the contact) at constant pressure, more uniform friction coefficient was achieved. The strong change on COF values for each 10 cycles were observed in both testing conditions as bold lines with colour change. The colour change was more outstanding for the test performed by decreasing the pressure; whereas, this was not the case for single run test performed in 100% RH.

Furthermore, when the wear tracks were analysed for these three testing conditions, and more debris and film deformation was seen for the test performed by interrupting the contact and by changing the pressure for *in situ* imaging. However, relatively less debris was formed at the centre of the wear track for the test performed in a constant pressure even though the contact was interrupted. Finally, the wear track has a smoother appearance for single run test as it was seen in the figure 9 which confirms the lowest friction coefficient for this specific testing condition.

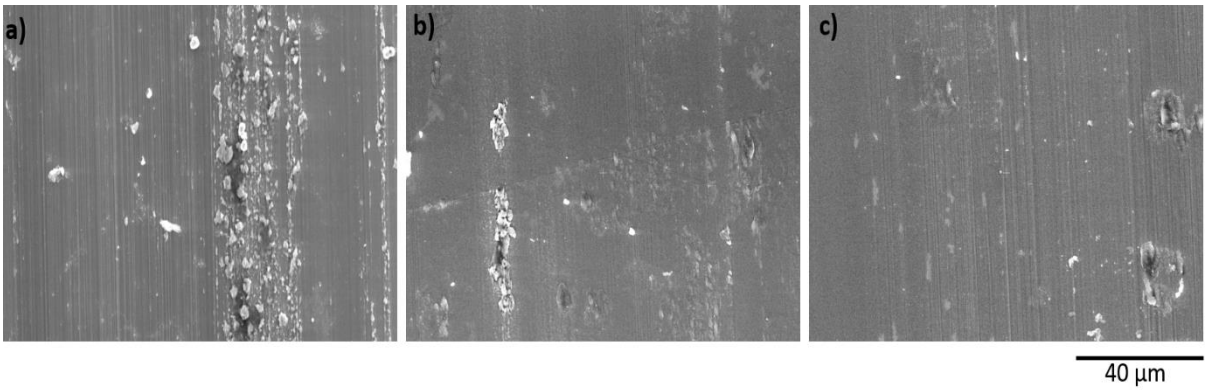

Figure 9: Centre of the wear tracks for the tests performed with the Ti-Ag film (Ag/Ti=0.72) at 100% RH a) by interrupting the contact and changing the pressure, b) by interrupting the contact at contact pressure, c) as single-run.

When the 3D profiles were analysed it was seen that the deformation mechanism under three different conditions was different. While the film deformed along the width of the wear track for the test performed *in situ* conditions with a pressure change, the wear track profile was relatively smoother for the test performed in constant pressure (test #2). However, in single run test, the deep deformation was detected only on the centre of the width of the wear track (Figure 10).

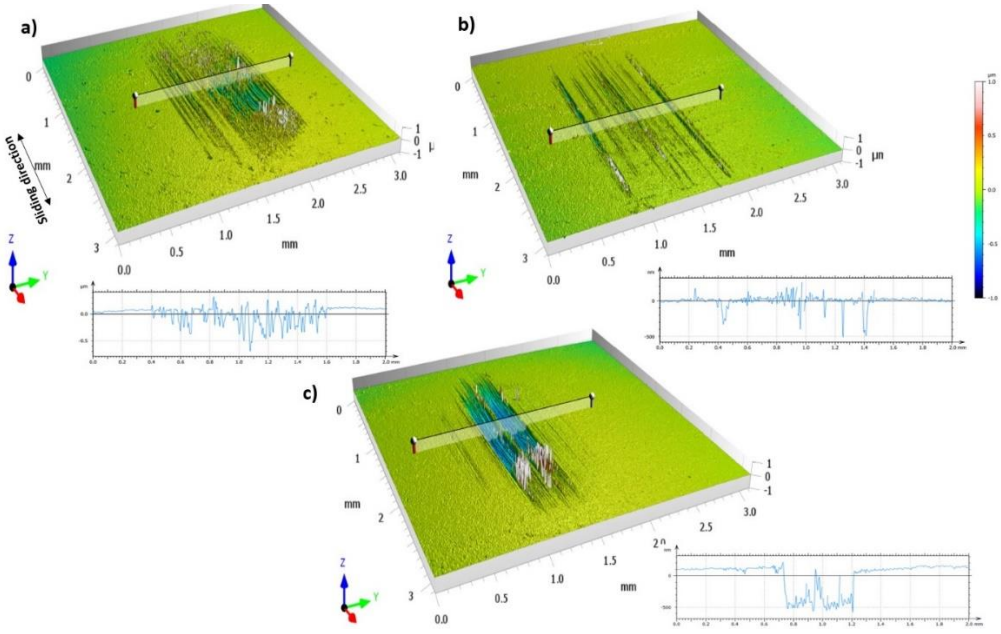

Figure 10: Wear track profiles of the tests performed with the Ti-Ag film (Ag/Ti=0.72) at 100% RH a) by interrupting the contact and changing the pressure, b) by interrupting the contact at contact pressure, c) as single-run.

When the EDS analysis were performed on the wear tracks formed with these three procedures, it was seen that there is more oxidation on the wear track for the test performed by interrupting the contact and changing the pressure (test #1). Additionally, on the dark regions where the particles were observed on the SE image, no silver was detected. Since the substrate material was not reached, these zones could be considered as either transferred ball material or oxide of titanium. Similar behaviour was examined also for the other two testing conditions; however, it was noticed that there is less oxygen detected for the film without pressure change (test #2) than the other one. Also, the less oxidized regions were obtained on the wear track formed in single-run tests (Figure 11). This difference on the oxide quantity could be correlated with the testing durations. In the first test, even the relative humidity of the chamber was modified, the sample was always exposed to a certain level of water vapour and it was the longest test by comparison to the other two procedures. For the second test performed by interrupting the contact at constant relative humidity, there is lower oxygen because this wear track exposed to water vapour for a shorter duration than the previous one. However, the contact was unloaded and the ball moved out from the contact point after every 10 cycles. Thus, this test was longer than the single run test which is the procedure that the lowest oxide amount was detected.

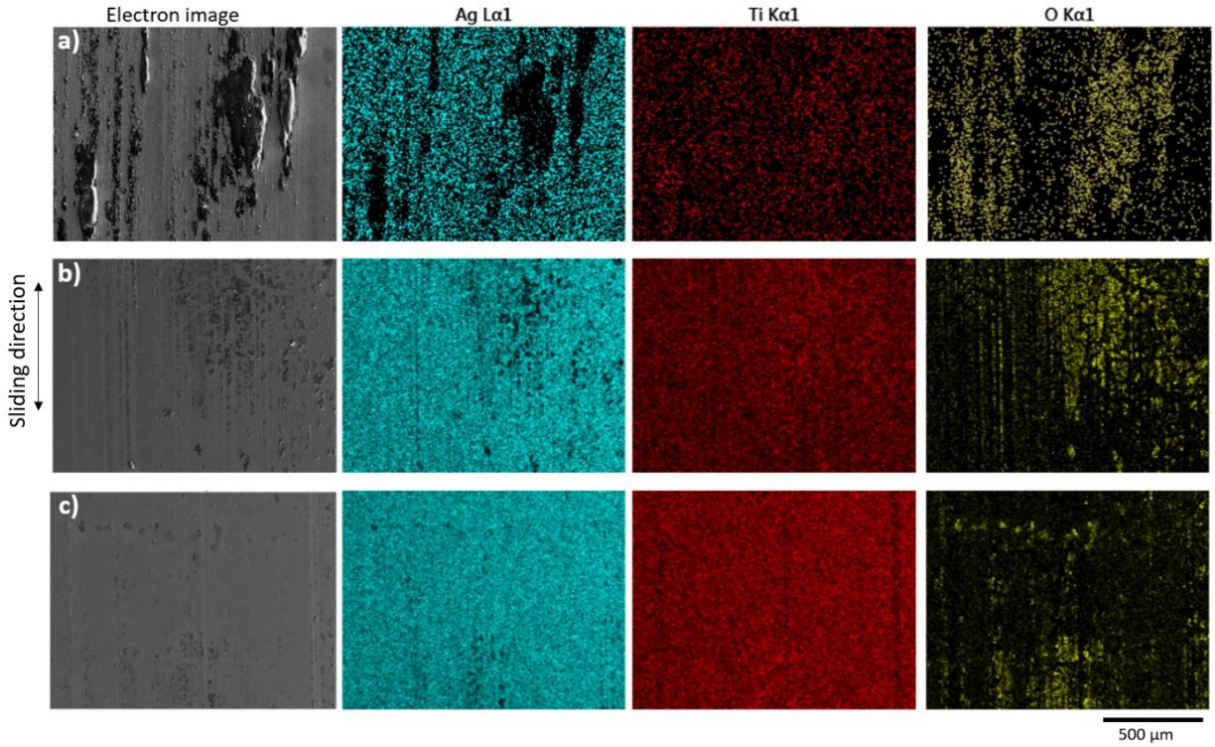

Figure 11: EDS analysis of the wear tracks for the tests performed with the Ti-Ag film (Ag/Ti=0.72) at 100% RH a) by interrupting the contact and changing the pressure, b) by interrupting the contact at contact pressure, c) as single-run.

Here, it could be expressed that the friction coefficient decreased with decreasing oxide layer formation on the wear track. For this high Ag-containing Ti-Ag film composition, silver oxide caused a negative effect on friction behaviour of the film.

On the other hand, when the balls rubbed to Ti-Ag films with Ag/Ti=0.72 analysed after these three testing procedures with EDS and the material transfer from film to ball was confirmed. There is more compact material transfer detected for the test performed by changing the pressure and interrupting the contact to do *in situ* analysis. The film particles were less compact on ball surface for the test #2. Here, the effect of constant pressure was observed as less oxygen detection on the ball surface. On the other hand, for the test performed in single run (at constant pressure with continuous contact), the film material was spread on the ball surface along the sliding direction and less transferred material was detected from film to ball (Figure 12). The remarkable difference of the ball surfaces is in line with the chemical analysis of the film wear tracks at 100% RH as it was shown in figure 6.19.

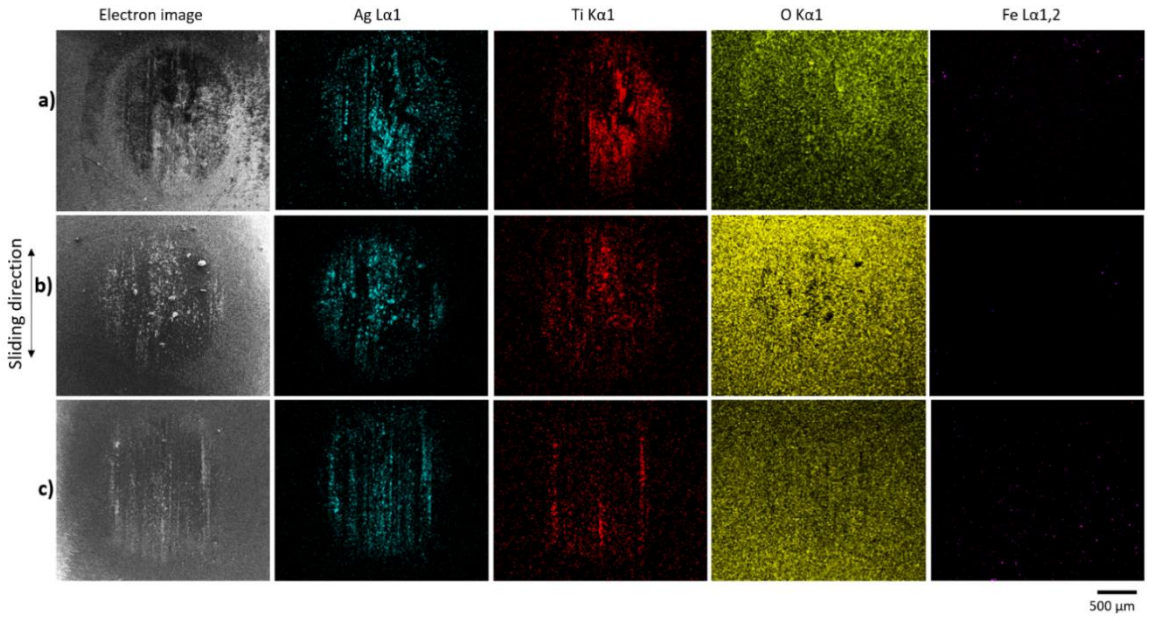

Figure 12: EDS analysis of the of the balls rubbed to Ti-Ag film (Ag/Ti=0.72) at 100% RH RH a) by interrupting the contact and changing the pressure, b) by interrupting the contact at contact pressure, c) as single-run.

Since the *in situ* analysis could not proceed for the last two testing procedure, the possible damaging mechanism was represented in the schema below, after several number of cycles. For the schema drawing, it was considered the compactness and alignment of the particles and the oxide layer formation during the sliding process (Figure 13). It was indicated that with increasing number of cycles, the thickness of the oxide layer was increased in addition to the large debris formation for the *in situ* test. However, for the test performed at constant pressure, even though the oxide layer formed, it is assumed that it has a lower thickness with the less debris formation both on the film and ball surface. Lastly, for the single run test, it is predicted that, the oxide layer thickness increased quite slowly from one cycle to another with a slight debris on both of the counter-parts.

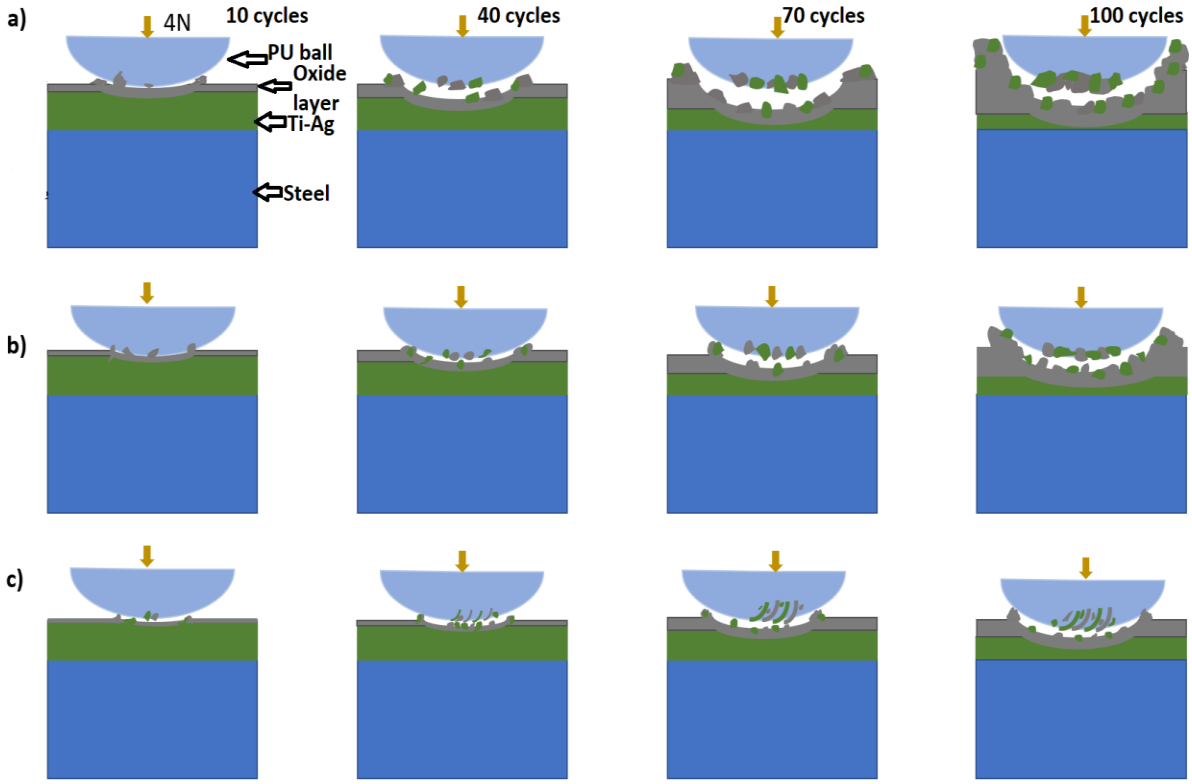

Figure 13: Schematic representation of contact conditions for the tests performed at 100% RH with Ti-Ag film (Ag/Ti=0.72) for a) by interrupting the contact and changing the pressure, b) by interrupting the contact at contact pressure, c) as single-run.

In conclusion, even though the pressure changed was mandatory for *in situ* analysis for the tests performed at 100% RH, it caused a negative effect on the wear mechanism of the coating by

increasing the friction coefficient and debris formation. When the pressure was kept constant and the contact was interrupted after every ten cycles without *in situ* imaging, a lower friction coefficient was obtained with a more stable curve for 100 cycles. Finally, for the test performed as single run, the effect of loading and unloading was eliminated and smoother curve was achieved for a lower mean COF. Unfortunately, for the last two methods dynamic investigation of the wear track was not possible. Ye, the 2nd test was selected in the following section (6.4.2.) for the analysis of effect of environment in post-mortem conditions since the testing procedure was the same as the tests performed in ambient air and 50% RH.

FOLIO ADMINISTRATIF

THESE DE L'INSA LYON, MEMBRE DE L'UNIVERSITE DE LYON

NOM : SAYILAN DATE de SOUTENANCE : 23/03/2023
(avec précision du nom de jeune fille, le cas échéant)

Prénoms : Aslihan

TITRE : Tribological Behaviour of Ti-Based Thin Film: A Small Scale *In Situ* Investigation

NATURE : Doctorat Numéro d'ordre : 2023ISAL0020

Ecole doctorale : Ecole doctorale matériaux de Lyon

Spécialité : Génie des matériaux

RESUME : The nature of interface in contact with skin, clothes or joints is one of the prime interests in the field of metallic biosensors. This interface can be enhanced through PVD processes in terms of chemistry and microstructure. Furthermore, dynamic evaluation of the contact interface at the early stage is essential to better understand the wear mechanism and to anticipate the efficient service life of the corresponding bio-device. Therefore, within this thesis, a laboratory-made micro-tribometer was developed and presented. This particular reciprocating ball-on-disk stage is coupled with an environmental SEM (eSEM) to characterise, at small scale, the tribological behaviour of the system under realistic *in situ* conditions.
To express the proof of concept, a preliminary analysis was performed with a conventional TiN PVD hard coatings, used as a model surface. The testing procedure for the dynamic approach during the run-in period throughout 100 cycles was defined in the controlled atmosphere in eSEM chamber (both in high vacuum and 50% relative humidity (RH)). When the tribological tests were performed, the wear track of the films was examined *in situ* after every 10 cycles, while the ball track was analysed in *post mortem* mode. Once validated, the mini-tribometer stage was applied for a more realistic metal used in biosensor systems: titanium. Indeed, this metal presents a high biocompatible character, coupled with interesting mechanical properties. The wear character of pure Ti film is still an issue, due to its columnar microstructure, which can be modified with an addition of proper alloying elements. In this sense, silver is an outstanding material to be alloyed with titanium for bio-sensor applications regarding its anti-bacterial character and ductile nature, as well its remarkable sliding behaviour in nanoparticle form. Within this thesis, Ti-Ag films were deposited with magnetron sputtering PVD process with several Ag contents. Various types of multiscale characterization (microstructural, chemical, electrical, mechanical) were performed to analyse the effect of Ag in the film composition. It was shown that increasing Ag content led to a denser microstructure with Ag-based nano-/micro-meter sized clusters distributed into the film matrix. Moreover, from a functional point of view, it also provided a slight improvement on hardness, Young's modulus and electrical conductivity of the films. During the *in situ* tribological analysis, the small-scale strategy of characterization that was specifically developed in this PhD, has highlighted a strong influence of the contact environment on its tribological behaviour. In particular, the effect of the humidity rate of the contact region on the tribological behaviour was deeply investigated, and the effect of Ag content on tribological behaviour of Ti-Ag films was studied. It was seen that temperature change to modify the humidity affects the tribological behaviour of polymer counter-face and Ag.

MOTS-CLÉS : Microstructural *in situ* characterisation, tribology, PVD thin films, environmental SEM, titanium, silver

Laboratoire (s) de recherche :
Université de Lyon, CNRS, UMR 5510, MATEIS, INSA-Lyon, F-69621 Villeurbanne, France
Université de Lyon, CNRS, UMR 5259, LAMCOS, INSA Lyon, F-69621, Villeurbanne, France

Directeur de thèse: Directeur de thèse: Prof. Philippe STEYER (MATEIS-INSA Lyon), HDR Sylvie DESCARTES (LAMCOS-INSA Lyon), Assoc. Prof. Nicolas MARY (MATEIS-INSA Lyon)

Président de jury :

Composition du jury : Prof. Cecile LANGLADE, Prof. Nicolas MARTIN, Prof. Luc PICHON, Assoc. Prof. Jose Filipe VILELA VAZ, HDR Chercheur Scientifique Juan Carlos SANCHEZ LOPEZ, Prof. Philippe STEYER, HDR-IR Sylvie DESCARTES, Assoc. Prof. Nicolas MARY